



HAL
open science

Étude d'un nouveau composé à propriété d'absorption multiphotonique dérivé du NADPH ciblant la NO-synthase

Huan Wang

► **To cite this version:**

Huan Wang. Étude d'un nouveau composé à propriété d'absorption multiphotonique dérivé du NADPH ciblant la NO-synthase. Agricultural sciences. École normale supérieure de Cachan - ENS Cachan, 2013. English. NNT: 2013DENS0049 . tel-00958076

HAL Id: tel-00958076

<https://theses.hal.science/tel-00958076>

Submitted on 11 Mar 2014

HAL is a multi-disciplinary open access archive for the deposit and dissemination of scientific research documents, whether they are published or not. The documents may come from teaching and research institutions in France or abroad, or from public or private research centers.

L'archive ouverte pluridisciplinaire **HAL**, est destinée au dépôt et à la diffusion de documents scientifiques de niveau recherche, publiés ou non, émanant des établissements d'enseignement et de recherche français ou étrangers, des laboratoires publics ou privés.

**THESE DE DOCTORAT
DE L'ECOLE NORMALE SUPERIEURE DE CACHAN**

Présentée par

Mademoiselle HUAN WANG

pour obtenir le grade de

DOCTEUR DE L'ECOLE NORMALE SUPERIEURE DE CACHAN

Domaine :

SCIENCES DE LA VIE ET DE LA SANTE

Sujet de la thèse :

**Multiphotonic Study of A New NADPH-derivative Compound
Targeting NO-Synthase**

Marie-Pierre Bourguignon	Directrice de recherche	Rapporteur
Bertrand Tavitian	Professeur	Rapporteur
Joanne Xie	Professeur	Examinatrice
Anny Slama-Schwok	Chargée de recherche	Examinatrice
Eric Deprez	Directeur de recherche	Directeur de thèse

Labortoire de Biologie et Pharmacologie Appliquée (LBPA)
ENS CACHAN/CNRS-UMR 8113, IDA
61, avenue du Président Wilson, 94235 CACHAN CEDEX (France)

Acknowledgement

When I start writing this section of my thesis, I couldn't believe that it is already the end of my PhD study. When I retrospect the three years in LBPA, all I could feel is full of gratitude. This thesis would not have been possibly finished without the helps and supports of many people who are gratefully acknowledged here.

I am much honored to have my thesis committee members Dr. Marie-Pierre Bourguignon, Dr. Bertrand Tavitian and Dr. Joanne Xie agreeing to read and evaluate this work. I thank them for providing an interest in my work. This thesis has benefited many comments from them.

My deepest gratitude goes first and foremost to Dr. Eric DEPRez, my supervisor, for his invaluable guidance, generous encouragement and continuous supervision with much patience throughout my PhD study. In fact, when I was a M2 student of MONABIPHOT Master Program, I did my "microthesis" in his team; later I decided to pursue my PhD study here. On one hand the project was very appealing to me; on the other hand I was greatly inspired by his passion for science. He is one of the exceptional scientists that I have ever seen who works extra diligently. It is my great luckiness and pleasure to be guided by him. During these years, he has offered me very impressive ideas and instructive suggestions with his profound knowledge and rich research experience. His rigorous scientific spirit and dedication for work are always a great encouragement to me.

I am sincerely grateful to Dr. Etienne Henry, a young scientist with solid background. He offered me crucial technical supports in fluorescence microscopy, as well as many valuable discussions. My sincere thanks equally go for our project collaborators: Dr. Anny Slama-Schwok (INRA, France) and Dr. Jean-Luc Boucher (Paris V, France), their insightful discussions helped me to develop a better understanding for the project; Dr. Chantal Dessy (UCL, Belgium), who provided me the professional training in cell culture.

It was a big pleasure to work in LBPA of ENS-Cachan, I received kindly helps from many of the members. I am grateful for Dr. Frédéric Subra, who gave me professional instructions in cell culture techniques; Dr. Sylvain Thierry, Dr. Olivier Delelis, who guided me in using flow cytometry; Dr. Patrick Tauc and Dr. Jean-Claude Brochon who gave me valuable discussions; Françoise Simon, who gave me the guidance in preparing the solutions. I treasure the time I spent together with my colleagues Rahima Chennoufi, Munir Soundasse and Eloïse Thierry, and I appreciate for their generous helps both at work and in daily life.

I have to especially express my gratitude to Prof. Isabelle Ledoux-Rak, who is the coordinator of MONABIPHOT Master Program. Without her, I would not have the chance to receive the high-class education in ENS-Cachan. Her agenda is always highly packed but she never refused to offer helps for students. I sincerely appreciate her tremendously efforts and supports, which left me very precious memories when I first came to France.

I would like to thanks all the members in the Foreign Affair Office of ENS-Cachan,

especially Madam Brigitte Vidal who helped us dealing with VISA, she is definitely the one that all the foreign students are grateful for her. I sincerely thank the secretaries in EDSP and LBPA, who helped me to solve the administrative problems and difficulties in daily life in France.

I am lucky to have many Chinese friends around me here: Na li, Yingying Chen, Xiaoqian Xu, Jiayao Li, Xiaoju Ni, Feifei Liang, Lue Huang, Xiao Wu, Qinggele Li, Yuanyuan Liao, Zhenzhen Yi, Fangzhou Zhang, Fan Yang, Zhe Sun, they shared my joy and my load when I am far away from my home country. They are my family in France.

My special thanks go for the most important person: my boyfriend Tobias Schudy. He is the firm backup in my heart and in my life. Without his encouragements and supports for my study, I would not have been able to walk through the obstacles with my courage. I appreciate his accompany from the bottom of my heart.

Lastly, I could never accomplish such a progress today without the supports from my parents. No matter where I am and what I do, they support me with unconditional love, understanding and encouragement throughout my life; they are the source of my power drive to pursue a life that I want to have.

In the end, I extend my regards and blessings to all of those who supported me in any respect during the completion of my PhD study. It is an unforgettable experience in my life.

Abbreviations

AI	Autoinhibitory (loop)
BAEC	Bovine Aortic Endothelial Cells
BH ₄	(6R)-5,6,7,8-tetrahydrobiopterin
BSA	Bovine Serum Albumin
CaM	calmodulin
CT	C-terminus
DMEM	Dulbecco's Modified Eagle Medium
DMSO	Dimethyl sulfoxide
EBM	Endothelia Cell Basal Medium
EEA	early endosome antigen
eNOS	endothelial NOS
EPR	Electron Paramagnetic Resonance
ER	Endoplasmic Reticulum
FABP	Fatty acid binding protein
FAD	Flavin Adenine Dinucleotide
FBS	Fetal Bovine Serum
FMN	Flavin Mononucleotide
FRET	Fluorescence Resonance Energy Transfer
fs	femtosecond
G6PDH	Glucose 6-phosphate dehydrogenase
GFP	Green Fluorescence Protein
HUVEC	Human Umbilical Vein Endothelial Cell
iNOS	Inducible NOS
IR	Inferred
K _d	equilibrium dissociation constant
L-Arg	L-Arginine
LEDGF	Lens Epithelium-Derived Growth Factor
MFI	Mean Fluorescence Intensity
NaCl	Sodium Chloride
NADPH	Nicotinamide Adenine Dinucleotide Phosphate

NIR	Near Infrared
nNOS	neuronal NOS
NO	Nitric Oxide
NOS	Nitric Oxide Synthase
NOSIP	NOS-interacting protein
NOSred	NOS reductase domain
NS	Nanoshutter
NT	Nanotrigger
P100 plate	100x20 mm culture plate
PBS	Phosphate Buffered Saline
PS	Penicillin-Streptomycin
RD-hinge	reductase domain hinge
ROS	Reactive Oxygen Species
rpm	round per minute
RVLM	rostral ventrolateral medulla
SDS	Sodium Dodecyl Sulfate
Ser	Serine
SOD	Superoxidase Dismutase
T-75 flask	75 cm ² culture flask
TBHP	Tert-butyl hydroperoxide
Thr	Threonine
UV	Ultra Violet
VEGF	Vascular Endothelial Growth Factor
VIS	Visible

Table of Content

INTRODUCTION	4
Objective of the study.....	4
Nitric Oxide and Nitric Oxide synthase	6
History	6
Nitric Oxide	6
Nitric Oxide Synthase (NOS)	8
Overall structure	8
Nomenclature of NOS isoforms	9
Comparison of the amino-acid sequences.....	10
Polypeptide structure	11
NOS dimerization	12
The catalytic mechanism of NOS	12
1. How electrons are transferred within the reductase domain?	12
2. The role of calmodulin binding	13
3. Mechanism of NO synthesis within oxygenase domain	16
Distribution of NOS isoforms in human body	17
Translocation of NOS among cellular compartments	20
Differential effects of NO derived from NOS isoforms	22
Regulation of NOS activity	23
CaM	23
Regulation by gene transcription	23
Activation/inhibition of signal transduction pathways.....	23
Modulation of enzymatic activity through protein-protein interaction.....	24
Inhibitors of Nitric Oxide Synthase	25
Experiment strategy	27
Nanotrigger (NT)	27
Principle	27
Molecular design.....	27
Nanoshutter (NS).....	30
Fluorescence Spectroscopy	32
Introduction to fluorescence.....	32
General parameters	35
Two-photon excitation.....	36
Principle	36
Theory.....	37

Parameter of two-photon absorption	38
Fluorescence microscopy	39
Epi-fluorescence microscopy	40
Confocal microscopy	41
Principle	41
Advantages	42
Two-photon microscopy using NIR/IR laser sources.....	43
Principle	43
Advantages	45
Confocal microscopy with two-photon laser scanning	47
Experimental design	48
<i>METHODOLOGY</i>	49
Spectroscopic and fluorescence properties of NS1	49
Fluorescence properties of NS1-NOS complex	50
NS1-protein bound selectivity assay.....	50
Cell culture	51
Gelatinization of the culturing surface (special treatment for HUVECs).....	52
Thawing of cells	52
Passage of cells.....	53
Freezing cells.....	53
Fixation and mounting	54
Immunostaining	54
Materials.....	54
Protocol	55
Imaging of NS1 ex vivo.....	56
Fluorescence detection of ROS generation in cells	57
<i>RESULT</i>.....	59
Introduction of “Rational design of a NADPH derivative imaging constitutive nitric-oxide synthases upon two-photon excitation”	59
Rational design of a NADPH derivative imaging constitutive nitric-oxide synthases upon two-photon excitation	63
Supplementary data I	69
Supplementary data II.....	88
Introduction of “Addressing to NADPH-dependent NO and Reactive Oxygen Species signaling with a photoactive NADPH Analogue”	89

Addressing to NADPH-dependent NO and Reactive Oxygen Species signaling with a photoactive NADPH Analogue.....	92
.....	95
Figures Legends	117
Figures	123
Supplementary data I	130
Supplementary data II	132
<i>DISCUSSION, CONCLUSIONS AND PERSPECTIVES</i>	<i>134</i>
<i>REFERENCES</i>	<i>141</i>

INTRODUCTION

Objective of the study

The aim of this study is to modulate the production of Nitric Oxide (NO) by targeting the enzyme responsible of its production, the Nitric Oxide Synthase (NOS). We designed a unique structure-based molecular tool called Nanoshutter (NOS inhibitor), which contains a nucleotide moiety mimicking the NADPH recognition site of NOS, as well as a chromophoric moiety characterized by a large two-photon absorption cross-section (σ_2), thus it is capable of inhibiting NOS catalysis and displays excellent biphotonic fluorescence imaging properties.

It is necessary to first understand the physiological role of NO in biological body. In mammals, NO is an endogenously produced free radical mediator involved in many (patho)physiological processes in the cardiovascular, nervous and immune systems (1). This highly reactive gas plays a key role in regulating cardiovascular homeostasis, influencing systemic and pulmonary blood pressure, vascular remodeling and angiogenesis. It displays both anti-viral and anti-bacterial properties and exerts important roles in apoptosis. The cardiovascular system is in a state of constant active vasodilation dependent on the generation of NO. Indeed, NO can be considered as the endogenous vasodilator (2). In tumor, NO could contribute to many of the abnormalities described in tumor vasculature such as hyporeactivity or unresponsiveness to vasoactive mediators (3) and maximum vasodilatation. It also plays a dual role in free tumor and solid tumor: when the NO is produced at high concentrations mostly in free tumors, NO has an antitumor activity. However, when the NO is produced at lower concentrations mostly in solid tumors, it promotes tumor growth.

The modulation of the NO level could lead to pathological processes, e.g. reduced NO production could lead to enhanced adhesion of platelets to the vessel wall, as it has been observed under conditions of atherosclerosis and diabetes, whereas the lack of NO could be involved in the restenosis sometimes observed after angioplasty (4). In blood cells, NO inhibits platelet aggregation (5), also inhibits adhesion to (i) collagen fibrils, (ii) endothelial cell matrix, and (iii) endothelial cell monolayers (6) (7). A decrease in the synthesis of NO may contribute in other pathways at the origin of diseases such as atherosclerosis and hypertension (8).

As a key enzyme, NOS plays a crucial role in the process of NO production. Regulation of NO by monitoring the activity of NOS could have profound potentialities in clinical treatment. This molecular tool may lead to a new avenue of controlling the release of free NO in cells with enhanced spatial and temporal resolution.

The following sections of Introduction will be divided into three parts: (i) From the biological point of view, the identification of NO and its chemical and biological properties will be reviewed. The introduction of NOS will be followed by the illustration of its structure, the nomenclature of NOS isoforms, the catalytically mechanisms of NO production, the distributions of NOS in human body, the regulation of NOS activity and finally, a rapid review of the known NOS inhibitors. (ii) On the basis of Nanotrigger (NT), a NOS activator which was studied in the previous project, the strategy of Nanoshutter (NS) will be presented. (iii) From the photo-physical point of view, a brief introduction of fluorescence principle and microscopy will be given, and the main fluorescence parameters will be presented. The emphasis will be stressed on the principle of two-photon excitation, which is a crucial tool in this study. Finally, the experimental design will be listed.

Nitric Oxide and Nitric Oxide synthase

History

In the early observations in 1980's, Nitric Oxide was considered as endothelium dependent relaxing factor (EDRF) (9) (10) (11). Based on pharmacological similarities between EDRF and NO generated from acidified NO_2^- , Furchgott suggested that EDRF may be NO (12). In 1987, the first evidence from the formation of NO by mammalian cells came from experiments in which EDRF released from vascular endothelial cells was detected by the chemical methods used to identify NO (13). In 1988, the amino acid L-arginine (L-Arg) was shown to be the precursor for the synthesis of NO by vascular endothelial cells (14), other data showed that the NO and citrulline are the co-products of the same enzymatic reaction; the corresponding enzyme is named NOS nowadays (15).

Nitric Oxide

NO is slightly soluble in many solvents and can diffuse relatively easily across biological membranes. Its solubility in water is low. According to Fick's laws of diffusion, the diffusion coefficient of NO is $4.8 \times 10^{-5} \text{ cm}^2 \text{ s}^{-1}$ in water at 37 °C (16) (17), similar to that of oxygen under comparable conditions (18). It has been estimated that the half-life of NO varies from about 1 s in blood-free perfused guinea pig heart to 30 s in physiological buffers (16).

The diffusion of NO in a biological context

In culture cells, NO stimulated by interferon has been detected at a distance of 100 to 500 μm from RAW 264.7 macrophages, yielding a diffusion radius equivalent to 10-to-50 cells (assuming an average macrophage diameter of 10 μm) (19). Theoretically, this can be used as a representative model for studying the diffusion of NO *in vivo*.

However, the estimation of the half-life of NO simply based on its diffusion radius is more complicated in biological systems as there are many interacting factors such as soluble guanylyl cyclase and hemoglobin, lipids, and free radicals (19) (20) (21). For example, in isolated rat aorta, the diffusion radius was shown to be 4-fold smaller in an aortic wall than in a homogeneous medium such as water (22). Recently the cholesterol content in membranes was reported to decrease NO diffusion by 20-40% (20) due to the changes in membrane fluidity caused by cholesterol. NO efflux produced by activated macrophages was also reduced by 41% in the presence of albumin and by 53-70% in the presence of liposomes, indicating that intracellular structures or biomolecules could also limit NO diffusion (19). In the case of high concentration of NO produced by iNOS, and in the presence of superoxide

anion, the formation of peroxynitrite also limits the diffusion of NO (16). In addition, the partitioning of NO between polar and non-polar media could play a major role in terms of localized effects (23). NO and O₂ have similar partition coefficients in non-polar media, being 70 times more soluble in hydrophobic than in hydrophilic media (24). Therefore, both molecules are more concentrated in a hydrophobic media, such as liposomes, lipoproteins, or biomembranes or within the hydrophobic pockets of proteins, than in polar-based environments (24) (25). Higher concentrations of NO and O₂ in a non-polar environment may result in chemical reactions favoring the formation of nitrogen oxides which has different chemical properties than NO (26) (27). The effects of NO in biological systems depend on its steady-state concentration and where it is being produced.

Nitric Oxide Synthase (NOS)

Overall structure

The known NOS enzymes are usually referred to as “dimeric” in their active forms; A substrate access channel extends from the active site towards the homo-dimer interface (28). Within this region, a second cofactor binding site is formed. In the bacterial enzymes, the precise identity of the cofactor is uncertain, however, for mammalian enzymes, it has been established that (6R)-5,6,7,8-tetrahydrobiopterin (BH₄) binds at the interface of the dimers and hydrogen bonding to the heme propionate group, an unique arrangement (29) (30)-(31) (32). The mammalian enzymes differ from the bacterial enzymes in their incorporation of a reductase domain by extension of the gene (33). Thus, mammalian NO synthases consist of **an oxygenase domain** (heme and BH₄ binding) and **a reductase domain** related by its sequence, structure and function to the NADPH-dependent microsomal cytochrome P450 reductase (known to be the primary electron donor to most mammalian P450s). Like P450 reductase, the NOS reductase domain (NOSred) can be further divided into FMN and FAD binding domains, linked together by a single polypeptide chain (34) (35). The FMN domain is connected to the oxygenase domain via a segment of polypeptide of about 30 amino acids in length, which forms a binding site for calmodulin (CaM) (33) (36) (37). **Fig.1** shows the overall organization of NOS.

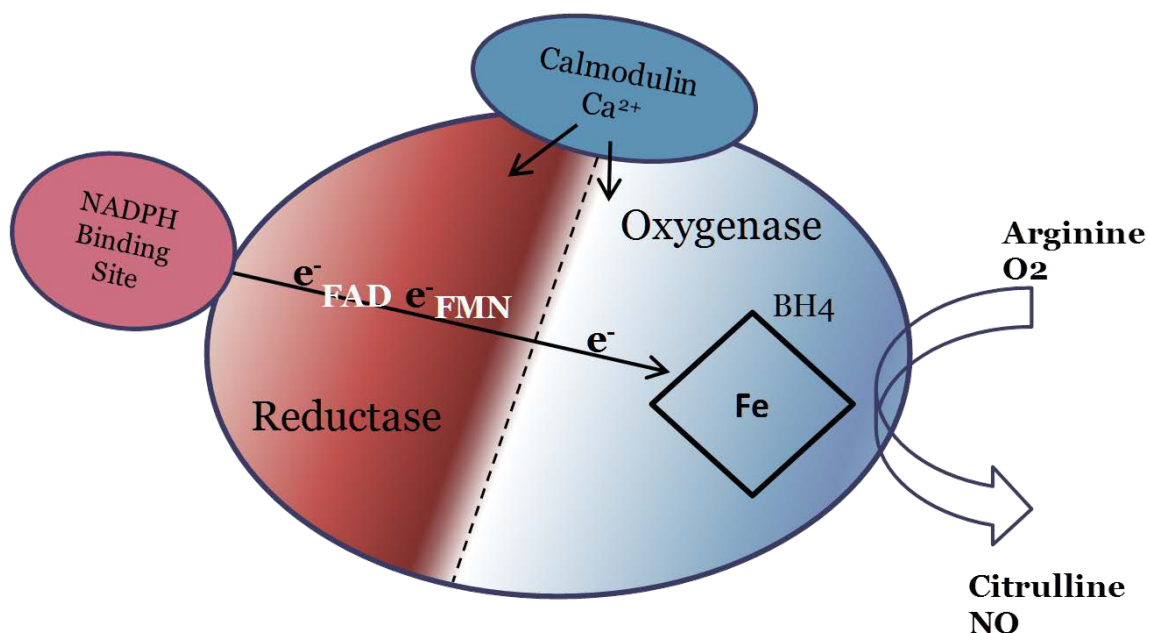


Fig. 1 Overall organization of NOS.

Electrons (e⁻) are donated by NADPH to the reductase domain of the enzyme and are transferred via FAD and FMN redox carriers to the oxygenase domain. At the oxygenase domain level, they interact

with the heme iron and BH_4 at the active site to catalyze the reaction of oxygen with L-Arg, generating citrulline and NO as products. The electron flow through the reductase domain requires the presence of bound Ca^{2+}/CaM . (Modified from Ref. (36))

Nomenclature of NOS isoforms

There mainly three NOS isoforms in mammals. The most common nomenclature of the three isoforms is: nNOS (also known as Type I, NOS-I and NOS-1) being the isoform first found (and predominating) in neuronal tissue, iNOS (also known as Type II, NOS-II and NOS-2) being the isoform which is inducible in a wide range of cells and tissues and eNOS (also known as Type III, NOS-III and NOS-3) being the isoform first found in vascular endothelial cells. To note, this nomenclature is not absolute. For example, nNOS was originally purified and cloned from neuronal tissues. However, nNOS is now known to be much more widely distributed, with an important level of expression in skeletal muscle. iNOS, originally purified and cloned from an immunoactivated macrophage cell line, has been identified in a myriad of mammalian tissues, and iNOS expression has been studied in many cell types such as cardiac myocytes, glial cells, and vascular smooth muscle cells. eNOS, the last of the three mammalian NOS isoforms to be isolated, was originally purified and cloned from vascular endothelium, but since has been discovered in cardiac myocytes, blood platelets, brain (hippocampus), etc. (38).

Another classification is based on the mechanism of expression, i.e. constitutive (eNOS and nNOS) or inducible (iNOS), and their respective calcium-dependent (eNOS and nNOS) or calcium-independent behaviors (iNOS). For eNOS and nNOS, resting intracellular Ca^{2+} concentrations are required for their binding calmodulin to be fully activated. By contrast, iNOS appears able to bind calmodulin with extremely high affinity. Now, it is known that the levels of gene expression of both eNOS and nNOS may also be induced under different physiological conditions (e.g. hemodynamic shear stress or endotoxic shock), and, conversely, that iNOS may function as a “constitutive” enzyme under physiological conditions in some cells (39). A comparison of the properties of these three major isoforms of the enzyme is shown in **Tab. 1** (From Ref. (40)).

	<i>Endothelial NOS (eNOS)</i> ^a (Type III NOS, NOS-3)	<i>Neuronal NOS (nNOS)</i> ^a (Type I NOS, NOS-1, bNOS)	<i>Inducible NOS (iNOS)</i> ^a (Type II NOS, NOS-2, macNOS, hepNOS)
Primary regulation	Ca^{2+} /calmodulin	Ca^{2+} /calmodulin	Gene expression
Subcellular location	Membrane \gg cytosol	Cytosol?	Cytosol \gg membrane
NO output ^b	Low (pmolar)	Low (pmolar)	High (μ molar)
Function	Cell signaling	Cell signaling	Cytotoxic Cytostatic Cytoprotective

Table. 1 Isoforms of NOS and their respective properties.

Comparison of the amino-acid sequences

Firstly, the NOSs were identified and described in 1989 (41), the three major isoforms were cloned and purified between 1991 (33) and 1994 (39). Three quite distinct isoforms of NOS have been identified, products of distinct genes, with various locations, regulation and catalytic properties as well as differential sensitivities to inhibitors; they share 51-57% homology at the amino acid level (42). The domains responsible for cofactor binding are all well conserved, with divergence in the segments connecting the domains, e.g. the CaM binding site and in a series of inserts (**Fig. 2**).

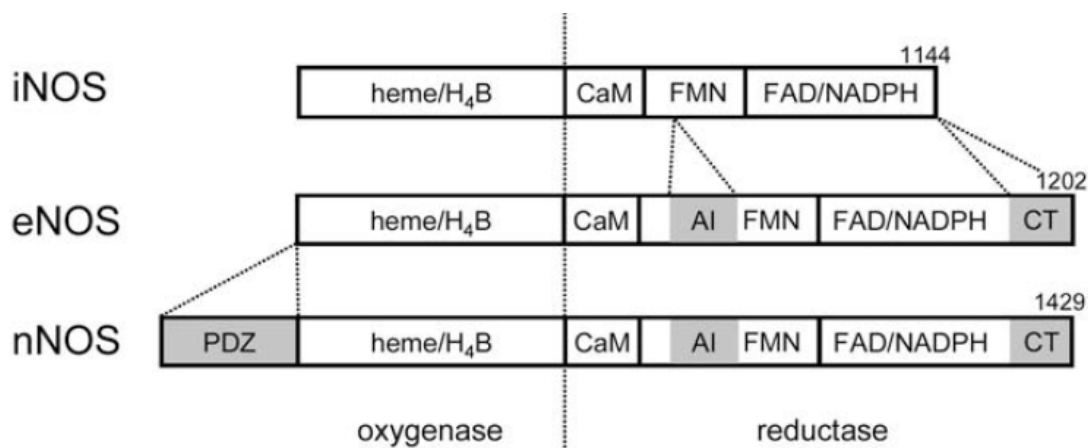


Fig. 2 Block gene alignment of NOS isoforms.

Fig. 2 (modified from Ref. (43)) indicates how the three different isoforms are related by amino-acid sequence (44).

Among the three isoforms, the inducible NO (iNOS) has the shortest sequence. Unlike the other two isoforms, iNOS binds CaM at all physiological Ca²⁺ concentrations and is not subject to Ca²⁺-dependent regulation (45).

The endothelial isoform (eNOS) has a modified CaM binding sequence and contains two significant inserts in the protein sequence. One is an autoinhibitory loop (AI) of 45 amino acids within the FMN domain; the other insert corresponds for an extension of the C-terminus (CT) of 42 amino acids with respect to P450 reductase.

The neuronal isoform (nNOS) contains the same modifications compared to eNOS. To note, nNOS also contains an N-terminal extension of about 200 amino acids, the PDZ domain which is involved in the subcellular localization of the protein (46).

These main characteristics are used to define the three isoforms, but there are other subtle differences in structure and sequence (47) (48).

Polypeptide structure

X-ray crystallography has enabled the high-resolution structure of most of the NO synthase polypeptide to be determined in series of fragments (**Fig. 3**). The structures of the iNOS (31) (32), eNOS (30) (31) and nNOS (49) (without the PDZ region) oxygenase domain in their dimeric forms with numerous different ligands have been determined and represent structural platforms for pharmaceutical developments.

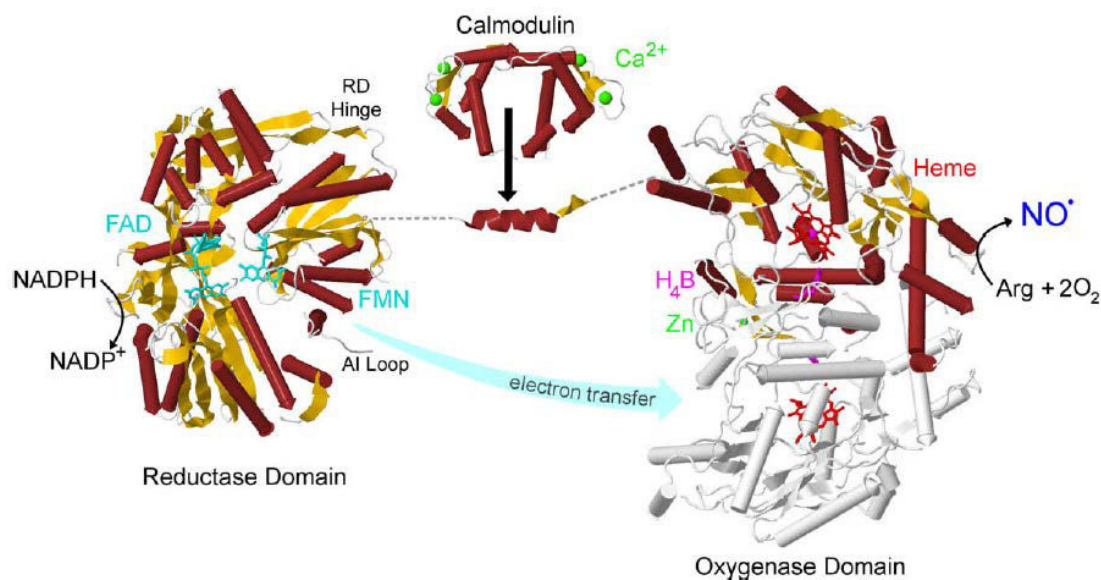


Fig. 3 Structures of the different fragments of NOS aligned in order of amino-acid sequence.

Fig.3 (from Ref. (50)) shows the dimeric oxygenase domain of nNOS (51), CaM-binding linker of eNOS with bound CaM (52) and the reductase domain of nNOS (34).

Regarding the reductase domain, only the X-ray structure of nNOS was resolved. The structure of the reductase domain of nNOS (34) was found to be very similar to that of P450 reductase (35), with the two cofactors FAD and FMN domains orientated within only 5 Å apart.

The additional polypeptides CT and AI inserted in the structure increased the contact area between the FAD and FMN domains. This factor alone probably influences the CaM dependency of the enzyme.

The CaM binding site connects the oxygenase and the reductase domains. Note that in the structure of eNOS, this area is an isolated peptide, allowing CaM binding (52), which adopts an α -helical conformation encapsulated by the four Ca²⁺-bound lobes of CaM.

In the case of nNOS, the relationship between the PDZ domain folds (53) and the oxygenase domain is not known, and to date, how these three components are assembled

to form the functional enzyme is not clear. However, it is known that the enzymes transfer electrons from the FMN domain of one subunit to the oxygenase domain of the other in a trans organization (54) (55) (56).

Besides, a comparison of human eNOS and iNOS oxygenase domain structures reveals that they share a similar overall molecular shape, as well as similar relative orientations of cofactors and stereochemistry within the catalytic center (30). The only significant difference in the arginine binding site is at position 382 where the Asp residue in iNOS is replaced by Asn in eNOS that lies about 9 Å from the substrate guanidinium.

NOS dimerization

Unlike the P450s, NOS is a homodimer and a substrate access channel extends from the active site towards the dimer interface (57).

The association of the NOS into active dimers involves a large interface in the oxygenase domain involving two regions of the primary structure of NOS (30) (32) (58). It is suggested that for iNOS, only the oxygenase domain is involved in the dimer formation (59), whereas for nNOS and eNOS, there are interactions between the reductase domains and the area between reductase and oxygenase domain which cross the dimer. Altogether, these interactions may play a key role in maintaining a tight dimeric organization. This may explain why iNOS dimer formation is more critically dependent on the presence of BH₄ compound to both nNOS and eNOS (60) (61).

Nevertheless, BH₄ together with heme and L-Arg all promote and/or stabilize the active dimeric form of all three isoforms. The presence of heme appears to be mandatory, with BH₄ arginine promoting and stabilizing dimer formation. In the case of nNOS, it was shown that addition of BH₄ and L-Arg to nNOS, already in its dimeric form, induced conversion into a more stable dimer which displayed unusual resistance to SDS (62). It is not clear whether this also occurs with the other isoforms. There is evidence suggesting that, in intact cells, dimers of iNOS are formed in an irreversible manner and cannot further dissociate into monomers (63).

The catalytic mechanism of NOS

1. How electrons are transferred within the reductase domain?

The supply of electrons for NO synthesis starts with the transfer of a hydride ion from NADPH directly to the N5 of the FAD in the reductase domain; the newly formed FAD hydroquinone must then transfer an electron to the FMN, which acts as a shuttle, passing

one electron at a time to the heme (64) (65) (66). The FMN forms an extremely stable neutral semiquinone, which is oxidized only very slowly in air (67) (68) (69) (70) (71). As previously mentioned, FAD and FMN cofactors are positioned around 5 Å apart (34) (35), in an optimal configuration facilitating the electron transfer from FAD to FMN; however, in this initial configuration, the FMN is unable to interact with the heme domain for subsequent efficient electron transfer. Thus FMN has to move substantially in order to donate its electron to the heme. It is likely that this conformational transition would require movement of the FMN domain relative to the FAD domain around the reductase domain hinge (RD-hinge, **Fig.3**)

Roles of the flavin domain

The essential role of the flavin cofactors is to allow a two-electron donor (NADPH) to donate electrons to a one-electron acceptor (heme), by forming stable semiquinone radical intermediates. The effect of CaM is most likely kinetic, rather than thermodynamic, since CaM-binding has little effect on the redox potentials of the flavins (69).

Interestingly the pathway of electron flow appears to “crossover” between different subunits of the dimer, e.g. the flavin domain of one polypeptide chain donates its electron to the heme domain of the other (72). The mechanistic reason for this is unclear, but the direct consequence is that the NOS monomer is inactive.

2. The role of calmodulin binding

The constitutive isoforms of NO Synthase (nNOS and eNOS) are both regulated by the free intracellular Ca^{2+} concentration, which induces binding of CaM to the enzymes (36) (61) (73). The EF hands of CaM bind to the recognition sequence in an antiparallel orientation to induce NO synthesis (74). The primary mechanism is activation of electron transfer from FMN to heme (64) (75), with CaM acting as an electronic switch. Other effects induced by CaM binding are acceleration of flavin reduction by NADPH, steady-state reduction of external electron acceptors such as dioxygen, ferricyanide and cytochrome c and an increase in flavin fluorescence. Indeed, all these effects are related to the overall activation mechanism. It was shown that most of the effects of CaM binding could be reproduced in the context of the isolated reductase domain (NOSred), indicating that the CaM binding site is still present on the reductase domain (70). As an example, the steady-state cytochrome c reductase activity of nNOSred increases by 10-fold upon CaM binding.

Since iNOS is Ca^{2+} -independent, comparisons between iNOS and eNOS/nNOS were used to probe the structural basis for the CaM-dependent activation mechanism.

The CaM binding sequence differs between the three isoforms, and has been shown to have a higher affinity in the case of iNOS. In this case, the complex is very stable and CaM cannot readily dissociate from iNOS (45).

In nNOS and eNOS there are two additional regions (AI and CT) inserted within the amino-acid sequence. The mutageneses of these regions by point mutation, deletion, insert swapping and domain swapping have established their roles: (i) Within the FMN domain there is an extra peptide AI (autoinhibitory loop). Deletion of this loop results in CaM binding at lower Ca^{2+} concentrations and an increase in the reductase domain activity in the absence of CaM (65) (76) (77) (78) (79) (80); (ii) At the C-terminal end, the constitutive NOSs are extended by CT. Deletion of this region has a similar effect, but also induces some NO synthesis activity in the absence of CaM (81). Deletion of both of these regions causes a great increase in reductase activity and CaM-free NOS activity, 40% higher relative to the wild-type CaM-bound rate for the endothelial isoform (82) (83). The small insertion in the FAD domain also affects the Ca^{2+} concentration dependence of the enzyme (84) and the reductase domain hinge (RD hinge in **Fig.3**) slows down the CaM-dependent heme reduction rate, especially in the case of eNOS (85). Besides, it appears that the AI and CT insertions increase the interface contact area between FAD and FMN. Indeed, all contacts within the FAD domain–FMN domain interface region appear to play a role in locking the conformation of the reductase domain closed then acts as AI domains. Moreover, it has been shown that, in a construct consisting of only the FMN and heme domains, the rate of electron transfer between the two cofactors remains CaM-dependent despite the absence of the FAD domain (86) (87).

Which steps are activated by CaM?

Taking into account the above-mentioned considerations, it is clear that the constitutive NOS activity is highly related to Cam binding. If we further divide the catalytic cycle of the reductase domain into three basic steps: (1) Hydride transfer from NADPH to FAD, (2) electron transfer from FAD to FMN and (3) electron transfer from FMN to heme, each has been shown to be dependent on the conformation of the enzyme, i.e., hinged open or closed (88). This implies that the reductase domain functions mechanically, with the hinging motion required to induce each step in turn. Therefore each step is also likely to be CaM-dependent (50). However, this subject is controversial and dependent on the interpretation of complicated pre-steady-state kinetics (70) (83) (88) (89) (90) (91) (92) (93) (94). The general proposed mechanisms based on the current understanding of each step are presented below:

In step (1), the rate is observed to be most likely dependent on the rate of movement of the FAD-stacking residue (89) (94), then immediately a charge-transfer complex containing NADP^+ and the reduced FAD is built. Although CaM appears to affect the rate of the

movement of the residue, the equilibrium of this complex is largely independent of CaM. So far the CaM-bound partially influences the rate of this step.

In step (2), according to biological electron transfer theories, the rate of electron transfer from FAD to FMN will be determined largely by the distance separating the cofactors and the possibility of coupled proton transfers (95). In nNOS (34), the distance from FAD to FMN is extremely short (5 Å) and has the greatest effect on rate. Until now, little is known about this step, because it is particularly difficult to observe an extremely rapid process. According to recent molecular modelling, NADPH binding locks the enzyme in a “hinge-closed” conformational state, in which the FMN module is closely associated with the FAD-NADPH binding domains (34) (87). In this state, electrons can be passed from FAD to FMN but not to outside electron acceptors such as cytochrome c. The “hinge-open” conformational state, in which effective electron transfer from FMN to the heme can take place, is facilitated by a major movement of the FMN module. It has been proposed that CaM accelerates this conformational change (34).

In step (3), Electron transfer from FMN to heme has been shown to be the rate-determining step for overall NO synthesis (64) (75) and involves a large-scale conformational change in which the FMN domain moves from an electron *input* state (in which the reductase domain is “hinge-closed”) to an electron *output* state in which the FMN is close enough to the heme to transfer an electron. Crystallographic and mutagenesis studies have identified the most likely interacting regions including the acidic cluster of residues on the surface of the FMN domain (92) and a basic patch of residues on the surface of the oxygenase domain (96) (97). The acidic patch also forms key contacts in the interface region of the reductase domain (34) (88) (98), whilst the basic residues surround is in direct contact with the heme. The contact regions in the *input* and *output* states appear therefore to be electrostatically controlled. In particular, the pathway of electron transfer from FMN to the heme, and the mechanism behind the activation of this electron transfer by CaM, are largely unknown. It has been proposed that the *output* state, in which FMN is close enough to transfer the electron to the heme, is only transiently. CaM could probably accelerate the conformational change leading to the *output* state.

3. Mechanism of NO synthesis within oxygenase domain

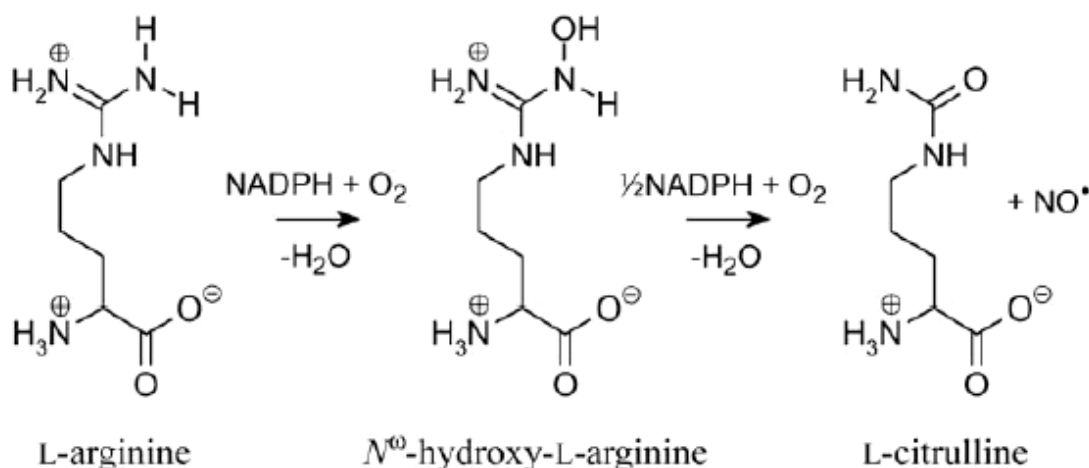


Fig. 4 NO synthesis from L-Arg.

The catalysis of NO is shown in **Fig. 4** (Ref. (51)). NO is produced within the oxygenase domain of NOS. NO is particularly interesting for the physiologists and biochemists, as it is part of the first mammalian pathway known to synthesize a gas as a signaling molecule. In terms of the chemical mechanism of NO synthesis, several aspects remain uncertain. There is inherent similarity between NOS and the cytochromes P450 (99) (100), cytochrome P450 could be considered as a starting model to discuss about the NO reaction. However, the added complexities for NOS thereby made the mechanism unique in enzyme chemistry, and some mechanical aspects remain unsolved.

The substrate L-Arg in the presence of O₂ is converted to NO and citrulline in the oxygenase domain via two consecutive mono-oxygenation reactions (36) (101) (102) (61). The first step requires the transportation of two electrons from the reductase domain to the heme, where oxygen activation takes place. This is a standard mono-oxygenation reaction which is typically similar to the one occurring in P450. The second step appears to consume only one electron and performs a similar di-oxygen activation reaction (102).

Using established P450 chemistry, yet far from definitive, it is possible to draw a catalytic cycle of NO production which includes the following aspects: Formation of the oxyferrous complex, one-electron reduction of this complex by BH₄ and release of NO from the ferrous NO complex by reduction of a BH₄ radical (103) (104).

Role of BH₄

A major breakthrough in our understanding of NO synthesis corresponded to the discovery of the role of BH₄, which has been identified as a critical cofactor for the NO production (105). The first clues of came from the observation that BH₄ accelerates the decay of the oxyferrous complex in the isolated NOS oxygenase domain (106) (107). In the

L-Arginine-bound state of the enzyme, oxygen binds to the ferrous heme and the resultant complex decays 100-fold faster in the presence of BH₄ (107) (108) (109). Now it is known that the two consecutive mono-oxygenation reactions start with di-oxygen bound to the ferrous heme, leading to the formation of a peroxy-bound heme complex that is reduced by an electron transfer from BH₄. In summary, BH₄ actually has several roles. (i) It binds within the dimer interface and helps to stabilize the quaternary structure of the active enzyme form (32) (62); (ii) It is required to act as an electron donor during oxygen activation. (iii) It is also required to recapture an electron from the ferrous nitrosyl complex in order to trigger NO release (103). In the particular case of endothelial NOS, two molecules of BH₄ bind to each eNOS dimer and facilitate electron transfer for L-arginine oxidation. It has also been demonstrated that BH₄ preserves eNOS dimerization and improves endothelial function (110). When BH₄ is limited, by decreasing its synthesis or increasing its oxidation, eNOS becomes uncoupled, and superoxide is produced (111). Thus BH₄ availability is essential for normal endothelial function (112).

Distribution of NOS isoforms in human body

It has been established that nNOS and eNOS are constitutively expressed, whereas iNOS is induced only during the immune response (113) (114). However, recently it has been observed that iNOS is constitutively expressed in neurons (115) (116), kidney (117), liver (118), lung (119), colon (120), and keratinocytes (121), whereas eNOS can be expressed at a level higher than its constitutive level under various conditions such as exercise (122), estrogen stimulation (123), hyperthermia (124), and shear stress (125) (126). Thus, based on current research reports, the expression and activity of the NOS isoforms appear to be cell-specific.

NO production and its effect not only depend on the type of cell, organ or organism where it is produced, but also varies in particular conditions. For example, NO produced by vascular endothelial cells is usually constitutive and in a relatively small amount, to maintain normal blood pressure and blood homeostasis (127). However, during septic shock, iNOS expression is induced in vascular endothelial cells, which in turn release high concentrations of NO, a process associated with vasoplegia, persistent hypotension, and decompensation (127) (128) (129).

Understanding the complexity of the localization of NO production and the implications of this compartmentalization in terms of cellular targets and downstream effects will contribute to the development of better strategies for treating or preventing pathological events associated with the increase, inhibition, or mislocalization of NO production.

Below are presented the locations of NOS isoforms in the main organs.

In the lung: The lung is composed of at least 40 different cell types, including vascular smooth muscle cells, endothelial cells, bronchial smooth muscle cells, neurons, pneumocytes, epithelial cells, and macrophages (130). Each of these cells has the ability to produce NO via one or more NOS isoforms (131) (132) (133) (134) (135).

Under healthy conditions, the three distinct NOS isoforms in different lung cells lead to various effects: increased iNOS level would result in increased lung mucus secretion in bronchial epithelia and alveolar macrophages in a specific manner, whereas the decreased expression of both eNOS and nNOS would lead to pulmonary hypertension and bronchoconstriction specifically in pulmonary vessels and bronchial smooth muscle. Nevertheless, it appears to be paradoxical that NO is known to dilate bronchia but bronchoconstriction was found in asthma patients whose exhaled NO is increased (136). This can be explained by the role of the oxidative/nitrative stress (136) (137). The strong induction of pulmonary iNOS, concomitant to the observed bronchoconstriction, could be due to the formation of unwanted side-products such as peroxynitrite which counteracts the expected bronchodilator effect (138) (139).

In the liver: In hepatocytes, NO can be synthesized by any of the NOS isoforms (118) (140), in another word, the 3 NOS isoforms are expressed in liver. Various cell–cell interactions, oxygen availability, and differential exposure to metabolic by-products and substances/substrates supplied by the mesenteric or cardiac circulation could modulate the production level and effects of NO in hepatocytes, depending on their localization in the liver (118) (141). It is hypothesized that the expression levels of the NOS isoforms and the effects of nitric oxide depend on the compartmentalization of the enzymes within a cell and also depend on the localization of the cells within an organ. In addition, the effect of NO derived from nNOS in periportal hepatocytes, could be different depending on the clinical condition stage. For instance, the level of nNOS increases primarily around perivenous hepatocytes in the late stages of experimental endotoxic shock, whereas, in Type 1 diabetes, nNOS is translocated to the nucleus in all types of hepatocytes regardless of their location within the organ.

In skeletal muscle: NO plays an important role in the skeletal muscle contraction (142) (143). All three NOS isoforms have been detected in rat skeletal muscles (144) (126). iNOS and eNOS are predominantly located in the sarcoplasm, whereas nNOS is present in sarcolemma only (144). It has been observed that mislocation of nNOS strongly contributes to muscular ischemia (145). Moreover, it was established a relationship between myopathies and the absence or decrease of nNOS level (146). This suggests that nNOS might be specifically involved in increasing blood flow at the muscle level, but not necessarily in the muscle contraction.

In central nervous system: The three NOS isoforms are all present in the RVLM (rostral ventrolateral medulla) which is a region containing glutamatergic neurons that participate in the increased sympathetic tone occurring after cardiac stimulation (147). Only nNOS is present in neurons (148), suggesting that nNOS participates in the central sympathetic response.

Subcellular localization of NOS: Since NO may be either stabilized or degraded through its interactions with various intracellular or extracellular chemical moieties, the initial localization of NOS within the cell is expected to influence the chemical fate and the subsequent biological function of NO. Almost every conceivable intracellular organelle has been postulated as a possible site for NO synthesis, from the plasma membrane to the cell nucleus, thereby raising the question: can NOS really be found everywhere? Perhaps the answer to this question is yes, but the supporting evidence varies in both quantity and quality (38).

The expression of each NOS isoform is cell-specific and within each cell, it appears that each isoform is located in a particular subcellular compartment. In a previous study performed in nNOS and eNOS knock-out mice, both groups of mice developed age-related cardiac hypertrophy, but only the nNOS knocked-out mice were found to be hypertensive (149). eNOS as the β -adrenergic receptor is located in cardiomyocyte caveolae, whereas nNOS is close to the sarcoplasmic reticulum (149). Thus, the different clinical outcomes of the two groups of mice were linked to the nNOS and eNOS compartmentalization as well as the protein-protein interaction network within cardiomyocytes .

Furthermore, nNOS and eNOS are also known to have opposing effects on the intracellular Ca^{2+} concentration and therefore participate together in controlling the contractility. eNOS inhibits the calcium influx produced by β -adrenergic agonists (mediated by L-type Ca^{2+} channels), while nNOS facilitates the calcium outflow from the sarcoplasmic reticulum. These opposite effects appear to be related to their various subcellular locations, which in turn determine the nature of the protein–protein network of each NOS isoform, e.g. eNOS with caveolin-3 and nNOS with ryanodine receptors (149). In the case of endothelial cells, confocal imaging of phosphorylated-eNOS and total eNOS pools has shown their co-localization with the Golgi region and plasmalemma in both transfected cells and native endothelial cells characterized by endogenous levels of expression (150).

Translocation of NOS among cellular compartments

It has been proposed that the translocation of NOS isoforms in response to various stimuli can affect cells in various ways, including modulations in the regulation of gene transcription, activation/inhibition of signal transduction pathways, and modulation of enzymatic activity via protein–protein interactions (151) (152). For example, the NOS-interacting protein (NOSIP) negatively regulates NO production by inducing nNOS and eNOS translocations to the cytoskeleton (actin), leading to inhibition of the activity of these enzymes (153) (154) (155).

Post-translational modifications of the NOS isoforms can affect their subcellular compartmentalizations. From this point of view, eNOS was the most well-studied isoform. As indicated above, the NOS isoforms are localized in various subcellular compartments. However, after a given stimulus, some of them have been known to change their locations, suggesting the occurrence of posttranslational modifications, such as phosphorylation, or the activation of translocation, a more complex process that occurs with the aid of specific protein–protein interactions. The mechanism by which localization influences eNOS activation is not completely understood. Until now, the representative model which describes the eNOS translocation corresponds to the active-inactive cycle which occurs concomitantly to the translocation between caveolin and Golgi complex (**Fig.5**). The activation and de-activation of eNOS is likely related to its phosphorylation /dephosphorylation and palmitoylation / depalmitoylation state. In un-activated endothelial cells, the association between eNOS and caveolin suppresses eNOS activity. After agonist activation (phosphorylation / dephosphorylation, palmitoylation / depalmitoylation), the increase in $[Ca^{2+}]$ promotes the calmodulin binding to eNOS and the dissociation of caveolin from eNOS. Then eNOS is transported to the Golgi complex. The activated eNOS–CaM complex synthesizes NO until $[Ca^{2+}]$ decreases, accounting for calmodulin dissociation. This dissociation is accompanied by a reformation of the inhibitory eNOS–caveolin complex, followed by transportation from Golgi to caveolin.

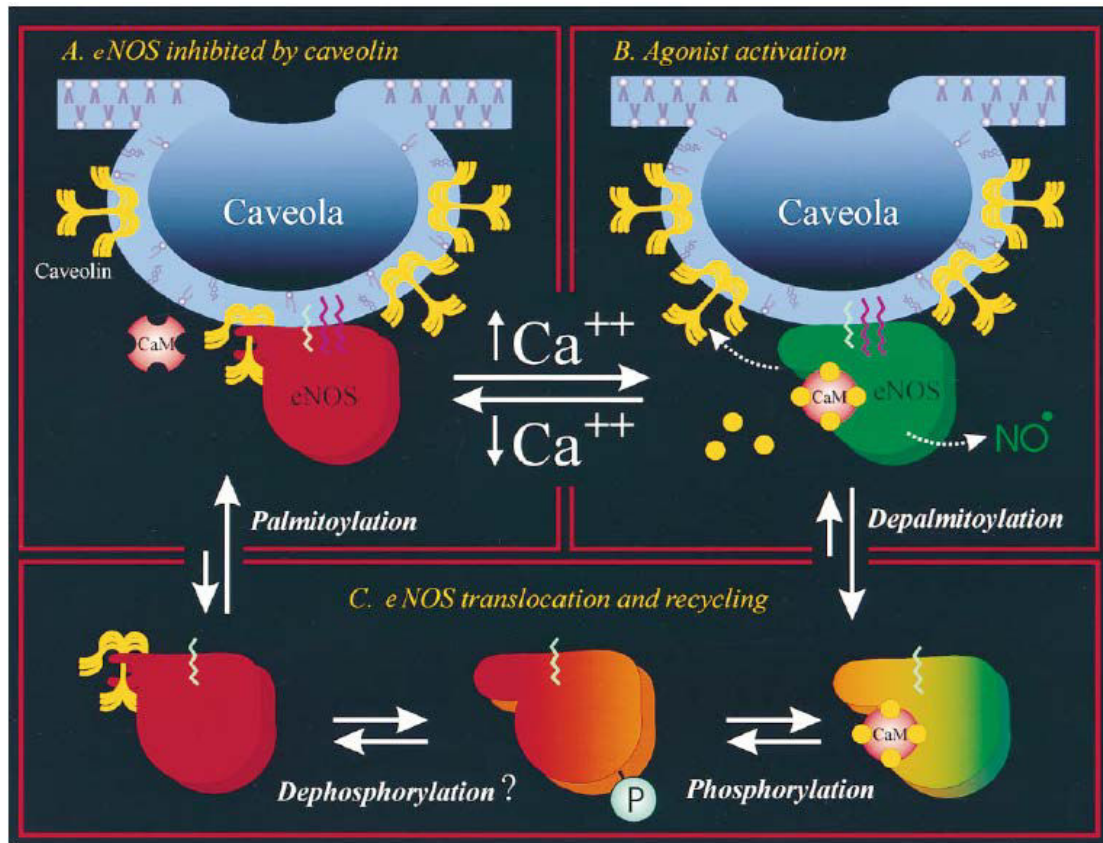


Fig. 5 The cycle of eNOS activation and deactivation.

(A) eNOS inhibited by caveolin. The interaction between eNOS and caveolin markedly attenuates enzyme activity in the resting endothelial cell. Panel A shows a plasmalemmal caveolae characterized by its distinctive lipid content and by the presence of homo-oligomers of the membrane-associated scaffolding protein caveolin. The interaction of eNOS with the scaffolding domain of caveolin maintains the enzyme in its inactivated state (red). eNOS is shown as being dually acylated by N-myristoylation (sky blue) and by two molecules of palmitate (purple). The calcium regulatory protein calmodulin (CaM), which is enriched in the caveolar fraction of plasma membranes, does not bind to eNOS in the absence of Ca^{2+} .

(B) Agonist activation. With agonist stimulation or other stimuli leading to an increase in the local $[Ca^{2+}]$ concentration, Ca^{2+} -bound CaM competitively displaces caveolin from eNOS, thereby allowing the required conformational changes within eNOS for the electron transfer and the subsequent NO synthesis by the activated enzyme (green).

(C) eNOS translocation and recycling. The decrease in $[Ca^{2+}]$ leads to the dissociation of calmodulin from eNOS and then the deactivation of the enzyme as caveolin rebinds to eNOS. In the model proposed here, the prolonged agonist activation leads to eNOS depalmitoylation, translocation, phosphorylation, and, subsequently, to the rebinding of caveolin as the enzyme becomes dephosphorylated and repalmitoylated at the caveolae level. To note, eNOS remains myristoylated throughout the translocation cycle, this modification probably guides the retargeting of the caveolin–eNOS complex to caveolae.

Figure illustration by Naba Bora, Medical College of Georgia, from Ref. (38)

It has also been observed that, under pathophysiological conditions the three NOS isoforms could be found in cell nuclei, suggesting that the nuclear NO production is also possible (156) (157) (158).

Differential effects of NO derived from NOS isoforms

NO in the lung is involved in many processes originating in various cell types: vasodilation at the endothelium, broncho-dilation at the inhibitory non-adrenergic/non-cholinergic nerve terminals, participation of macrophages in phagocytosis, and production of mucin by the bronchial epithelial cells (131) (134) (159). These diverse functions have to be coordinated and controlled to support adequate blood flow and air flow under normal conditions as well as when allergens or immunogens trigger an inflammatory response (134).

NO and derived reactive species (known as reactive nitrogen species) play an important role in diverse inflammatory pulmonary diseases (160). Elevated levels of NO have been found in the exhaled air of asthma patients (135) (161), consistent with the increased iNOS gene expression (135) (162). During endotoxic shock, NO could be one of the major molecular mediators involved in the changes in pulmonary blood distribution (163). On one hand, pulmonary blood flow increases at early stages, raising the volume of oxygenated blood in vital organs. On the other hand, during the late stages of shock, massive pulmonary vasodilation is elicited in response to the dramatic increase in the NO level produced by iNOS.

In liver, the changes of hepatic blood circulation due to the endotoxic shock displays an opposite behavior to those observed in lung (163). It has been assumed that in the early stages of shock in liver, the portal vein circulation is restricted to supply blood flow to organs out of liver, whereas the observed vasoplegia in the late stages (164) is mainly due to NO production originating from the increased nNOS activity (127).

NO plays an important role in skeletal muscle contraction (143) (144). In central nervous system, NO synthesized by nNOS plays a key role in increasing central sympathetic outflow. The increased iNOS-mediated production of NO, which is induced by oxidative stress, significantly increases the central sympathetic tone. Interestingly, it was observed that the over-expressed NO derived from eNOS has an opposite effect (165). These different outcomes could be explained by the differential localization of NOS isoforms and the subsequent "local" effects of NO on downstream targets; thus the overall fluctuations in the production of NO do not explain localized effects.

At the subcellular level, NO regulates mitochondrial respiration, depending on the ratio of oxygen-to-NO (166), through both competitive and noncompetitive mechanisms (167). As

mentioned above, it has been observed that under pathophysiological conditions the three NOS isoforms could be found in cell nuclei.

Regulation of NOS activity

CaM

CaM was the first protein shown to interact with NOS (37) and is necessary for the enzymatic activity of all three isoforms. As previously mentioned, the Ca^{2+} -dependency of NOS distinguishes the NOS isoforms between the nNOS/eNOS group and iNOS. CaM binding increases the rate of electron transfer from NADPH to the flavin in the reductase domain (70) (168); it also triggers electron transfer from the reductase domain to the heme in the oxygenase domain (75). nNOS and eNOS differ in their primary structure from iNOS with a AI loop in the middle of the FMN-binding subdomain. Deletion of AI loop led to several interpretations: in the case of eNOS, it was shown that the required $[\text{Ca}^{2+}]$ to activate the enzyme decreased significantly, leading to a loss of regulation by Ca^{2+} /CaM, a situation which is similar to iNOS (79). In the case of nNOS, the deletion of AI loop appears to lead to a Ca^{2+} /CaM-independent heme reduction (65).

Regulation by gene transcription

Under some pathophysiological conditions, the NOS isoforms could be found in cell nuclei, suggesting that the regulation of NO production could occur at the level of gene transcription (169). In one study it was found that during the first 6 days in the cultured cells, nNOS was localized in the cytosol; however, at the 7th day, nNOS was mainly present in the nuclei. This phenomenon is concomitant with both the observed production of NO in nucleus and the decrease of iNOS protein expression (170). These results suggest that the presence of nNOS in nuclei represses the transcription of the iNOS gene (157). Another example shows the regulation of iNOS by translocation of eNOS in nuclei: when stimulating the rat hepatocytes with a G-protein-coupled receptor agonist which activates eNOS, eNOS was then translocated from the cytoplasm to the nucleus (171). Afterwards, the eNOS-dependent NO production modulated the iNOS gene transcription.

Activation/inhibition of signal transduction pathways

Until now, the most extensive study of NOS regulation was done on eNOS. eNOS is primarily found in the Golgi complex and plasmalemmal caveolae of endothelial cells (172) (173). The activity of eNOS is highly related to its localization. When eNOS form a complex with caveolin which is located in caveolae, the enzyme activity is inhibited, whereas it is more active in the Golgi complex. To note, its activity in the *cis*-Golgi is higher than in the *trans*-Golgi complex, mitochondria, or nucleus (174). This could result from a facilitated access to calcium stores in the *cis*-Golgi complex under normal conditions.

It has been shown that serum starvation increases the perinucleus location of the eNOS/ caveolin complex in cultured endothelial cells isolated from bovine aorta (175). In cultured endothelial cells in the presence of insulin, eNOS is phosphorylated and the eNOS/ caveolin complex is translocated to the caveolae in response to the palmitoylation of caveolin, suggesting that insulin inhibits eNOS activity through a phosphorylation pathway (176). In high-fat-fed mice, insulin-induced eNOS phosphorylation in the aorta is decreased, suggesting that eNOS phosphorylation may have a role in the endothelial cell dysfunction that characterizes obesity and insulin resistance (177).

Fluid shear stress elicits phosphorylation of eNOS and an increase in calcium-independent NOS activity (178) (179). Several studies have shown that Ser¹¹⁷⁷ of eNOS is phosphorylated by the protein kinase Akt (180) (181), which results in an increase in electron flux through the reductase domain and an increase in NO production (182). In contrast, the phosphorylation of nNOS at Ser⁸⁴⁷ by CaM-dependent kinases leads to a decrease in NOS activity (183) (184).

The five known Serine / Threonine phosphorylation sites in eNOS and the effects of phosphorylation at these sites on eNOS activity are summarized in **Fig. 6** (from Ref. (185)). Activity of eNOS is increased by phosphorylation at both Ser¹¹⁷⁷ and Ser⁶³³ (181) (186) (187). In contrast, phosphorylation at Thr⁴⁹⁵ in the CaM binding domain is inhibitory (188) (189). The effects of phosphorylation at Ser¹¹⁴ and Ser⁶¹⁵ positions remain controversial (188).

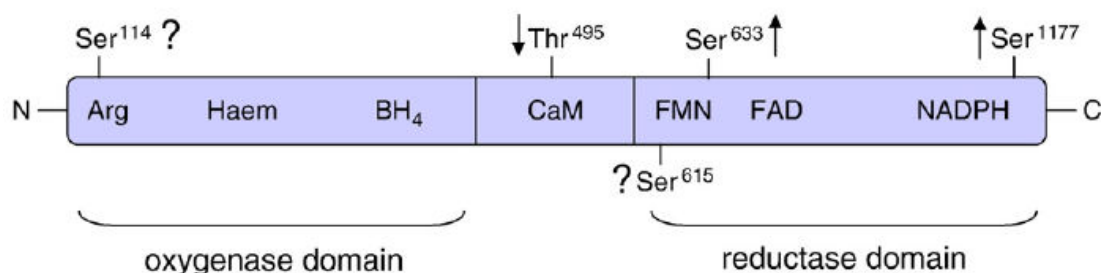


Fig. 6 Phosphorylation sites of eNOS.

The arrows indicate the effect of phosphorylation on the eNOS activity: Phosphorylation of Ser⁶³³ and Ser¹¹⁷⁷ increases eNOS activity, whereas phosphorylation of Thr⁴⁹⁵ is inhibitory. The effects of phosphorylation of Ser¹¹⁴ and Ser⁶¹⁵ remain controversial. Ser-serine, Thr-threonine, Arg-arginine.

Modulation of enzymatic activity through protein-protein interaction

The NOS interaction protein (NOSIP) is expressed in heart, brain, lung, as well as in endothelial cells (155). NOSIP is translocated from the nucleus to the cytoplasm in the G2 phase of the cell cycle (153) (154). By interacting with nNOS and eNOS, NOSIP negatively regulates NO production by inducing nNOS and eNOS translocation to the actin cytoskeleton and therefore inhibiting their enzymatic activity (154) (155).

Inhibitors of Nitric Oxide Synthase

To date, many NOS inhibitors have been described. They belong to distinct inhibitor groups depending on the binding site and the mechanism of action. Among all the inhibitors, the main target is in the oxygenase domain of NOS.

L-Arginine-based inhibitors: All the NOS isoforms can be inhibited (to a different extent) by N^ω-substituted L-Arginine analogues. Some analogues of L-Arg do exhibit some isoform selectivity, mostly towards the constitutive isoforms. The mechanisms of inhibition of NOS activity by these compounds vary, but they all involve occupation of the substrate binding site, thus they competitively prevent the NO production. The L-Arg-based inhibitors have been used widely in 1990's and have demonstrated beneficial effects in various forms of shock, inflammation and central nervous system disorders (1) (190) (191) (192) (193). However, in addition to their lack of marked isoform selectivity and due to non-specific effects, they also lead to numerous side-effects, such as increase in the chronic renal failure (194) (195) and in hypercholesterolemia.

Calmodulin inhibitors: The calmodulin-dependent NOS isoforms (eNOS and nNOS), as CaM-dependent enzymes, can be inhibited by calmodulin inhibitors, such as calmidazolium. iNOS, which contains calmodulin in a tightly bound form, is not sensitive to these agents (196).

BH₄ inhibitors: Mainly, there are two classes of BH₄ inhibitors. The first class corresponds to compounds which target the BH₄ binding site of NOS; the second class corresponds to compounds that reduce BH₄ synthesis (thereby decreasing the apparent production of BH₄). A range of compounds have been identified which appear to interact with the pterin site. However, the interactions of some of these pterin-site inhibitors with NOS reveal unexpected complexity (197) (198). The use of BH₄ synthesis inhibitors has several drawbacks because BH₄ is also a co-factor of many other enzymes, such as tyrosine hydroxylase and tryptophan hydroxylase, so inhibition of BH₄ production may lead to unwanted side-effects such as reduced biosynthesis of dopamine, epinephrine, norepinephrine, and serotonin (199) (200).

Heme-binding inhibitor: In monomeric murine-iNOS heme domain crystallized in the presence of imidazole, two imidazole molecules are bound to each monomer, one directly bound to the heme iron and the other one bound to the L-arginine-binding region (97). Various anti-fungal imidazole derivatives have been shown to inhibit NOS activity, not only by interacting with the heme in the active site of the oxygenase domain but also by acting in competition with CaM (201). To note, a class of substituted pyrimidine imidazoles has been identified which does not directly inhibit NOS activity at the catalytic level, but possibly inhibits dimerization of iNOS during its synthesis and assembly (63).

Flavin protein inhibitors: Flavin-adenine dinucleotide and flavin mononucleotide are both redox co-factors and, by analogy with their function in P450 reductases, are involved in the transfer of electrons from NADPH to the catalytic center. It has been suggested that the flavoprotein inhibitor, diphenyleneiodonium, exerts its inhibition of NOS activity by its irreversible effects at the FAD binding site level (202).

To note, of all the inhibitors listed above, the majority of them target the oxygenase domain of NOS, there is only one flavin inhibitor which targets the reductase domain. In contrast, the NS1 compound used in our study (described in the results section of this manuscript) was designed as a NADPH derivative, conjugated with a two-photon absorption chromophoric unit. NS1 represents the first inhibitor targeting the NADPH binding site of the reductase domain of NOS.

Experiment strategy

The concept of Nanoshutter (NS) was raised on the basis of the reverse molecule named as Nanotrigger (NT) which was studied in advance (203) (204). With respect to the time order regarding the developments of the two strategies, I will give the introduction of NT first.

Nanotrigger (NT)

Principle

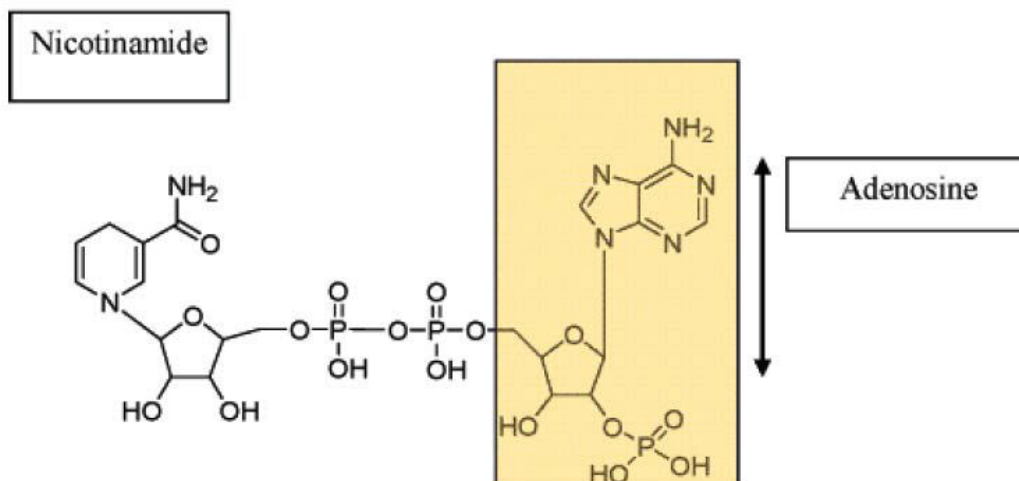
The aim of NT is to control NO-dependent vasodilation in tumor blood vasculature in a precise spatial and temporal manner (203). Due to the heterogeneity of tumor blood vessels, the efficiency of chemotherapy is often limited by poor drug delivery and penetration depth under hypoxia conditions. If there would be a drug which could increase NO production directly leading to vasodilation and if this action could be switched on and off by light in a synchronous manner, it would be conveniently applied as an adjuvant treatment in chemotherapy. Based on this concept, NT was designed to target NOS and activate NO catalysis upon two-photon excitation.

Molecular design

As previously mentioned, the electrons are donated by NADPH to the reductase domain of NOS and proceed via FAD and FMN redox carriers to the heme group in the oxygenase domain, where the proper NO formation occurs. On the basis of the NADPH structure, a molecular tool that would mimic NADPH (NADPH analogue) to ensure efficient binding to the enzyme, but meanwhile would trigger electron transfer to flavins only upon appropriate photon activation, would be of particular interest. Such a compound could be used to trigger the primary electron transfer to NOS *in situ* on demand, and the ultrafast laser pulse as the external command is particularly appealing for photon activation. Notably, one of the main characteristics of NT and also a crucial point is: the electron delivery from NT to flavin could only happen upon photon activation; without photon activation, the redox potential is not high enough to trigger electron delivery.

With this aim in mind, the strategy was to design a NT that allows efficient and selective biphotonic activation, in particular for future developments/applications at the tissue level. The detail of the design is shown in **Fig. 7** (205).

A: NADPH



B: Nanotrigger

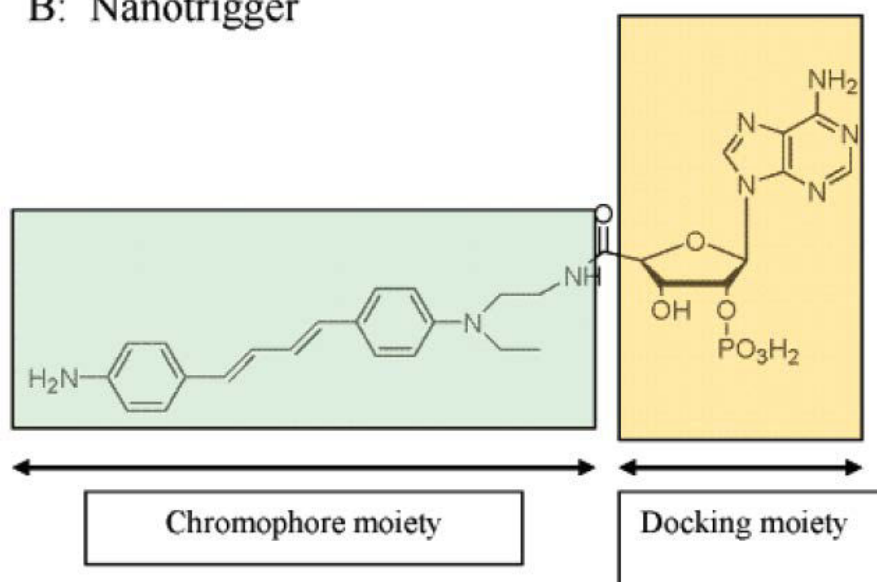


Fig. 7 Design of Nanotrigger

NT is based on the combination of (i) a molecular recognition unit that allows selective and efficient binding of NT to the NADPH binding site in NOS. Crystallographic data of NADPH-containing proteins showed that the main recognition motif of NADPH in its binding site are found in the nucleotide part, with the sugar, adenine rings, and the final phosphate linked by numerous H-bonding interactions with the proteins, in particular by means of highly conserved arginine residues. Additionally, arginine residues interact electrostatically with the 2' phosphate group of NADPH nucleotide moiety. The design conserved the overall shape and length of the nucleotide part of NADPH to confer a proper binding of NT to NADPH binding site. (ii) a chromophoric unit takes the place of the nicotinamide part, which

would become strongly reducing upon photon excitation and would transfer electron, thanks to the presence of an electron donor group (NH₂), to the flavins of NOS to initiate the catalysis. The NT design is based on a quadrupole system of the type Q_n as a generic chromophoric unit, which has a large reducing potential in the excited state than in the ground state (206). The number of n determines the total length of NT; when the n value increases, the maximum of absorption shifts to longer wavelengths and the two-photon absorption cross-section also increases in the red-NIR region (207). Moreover, an extended conformation of NT by means of conjugated double bonds and a peptidic linker between chromophore and nucleotidic moieties could “lock” the enzyme in an active conformation, favorable for the electron transfer. The extended conformation of the NT should also maximize the delocalization of the π electrons on the chromophore, with subsequent favorable properties of one- and two-photon absorption.

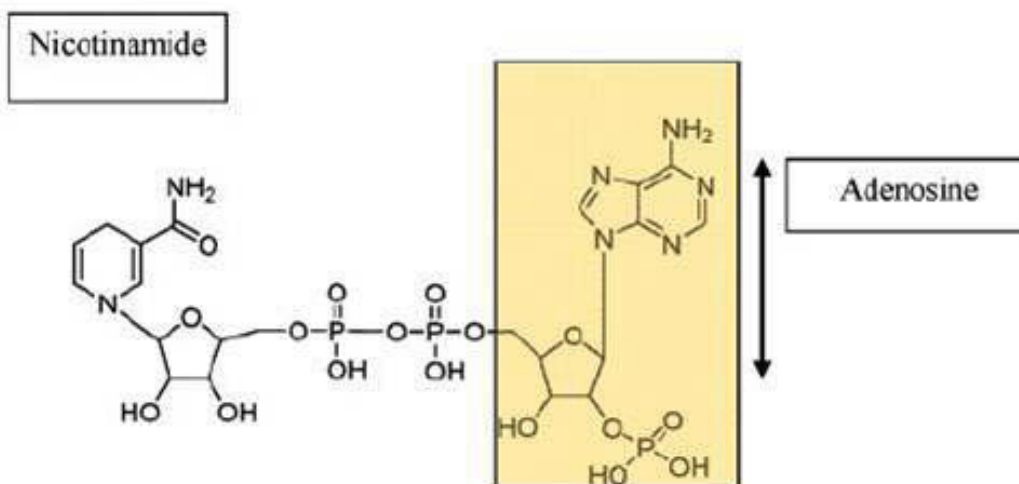
The validity of the Nanotrigger concept was realized with NT1 as the representative molecule. NT1 combines the docking moiety of NADPH and a derivative of quadrupole Q₂ as the chromophoric unit, where the terminal group NH₂ is meant to enhance the water solubility and reinforce the affinity for the NADPH binding site in NOS (205). In the study of NT1, experimental data showed a competitive binding of NT1 and NADPH in the NOS cofactor binding site, and electron injection was triggered upon two-photon activation within an extreme short period (20ps). The increase in the NO production upon light irradiation of NT1 was validated *in vitro* using EPR for detection of NO. The amount of NO formed by using NT1 was three times higher than that produced by the enzyme activated with NADPH (204). So far, in terms of NO activation, this synchronous modulation of NO meets the need for vasodilation, and practically should avoid undesirable angiogenesis. NT ($\sigma_2 = 160 \text{ GM at } 790 \text{ nm}$) has a 1800 times larger two-photon cross-section than NADPH and 110 times larger than FAD; such a two-photon absorption property would favor the deep penetration for *in situ* experiment. In summary, NT1 performed tunable NO modulation in a precise spatial and temporal manner, providing a promising perspective in adjuvant treatment in chemotherapy.

Nanoshutter (NS)

The terminal group NH_2 at the photoactive moiety in NT is an electron donor, which is able to deliver electron to FAD due to an increase in the redox potential of NT upon one- or two-photon excitation. If we replace this electron donor by a terminal electron acceptor group, it will be possible to transform a NOS activator into a NOS inhibitor that presents electron flow and then initiation of NO catalysis. The inhibitor family was then named Nanoshutter (NS). In contrast to the NT-induced vasodilation, the expected consequence of NS is the induced vasoconstriction in an alternative anti-angiogenic approach. Structurally, NT and NS share the same docking subunit which competitively binds to the recognition site of NADPH within the reductase domain of NOS. By contrast, regarding the chromophoric moiety, NS differs from NT in a sense that the electron donor group in NT was replaced by an electron acceptor group in NS (NO_2 in NS1).

Compared with NT, the prototype of NS meets the similar criteria as in the case of NT, NS should be capable of binding to NOS and its affinity should be at least equivalent to the natural NADPH cofactor. NS should display good two-photon absorption and fluorescence properties for imaging NOS at the cellular and tissue levels. The major difference between NS and NT lies in its chromophoric moiety, where an electron acceptor such as NO_2 group (instead of the electron donor NH_2 group in NT) should be able to prevent the electron flow when NS binds to NOS. Moreover, as the NO_2 group is also known as to be a fluorescence quencher in polar solvents, a significant fluorescence recovery of NS1 is expected upon its binding to NOS. NS1 should be characterized by distinct fluorescence properties between its free and bound states. Consequently, the binding of NS to NOS could be easily monitored by analyzing the enhancement of its emission fluorescence signal. Well of course the chromophoric moiety in NS should also display a large two-photon cross-section, not for electron injection as in the case of NT, but for multi-photon imaging of NOS. Based on these criteria, the structure of NS is given in **Fig. 8 B** and compared to the structure of NADPH (**Fig. 8 A**). The molecular synthesis was done by our collaborator Dr Jean-Luc Boucher, (University Paris V). The prototype of NS compound used through this study was named as NS1, possessing a NO_2 electron acceptor group.

A: NADPH



B: NS1

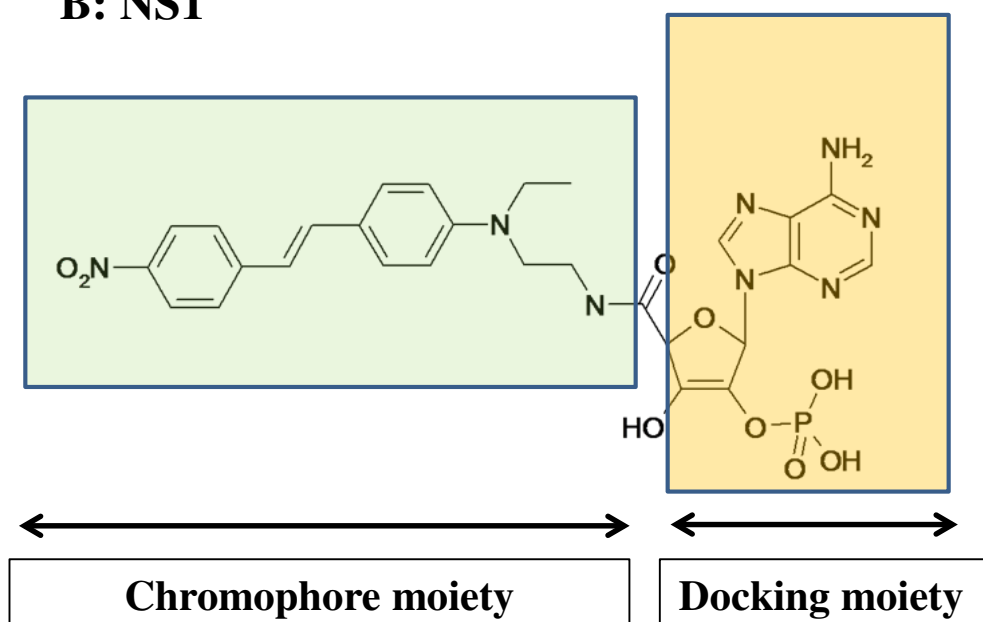


Fig. 8 Design of Nanoshutter.

Fluorescence Spectroscopy

Through this study, fluorescence was used as a crucial tool to reveal the interaction between NS1 and NOS proteins both *in vitro* and *ex vivo*. Due to the presence of the terminal NO₂ group of NS1, the NS1 compound displays a weak fluorescence emission in polar solvents. The fluorescence properties of NS1 should be very sensitive to the environment, in terms of emission spectrum as well as fluorescence quantum yield. Thus, NS1 was expected to display distinct fluorescence properties between free and bound states. This property was first used to assess *in vitro* the binding of NS1 to the three NOS isoforms. The selectivity of NS1 was also tested by using other proteins containing or not a NADPH binding site. Furthermore, taking into consideration that the fluorescence signal is a hallmark of the NOS-bound state of NS1, we also used the specific fluorescence emission of NS1 to image eNOS in the cellular context, especially in endothelial cells. Another advantage of NS1, is related to its photophysics, more particularly on its non-linear light absorption properties. Indeed, NS1 was designed to have a chromophoric moiety characterized by a large two-photon absorption cross-section. This property should allow to investigate the binding process of NS1 to NOS, by analyzing the proper fluorescence property of NS1, without any complication due to the overlap with the auto-fluorescence of NOS (due to the presence of flavin groups; absorption at 450nm). Indeed, flavins are characterized by very low two-photon absorption cross sections and their participation in the overall spectrum could be largely eliminated upon two-photon excitation, using an excitation wavelength in the NIR/IR region of spectrum.

In this context, I will give below a brief review of the principle of fluorescence and the general properties and parameters used in fluorescence studies (excitation and emission spectra; fluorescence quantum yield, fluorescence lifetime and the sensitivity of the fluorescence signal to the environment). The theory and the main applications in fluorescence imaging of the two-photon excitation process will be also briefly presented. The illustration of fluorescence microscopies will be mainly emphasized on confocal and two-photon microscopies which were largely used in this study.

Introduction to fluorescence

When the first fluorescence was observed by Sir John Frederick William Herschel in a quinine solution in 1845 (208), a new gate was opened in science. During the past hundreds years, there has been a remarkable growth in the use of fluorescence in various fields: primarily considered as research tools in biochemistry and biophysics, the application of fluorescence was more recently expended to cell biology. Nowadays, spectrofluorimetry and fluorescence imaging are widely used methodologies with many applications in

biotechnology, flow cytometry, medical diagnostics, DNA sequencing, forensics, genetic analysis and cell or intravital imaging. With its highly sensitive detection, there is no longer the need for the expense and difficulties of handling radioactive tracers for most biochemical measurements. There has been dramatic growth in the use of fluorescence for molecular and cellular imaging, which can reveal the localization and intracellular trafficking of molecules, sometimes at the level of single-molecule detection (209).

Fluorescence is a process that belongs to the ubiquitous luminescence family of processes in which molecules emit light from electronically excited states created by either a physical (for example, absorption of light), mechanical (friction), or chemical mechanism. The generation of luminescence through excitation of a molecule by ultraviolet or visible light photons is a phenomenon termed photoluminescence, which is formally divided into two categories, fluorescence and phosphorescence, depending on the electronic configuration of the excited state and the emission pathway (the relaxation of the excited state occurs in a singlet or triplet configuration, respectively). Photoluminescence may exist, originating from absorption of two or more infrared photons. This is the case for example of multiphoton fluorescence (see below).

The categories of molecules capable of undergoing electronic transitions that ultimately result in fluorescence emission are known as fluorescent probes, fluorochromes, or simply dyes. Fluorochromes that are conjugated to a larger macromolecule (such as a nucleic acid, lipid, or protein) through adsorption or covalent bonds are termed as fluorophores. In general, fluorophores are divided into two broad classes, termed intrinsic and extrinsic, respectively. Intrinsic fluorophores, such as aromatic amino acids in proteins, neurotransmitters, porphyrins, redox cofactors (FAD, FMN, NADPH) and the chromophoric triad in the green fluorescent protein, are naturally occurring fluorophores in biological molecules. Extrinsic fluorophores are synthetic dyes that are bound (non-covalently or covalently) to biological molecules and serve as fluorescent flags. In this study, the NS1 compound was designed and synthesized as a conjugated extrinsic fluorophore which serves to probe the NOS protein in the cellular context.

The processes that occur between the absorption and emission of light are usually illustrated by the **Jablonski diagram (Fig. 9)**.

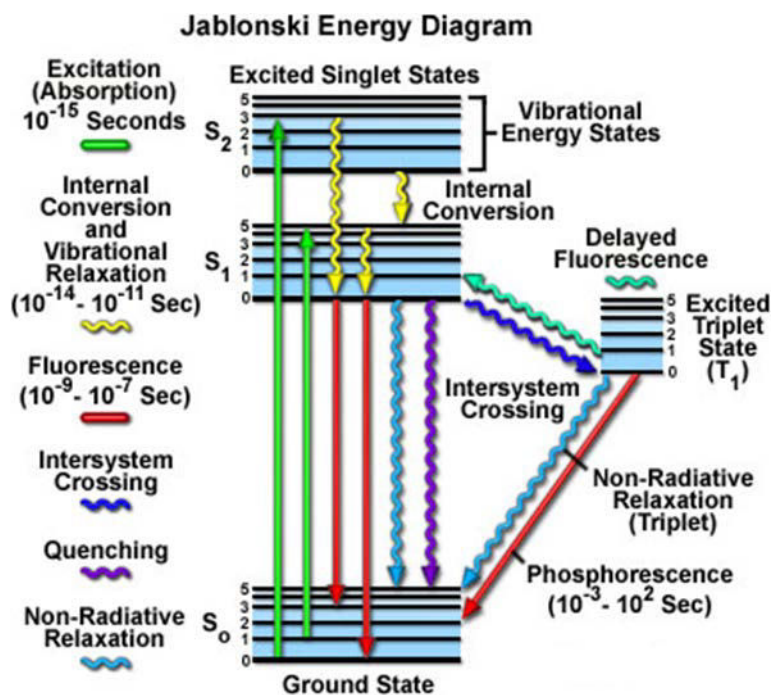


Fig. 9 Jablonski diagram.

The singlet ground (S_0) state, as well as the first (S_1) and second (S_2) excited singlet states as a stack of horizontal lines (—). In Fig.7, the thicker lines represent electronic energy levels while the thinner lines denote the various vibrational energy states (rotational energy states are ignored). Transitions between the states are illustrated as straight (\rightarrow) or wavy arrows ($\sim\rightarrow$), depending upon whether the transition is associated with absorption or emission of a photon (\rightarrow) or results from a molecular internal conversion or other non-radiative relaxation process ($\sim\rightarrow$).

Fluorescence: In excited singlet state, one electron in the excited state is paired (opposite spin) to a 2nd electron in the ground state orbital. Consequently, the return to the ground state is spin-allowed and occurs rapidly by emission of a photon. The emission rates are typically 10^8 s^{-1} , so that the typical fluorescence lifetime is near 10 ns.

Phosphorescence: This process corresponds to the emission of light occurring from a triplet excited state in which the electron in the excited orbital has the same spin orientation as the ground state electron. The transition to the ground state is then forbidden and the corresponding emissions rates are slow ($10^3 - 10^0 \text{ s}^{-1}$). So the phosphorescence lifetimes are typically milliseconds-to-seconds.

Stokes' shift: the energy of emitted photons is typically lower than the energy of photons responsible for the excitation (the excited-state molecule loses energy to its surroundings and the electron energy after light absorption ($E_{S_1,n}$ where $n > 0$) relaxes back to the lowest vibrational state of the lowest excited energy state ($E_{S_1,0}$). As $E_{S_1,n} > E_{S_1,0}$, where $E = hc/\lambda$ (E is the energy, c is the velocity of light, λ is the wavelength and h is the Planck's constant), consequently, the photons are emitted at a longer wavelength compared to the

absorption/excitation wavelength: $\lambda_{em} > \lambda_{ex}$, where λ_{em} and λ_{ex} correspond to emission and excitation wavelengths, respectively.

Photo-bleaching: Most fluorophores can repeat the excitation-and-emission cycle many hundreds to thousands of times before the highly reactive excited state of the fluorophore is subjected to a process termed photo-bleaching where the fluorophore is trapped in a dark state. The exact mechanism is not well-known, probably not unique but it is assumed to be linked to a transition from the excited singlet state to the excited triplet state. The excited triplet state is relatively long-lived and is chemically more reactive. Each fluorophore has different photo-bleaching characteristics.

General parameters

The molar extinction coefficient (ϵ) is an intrinsic property to describe the probability of a chemical compound to absorb light at a given wavelength. According to the Beer-Lambert Law: $A = \epsilon lc$ (210), where A is the absorbance, c is the concentration of the sample and l is the path length that light travels through the sample. The unit of ϵ is $M^{-1}cm^{-1}$.

The fluorescence lifetime (τ) is the average time spent by the fluorophore in the excited state before emitting light. As an important character, the fluorescence lifetime defines a temporal window in which information about fluorophore environment is available, i.e. static and dynamic. In the latter case, fluorescence emission will be sensitive to any change in the fluorophore environment (originating for instance from molecular diffusion) occurring during the emission lifetime. The measurement of lifetime can be derived from the decay analysis of fluorescence intensity upon simultaneous excitation of an ensemble of molecules:

$$I(t) = I_0 e^{-t/\tau}$$

Where I_0 is the initial fluorescence intensity immediately after the excitation pulse, τ is defined as the time in which the initial fluorescence intensity decays to I_0/e .

Another way to define the lifetime corresponds to the relationship with the kinetic constants of all de-excitation processes:

$$\tau = 1 / (k_{rad} + k_{non-rad})$$

Where k_{rad} is the rate constant of the radiative de-excitation pathway, $k_{non-rad}$ is the sum of all rate constants related to all non-radiative de-excitation pathways (heat release, collisional quenching, inter-molecular energy transfer).

The fluorescence quantum yield (Q) is the ratio between the number of photons emitted and the number of photons absorbed. The fraction of fluorophores that decays through radiative emission is related to the fluorescence quantum yield by:

$$Q = k_{\text{rad}} / (k_{\text{rad}} + k_{\text{non-rad}})$$

When the non-radiative pathways are minor (i.e. $k_{\text{non-rad}}$ is negligible), thus the quantum yield is close to 1. In this case, we define the natural or intrinsic lifetime: $\tau_N = 1 / k_{\text{rad}}$.

Influence of the local environment

Solvent effect: in the more polar solvents, due to the larger dipole moments of surrounding solvent molecules, the energy transfer from the fluorescent molecule to the surrounding solvent molecules increases. Typically, the fluorophore has a larger dipole moment in the excited state (μ_E) than in the ground state (μ_G). Following excitation, the solvent dipoles can reorient or relax around μ_E , which lowers the energy of the excited state, hence leads to emission spectral shifts toward the red side of the spectrum, according to the Lippert Equation. The fluorescence lifetime of fluorophores tends to be shorter in polar solvents as well.

The overall solvent effects are complicated. In general, only fluorophores which are polar themselves will display a large sensitivity to solvent polarity. Non-polar molecules are much less sensitive to solvent polarity. In addition to general solvent effects mentioned above, some specific solvent effects also influence the spectral shift or/and the quantum yield, such as the hydrogen bonding.

Two-photon excitation

Principle

In the Jablonski Diagram shown above, fluorescence corresponds to the absorption of light at one wavelength followed by emission of light at a longer wavelength. An incoming photon gives its energy to an electron, knocking it into an excited state, a higher energy level that the electron can occupy only transiently. Soon, in nanoseconds, the electron loses this energy and drops back to its ground state. The energy can be emitted as another photon. Because of the relaxation of the vibrational states prior to emission, the emitted photon has less energy than the one used for excitation of the molecule, and the lower energy corresponds to a longer wavelength. Two-photon excitation absorption, paradoxically, excites fluorescence with photons of longer wavelength than the emitted light. However, this process does not violate any of the laws of physics, because it raises the electron to its excited state with two photons of half the required energy, arriving almost simultaneously in space and in time on the fluorochrome (**Fig. 10**). The electron reaches the same final excited

state as in one-photon excitation, using an intermediary virtual state (horizontal dashed line in the right panel of **Fig. 10**). The subsequent fluorescence emission and all fluorescence properties (e.g. emission wavelength and fluorescence lifetime) are identical to those observed upon one-photon excitation. As a consequence, in the two-photon excitation, the dye which normally requires UV or VIS in the one-photon excitation process can be excited with NIR or IR light. However, the two-photon excitation pathway is not always identical to the one-photon process, because of the interaction of two photons with the fluorophores; the selection rules for light absorption are, in principle, different from those for one-photon absorption (211).

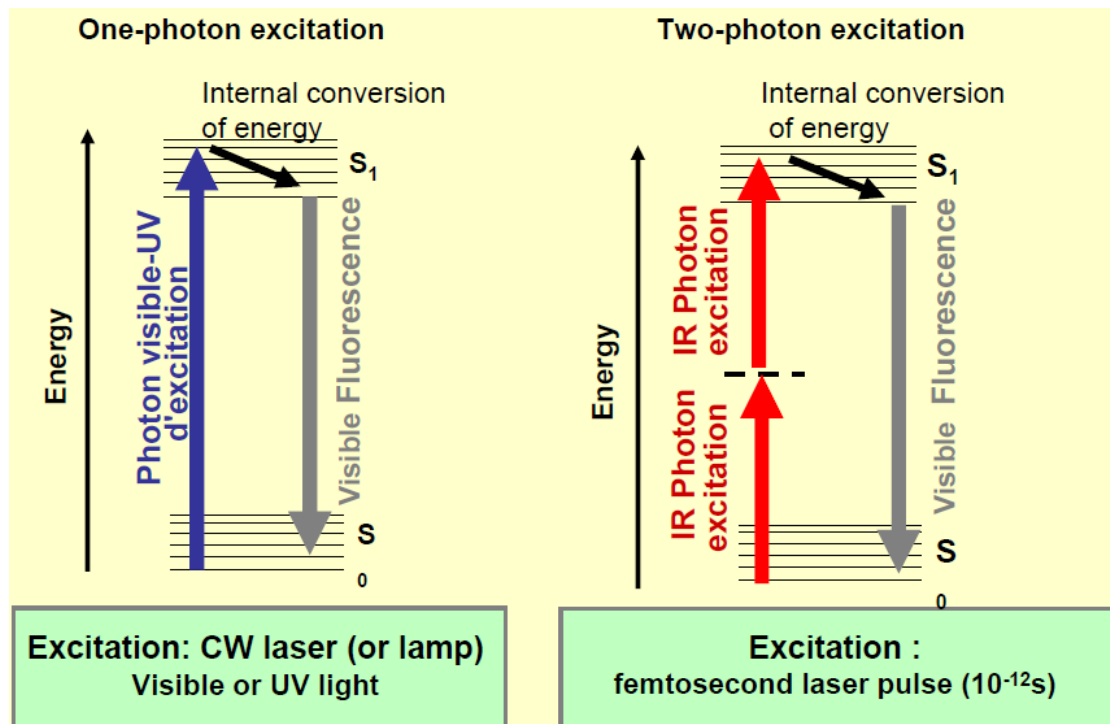


Fig. 10 One- and two-photon excitation diagrams.

Theory

In order to excite a single molecule by two photons simultaneously, it obviously requires a very large photon flux impinging on the specimen. Excitation therefore is likely to occur only at the focus of the illumination light. Above and below this point, the photons are not sufficiently concentrated, and two-photon absorption does not occur. Indeed, the probability of two photons arriving at a point at the same moment depends on the probability of one photon being in the area multiplied by the probability of another photon being in the same area. This possibility depends on the square of the flux density of photons. Hence the consequence of this dependency is that if the light is focused on a small diffraction-limited spot, the probability that two-photon excitation occurs will depend on the square of the intensity distribution at the focus. Since the probability of the two-photon

absorption processes is very low, it requires short and intense pulse which can be obtained using pulsed laser source with high powers (212).

Parameter of two-photon absorption

The absorption cross section is a term commonly used to describe the amount of light being absorbed by a particular fluorophore when exposed to light excitation. As previously mentioned, the unit of the molar absorption coefficient (ϵ) for one-photon absorption is $M^{-1}cm^{-1}$; in the case of the single photon absorption the letter σ is used to denote the molecular cross-section (unit is cm^2). In the one-photon absorption process, the cross-section is comparable to the size of fluorophores (213).

In contrast, the two-photon absorption cross-section is commonly measured in Göppert-Mayer (GM) unit, where $1 GM = 10^{-50} (cm^4 \cdot s)/\text{photon}$. Maria Göppert-Mayer was a physicist, who developed the theory for two-photon absorption processes (214). The physical origin of the two-photon cross-sections can be understood as follow:

For one-photon absorption the number of photons absorbed per second (NA_1) is given by

$$NA_1 (\text{photon/s}) = \sigma_1 (cm^2) I (\text{photon}/cm^2 \cdot s)$$

Where I is the flux of photons and σ_1 is one-photon absorption cross-section. The cross-section (in cm^2) is multiplied by the number of photons passing near the molecule per second to yield the number of photon absorbed per second. To obtain NA_1 in photons per second, the cross-section must be in units of cm^2 .

For two-photon absorption, the number of photons absorbed per second via a two-photon process (NA_2) is given by

$$NA_2 (\text{photon/s}) = \sigma_2 I^2 (\text{photon}/cm^2 \cdot s)^2$$

In order for the units to match on both sides of the equation, the units of σ_2 must be $cm^4 \cdot s/\text{photon}$ (213).

Table 2 shows some examples of two-photon cross-section values characterizing commonly used biological fluorophores and intrinsic chromophores excited in the NIR-IR region of the spectrum (215) (216).

Fluorophores	Two-photon absorption cross-section (GM)	Excitation Wavelength (nm)
wild-type GFP	6	~800
enhanced GFP	7	~960
NADPH	$5 \times 10^{-2} / 5 \times 10^{-6}$	~700/900
FAD/FMN	0.1/0.8	~700/900
Fluorescein (PH11)	38±9.7	~782

Table. 2 Two-photon excitation properties of selected fluorophores and chromophores.

Fluorescence microscopy

Fluorescence microscopies provide attractive advantages over conventional light microscopes. They can be employed as novel non-invasive biomedical tools in a great variety of domains such as three-dimensionally resolved fluorescence imaging to obtain important information about subcellular localization and co-localization of biomolecules, molecular tracking, study of molecular interactions (FRET, fluorescence resonance energy transfer), optical diagnostics and probing of chemical compounds (e.g. calcium).

Fluorescence microscopy is comparable to the conventional light microscopy with additional features to enhance its capabilities. On the basis of conventional wide-field epi-fluorescence microscopy, technically more advanced confocal microscopy alone or with the addition of pulsed IR laser source for two-photon fluorescence imaging has allowed to improve several aspects of fluorescence imaging such as spatial resolution (particularly in the Z direction), faster running speed and capability in deep penetration scanning as well as 3D reconstruction. Here, the emphasis is mainly stressed on the confocal and multi-photon microscopies, which were mainly applied in this study. **Fig. 11** shows the comparisons of wide-field microscopy, confocal microscopy and two-photon microscopy set-ups (217).

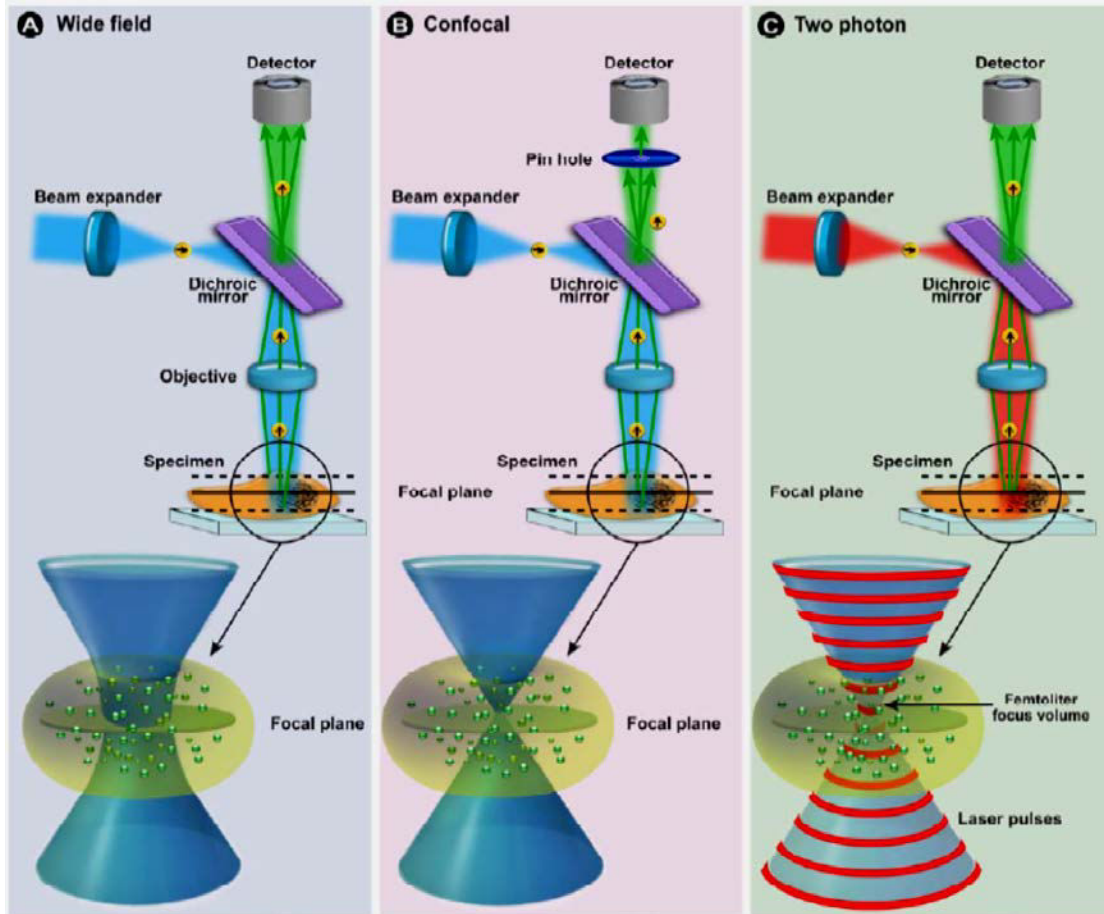


Fig. 11 Set-ups of conventional wide-field microscopy, confocal microscopy and two-photon microscopy.

Epi-fluorescence microscopy

Epi-fluorescence microscopy is typically equipped with a mercury-vapor lamp as light source and emission filters (**Fig. 12** shows the simplified scheme of epi-fluorescence microscopy). The light emitted by the lamp is first filtered by the excitation filter; the exciting radiation is reflected onto the sample by a dichroic mirror or beam splitter, then emission radiation goes through the mirror, and is further filtered by an emission filter before reaching the detector.

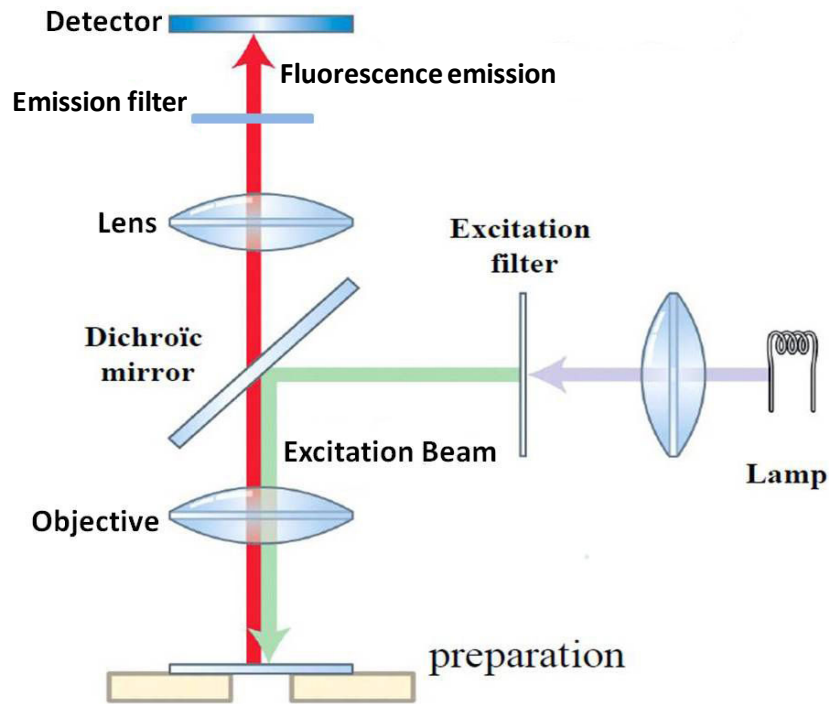


Fig. 12 Epi-fluorescence light path

As a wide-field optical microscope, the fluorescence emitted by the specimen often occurs through the entire excited volume which made it impossible to have spatial selectivity especially in the Z-axis. Besides, due to the light scattering around the observing area, the image may appear blurring. The thickness of a sample imaged by epi-fluorescence microscopy is limited within 2 μm .

Confocal microscopy

Principle

A confocal microscope is a scanning microscope which scans the sample with a focused beam and builds up an image point by point. The two major characteristic elements in confocal microscopy include (i) the pinhole, (ii) the laser source. The critical difference between the confocal and wide-field microscope is: there is a small pinhole placed in front of the detector in a confocal microscope, therefore it is able to effectively filter out the out-of-focus light from above and below the point of focus in the object. **Fig. 13** shows that only the light in-focus (solid lines) could pass through the small spot at the pinhole and then is able to reach the detector, whereas the light from out-of-focus (dashed lines) will be eliminated. Therefore the confocal image precisely contains in-focus information (218).

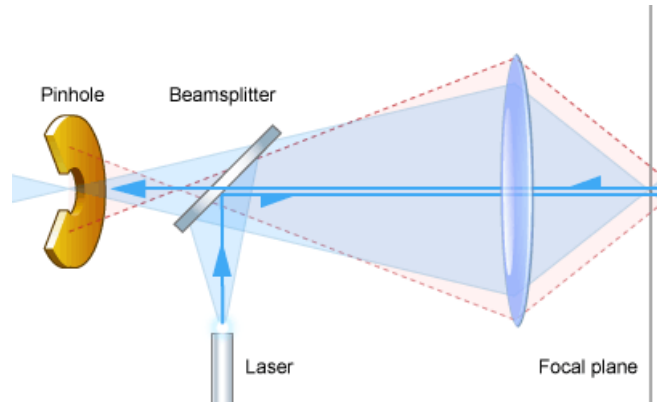


Fig. 13 The light paths of in-focus and out-of-focus in a confocal optical system.

Advantages

Confocal microscopes possess several advantages over conventional microscopes. First, the image contrast (signal-to-noise ratio) is increased due to the reduced out-of-focus light. Besides, confocal microscopy produces images of improved resolution. The resolution (d) of an optical microscope is defined as the shortest distance between two points on a specimen that can still be distinguished by the observer or camera system as separate entities. This parameter indicates the resolution capability in imaging. The smaller distance is, the better resolution of the microscopy is. As shown below (where NA is the numerical aperture), the lateral resolution (x - y plan) of confocal microscopy is improved up to 1.4 times greater than conventional wide-field microscopy. The axial resolution (Z -axis scanning) is improved as well, which facilitate the examination of thick specimens.

$$\text{In wide-field microscopy: } d_{xy} = 0.61 \lambda_{em} / NA, d_z = 2 \lambda_{em} / NA^2$$

$$\text{In confocal microscopy: } d_{xy} = 0.4 \lambda_{em} / NA, d_z = 1.4 \lambda_{em} / NA^2$$

Another key advantage of confocal microscopy is the optical sectioning capability. In the conventional microscopy, we are restricted to one plane, the plane of best focus. This restriction can be overcome by confocal microscopy. The image of a thick object specimen can be reconstructed by monitoring individual x - y planes in the z -direction, each slice produces a sharp image. Using specific software, a complete 3-dimensional representation of the sample can be reconstructed.

Figure 14 shows the comparison of the image of PtK2 cells (Male Rat Kangaroo Kidney Epithelial cells) under conventional wide-field microscopy and confocal microscopy.

Conventional fluorescence microscopy

Confocal fluorescence microscopy

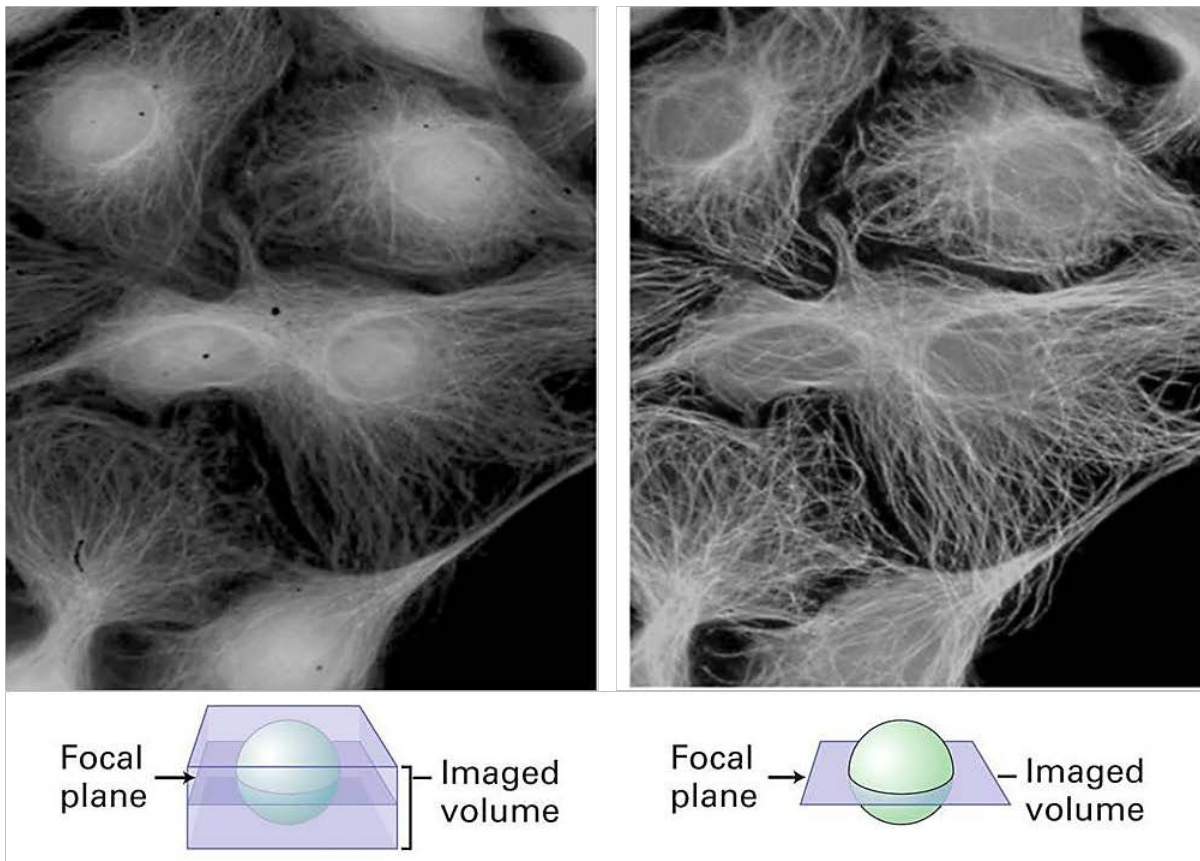


Fig. 14 Comparison of the images of PtK2 cells obtained by conventional and confocal microscopies.

Two-photon microscopy using NIR/IR laser sources

Principle

There are two major applications of NIR microscopy in life sciences. On one hand are the laser tweezers for optical micromanipulations, which are based on highly focused continuous wave NIR laser radiation with typical mean powers of 100-100mW. The other important application of NIR microscopy uses two-photon or three-photon excitation thus enables 3D fluorescence imaging or photo-induced uncaging of compounds.

As previously mentioned, the two-photon excitation of electronic states, based on the simultaneous absorption of photons, was first theoretically predicted in 1931. After 30 years, the first nonlinear multi-photon absorption was experimentally observed by Kaiser and Garrett with a ruby laser pulses in the ultraviolet absorption band of europium-doped CaF_2 (219). However, it took another 30 years until the first two-photon fluorescence imaging of living specimens using a 100 fs NIR dye laser was published (220). Today, tunable mode-locked Ti: sapphire lasers operate at 70-80 MHz repetition rate with 80-120 fs pulses and are commonly used to perform two-photon fluorescence experiments.

A key feature of two-photon microscopy is the limitation of the fluorescence excitation within a small focal volume (typically of one femtoliter or less). The excitation probability is proportional to the square of the laser intensity. The nonlinear nature of two-photon excitation implies that absorption occurs most strongly near the focal plane, where the photon flux is the highest (216). **Fig. 15** shows the fluorescence emissions in a diluted fluorescein solution upon one- or two-photon excitations, respectively. The fluorescence emission occurred along the entire light path, using visible light for one-photon excitation. In contrast, the fluorescence emission by two-photon excitation (using a pulsed IR laser source) only occurred in a very small volume at the focal point, illustrating that only molecules near the focus of the laser beam are excited, a consequence of the highly non-linear effects of the multiphoton excitation process.

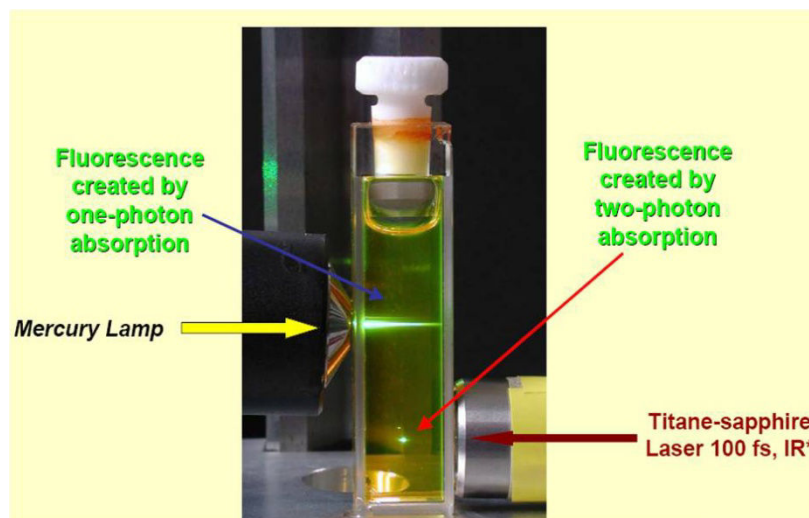


Fig. 15 A comparison of one- and two-photon excitation profiles.

A fluorescein solution is excited using one-photon excitation (Mercury lamp) via a numerical-aperture objective; the fluorescence emission is observed throughout the path of the light beam. For two-photon excitation (Ti:Sapphire laser) by using a second objective with the same numerical aperture, the fluorescence emission occurs only within a 3D localized spot (E. Guiot, PhD Thesis, Orsay, 2001). In the latter case, the fluorescein does not absorb IR light outside the focal spot.

The two-photon excitation process produces the same imaging properties as confocal microscopy, without any need of a pinhole in front of the detector. The optical sectioning in two-photon microscopy is analogous to that in confocal microscopy (211). However, in two-photon microscopy, the optical sectioning of the sample is achieved at excitation through the use of a mode-locked Ti:sapphire laser which operates in the near-infrared, whereas the optical sectioning occurs at emission in confocal microscopy due to the presence of the pinhole. Moreover, the position of a detector in a two-photon system is variable allowing the flexibility of the detection geometry, whereas this position is fixed in a confocal microscope (see **Fig. 16**).

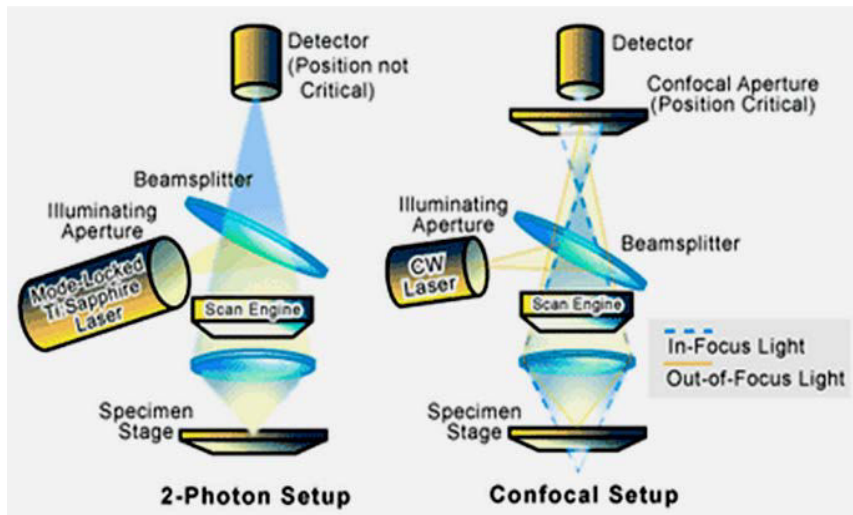


Fig. 16 Laser scanning confocal microscope setup versus two-photon confocal microscope setup.

Advantages

The first advantage of multiphoton microscopy is that there is no need of a pinhole as for confocal microscopy, so the two-photon microscopy can be depth-selective even with a wide-field detector.

Because two-photon absorption events can take place only at the focus of the illuminating light, the fluorescence as well as the potential photo-bleaching and photo-damage related to fluorescence excitation are also confined to the vicinity of the focal point (221), hence the signal-to-noise ratio is substantially improved. In the conventional confocal microscopy approach, we select the emission information from the focused spot by using the pinhole. However, the cone of light above and below this spot is still capable of exciting and bleaching the sample. The selection of observation area occurs at excitation and emission for multi-photon and confocal microscopies, respectively. These selection modes have consequences on the overall bleaching of the sample.

Most conventional light microscopes used in life sciences are based on the use of ultraviolet (UV) and visible (VIS) radiation for optical analysis and microsurgery (222) (223). The imaging methods include (i) 2D fluorescence microscopy using discrete excitation lines of high pressure mercury lamps and (ii) 3D confocal laser scanning fluorescence microscopy with excitation radiation of He-Ne lasers, argon/krypton ion lasers, He-Cd lasers and laser diodes. Most endogenous fluorophores in cells, such as tryptophan, NADPH and flavin, require UV or blue excitation wavelengths. Important exogenous fluorophores, such as the DNA markers Hoechst and DAPI as well as the calcium indicators possess absorption bands in

the UV only, whilst the other exogenous fluorophores are designed to match the laser and mercury lamp emission lines. However, the disadvantages of UV and short wavelength VIS radiation in conventional light microscopy lie in low light penetration depth and the potential of severe photo-damage to living cells (224).

Scattering of light in a turbid medium is directly related to wavelength. The imaging by UV-VIS excitation is often limited by the penetration depth and longer wavelengths penetrate much better into cells. In the case of two-photon excitation, the penetration of the excitation wavelength (NIR or IR) into tissue ($>200\mu\text{m}$) (225) is improved by at least a factor of two due to its longer wavelength accounting for an inherent decrease in the scattering parameter. Furthermore, the absorption of intrinsic fluorophores in the tissue or cells such as collagen, elastin, flavins, NADPH mainly occurs in the UV-VIS region and also limits light penetration. Usually, the red region (600-700 nm) is referred to as the optical window of cells and tissues owing to the lack of efficient endogenous absorbers in this spectral range and the subsequent high light penetration depth of the order of a few millimeters in most tissues. The optical window can be extended thanks to the two-photon absorption up to ~ 950 nm. The absorption by endogenous fluorophores can then be also overcome by using NIR/IR excitation wavelengths. Note that the IR light absorption by water is high above 950 nm (the absorption coefficient of water in the 400-700 nm range is much below than 0.1 cm^{-1} (226) but its absorption becomes strong above 950 nm and is not considered as negligible). The 700-950 nm spectral window is thus the optimal spectral region for performing two-photon fluorescence imaging.

Because the two-photon excitation wavelength is red-shifted to twice the maximum absorption wavelength under one-photon excitation, there is a good separation between two-photon excitation and emission spectral regions (221). This wide separation allows the emission intensity to be isolated easily from the high-intensity excitation. As a consequence, in some examples of one-photon absorption probes, the overlap between the excitation and emission spectra prevents the shorter emission wavelength region to be studied, whereas such a problem is avoided under two-photon excitation (227).

Long-wavelength light is less energetic and then much less damaging to living cells than UV-VIS light. It has been shown that single cells fluorescence microscopy with 365 nm radiation from a conventional 50 W high pressure mercury lamp results in failed cellular reproduction, modifications in intracellular redox state and DNA strand breaks, this photo-damage happened within seconds (228). Many experiments have demonstrated extended cell viability during multi-photon imaging compared with equivalent single-photon imaging experiments. For instance, using continuous-wave single-frequency and multi-frequency NIR lasers with 100 mW power at the entrance of the objective and a high numerical aperture objective, König has demonstrated the viability of cells under two-photon excitation (228) (229). Fluorescence occurred only in a sub-femtoliter focal

volume. Despite high light intensities in the optical trap, the temperature increase is less than 2 K, thus excluding thermal toxic effects under these power conditions (230). In contrast to conventional one-photon laser scanning microscopy, femtosecond laser microscopy can be performed with a peak intensity of about 200 GW cm^{-2} for hours without significant impact on the cellular reproduction and vitality. Squirrell et al (231) exposed hamster embryos to NIR femtosecond laser pulses of a multi-photon fluorescence microscope for 24 hrs, no impact on embryo development was found. In summary, from the bio-safety point of view, two-photon fluorescence imaging appears to be a safe novel optical sectioning technique within a particular intensity window.

Confocal microscopy with two-photon laser scanning

To counterbalance the benefits and limitations of confocal and two-photon microscopy, in this study, our imaging set-up was equipped with a confocal microscope with a combination of two-photon laser scanning. In addition of the continuous one-photon laser sources at visible region (He-Ne laser at 543 and 633nm, Ar laser at 458, 476, 488 and 514 nm), a femtosecond pulsed laser tunable in the NIR region (720-920 nm) was used for imaging endothelial cells (HUVEC) in the presence of NS1 with improved signal-to-noise ratio. Moreover, the two-photon excitation approach was also used for *in vitro* studies related to the binding of the NS1 compound to its NOS target. As NOS contains flavins, the two-photon approach was much more efficient compared to the conventional one-photon approach for monitoring the proper binding process of NS1 to the recombinant NOS, since the autofluorescence of flavins is strongly minimized under two-photon excitation only (not under one-photon excitation conditions).

Experimental design

The project of Nanoshutter corresponds to a collaborative project which is interdisciplinary in nature, at the cross-road of chemistry, molecular modelling, photophysics, fluorescence imaging, enzymology and physiology. The general approach for studying NS1 includes the contributions of skills in biology, physics and chemistry. First, the design of the NS1 compound and the prediction of its binding ability at the nNOS reductase domain level was theoretically supported by the molecular modelling (Anny Slama-Schwok, INRA, Jouy-en-Josas). Our chemist collaborator (J-L Boucher, University Paris V) realized the synthesis of NS1 compound and performed enzymologic study.

During my thesis, I present my work in the field of photophysics and cell biology, including the investigations of the spectroscopic properties of NS1 *in vitro* and at the imaging profiles at cellular level. The extended physiological studies of NS1 at the tissue level (vasoconstriction/vasorelaxation study in isolated mouse aorta rings, inhibition of endothelial tube formation) was mainly carried by Chantal Dessy (UCL, Belgium) who is specialized in cardiovascular research. Additional data related to the differential effects of NS1 on normal melanocytes and melanoma cells were provided by Stéphane Rocchi (University Sophia Antipolis, Nice). In this collaborative context, my work was mainly devoted to the characterization of NS1 in terms of photophysics and fluorescence properties, the use of these properties for the study of the NS1/NOS complexes in both contexts, *in vitro* and in the cellular context. In the latter case, the study of NS1 in terms of subcellular localization was performed using endothelial cells such as HUVEC cells. The consequence of NS1 on the ROS production in different cell lines was also analyzed by flow cytometer. Below, I explained the main methodologies I used during my thesis. The design of experiments follows the progress of this study and is listed as below:

Spectroscopic and fluorescence *in vitro* characterizations of NS1: absorption and emission spectra upon one- and two-photon excitations were characterized in both polar and non-polar solvents.

1. *In vitro* study of the formation of NS1-NOS complexes using one- and two-photon fluorescence experiments.
2. *In vitro* study of the binding selectivity of NS1 to NOS compared to other proteins.
3. Imaging of NS1 in living cells. Study of the kinetics of NS1 internalization.
4. Sub-cellular co-localization of NS1 with cell organelles using cell trackers.
5. Sub-cellular co-localization of NS1 with eNOS/Cav-1 using immunostaining.
6. Fluorescence detection of ROS generation in living cells.

METHODOLOGY

Spectroscopic and fluorescence properties of NS1

Materials and equipment:

NS1 (chemical formula: $C_{28}H_{31}N_8O_9P$, molecular weight 654.6 g/mol) was synthesized by the chemist collaborator Jean Luc Boucher (UMR CNRS 8601, Paris V). All the NOS were kindly provided by our collaborator Valdimir Berka and Ah-Lim Tsai (University of Texas Health Center): Recombinant full-length rat nNOS, murine iNOS and bovine eNOS were expressed in *E. coli* cell line BL21 (DE3) whereas eNOS reductase domain was expressed in yeast and purified as described (231) (232). Purified nNOS, eNOS, iNOS and eNOSred were more than 95 % pure as determined by SDS-PAGE stained with Coomassie Blue. Dimethyl sulfoxide (DMSO) A.C.S. Spectrophotometric grade was purchased from Sigma. Tris-buffer was prepared using Tris (hydroxymethyl) aminomethane, Molecular Biology Grade (Euromedex). Sodium chloride (NaCl) was from Merck (Germany).

UV-visible absorption spectrum of NS1 was carried out with an Uvikon XL spectrophotometer (Bioserv). NS1-binding isotherms were built using NOS in 50 mM Tris pH 7.5 containing 150 mM NaCl at 25 °C, either under one-photon (1-PE) or two-photon excitation (2-PE) conditions. For one-photon experiments, fluorescence excitation and emission spectra were recorded on a Eclipse (Varian) spectrofluorimeter, equipped with a thermostatic cell holder, using aerated 80 μ l solutions placed in micro cells (Hellma, Paris, France). The emission spectra were recorded with excitation and emission slits set at 5 nm. Two-photon excitation and emission spectra were recorded using a home-built set-up. Briefly, a 80-MHz mode-locked Mai-Tai[®] Ti:Sapphire tunable laser (690-1040 nm, 100 fs laser pulse; Spectra Physics, Mountain View, CA, USA) was focused onto the sample (80 μ l) placed in a quartz micro cell. The two-photon fluorescence was collected at 90 degrees and was further filtered by a Semrock FF01-842/SP filter to reject the residual excitation light. The fluorescence signal was focused into an optical fiber connected to a SpectraPro-275 digital spectrograph (300 lines/mm) coupled to a liquid nitrogen cooled CCD detector (1024 \times 256 pixels; Princeton Instruments Acton, MA, USA). The wavelength calibration of the spectrograph was done using a high pressure mercury lamp. Excitation power was set between 50 and 100 mW and the acquisition time varied between 1 and 60 s. The fluorescence quantum yield and the two-photon cross-section (σ_2) of NS1 in DMSO were determined using rhodamine B as a reference.

Fluorescence properties of NS1-NOS complex

NOS was dissolved in Tris-buffer 50 mM, [NaCl] = 150 mM, pH 7.5. The concentration of NOS was calculated by means of measuring absorption spectra, according to the Beer-Lambert law $C=A/\epsilon L$, where A value corresponds to the maximum absorbance and ϵ corresponds to the molar extinction coefficient. ϵ is 23,400 L·mol⁻¹·cm⁻¹ for the reductase domain of NOS at 456 nm, and 100,000 L·mol⁻¹·cm⁻¹ for the holoenzyme at 395 nm.

The formation of the NS1-NOS complex was carried out by titrations of NOS by NS1. In a series of quartz cuvettes, the final concentration of protein was fixed at 5 μ M, and the final concentration of NS1 added in each cuvette increased from 0 μ M (protein only) to 30 μ M. Tris-buffer (50mM, ph 7.5) was added to reach the same total volume of solution in all cuvettes. The NaCl concentration was 150 mM.

The mixtures of NS1 and Tris-buffer in the cuvettes were prepared at the same time, and then NOS was added before excitation. The one- and two-photon fluorescence emissions were measured using the settings mentioned above. Briefly, the emission intensities at 700 and 630 nm, for one and two photon experiments, respectively, were recorded upon excitation at 460 and 940 nm, respectively, and plotted as a function of NS1 concentration. In two photon experiments, the maximum emission wavelength of NS1/NOS complex, 630 nm, was used since no participation of the NOS autofluorescence was evidenced. In contrast, in the case of one photon experiments, the emission wavelength which served as a reference (i.e. 700 nm) was red shifted compared to 630 in order to minimize the participation of the autofluorescence. In each case, the Kd value corresponds to the NS1 concentration that leads to half of the maximal fluorescence signal (obtained at the plateau).

NS1-protein bound selectivity assay

Myoglobin was purchased from Sigma, M0630. Glucose 6-phosphate dehydrogenase (G6PDH) was purchased from Sigma, 1001153534. *E. Coli* RecQ helicase and Lens epithelium-derived growth factor (LEDGF) were purified by the previous PhD student Na LI during her thesis (234) (235). Fatty acid binding protein (FABP) was purified by the previous PhD student Jiayao Li during his thesis (236).

Method: the above-mentioned binding assay was performed by titration of NS1 to the three NOS isoforms (i.e. eNOS, nNOS and iNOS) and the proteins listed above. The protein concentration was typically in the 5-10 μ M range; increasing concentration of NS1 was added into the cuvette (2.5, 5, 10, 15, 30, 50 and 100 μ M) and the fluorescence emission upon one- or two-photon excitation was measured at each concentration point.

One- and two-photon images of living NS1-treated HUVECs were obtained using a SP2 confocal microscope (Leica MicroSystems, France), using a laser line at 488 nm or a 80-MHz mode-locked Mai-Tai® Ti:Sapphire laser (720-920 nm, 100 fs laser pulse; Spectra Physics, USA) tuned to 840 nm, respectively (the emission range was set between 520 and 680 nm).

Cell culture

Materials:

Human Pre-screened Umbilical Vein Endothelial Cells (HUVEC) and Endothelial Cell Basal Medium (EBM) were purchased from ECACC (Distributor: Sigma, Cat[#] for HUVECs is 06090721, Cat[#] for EBM is 210-485). A7R5 cells (the smooth muscle cell line from rat aorta) were purchased from ATCC® CRL-1444™. Hela cells were kindly provided by Dr. Frederic Subra in LBPA, ENS-Cachan. DMEM (1X) + GlutaMAX™-I Dulbecco's Modified Eagle Medium was purchased from Gibco, UK. 2% Gelatin was purchased from Sigma (Cat[#] G1393). Penicillin-Streptomycin was purchased from Gibco (Cat[#] 15140). 0.05% Trypsin-EDTA 1x was purchased from Gibco (Cat[#] 25300-054). Fetal Bovine Serum (FBS) Standard Quality was purchased from PAA (Cat[#] A15-101). Phosphate Buffered Saline (PBS 1x) was from Gibco (Cat[#] 18912-014). Dimethyl sulfoxide (DMSO) A.C.S. Plant cell culture grade was purchased from Sigma, France, (Lot[#] SHBB5172V). Fixation Buffer was purchased from BD Cytifix™. Microscope Cover Glasses, 18 mm ø, were purchased from Marienfeld, Germany. Willco-dish® was purchased from Willcowells, Netherlands (Ref. No. GWSB 3522). The culture medium was EBM with 1% Penicillin-Streptomycin for HUVECs, DMEM with 10% FBS and 1% Penicillin-Streptomycin for A7R5 and Hela cells, respectively.

Equipments:

The 37°C/CO₂ humidified incubator was purchased from SANYO (Type: MCO-5AC). The thermostatic water bath was purchased from Fried Electric. The bench-top refrigerated centrifuge was purchased from Jouan (Type: CR412). The laminar flow cabinet was purchased from Sterile-VBH. The inverted phase contrast microscope was purchased from NIKON TMS.

Methods:

The following operations concerning cell biology such as the gelatinization of the culturing surfaces, thawing of cells, passage of cells and freezing cells were carried out in the Class II laboratory of ENS-Cachan equipped with laminar flow. HUVECs were incubated with EBM medium, A7R5 and Hela cells were incubated with DMEM +10% FBS+1% PS. Confluent cells at the 4th-7th passage were collected for experiments.

The general preparations such as thawing, passaging and freezing cells for culturing HUVEC, Hela and A7R5 cells are in common; except for the attachment of HUVECs which requires the gelatin-coated surface, there is an extra step to gelatinize the flasks and/or plates before culturing, described below.

Gelatinization of the culturing surface (special treatment for HUVECs)

This preparation is a special procedure for HUVECs: in order to favor better cell adhesion on the surface, it is necessary to prepare gelatin-coated surface in flasks or plates.

Procedure: 2% gelatin was warmed in 37°C water bath until it changed from gel to fluid, then it was diluted with sterilized water giving a final concentration of 0.2%. The amount of gelatin used to cover the culture surface varies in different culture containers: e.g. for covering the 75 cm² culture flasks (T-75 flask), 7 ml of gelatin was needed; for 100x20 mm culture plates (P100 plate), 3-4 ml of gelatin was needed; and for 6-well culturing plates, 1ml of gelatin was added per well. For the preparation of the coverglasses, they were first disinfected with pure ethanol, rinsed with sterilized water and dried; then, 500 µl of gelatin was added homogeneously on the surface. The culturing containers were placed at room temperature in the Laminar Flow Cabinet for 20 min with their covers closed. Then, the rest of gelatin in the containers was removed, leaving the covers open until the thin layer of gelatin on the surfaces was dried. After gelatinization, the flasks and plates were labeled and sealed with parafilm.

Thawing of cells

Cells were kept either in liquid nitrogen for longer storage (1-3 years) or in -80°C refrigerator for shorter storage (3-6 months). When the vials of cells were taken out from hypothermia environment, the cap of the vial was turned a quarter to release any liquid nitrogen that may be trapped in the threads, and re-tighten before thawing in the water bath. The cells were quickly thawed in a 37°C water bath, by placing the lower half of the vial into the water. When there was only small amount of ice left in the vial, the exterior of vials was then decontaminated with 70% alcohol and the cap was removed. The cells were re-suspended with 4 ml of culture medium at 4°C and replaced in the 15 ml sterile conical tube. Cells were centrifuged at 4°C for 5min with 1000 rpm speed. After removing the supernatant carefully in the tube, the preheated culture medium at 37°C was added and gently aspirated, then the mixture of cells and culture medium was replaced into the culture container; for the T-75 flask and P100 plates, 12 ml and 8 ml of medium was added, respectively. Cells were placed in the incubator at 37°C with 5% CO₂ overnight, then the medium was changed to remove all traces of DMSO.

Passage of cells

When the cells reached to 90 to 100% of confluence rate, it was necessary to subculture the cells. The culture medium, 0.05% trypsin-EDTA and PBS were preheated in 37°C water bath for 15 min. The medium in the culture container was removed first. The cells were then rinsed with PBS to remove the trace of the serum; 2 ml of trypsin was added into the T-75 flasks or P100 plates. The culture containers were rocked gently to ensure that the solution covers all the cells, then placed in the incubator for 2-3 min. As soon as the adherent cells became round, they were ready to be detached from the surface. The rounded cells were released from the culture surface by hitting the sides with mild strength. 8ml of medium was then added to stop the digestion of trypsin. The mixture was gently aspirated, then transferred into a 15 ml sterile conical tube and centrifuged at 1000 rpm for 5 min at 4°C. The flask/plate was examined under the microscope. After centrifugation, the supernatant was aspirated from the tube without disturbing the cell pellet. The tip of the conical tube was flicked with finger to loosen the cell pellet. The passage ratio varied among different cell lines. Usually the HUVEC or A7R5 cells in one T-75 flask with 90-100% confluence can be distributed into two-to-three T-75 flasks containing 12 ml medium; one P100 plate with 90-100 % confluence can be distributed into three-to-four P100 plates containing 8 ml medium. In the case of HeLa cells, a T-75 flask with confluent cells can be distributed into ten-to-fifteen T-75 flasks. For HUVEC cell experiments, cells were seeded in gelatin-coated 6-well plates which contain coverglasses. Cell counts were around 1×10^5 /well, and the volume of medium was 1.5-2 ml.

Freezing cells

The medium for freezing cells was prepared with 90% FBS and 10% DMSO, then stored at 4°C. The procedure of treating the cells was the same as the subculture steps described above, until removing supernatant after centrifugation. Cells were counted under microscope to guarantee that each vial contained $1.5 \sim 2 \times 10^6$ cells in 1 ml freezing medium. It is crucial to decrease the temperature in the vials gradually and slowly. The steps of freezing vial were: (i) placing the vial at 4°C for one hour, (ii) moving the vial to -20°C for two to three hours, (iii) placing the vial at -80°C overnight and, finally, (iv) storing the vial in liquid nitrogen.

Fixation and mounting

Cells were cultured on coverglasses which were placed inside the wells of 6-well plates. When they reached confluence, the medium was removed, and cells were rinsed with PBS 1X for three times. 200 µl fixation buffer was then gently dropped onto the coverglass to form a homogeneous layer of liquid on the surface; the plate was placed at room temperature for 10-15 min, avoiding light. Finally, each coverglass in the well was rinsed with 2 ml of PBS 1X for twice.

One drop of mounting medium (10 µl) was added onto the surface of microscope slide (76x26mm), then the coverglasses was slowly attached onto the drop, avoiding air bubbles and making sure that the side cultured with cells was attached to the surface of microscope slide. After the mounting medium was dried, the circumferences of coverglasses were sealed with transparent nail polish. The slides were stored at 4°C, protected from light.

Immunostaining

Materials

Antibodies:

1st antibodies: Goat polyclonal to Caveolin-1 was purchased from Abcam® (Ref. No. ab36152). Rabbit polyclonal to EEA 1-Early endosome marker was purchased from Abcam® (Ref. No. ab2900). Purified Mouse monoclonal anti-eNOS/NOS type III was purchased from BD (Ref. No. 610297).

2nd antibodies: Alexa Fluro® 594 donkey anti-goat IgG (H+L), Alexa Fluro® 594 goat anti-rabbit IgG (H+L) and Alexa Fluro® 594 goat anti-mouse IgG (H+L) were purchased from Invitrogen.

Reagents: Saponin from Quillaja bark was purchased from Sigma, Germany. Mounting medium-SlowFade® Gold antifade reagent with DAPI was purchased from Invitrogen, USA. Bovine Serum Albumin (BSA) was purchased from Euromedex, France.

Protocol

The different steps for immunostaining are described below:

- 1) Cells were seeded on the coverglasses and cultured in the incubator at 37 °C until they were confluent.
- 2) After the addition of NS1, cells were rinsed three times with PBS buffer.
- 3) Cells were fixed using the fixation procedure as described above.
- 4) After fixation, cells were rinsed with PBS buffer twice, for 5 min each.
- 5) The cell membranes were permeabilized with PBS-Saponin 0.5% solution for 10 min.
- 6) Cells were rinsed with PBS-BSA 3% buffer twice.
- 7) The PBS-BSA 3% buffer was used to block the non-specific antibody bindings for 30 min.
- 8) The 1st antibody was diluted in the PBS-BSA 3%- Saponin 0.5% buffer, and the drops of the mixture were added to the coverglasses, making sure that the entire surface was covered by the solution. Cells were incubated with the 1st antibody for 60 min at room temperature. During the incubation, the coverglasses were placed in the culture dish, on top of the wetted paper, and the cover of the culture dish was sealed with parafilm, to prevent the evaporation of the solution.
- 9) After the incubation, cells were rinsed with PBS-BSA 3%- Saponin 0.5% buffer twice, for 5 min each.
- 10) The 2nd antibody was diluted in PBS-BSA 3%- Saponin 0.5% buffer, and incubated with the cells for 45min at room temperature.
- 11) Cells were rinsed with PBS-BSA 3%- Saponin 0.5% buffer twice, for 10 min each.
- 12) Last, the cells were rinsed with PBS buffer.
- 13) The coverglasses were carefully taken out from the culture wells, using a tweezers, and mounted on the microscope slide.

Imaging of NS1 ex vivo

Living cells imaging

For living cell imaging, cells were cultured in Willco-dish until they were confluent. The Willco-dishes were then placed in the chamber fixed at the focal plane of the confocal microscope, this chamber was coupled with CO₂ and a temperature controlling system to provide the same conditions as in the incubator (37°C, 5% CO₂). The cells were placed in the chamber sealed with cover.

In the kinetics study of NS1 internalization, cells were incubated with 5-10 μM of NS1. During the observation, the CCD camera took the picture of epi-fluorescence from the same cell at a series of time points.

In the colocalization study of NS1 with cell organelles such as endoplasmic reticulum (ER), mitochondria and Golgi complex, cells were labeled by trackers which are compatible with living cell imaging. ER-Tracker™ Red dye ($\lambda_{ex/em}$ = 587/615 nm), MitoTracker® Deep Red ($\lambda_{ex/em}$ = 644/665 nm) and BODIPY® TR C 5 ceramide complexed to BSA ($\lambda_{ex/em}$ = 589/617 nm) were purchased from Invitrogen. For co-localization with ER or mitochondria, cells were co-incubated with NS1 (5-10 μM) with either ER or mitochondria tracker, respectively, for 30 min, according to the manufacture's protocol. For co-localization with the Golgi complex, cells were incubated first with the BODIPY TR ceramide complex (3μM) for 60 min, and further incubated with NS1 (5μM) for 30 min, according to the manufacture's protocol.

Fixed cell imaging:

In the colocalization study of NS1 with eNOS, Caveolin-1 and Early endosome, the cells were incubated first with NS1 (5-10 μM for 60min), then were labeled with eNOS, Caveolin-1 or EEA (for early endosome) antibodies followed by immunostaining procedure, according to the protocol described above.

Imaging settings for colocalization experiments:

The objective of confocal microscope was 63X. The 1-photon excitation wavelength for NS1 was 488nm. The 1-photon excitation wavelength for red trackers (Endoplasmic reticulum, Mito tracker and Golgi tracker) as well as immune-labeling markers (eNOS, Calveolin-1 and EEA) was 543 nm. The 2-photon excitation wavelengths for DAPI (to image the nuclei) and NS1 were 740 nm and 840 nm, respectively. The output excitation power was in the 5-20 mW range. The emission ranges were 410-510 nm for DAPI, 520-680 nm for NS1 and 590-700 nm for red trackers/markers.

Fluorescence detection of ROS generation in cells

To measure the variation of cellular oxidative stress in the presence of NS1, CellROX® Deep Red Reagent ($\lambda_{\text{ex/em}} = 644/665$ nm) purchased from Invitrogen was used to indicate the ROS generation. The fluorescence detection of ROS was measured by a FACS Calibur flow cytometer (Becton-Dickinson, USA). Tert-butyl hydroperoxide (TBHP) (Sigma), was used as a positive control for ROS detection.

$1-1.5 \times 10^5$ cells were seeded in 12-well plates. When the cells reached confluence, they were pre-incubated with increasing concentrations of NS1 for 30 min, and then further incubated with 2 μM CellROX® Deep Red Reagent for 30 min. Each concentration point was duplicated or triplicated. In the case of TBHP treatment, cells were pre-incubated with 400 μM TBHP for 2 hours before addition of CellROX® Deep Red Reagent. After CellROX® Deep Red treatment, the cells were trypsinized, collected and centrifuged at 1,000 rpm for 5 min. The cell pellets were resuspended in PBS containing 30% of enzyme-free Cell Dissociation Buffer (Gibco®) in order to avoid cell aggregation. The cell counts for each analysis by flow cytometry were 12,000-20,000.

The fluorescence signals of NS1 and CellROX® Deep Red reagent were measured by using FL-1 and FL-4 channels which correspond to distinct wavelength ranges. Indeed, the emission filters for FL1 and FL4 were 530 ± 30 nm and 661 ± 16 nm, respectively. The MFI (Mean Fluorescence Intensity) related to the fluorescence emission was used to interpret the modulation effect of NS1 on ROS formation. The measured MFI in FL-4 channel obtained for a given NS1 concentration was normalized by the MFI obtained in the absence of NS1 (i.e. as a measurement of the basal cellular level of ROS in the cells, CellROX® Deep Red Reagent alone was also measured in FL-4 channel), giving the fluorescence enhancement factor. The increase in the NS1 signal as a function of NS1 concentration incubated with cells was checked using the FL-1 channel.

Note: The materials and methods section is only related to experiments which were performed by me during the thesis. To avoid any redundancy, the details related to the experiments performed by our different collaborators will be described in the results chapter (particularly in the “Materials and Methods” section relative to the article published in PNAS and the submitted article, respectively). The molecular modelling was performed by the project collaborator A. Slama-Schwok and B. Tarus (INRA, Jouy-en-Josas). The chemical synthesis of NS1 and derivatives were performed by Y. Li and J-L Boucher (University Paris V). The NO and ROS measurements by Electron Paramagnetic Resonance (EPR) in endothelial cells and isolated mice aortic rings were performed by C. Dessy, M. Romero-Perez and I. Lobysheva (UCL, Belgium). Our collaborators in UCL also performed vasorelaxation/vasoconstriction experiments on isolated mice aortic rings. The ROS detection

by EPR in PMA-activated macrophages was performed by J-L. Boucher (University Paris V). The effect of NS1 on the angiogenic process was performed by C. Dessy and I. Lobysheva (UCL, Belgium). The effect of NS1 on normal melanocytes and melanoma cells was performed by S. Rocchi (university Sophia-Antipolis, Nice).

RESULT

Introduction of “Rational design of a NADPH derivative imaging constitutive nitric-oxide synthases upon two-photon excitation”

Yun Li*, Huan Wang*, Bogdan Tarus, Miguel Romero Perez, Laurence Morellato, et al. PNAS 2012July
(* Co-first authors)

In this publication, we report the design and synthesis of the NADPH analog Nanoshutter (NS1). We characterized the *in vitro* fluorescence properties of free NS1 and NOS-bound NS1. We also assessed the inhibition of NOS catalytic activity, as well as the selectivity of targeting by comparing the binding of NS1 to several recombinant proteins: (i) proteins that do not contain any NADPH binding site such as Lens epithelium-derived growth factor (LEDGF), Fatty acid binding protein (FABP), Myoglobin and *E. Coli* RecQ Helicase; (ii) proteins distinct from NOS that contain a NADPH binding site such as Ferredoxin reductase and glucose 6-phosphate dehydrogenase (G6PD) and (iii) the three NOS isoforms: eNOS, nNOS and iNOS. Furthermore, we demonstrated the *in vivo* imaging capability of NS1 in endothelial cells and the colocalization with subcellular organelles and eNOS.

In the biological context, NO participates in profound physiological and pathological activities in cardiovascular, nervous and immune systems. Modulation of the production of NO has been a central issue in biological and clinical research since NO was discovered 80 years ago. Because the only pathway for NO synthesis inside human body is the oxidation of L-arginine catalyzed by NO Synthase, scientists has dedicated to develop various NOS inhibitors. The majority of them actually target the oxygenase domain of NOS. However, this mechanism has significant backwards: on one hand, they are limited by the lack of specificity among NOS isoforms and many other potential targets; on the other hand, they are incapable of avoiding NOS uncoupling and the associated formation of the well-known reactive oxygen species (ROS). Any compound that targets NOS in the oxygenase domain, for instance, cannot prevent the ROS formation originating from electron leakage. Such a consequence may occur with arginine analogs but also with compounds that target BH₄. Indeed, BH₄ as a critical cofactor in the oxygenase domain has been identified to preserve NOS dimerization (111). The decrease in NOS activity by targeting its oxygenase domain will be associated with disruption of NOS dimers, producing ROS (NOS uncoupling) rather than NO as proposed in (237). Even though the structure of the reductase domain of NOS was solved, so far there is only one flavin inhibitor which targets the FAD binding site, and its

inhibition effect is irreversible.

In contrast to the conventional NOS inhibitor, the purpose of this study was to design a novel inhibitor which competitively targets the NADPH binding site in the NOS reductase domain. This compound should also display two photon excitation and emission properties compatible with *in vitro* and *ex vivo* characterization of the complex formation. To reach the optimal effects, we took into account several criteria including NOS-NS1 affinity, electron flow blockage capability, good two-photon cross-section enabling multi-photon imaging, and distinct fluorescence properties between the free and the NOS-bound NS1 compound.

With these conditions in mind, the design of NS1 was firstly guided by molecular modelling (performed by B. Tarus and A. Slama-Schwok, INRA, Jouy en Josas). The nucleotide recognition motif of NADPH was retained in NS1, allowing a proper targeting to the NADPH site of NOS, while a stilbene moiety was used to replace the nicotinamide moiety of NADPH. Compared to NT1 in the previous study (Nanotrigger) (205), NS1 was designed to have the identical recognition moiety, but the chromophoric moiety (stilbene) of NS1 was shorter than that of NT1 (1,4-diphenyl-butadiene), and the terminal group of NS1 was an electron acceptor group (NO_2) instead of an electron donor group (NH_2) in NT1. In addition to the ability of the NO_2 group to prevent electron flow, this group is also known to confer environment modulation of fluorescence properties. Although the stilbene linker should decrease the two-photon absorption cross-section, the stilbene of NS1 leads to a better steric fit to the NADPH site than the butadiene of NT1 as predicted by molecular modelling. Moreover, the synthesis of NS1 is based on a seven-step procedure, allowing an easier synthesis compared to the fifteen-step procedure for NT1 (203).

NS1 dissolved in DMSO has an absorption maximum at 460 nm, with an extinction coefficient of $\epsilon = 21,000 \text{ M}^{-1}\text{cm}^{-1}$. Under one- and two-photon excitation, at 460 nm and 940 nm, respectively, the emission peak was centered at 760 nm. As expected, NS1 displayed high sensitivity to the polarity of the solvent. By varying the amount of DMSO in the Tris buffer (pure DMSO, 66% DMSO: 33% Tris buffer (v/v), 33% DMSO: 66% Tris buffer (v/v), pure Tris buffer), we found that the fluorescence emission of NS1 dropped off when the content in DMSO decreased. NS1 also displayed a satisfactory two-photon cross-section (σ_2) of 130 and 65 GM in the 800-860 and 920-950 nm ranges, respectively, although these σ_2 values are less than the σ_2 value characterizing NT1 (160 GM at 790 nm). However, the σ_2 value of NS1 is good enough for both two-photon *in vitro* studies and multiphoton fluorescence imaging.

In comparison with the weak fluorescence emission of the free NS1 in aqueous buffer, a substantial recovery of fluorescence emission of NS1 was observed in the NOS context. This interesting property was used for measuring the affinity characterizing the NOS-NS1 complex. The titration was performed under both one- and two-photon excitation conditions, and similar K_d values (around 4.2 μM) were found, suggesting an effective binding of NS1 to NOS

with a good affinity comparable with the K_m value related to the binding of NADPH to NOS. Notably, due to the participation of fluorescence emission from flavins in NOS, the quantification of the binding process was rather difficult under 1-photon excitation conditions. Indeed, it was possible to estimate the K_d value but only from emission intensities in the red region of the spectrum characterized by a low signal. In contrast, the contribution of NOS auto-fluorescence signal was totally eliminated in the case of two-photon excitation, therefore, the pure binding information related to the formation of the NOS-NS1 complex was revealed under two-photon excitation.

Furthermore, NS1 displayed good selectivity upon binding in terms of quantum yield. There was an enhancement of fluorescence emission of NS1 bound to the three NOS isoforms, however to different extents (eNOS>nNOS>>iNOS). To note, although the quantum yield of NS1 depends on the isoform context, the three NOS isoforms displayed similar K_d values. In the presence of other proteins which contain or not a NADPH binding site, NS1 displayed poor quantum yields. A possible explanation for the difference of quantum yields observed among the three NOS isoforms is suggested by molecular dynamic simulations: it was found that NS1 probed a more hydrophobic environment in eNOS than in iNOS and nNOS.

Stopped-flow experiments and oxyhemoglobin assay showed that NS1 was able to compete with NADPH binding to nNOS and subsequently inhibit the NO formation, in dose-dependent and reversible manners. So far, the *in vitro* experiments demonstrated that NS1 meets the criteria of molecular design, NS1 reached the initial goal to inhibit NOS activity and displayed a good two-photon absorption property.

To get deeper insight into the effect of NS1 in a real biological environment, we performed fluorescence imaging and colocalization experiments of NS1 *ex vivo*. The endothelial cell line (HUVEC) which contains eNOS was chosen in these experiments, because the eNOS context led to the highest quantum yield of NS1, as probed in the selectivity assay *in vitro*. In living cells, under both one- and two-photon excitation conditions, a significant and specific fluorescence emission was rapidly observed after the addition of NS1 in the medium, indicating a rapid and efficient internalization of NS1 in HUVEC cells. Moreover, the fluorescence signal was consistently highlighted in the perinucleus region, sometimes with detectable signals at the plasma membrane. This is in accordance with the fact that eNOS in endothelial cells is mainly localized in the Golgi complex and the plasma membrane. To find out the potential targets of NS1 inside the cell, we performed colocalization imaging between NS1 and several cell organelles, as well as eNOS immunofluorescence labeling. We observed the colocalization between NS1 and Golgi, more importantly between NS1 and eNOS, suggesting that NS1 actually targets eNOS in endothelial cells.

In summary, NS1 fulfilled the purpose of this study, firstly as a unique NOS inhibitor, it

targets the reductase domain of NOS and competitively inhibits the enzyme activity. The chromophoric moiety displayed a unique two-photon property *in vitro* and *in vivo*. These features may lead to a new road for non-invasive real-time imaging, and to perspective clinical applications in the study of NO-dependent diseases.

Rational design of a fluorescent NADPH derivative imaging constitutive nitric-oxide synthases upon two-photon excitation

Yun Li^{a,1}, Huan Wang^{b,1}, Bogdan Tarus^{c,1}, Miguel Romero Perez^d, Laurence Morellato^a, Etienne Henry^b, Vladimir Berka^e, Ah-Lim Tsai^e, Booma Ramassamy^a, Hamid Dhimane^a, Chantal Dessy^d, Patrick Tauc^b, Jean-Luc Boucher^a, Eric Deprez^{b,1,2}, and Anny Slama-Schwok^{c,1,2}

^aLaboratoire de Chimie et Biochimie Pharmacologiques et Toxicologiques, Centre National de la Recherche Scientifique UMR8601, Université Paris Descartes, 75270 Paris, France; ^bLaboratoire de Biologie et Pharmacologie Appliquée, Centre National de la Recherche Scientifique UMR8113, ENS-Cachan, 94235 Cachan, France; ^cLaboratoire de Virologie et Immunologie Moléculaires, Institut National de la Recherche Agronomique UR892, 78350 Jouy en Josas, France; ^dPole of Pharmacology and Therapeutics, FATH5349, Institute of Experimental and Clinical Research, Université catholique de Louvain Medical Sector, B-1200 Brussels, Belgium; and ^eDivision of Hematology, Department of Internal Medicine, University of Texas Health Science Center at Houston, TX 77030

Edited by* Gregory A. Petsko, Brandeis University, Waltham, MA, and approved June 25, 2012 (received for review April 3, 2012)

We report the structure-based design and synthesis of a unique NOS inhibitor, called nanoshutter NS1, with two-photon absorption properties. NS1 targets the NADPH site of NOS by a nucleotide moiety mimicking NADPH linked to a conjugated push-pull chromophore with nonlinear absorption properties. Because NS1 could not provide reducing equivalents to the protein and competed with NADPH binding, it efficiently inhibited NOS catalysis. NS1 became fluorescent once bound to NOS with an excellent signal-to-noise ratio because of two-photon excitation avoiding interference from the flavin-autofluorescence and because free NS1 was not fluorescent in aqueous solutions. NS1 fluorescence enhancement was selective for constitutive NOS in vitro, in particular for endothelial NOS (eNOS). Molecular dynamics simulations suggested that two variable residues among NOS isoforms induced differences in binding of NS1 and in local solvation around NS1 nitro group, consistent with changes of NS1 fluorescence yield. NS1 colocalized with eNOS in living human umbilical vein endothelial cells. Thus, NS1 constitutes a unique class of eNOS probe with two-photon excitation in the 800–950-nm range, with great perspectives for eNOS imaging in living tissues.

chemical biology | inhibition of enzymatic catalysis | structure-based design and molecular modeling | two-photon fluorescence imaging | fluorescence spectroscopy

In mammals, NO is a gaseous signaling mediator that exerts a wide range of key physiological functions, including blood pressure regulation, neurotransmission, and immune responses (1). NO is formed by nitric-oxide synthases, a family of hemoproteins that catalyzes the oxidation of L-arginine leading to L-citrulline and NO (2, 3). NOS catalysis is driven by reducing equivalents supplied by NADPH. NOS enzymes are constituted by oxygenase and reductase domains linked by a calmodulin (CaM)-binding domain. The oxygenase domain binds the heme, L-arginine, and the cofactor (6R)-5,6,7,8-tetrahydro-L-biopterin (H₄B). The reductase domain binds two flavins, FMN and FAD, and NADPH (4). CaM binding allows the electron transfer from FMN to the heme (2, 3). The biological activities of NO are closely linked to the specific NOS isoform involved in its synthesis and deregulation of its biosynthesis leads to various pathologies (5). Data support the notion that inhibition of the inducible and neuronal isoforms iNOS and nNOS have therapeutic utility in the treatment of a variety of diseases, including septic shock, neurodegeneration, inflammation, and cancer (5, 6). It was shown that the endothelial isoform eNOS participates in tumor initiation and maintenance, thus its inhibition could be beneficial in this context (7, 8). Based on crystallographic studies (9, 10), much effort was dedicated to the development of specific NOS inhibitors

by targeting the heme site. However, most of these inhibitors are not specific and cannot avoid NOS uncoupling and formation of deleterious radical oxygen species (ROS) at the reductase domain. Although the structure of nNOS reductase domain has been solved (4), no specific compounds targeting this domain are available, and only diphenyliodonium (DPI) and its analogs nonselectively and irreversibly react with flavins (11). The NADPH-binding site is highly conserved among redox enzymes. The crystallographic data of NADPH-containing proteins showed that the main recognition elements in their binding site involve conserved arginines that interact electrostatically with the 2' phosphate group of NADPH nucleotide moiety. The nicotinamide part of NADPH can be flexible and undergoes conformational changes depending on the NADP(H) enzymes and their specific catalysis. In recent studies, we have characterized a NADPH analog called nanotrigger, NT1, targeting the NADPH site in NOS reductase domain (12–14) (Fig. 1A). NT1 contained a conjugated, photoactivatable chromophore substituted with two donor groups that replaced the nicotinamide moiety of NADPH. Following photoactivation, the terminal amine group of excited NT1* was able to inject electrons to the FAD acceptor, thereby initiating the electron flow. This initiation and synchronization of NOS catalysis upon one- or two-photon excitation (1-PE or 2-PE, respectively) led to light-induced NO formation (12–14).

Here, we designed a unique prototype of NOS inhibitor, called nanoshutter (NS1), with intrinsic fluorescence imaging properties. To this purpose, we designed a compound that meets the following criteria: (i) NS1 should demonstrate a good affinity for NOS, at least comparable to the affinity of the natural hydride donor NADPH; (ii) injection of electrons to FAD should be prohibited by bound NS1 to NOS; (iii) NS1 should have a good two-photon cross-section, compatible with multiphoton imaging; (iv) free and bound NS1 should possess different fluorescence properties. We designed a compound bearing a nucleotide moiety as recognition motif of the NADPH site linked by an alkyl chain to a new chromophore substituted with an acceptor and a donor group, thus engineering a push-pull photoactive element

Author contributions: Y.L., J.-L.B., C.D., E.D., and A.S.-S. designed research; Y.L., H.W., B.T., M.R.P., L.M., E.H., V.B., and P.T. performed research; B.T., V.B., A.-L.T., P.T., and J.-L.B. analyzed data; and E.D. and A.S.-S. wrote the paper.

The authors declare no conflict of interest.

*This Direct Submission article had a prearranged editor.

¹Y.L., H.W., B.T., E.D. and A.S.-S. contributed equally to this work.

²To whom correspondence may be addressed. E-mail: Anny.Schwok@gmail.com or deprez@lbpa.ens-cachan.fr.

This article contains supporting information online at www.pnas.org/lookup/suppl/doi:10.1073/pnas.1205645109/-DCSupplemental.

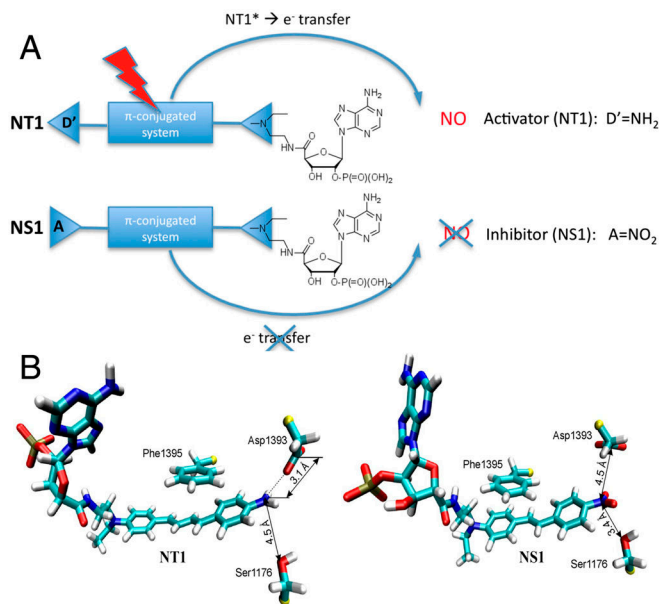


Fig. 1. Design and molecular modelling studies of the nanotrigger NT1 and the nanoshutter NS1. (A) Principles of activation and inhibition of NOS by NT1 and NS1. Because of its terminal nitro-phenyl (electron acceptor) group that cannot inject the reducing equivalents required for the initiation of catalysis, NS1 is expected both to bind to the NADPH site and to inhibit competitively the electron flow to the FAD acceptor (in contrast to the electron donor-containing compound NT1). Additionally, significant modulations of the fluorescence emission by the polarity (λ_{\max}) and the presence of water (quantum yield, Φ) of the environment are expected. (B) Close-up view of the terminal groups of NT1 diene chromophore and NS1 stilbene chromophore in $n\text{NOS}_{\text{red}}$; FAD is omitted for clarity (12–14).

(Fig. 1A). Such a chromophore is expected to have a high dipole moment caused by the electron delocalization in the excited state that should lead to nonlinear absorption properties (15). The NS1 chromophore carries a conjugated stilbene substituted with the donor–acceptor pair instead of the diene moiety of NT1 (13) (Fig. 1B). Finally, the terminal electron acceptor was chosen to be a nitro group that should block the electron flow, inhibit NOS catalysis, and modulate the fluorescence properties of NS1 with the environment (16). A change in fluorescence emission between free and NOS-bound states of the engineered NS1 compound was then expected. This work paves the way for a unique family of NOS inhibitors with imaging applications.

Results

Molecular Modelling. We showed that NS1 fits into the narrow NADPH site of the reductase domain of $n\text{NOS}$ ($n\text{NOS}_{\text{red}}$) using docking and molecular dynamic simulations based on the structure of this domain (4). We used a stilbene moiety instead of the 1,4-diphenyl-butadiene moiety of NT1 for replacement of the nicotinamide part of NADPH. This choice of a shorter stilbene moiety was guided by initial modelling studies, which had suggested that a shorter compound than NT1 with the same terminal donor group could fit tighter to this site. Our design retained the nucleotidic recognition motif of NADPH that confers proper targeting to the NADPH site, based on previous studies that led to the discovery of NT1 (12–14, 17). The designed inhibitor NS1 was docked in $n\text{NOS}_{\text{red}}$ by replacement of the embedded NADPH (4). Each complex, NS1- $n\text{NOS}_{\text{red}}$ or NT1- $n\text{NOS}_{\text{red}}$, was placed in a box of explicit water molecules; after energy minimization, we assessed the fit of both NS1 and NT1 within the NADPH site by running trajectories of 10 ns. The main interaction energy of NS1 and NT1 with the protein originated in their terminal phosphate group that recognized the conserved arginine residues in the NADPH-binding site, in particular Arg1400, Arg1314, Arg1284,

and Arg1010. This modelling demonstrated a similar recognition of the nucleotidic part of NS1 to that seen with NADPH (17) (SI Appendix, Fig. S1 and Table S1). The chromophore moieties of NS1 and NT1 were inserted close to FAD, removing the stacking interaction of Phe1395 with FAD observed in the crystal structure (4). The partly charged oxygen of the terminal nitro group of NS1 induced a reorientation of the δ -oxygen of Asp1393 by electrostatic repulsion between them (Fig. 1B). The van der Waals energy terms of both chromophores had similar negative values, contributing to their correct docking despite unfavorable electrostatic energies, 25 ± 5 and 9 ± 4 kcal/mol for NS1 and NT1, respectively. The better steric fit of the stilbene chromophore to the NADPH site was reflected by a more favourable linker term for NS1 binding than for NT1 (-57 ± 6 and -38 ± 7 kcal/mol, respectively) (SI Appendix, Table S1). In NT1, the positioning of the longer diene chromophore probably required some adjustments. Altogether, the nucleotidic part was identical in both molecules and there was compensation between the linker and chromophore energy terms, which led to similar interaction energies for both NS1 and NT1, suggesting that NS1 could display an affinity for $n\text{NOS}$ (or $e\text{NOS}$) close to that of NT1.

Synthesis, Spectroscopic, and Fluorescence Properties of NS1 in Solution. The synthesis of the target compound NS1 (Fig. 2A) consisted of a seven-step procedure (see Methods and SI Appendix, Fig. S2). The absorption spectra of NS1 and its chromophore

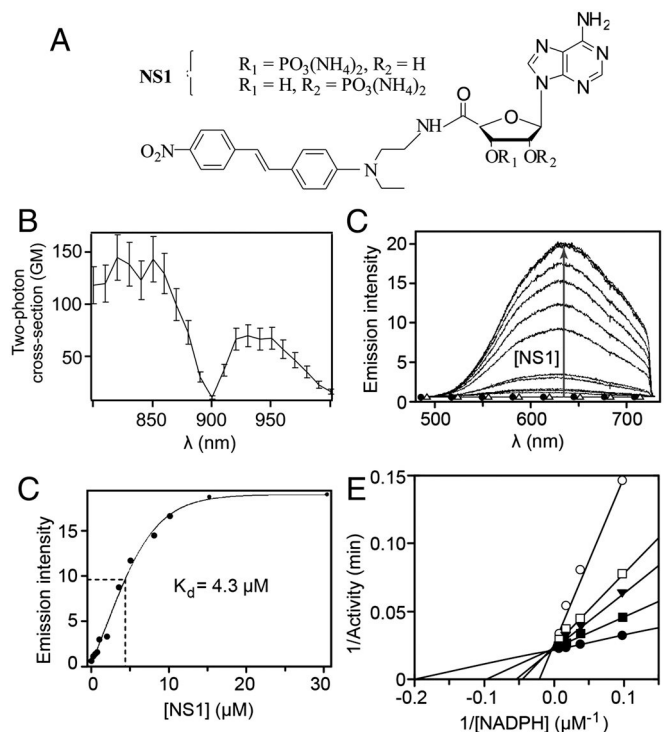


Fig. 2. Binding of NS1 to $n\text{NOS}$ monitored by fluorescence emission upon 2-PE and subsequent inhibition of NOS activity. (A) Structure of NS1; (B) two-photon excitation spectrum of NS1 in DMSO. The fluorescence quantum yield and the two-photon cross-section (σ_2) were determined using rhodamine B as a reference and were found to be equal to 0.0045 and 65 GM at 940 nm, respectively (σ_2 of approximately 130 GM at 840 nm). (C) Increase in NS1 fluorescence ($\lambda_{\text{ex, 2-PE}} = 940$ nm) upon binding to $n\text{NOS}$ (5 μM). No fluorescence emission was detected in Tris buffer upon 2-PE of $n\text{NOS}$ alone (Δ) or NS1 alone (30 μM , \bullet); (D) corresponding binding isotherm. The binding isotherm was fitted using a one-binding site model, leading to an apparent dissociation constant for NS1 binding of 4.3 ± 0.6 μM . (E) Inhibition by NS1 of the formation of NO by $n\text{NOS}$: competition experiments between NADPH and NS1. The double-reciprocal plots of $n\text{NOS}$ activities measured in the presence of various concentrations of NADPH (up to 100 μM) are shown in the absence (\bullet) or in the presence of 5 (\blacksquare), 25 (\blacktriangledown), 50 (\square), or 100 (\circ) μM NS1.

moiety were similar, with a maximum similar to the related 4-*N*, *N*-dimethylamino-4'-nitrostilbene (16, 18). NS1 had an absorption maximum at $\lambda_{\max} = 460$ nm with an extinction coefficient $\epsilon = 21,000 \text{ M}^{-1} \text{ cm}^{-1}$ in DMSO (*SI Appendix, Fig. S3A*); upon excitation at 460 nm, NS1 presented a broad emission peak centred at 740 nm (*SI Appendix, Fig. S3B*). The two-photon cross-section of NS1 was found to be σ_2 of approximately 130 and 65 GM (Göppert-Mayer; 1 GM = $10^{-50} \text{ cm}^4 \cdot \text{s}/\text{photon}$) in the 800–860 and 920–950 nm ranges, respectively, in DMSO (*Fig. 2B*). As expected, NS1 fluorescence was strongly sensitive to the presence of water (*SI Appendix, Fig. S3B and C*), its fluorescence was undetectable in aqueous solutions under either one-photon excitation condition (at 435 or 460 nm) or two-photon excitation condition ($\lambda_{\text{ex},2\text{-PE}} = 840$ or 940 nm).

Fluorescence Properties of NS1–NOS Complexes. Addition of NS1 to purified NOS led to the recovery of bound NS1 fluorescence as compared to free NS1 being non fluorescent in aqueous buffer. This made possible the biochemical monitoring of NS1 binding to NOS using one- or two-photon fluorescence experiments. Under 1-PE conditions, the intrinsic emission properties of the NS1–nNOS complex were difficult to extract because the fluorescence of nNOS flavins and the fluorescence of NS1 overlapped. NS1 contribution was extracted by monitoring the emission at 700 nm in a spectral region where flavin autofluorescence was not significant. Although NS1 fluorescence was low at 700 nm, NS1 binding to nNOS could be recorded and led to the determination of an apparent K_d of 4.2 μM (*SI Appendix, Fig. S4*). We reasoned that if the two-photon fluorescence of nNOS is weak (as expected, taking into account the very low σ_2 value of flavins—see *Discussion*), the 2-PE approach should be more appropriate for monitoring the fluorescence recovery of NS1 upon binding to nNOS. Indeed, both the intrinsic fluorescence of nNOS and free NS1 fluorescence (up to 30 μM) were undetectable under 2-PE condition (*Fig. 2C*). Stepwise additions of NS1 to nNOS resulted in an increase of NS1 fluorescence emission (*Fig. 2C*), which corresponded to pure emission spectra of NS1 in the nNOS–NS1 complex, allowing quantitative analysis of the binding process (*Fig. 2D*). The apparent $K_d = 4.3 \pm 0.6 \mu\text{M}$ was consistent with the 1-PE value. The emission of NS1 was blue-shifted in the protein context (630 nm) compared to DMSO (740 nm), consistent with the influence of solvent polarity on emission maxima of nitrostilbene derivatives (16). Binding of NS1 to full-length eNOS, iNOS, or eNOS_{red} yielded comparable results in terms of affinity, but with substantial differences in the quantum yield characterizing each complex (see below).

Inhibition of NOS Catalytic Activity by NS1. The ability of NS1 to inhibit the NADPH-mediated hydride transfer to nNOS was studied by stopped-flow measurements. Fast mixing of nNOS with NADPH resulted in a fast decrease of the NADPH absorption, corresponding to a two-phase model (*SI Appendix, Fig. S5*). A significant slowdown of the fast phase of NADPH consumption that contributed approximately 65% of the decay at 340 nm was observed in the presence of NS1. NS1 competed with NADPH on nNOS reduction in a dose-dependent manner, presenting a typical saturation curve, and led to an apparent inhibition constant $K_i = 15 \pm 4 \mu\text{M}$. This value compares well with those obtained previously with NT1, $K_i = 7 \pm 3 \mu\text{M}$ (13, 17), showing that NS1 and NT1 display similar affinities for the NADPH site of constitutive NOS, as suggested by our molecular modelling study.

Because NS1 abolished the electron-transfer flux from NADPH to the flavins in the reductase domain of nNOS, NO formation should also be inhibited. The ability of NS1 to inhibit NO formation was assessed using the oxyhemoglobin assay. NS1 inhibited the formation of NO catalyzed by nNOS in a dose-dependent manner with a half-inhibitory concentration (IC_{50}) at $65 \pm 8 \mu\text{M}$ in the presence of 100 μM NADPH and L-arginine

(*SI Appendix, Fig. S6A*). We then investigated the mechanism of inhibition by varying NADPH and NS1 concentrations. The double-reciprocal plot of NO formation activity as a function of [NADPH] led to a K_m value of $5.5 \pm 0.5 \mu\text{M}$ in the absence of NS1 (intercept with the x axis; *Fig. 2E*). NS1 inhibition was competitive with NADPH as demonstrated by changes of the apparent K_m values ($K_{m \text{ app}}$) without significant effect on the V_{\max} values with varying NS1 concentration. The plot of $K_{m \text{ app}}$ values as a function of [NS1] led to a K_i value ranging between 13 and 18 μM (*SI Appendix, Fig. S6B*). The value of $K_i = 3.4 \mu\text{M}$ deduced from $\text{IC}_{50} = 65 \mu\text{M}$ using the Cheng-Prusoff relationship is consistent with the values of $K_d = 4.3 \mu\text{M}$ and $K_i = 15 \mu\text{M}$ obtained in 2-PE and stopped-flow experiments, respectively, and compares well with NADPH affinity ($K_m = 5.5 \pm 0.5 \mu\text{M}$). Further experiments using the dilution method showed that the inhibition of NO formation by NS1 was reversible. NS1 appears as a unique prototype inhibitor that competes with NADPH for binding in the reductase domain.

In Vitro Selectivity in the Fluorescence Enhancement of Protein-Bound NS1. The relative two-photon fluorescence intensity of NS1 bound to various proteins was next assessed. NS1 did not display significant fluorescence enhancement in the presence of proteins lacking a NADPH-binding site (*Fig. 3A*). For instance, NS1 non-specifically binding to the fatty acid-binding protein (FABP) accounted for only 5% of the fluorescence signal observed with eNOS-bound NS1. Thus, NS1 differs from nonspecific probes such as the well-known ANS compound (anilinonaphthalene sulfonic acid), whose fluorescence is largely enhanced by multiple interactions in inner protein cavities, in particular upon binding to FABP (19). Among the NADPH-binding proteins, including the three NOS isoforms, NS1 binding to eNOS and nNOS led to the largest fluorescence enhancement (eNOS > nNOS \gg iNOS). The fluorescence quantum yield of NS1 was found to be strongly dependent on the protein context, indicating that NS1 within the NADPH-binding site probed distinct local solvent environment in each NOS isoform. In contrast, NS1 was only weakly fluorescent when bound to ferredoxin reductase or glucose-6-phosphate dehydrogenase (G6PDH). Interestingly, the two-photon fluorescence emission of eNOS-bound NS1 was found to be even higher than the value found in DMSO (approximately 45-fold higher) (*Fig. 3A, Inset*). Thus, NS1 is highly selective between constitutive and inducible NOS. These results were promising for further cellular investigations.

Structural Insight of NS1 Binding to NOS Isoforms Based on Molecular Dynamics Simulations. We attempted to explain the modulation in fluorescence yields of NS1 bound to the three NOS isoforms by additional structural insight; homology modelling was used to generate eNOS and iNOS reductase domains (17). NS1 bound to nNOS or eNOS by three arginine residues interacting with its phosphate group (*SI Appendix, Fig. S7*). Among these arginines, R1400 in nNOS was replaced in iNOS by S1130 unable to form an H-bond with NS1 phosphate. Note that S1130 is located on the same linker as the catalytic D1123, allowing an information flow between the nucleotidic part of NS1 and the chromophore terminal. In addition, the solvation around NS1 terminal NO_2 was highest in iNOS among the three NOS (*SI Appendix and Fig. 3B and C*) and *SI Appendix (Fig. S8)*. The importance of water in active sites of proteins has been shown by pioneer works of Douzou and co-workers (20). In iNOS, the NO_2 group of the chromophore was more distant to the hydrophobic patch forming the edge of the binding site. This patch was composed by three F and one Y in iNOS and nNOS instead of four F in eNOS. Y1077 made H-bonds with either water or nearby hydrophilic residues, which caused the hydrophobic patch to be less packed, and more water (partly from iNOS dimeric interface) accessed the NO_2 group (*SI Appendix, Fig. S8*). In contrast,

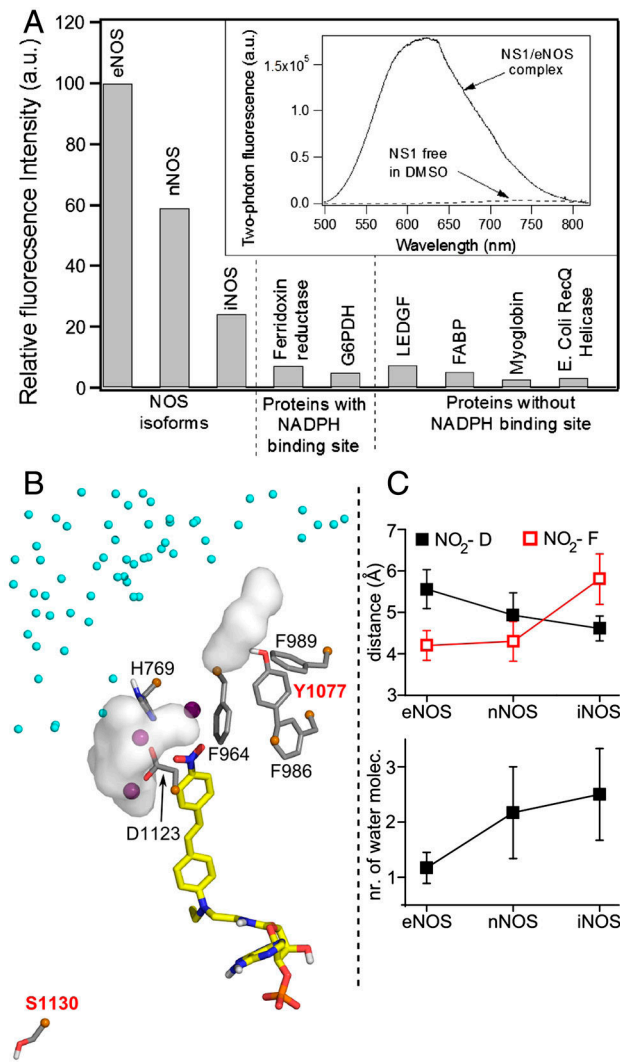


Fig. 3. (A) Fluorescence intensity of NS1 bound to various proteins upon two-photon excitation (normalized by the maximum intensity value corresponding to eNOS). The experiments shown in Fig. 2C and D were repeated with NOS isoforms and proteins with ferredoxin reductase, glucose-6-phosphate dehydrogenase (G6PDH), or without [lens epithelium-derived growth factor (LEDGF), fatty acid-binding protein (FABP), myoglobin, and *E. Coli* RecQ helicase] a NADPH-binding site; 5 μ M of protein was mixed with increasing concentrations of NS1 until the fluorescence intensity reached a plateau. The relative fluorescence intensity was calculated based on the plateau value. The apparent dissociation constants of NS1 from the NOS isoforms determined using 2-PE fluorescence display similar affinities for NS1, $K_d = 4\text{--}5\ \mu\text{M}$. (Inset) Two-photon fluorescence emission of NS1 (ex 940 nm) bound to eNOS or free in DMSO. (B) Zoom on the solvation near the nitro terminal of NS1 chromophore bound to iNOS reductase domain. Three water molecules located at 3.5 Å from the NO₂ extremity of NS1 are shown by purple spheres. The white surfaces are solvent molecules at 3.5 Å from D1123 and (variable) Y1077, the latter being part with F986, F989, and F964 to the hydrophobic patch at the edge of NS1-binding site; contribution of water from iNOS dimeric interface (small cyan spheres) is observed; (C) The distance to the conserved D decreases while the distance to F (F998, F1234, F964) and the number of water surrounding D (D1157, D1393, D1123) increases in the order e/n/iNOS (*SI Appendix, Fig. S8*).

the proximity of NO₂ to a well-packed hydrophobic patch limited access to water-solvating D1127 in eNOS; thus, NS1 terminal probed a more hydrophobic environment. This hypothesis fits well with NS1's probing the most hydrophobic environment in eNOS, thus the largest fluorescent yield. Indeed, specific solvent effects depending on the water content modulate NS1 fluores-

cence yield without $\lambda_{\text{max,em}}$ shift in solution and in NOS isoforms (*SI Appendix, Fig. S3* and Fig. 3A).

NS1 Imaging in Endothelial Cells. The fluorescence selectivity of NS1 for constitutive NOS prompted us to test if NS1 would specifically highlight eNOS in living cells. A rapid uptake of NS1 (maximum 10 min) by living human umbilical vein endothelial cells (HUVECs) was easily monitored upon excitation in the near infrared, showing the suitability of NS1 for 2-PE fluorescence studies of living cells (Fig. 4). (A comparison between 1- and 2-PE images for identical living cells is shown in *SI Appendix, Fig. S9*). NS1 displayed an intense fluorescence signal in the cytoplasm, especially in the perinuclear region and, to a smaller extent, at the cell membrane (Figs. 4A and 5A and D). The dots at the cell membranes were prominent at high cell confluence, in agreement with the role of eNOS in the maintenance of tight cell-to-cell junctions (21). The subcellular localization of NS1 within organelles was then further investigated by colocalization experiments. NS1 mainly colocalized with the Golgi apparatus (Fig. 4E–H). NS1 did not colocalize with the endoplasmic reticulum, cell nucleus, or mitochondria, whereas only partial colocalization was observed with early endosome (EEA1) (*SI Appendix, Fig. S10*). The two main locations of NS1 (Golgi and plasma membrane) are compatible with the subcellular localization of eNOS (22). Using specific immunostaining of eNOS combined to one- (Fig. 5A–C) or two-photon (Fig. 5D–F) imaging of NS1, we observed an excellent colocalization of NS1 and eNOS in the perinuclear region and at the plasma membrane level, showing that NS1 actually targets eNOS in HUVEC cells. Because the 2-PE process avoided cellular autofluorescence, the signal-to-noise ratio was remarkably higher using two-photon compared to one-photon imaging, as judged by the more restricted colocalization area obtained using $\lambda_{\text{ex}} = 840\ \text{nm}$ instead of 488 nm.

Discussion

NS1 fulfilled a double functionality: (i) a new prototype of a reversible NOS inhibitor, targeting the reductase domain in a specific manner and competing with NADPH; (ii) a unique fluorescent compound with 2-PE properties when bound to constitutive eNOS or nNOS. These two functions result from a rational design of a push–pull nitroaminostilbene chromophore moiety that cannot inject reducing equivalents required for triggering NOS catalysis, and that is highly sensitive to solvent polarity and to the presence of water in terms of fluorescence quantum yield (16).

Available NOS inhibitors include analogs of substrate L-arginine, calmodulin antagonists, and irreversible flavin inhibitor DPI and its analogs (11) as nonspecific inhibitors of electron transfer. NS1 represents a unique prototype of NOS inhibitor that competes with the initial hydride donor NADPH for binding to the reductase domain. Consequently, NS1 appears as a site-specific, reversible inhibitor that prevents both NO formation and NOS uncoupling by blocking the electron flow (flavins and heme). As such, avoiding the formation of toxic ROS and NO concentrations offers great perspectives, in particular for therapeutic strategies for, on the one hand, targeting nNOS and iNOS in the treatment of neurodegeneration, inflammation, and cancer (5), and, on the other hand, controlling eNOS activity and inhibiting deleterious effects of NO produced by eNOS in metastasis (7). Because eNOS constitutes the major source of NO production in endothelial cells and is an important regulator of cardiovascular homeostasis, further work is in progress for improving the isoform selectivity of NS1 in terms of molecular recognition, as well as for developing a photoactivation strategy for spatial and temporal control of eNOS inhibition by a two-photon-induced process.

In terms of NS1 imaging, a specific fluorescence enhancement upon binding to constitutive NOS was observed, with a preference for eNOS over nNOS. Compared to available NOS ligands,

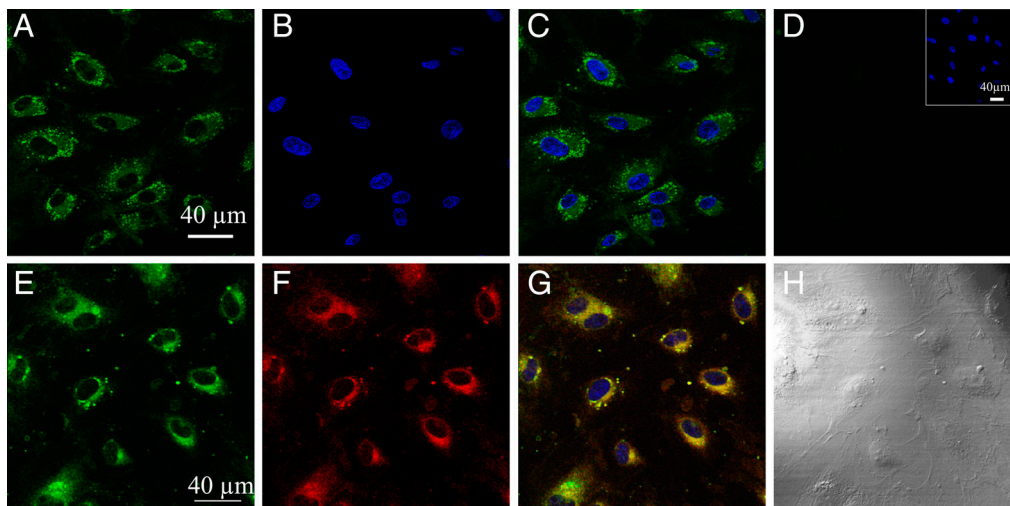


Fig. 4. Imaging of living HUVECs using the two-photon fluorescence properties of NS1 and colocalization with the Golgi complex. HUVECs were treated with 5 μ M NS1 and further observed under 2-PE (840 nm; emission at 520–680 nm) (A); (B) nucleus staining of NS1-treated HUVECs (2-PE, 740 nm; emission at 410–510 nm) by Hoechst 33342; (C) merged image of A and B; (D) control two-photon image of nontreated HUVECs at the same setting (*Inset*, nucleus staining of control cells); (E–H) colocalization imaging of NS1 and the Golgi complex—living HUVECs were treated with NS1 (5 μ M) and Golgi tracker (BODIPY TR ceramide; 5 μ M) for 60 min. (E) Shows the imaging channel of NS1 (1-PE, 488 nm; emission at 520–680 nm). (F) Shows the imaging channel of the Golgi tracker (1-PE, 543 nm; emission at 600–650 nm); (G) merged image of E and F (with nucleus staining). Yellow areas indicate colocalization of NS1 and the Golgi apparatus; (H) shows the corresponding differential interference contrast microscopy transmission image. Colocalization experiments with ER, mitochondria, and EEA1 are shown in *SI Appendix*, Fig. S10.

NS1 has the additional benefit of real-time imaging eNOS in living endothelial cells with excellent signal-to-noise ratio. This is of special interest because confinement effects on the subcellular location of eNOS have a profound effect on eNOS activity and are altered in pathological states (23). NS1 was highly photostable, without fading or blinking compared to fluorescent proteins (FP) or quantum dots (QD), respectively, and probed endogenous expression profiles of eNOS in contrast to exogenous fusion or QD-labeled proteins. Moreover, NS1 internalization did not require permeation mandated for immunostaining when using antibodies against eNOS. The excellent signal-to-noise ratio primarily relies on NS1 fluorescence enhancement by binding

to eNOS with negligible fluorescence either free or with nonspecific proteins. Additionally, NS1 is well-suited for two-photon studies because it has a much higher two-photon cross-section ($\sigma_2 = 130$ and 65 GM at 840 and 940 nm, respectively) than that of flavins and NAD(P)H (24, 25) [σ_2 (flavins) = 0.8 and 0.1 GM at 700 and 900 nm, respectively, or σ_2 (NADPH) = $5 \cdot 10^{-2}$ and $5 \cdot 10^{-6}$ GM at 700 and 900 nm, respectively]. Thus, the intrinsic advantage of NS1 relies on its two-photon absorption properties and ability for monitoring native eNOS using 2-PE without background or free NS1 contribution.

In conclusion, NS1 is a promising tool for noninvasive imaging of living tissues and isolated organs with an enhanced spatial resolution and a better light penetration in living tissues, leading to potential applications for monitoring eNOS within tumor cells as melanoma. Improvement of the selectivity of the NS1 prototype toward nNOS should afford an interesting pharmacological and imaging tool for neurodegenerative diseases.

Methods

Molecular Modelling. Molecular dynamics simulations of nNOS–NS1 and nNOS–NT1 complexes were carried out using the program NAMD with the CHARMM27 force field (26). eNOS and iNOS reductase domains were generated by homology modelling based on the structure of the nNOS isoform (1TLL) (4). The solvent was treated explicitly. Electrostatic interactions were calculated with no truncation, using the particle mesh Ewald summation algorithm. The van der Waals interactions were smoothly shifted to zero between 10.0 Å and 12.0 Å. The list of the nonbonded interactions was truncated at 13.5 Å. The lengths of the bonds containing hydrogen atoms were fixed with the SHAKE algorithm, allowing us to use an integration time of 2 fs. Trajectories of 10 ns each were produced for nNOS-bound NS1 and NT1 and for the eNOS–NS1 and iNOS–NS1 complexes.

Synthesis of NS1. The substituted aldehyde **3** was prepared from *N*-ethyl-aniline and phthalimido-acetaldehyde **1** in the presence of $\text{NaBH}(\text{OAc})_3$, followed by a Vilsmeier formylation of disubstituted aniline **2**. The Knoevenagel-type condensation of 4-nitrophenyl-acetic acid with **3** led to the pure *E*-4-(4-nitrostyryl)aniline derivative **4**. The phthalimido group was removed using the NaBH_4 -HOAc method (27). A peptide coupling reaction with HBTU in anhydrous DMF assembled the chromophore **5** and the 2'-3'-*iso*-propylidene adenosine 5-carboxylic acid **6** (28). After HCl deprotection of the *iso*-propylidene moiety of compound **7**, diol **8** was phosphorylated at positions 2' and 3' by treatment with chlorodiethylphosphate in anhydrous CH_2Cl_2 . Further acidic hydrolysis of the diethylphosphate afforded the

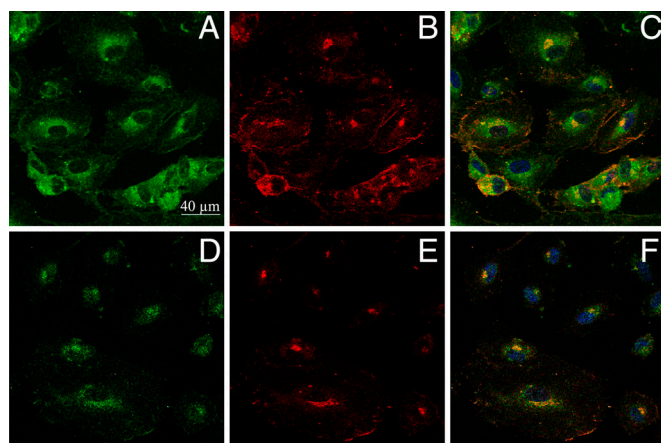


Fig. 5. Colocalization imaging of NS1 and eNOS. Living HUVECs were treated with NS1 (10 μ M) for 60 min prior to fixation and immunostaining of eNOS. Primary and secondary antibodies for immunostaining were purified mouse anti-eNOS/NOS Type III and AlexaFluor 594 goat anti-mouse IgG (H + L), respectively. (A and D) Imaging channel of NS1 [1-PE (488 nm) and 2-PE (840 nm), respectively; emission at 520–680 nm]; (B and E) imaging channel of eNOS (1-PE, 543 nm; emission at 590–700 nm), corresponding to A and D, respectively; (C) merged image of A and B; (F) merged image of D and E. Yellow to orange areas indicate colocalization of NS1 and eNOS. Nucleus staining by Hoechst 33342 is also shown in C and F. Upon prolonged incubations (1–3 h) with NS1 (1–10 μ M), the cells did not modify their shapes without fading of NS1 signal upon 1-PE and 2-PE.

expected NS1 as a mixture of isomeric compounds **9** and **10** bearing the P(O)(OH)₂ group at positions 2' and 3' in a 40:60 ratio, respectively (see *SI Appendix, Fig. S2*).

Expression and Purification of Proteins. Recombinant rat nNOS, murine iNOS, and bovine eNOS were expressed in *Escherichia coli* BL21 cells whereas eNOS reductase domain was expressed in yeast and purified as described (29, 30).

Spectroscopic Characterization of Free or NOS-Bound NS1. UV-visible absorption spectrum of NS1 was carried out with an Uvikon spectrophotometer. Fluorescence excitation and emission spectra under one-photon excitation condition were recorded on an Eclipse (Varian) fluorimeter. Two-photon excitation and emission spectra were recorded using a home-built setup. Briefly, an 80-MHz mode-locked Mai-Tai Ti:Sapphire tunable laser (690–1,040 nm, 100-fs laser pulse; Spectra Physics) was focused onto the sample placed in a quartz micro cell. The fluorescence was collected at 90°, filtered by a Semrock FF01-842/SP filter, and focused into an optical fiber connected to a SpectraPro-275 digital spectrograph coupled to CCD detector (Princeton Instruments).

Stopped-Flow Experiments. Kinetics of the reaction between nNOS (5 μM) and NADPH were measured at 24 °C in an anaerobic chamber (Coy Laboratory Products Inc.) using a Bio-SEQUENTIAL DX-18MV stopped-flow instrument (Applied Photophysics). The solutions of NADPH (25 μM) and NS1 (0–100 μM) were prepared in oxygen-free buffer. Reaction rates were calculated by fitting data to single- or double-exponential functions using Applied Photophysics software.

Effect of NS1 on the Formation of NO Catalyzed by nNOS. The initial rates of NO formation were determined at 37 °C in 1-cm path-length cuvettes (150 μl) on

a Uvikon 941 spectrophotometer using the oxyhemoglobin assay. The NO-mediated conversion of oxyhemoglobin to methemoglobin was monitored by repetitive scanning between 380 and 480 nm every 0.2 min. All values are means ± SD from 3–4 experiments.

Imaging of Living HUVEC Cells in the Presence of NS1 and Colocalization Experiments. NS1 was incubated with HUVECs (Sigma, at fourth passage) for 30 min using fresh medium before observation. One- and 2-photon images of living NS1-treated HUVECs were obtained using a SP2 confocal microscope (Leica Microsystems) and a laser line at 488 nm or an 80-MHz mode-locked Mai-Tai Ti:Sapphire laser (720–920 nm, 100-fs laser pulse; Spectra Physics) tuned to 840 nm, respectively (the emission range was set between 520 and 680 nm). Colocalization experiments of NS1 with endoplasmic reticulum (ER), mitochondria, or Golgi complex were performed on living HUVEC cells using ER-Tracker Red dye, MitoTracker Deep Red FM, or BODIPY TR ceramide complexed to BSA (Invitrogen), respectively. Colocalization of NS1 with early endosome (EEA1) or eNOS was performed by immunostaining on fixed cells using rabbit polyclonal to EEA1 marker (Abcam) or purified mouse anti-eNOS/NOS Type III (BD-Biosciences), respectively, as primary antibodies.

ACKNOWLEDGMENTS. The authors thank Dr. Lambry for providing initial parameter files and Dr. Lee-Ho Wang (University of Texas Health Science Center at Houston, TX) for providing protein samples. This work was funded by the French National Research Agency Grant (ANR-PCV108-006-01 to A.S.-S., J.-L.B., and E.D.) and fellowships (to B.T. and L.M.) and National Institutes of Health Grant HL095820 (to A.-L.T.). This work was granted access to the High Performance Computing (HPC) resources of Institut du Développement et des Ressources en Informatique Scientifique (IDRIS) made by Grand Equipement National de Calcul Intensif (GENCI) under Grant 2010-99636 (to A.S.-S. and B.T.).

- Moncada S, Palmer RM, Higgs EA (1991) Nitric oxide: Physiology, pathophysiology and pharmacology. *Pharmacol Rev* 43:109–142.
- Jachymova M, et al. (2005) Recruitment of governing elements for electron transfer in the nitric oxide family. *Proc Natl Acad Sci USA* 102:15833–15838.
- Li H, Poulos TL (2005) Structure-function studies on nitric oxide synthases. *J Inorg Biochem* 99:293–305.
- Garcin ED, et al. (2004) Structural basis for isozyme-specific regulation of electron transfer in nitric-oxide synthase. *J Biol Chem* 279:37918–37927.
- Pacher P, Beckman JS, Liaudet L (2007) Nitric oxide and peroxynitrite in health and disease. *Physiol Rev* 87:315–424.
- Silverman RB (2009) Design of selective neuronal nitric oxide synthase inhibitors for the prevention and treatment of neurodegenerative diseases. *Acc Chem Res* 42:439–451.
- Lim KH, Anrile BB, Kashatus DF, Counter CM (2008) Tumour maintenance is mediated by eNOS. *Nature* 452:646–649.
- Lahdenranta J, et al. (2009) Endothelial nitric oxide synthase mediates lymphangiogenesis and lymphatic metastasis. *Cancer Res* 69:2801–2808.
- Crane BR, et al. (2000) Structures of the N(omega)-hydroxy-L-arginine complex of inducible nitric oxide synthase oxygenase dimer with active and inactive pterins. *Biochemistry* 39:4608–4621.
- Raman ED, et al. (1998) Crystal structure of constitutive endothelial nitric oxide synthase: A paradigm for pterin function involving a novel metal center. *Cell* 95:939–950.
- Stuehr DJ, et al. (1991) Inhibition of macrophage and endothelial cell nitric oxide synthase by diphenyliodonium and its analogs. *FASEB J* 5:98–103.
- Beaumont E, et al. (2009) NO formation by neuronal NO-synthase can be controlled by ultrafast electron injection from a nanotrigger. *ChemBioChem* 10:690–701.
- Beaumont E, et al. (2007) Synchronous photoinitiation of endothelial NO synthase activity by a nanotrigger targeted at its NADPH site. *J Am Chem Soc* 129:2178–2186.
- Beaumont E, et al. (2008) Two photon-induced electron injection from a nanotrigger in native endothelial NO-synthase. *ChemPhysChem* 9:2325–2331.
- Akemann W, Laage D, Plaza P, Martin MM, Blanchard-Desce M (2008) Photoinduced intramolecular charge transfer in push-pull polyenes: Effects of solvation, electron-donor group, and polyenic chain length. *J Phys Chem B* 112:358–368.
- Lapouyade R, Kuhn A, Letard JF, Rettig W (1993) Multiple relaxation pathways in photoexcited dimethylaminonitro- and dimethylaminocyno-stilbenes. *Chem Phys Lett* 208:48–58.
- Lambry JC, Beaumont E, Tarus B, Blanchard-Desce M, Slama-Schwok A (2010) Selective probing of a NADPH site controlled light-induced enzymatic catalysis. *J Mol Recognit* 23:379–388.
- Paper V, Pines D, Likhenstein G, Pines E (1997) Photophysical characterization of trans-4,4'-disubstituted stilbenes. *J Photochem Photobiol A* 111:87–96.
- Kirk WR (2005) The binding of 1,8 ANS congeners to I-FABP and comparison of some hypotheses about ANS' spectral sensitivity to environment. *Biochim Biophys Acta* 1748:84–93.
- Di Primo C, Deprez E, Hoa GH, Douzou P (1995) Antagonistic effects of hydrostatic pressure and osmotic pressure on cytochrome P-450cam spin transition. *Biophys J* 68:2056–2061.
- Rath G, Dessy C, Feron O (2009) Caveolae, caveolin and control of vascular tone: Nitric oxide (NO) and endothelium derived hyperpolarizing factor (EDHF) regulation. *J Physiol Pharmacol* 60(Suppl 4):105–109.
- Fulton D, et al. (2002) Localization of endothelial nitric-oxide synthase phosphorylated on serine 1179 and nitric oxide in Golgi and plasma membrane defines the existence of two pools of active enzyme. *J Biol Chem* 277:4277–4284.
- Villanueva C, Giulivi C (2010) Subcellular and cellular locations of nitric oxide synthase isoforms as determinants of health and disease. *Free Radic Biol Med* 49:307–316.
- Huang S, Heikal AA, Webb WW (2002) Two-photon fluorescence spectroscopy and microscopy of NAD(P)H and flavoprotein. *Biophys J* 82:2811–2825.
- Xu HN, Nioka S, Glickson JD, Chance B, Li LZ (2010) Quantitative mitochondrial redox imaging of breast cancer metastatic potential. *J Biomed Opt* 15:036010.
- Folloppe N, MacKerell AD (2000) All-atom empirical force field for nucleic acids: I. Parameter optimization based on small molecule and condensed phase macromolecular target data. *J Comp Chem* 21:86–104.
- Benkeser RA, Laugal JA, Rappa A (1984) Safe method for reduction of aromatic compounds. *Tetrahedron Lett* 25:2089–2092.
- Robin AC, et al. (2007) A NADPH substitute for selective photo-initiation of reductive bioprocesses via two-photon induced electron transfer. *Chem Comm* 43:13333–13336.
- Moali C, Boucher JL, Sari MA, Stuehr DJ, Mansuy D (1998) Substrate specificity of NO synthases: Detailed comparison of L-arginine, homo-L-arginine, their N omega-hydroxy derivatives, and N omega-hydroxy-L-arginine. *Biochemistry* 37:10453–10460.
- Du M, Yeh HC, Berka V, Wang LH, Tsai AL (2003) Redox properties of human endothelial nitric-oxide synthase oxygenase and reductase domains purified from yeast expression system. *J Biol Chem* 278:6002–6011.

SUPPLEMENTARY INFORMATION

Rational design of a fluorescent NADPH derivative imaging constitutive nitric oxide synthases upon two-photon excitation.

Yun Li^{*,||}, Huan Wang^{†,||}, Bogdan Tarus^{‡,||}, Miguel Romero Perez[§], Laurence Morellato^{*}, Etienne Henry[†], Vladimir Berka[¶], Ah-Lim Tsai[¶], Booma Ramassamy^{*}, Hamid Dhimane^{*}, Chantal Dessy[§], Patrick Tauc[†], Jean-Luc Boucher^{*}, Eric Deprez^{†,**} and Anny Slama-Schwok^{‡,**}.

[^{*}] Laboratoire de Chimie et Biochimie Pharmacologiques et Toxicologiques, CNRS UMR8601, Université Paris Descartes, Paris, France.

[[†]] Laboratoire de Biologie et Pharmacologie Appliquée (LBPA), CNRS UMR8113, ENS-Cachan, Cachan, France.

[[‡]] Laboratoire de Virologie et Immunologie Moléculaires, INRA UR892, Jouy en Josas, France.

[[§]] Pole of Pharmacology and Therapeutics, FATH5349, IREC, UCL Medical Sector, B-1200 Brussels, Belgium.

[[¶]] Division of Hematology, Department of Internal Medicine, University of Texas Health Science Center at Houston, Texas, USA.

^{||} These co-first authors contributed equally to this work

^{**} Eric Deprez and Anny Slama-Schwok contributed equally to the work.

Corresponding authors: Dr Anny Slama-Schwok Anny.Schwok@gmail.com,
And Dr Eric Deprez deprez@lbpa.ens-cachan.fr

Table of contents

	Contents
Supplementary Table	Table S1: Page 2
Supplementary Figures	Fig. S1-S10: Pages 2-13
Supplementary Methods	Page 14-17
Supplementary References	Page 18-19

SUPPLEMENTARY TABLE:

Table S1. Comparison of the interaction energies of bound NS1 and NT1 at the NADPH site of nNOS_{red} as determined by molecular modelling.

Energy (kcal/mol)	NS1 in nNOS _{red}	NT1 in nNOS _{red}
Nucleotidic moiety:	- 458 ± 57	- 423 ± 26
Linker:	- 57 ± 6	- 38 ± 7
Chromophore:		
- Total	- 14 ± 7	- 26 ± 4
- van der Waals term	-39 ± 4	- 35 ± 3
- Electrostatic term	25 ± 5	9 ± 4
Total	- 529 ± 68	- 487 ± 25

SUPPLEMENTARY FIGURES:

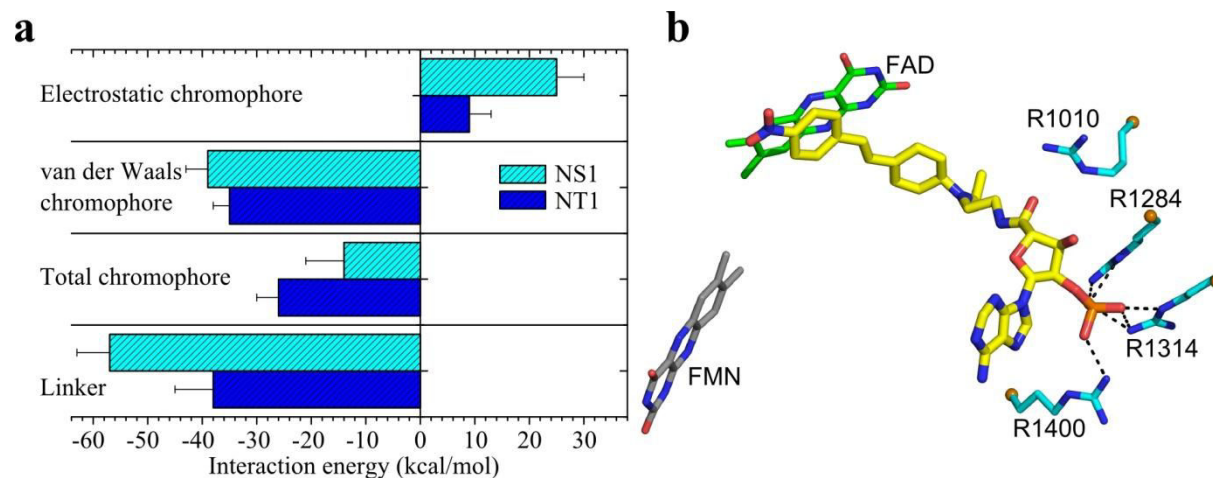


Fig. S1: (a) Effects of the linker and the chromophoric terminal group (NH_2 or NO_2) of NT1 or NS1 on the recognition of nNOS_{red} at the NADPH site. Comparison of the interaction energies of the chromophore and linker parts of NS1 and NT1 with nNOS_{red} (see also Table S1): the unfavorable electrostatic term is compensated by the van der Waals (VdW) interaction energies of the chromophore and the linker. **(b) NS1 binding in the NADPH site of nNOS reductase domain.** Overall binding of NS1 at the NADPH site by multiple H-bonds with conserved arginine residues of nNOS_{red} : the phosphate group of NS1 interacts with R1284, R1314 and R1400 and the carbonyl of the amide linker forms transient H-bond with R1010 while its chromophore terminal nitrophenyl group stacks on FAD.

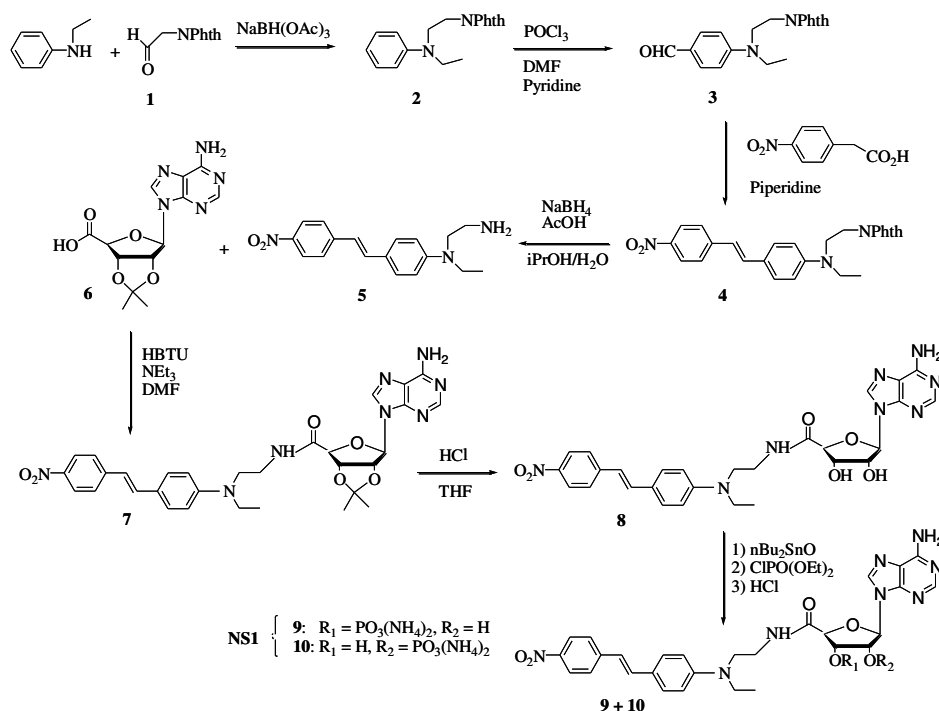


Fig. S2: Synthetic steps leading to NS1. The disubstituted aniline **2** was prepared by reductive amination of phthalimido-acetaldehyde **1** by *N*-ethylaniline in the presence of $\text{NaBH}(\text{OAc})_3$. The substituted benzaldehyde **3** was prepared by a Vilsmeier's formylation of compound **2** under usual conditions (POCl_3 in DMF containing pyridine). The Knoevenagel's type condensation of 4-nitrophenyl-acetic acid with **3** led to the pure *E*-4-(4'-nitrostyryl)aniline derivative **4**. As the commonly used NH_2NH_2 method failed to deprotect the phthalimido group, it was removed using the NaBH_4 -HOAc method giving the expected chromophore **5**. A peptide coupling reaction with HBTU in anhydrous DMF linked the chromophore **5** and the 2'-3'-*iso*-propylidene adenosine 5-carboxylic acid **6**. After HCl deprotection of the *iso*-propylidene moiety of compound **7**, diol **8** was phosphorylated at positions 2'- and 3'- by treatment with chlorodiethylphosphate in anhydrous CH_2Cl_2 . Further acidic hydrolysis of the diethylphosphate afforded the expected compound NS1 as a mixture of two regioisomers **9** and **10** that bear the $\text{P}(\text{O})(\text{OH})_2$ group at positions 2'- and 3'- in a 40:60 ratio, respectively. See Supplementary Methods for more information.

These two isomers could be separated by analytical HPLC. Because these isomers can interconvert (1) and we estimated the K_d difference of the 2' over the 3' isomer not to exceed a factor 2-3, we did not attempt to set up conditions for a preparative separation of the 2' and 3' isomers (See Supplementary Methods for more information).

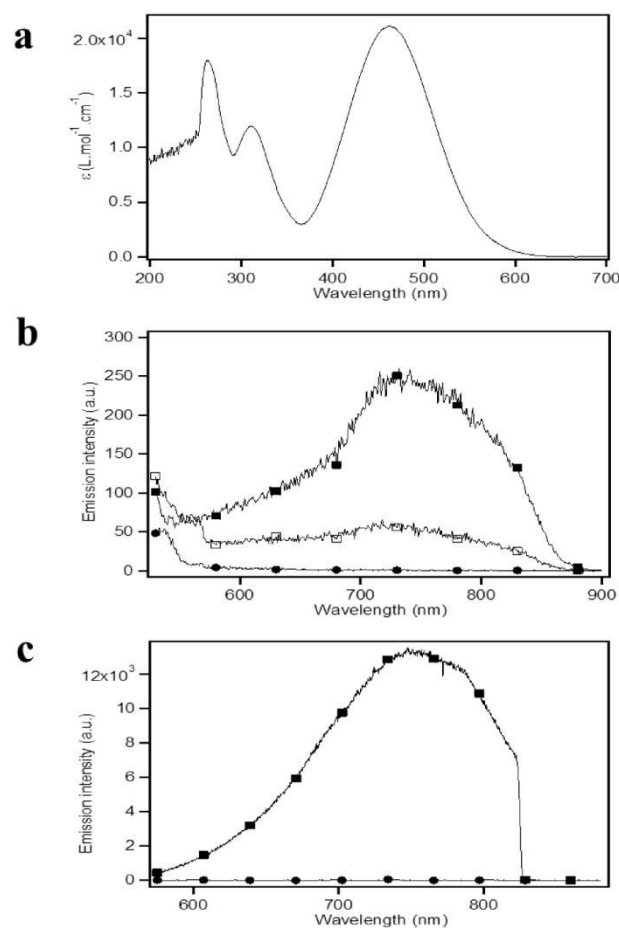


Fig. S3: Spectroscopic and fluorescence properties of NS1 in solution. (a) Absorption spectrum of NS1 in DMSO. (b) Fluorescence emission spectrum of NS1 (10 μM) upon one-photon excitation ($\lambda_{\text{ex,1-PE}} = 460 \text{ nm}$) in DMSO alone (black squares), in a DMSO : water mixture (67% : 33%, v:v) (white squares), or in 50 mM Tris buffer pH 7.5 containing 150 mM NaCl (black circles). (c) Fluorescence emission spectrum of NS1 (10 μM) upon two-photon excitation ($\lambda_{\text{ex,2-PE}} = 940 \text{ nm}$) in DMSO (black squares) or in 50 mM Tris buffer pH 7.5 containing 150 mM NaCl (black circles). The fluorescence quantum yield (Φ) and the two-photon cross-section (σ_2) of NS1 in DMSO were determined using rhodamine B as a reference and were found to be equal to 0.0045 and 65 GM at 940 nm, respectively. 1 Göppert-Mayer = $10^{-50} \text{ cm}^4 \cdot \text{s}/\text{photon}$.

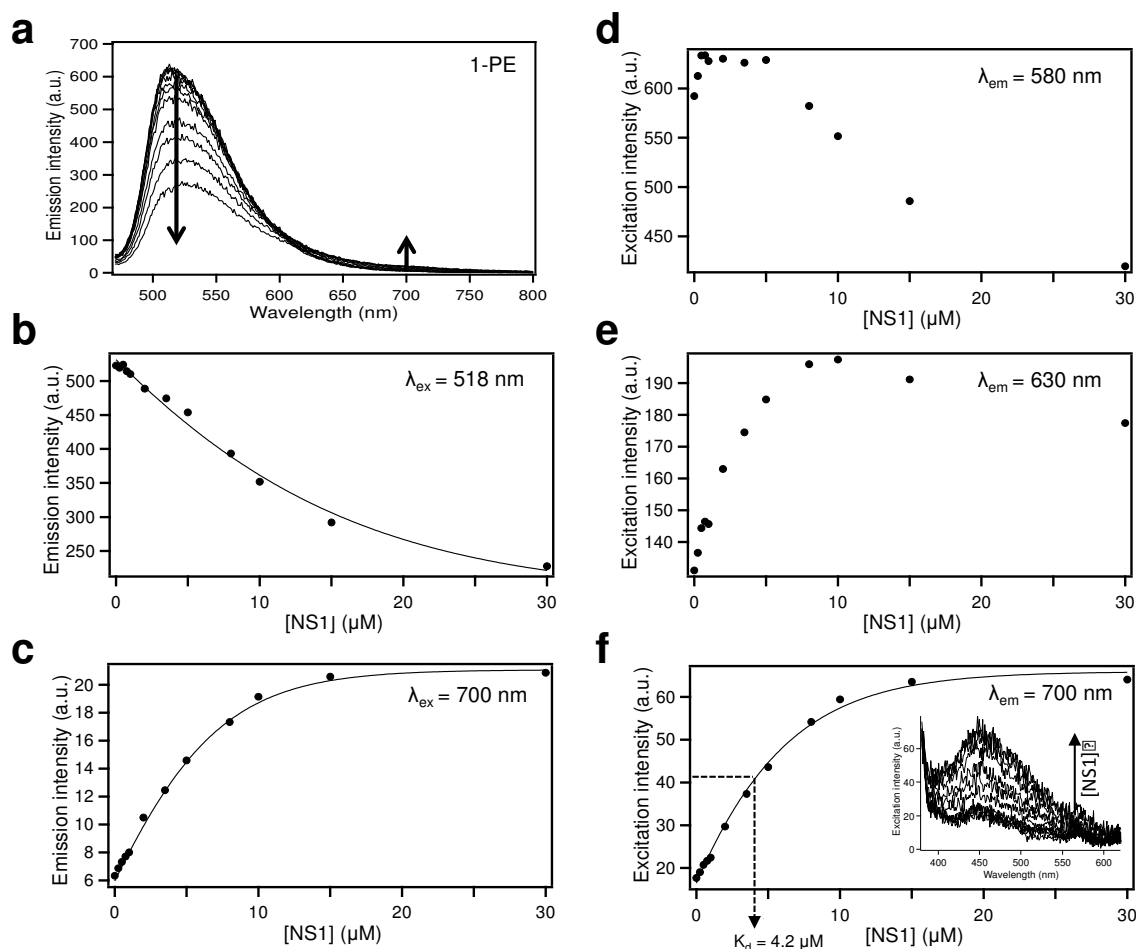


Fig. S4: Binding of NS1 to nNOS (5 μM) monitored by one-photon excitation fluorescence (1-PE). (a) Influence of NS1 on the fluorescence emission spectrum of nNOS ($\lambda_{\text{ex,1-PE}}$, 460 nm). The arrows indicate the decrease or increase in emission intensities at 518 or 700 nm, respectively, when increasing [NS1] (quantified in panels b-c). Panels (d-f), the excitation intensity in the 430-490 nm range was plotted against [NS1]; λ_{em} : 580 (d), 630 (e) or 700 nm (f) (inset: excitation spectra showing a continuous increase in the excitation intensity upon increasing [NS1]).

Using $\lambda_{\text{ex}} = 460$ nm, the emission intensity (518 nm) continuously decreased when increasing [NS1] (Fig. S4a). Concomitantly, the intensity increased on the red side of the emission spectrum (>610 nm), where the contribution of NS1 fluorescence is expected to be larger than the contribution of nNOS. Both changes in the intensity values reached a plateau upon increasing [NS1], indicating that NS1 actually bound to nNOS (Fig. S4b-c). As NS1 was not fluorescent in aqueous buffer, this indicated a recovery of NS1 fluorescence upon binding to nNOS. The decrease of the intensity (518 nm) is most likely due to a resonance energy transfer between FAD (donor) and NS1 (acceptor) that results from the significant overlap of FAD emission and NS1 absorption. Regarding the excitation intensity in the 430-490 nm region, using $\lambda_{\text{em}} = 580$ or 630 nm (Fig. S4d-e), a decreasing phase was observed when plotting the excitation intensity as a function of [NS1], consistent with the observed decrease in the emission intensity at 518 nm as mentioned above. This decreasing phase was less pronounced at 630 compared to 580 nm as the contribution of nNOS fluorescence relative to that of NS1 decreased by using a red-shifted λ_{em} . No decreasing phase was observed with $\lambda_{\text{em}} = 700$ nm, allowing quantitative titration of nNOS with NS1. A typical hyperbolic binding isotherm was obtained at this λ_{em} only (Fig. S4f; $K_d = 4.2 \pm 1.1$ μM), but with a rather modest change in its intensity. The excitation maximum of NS1 bound to nNOS, 450 nm, was similar with NS1 absorption/excitation maximum in DMSO (Fig. S4f, inset).

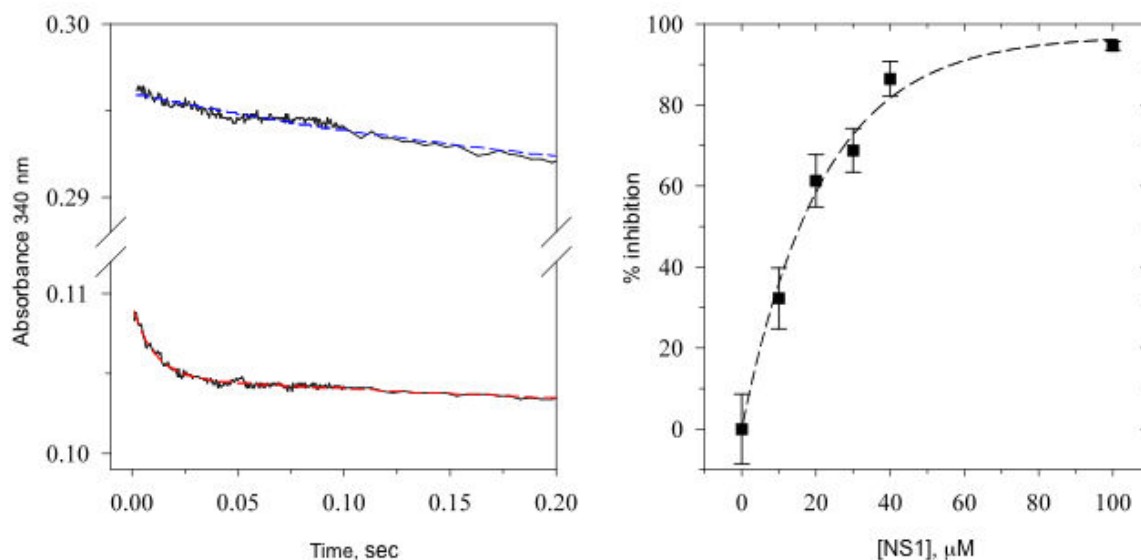


Fig. S5: Inhibition by NS1 of hydride transfer from NADPH to FAD in nNOS monitored by stopped-flow experiment. Left panel shows the raw absorbance changes at 340 nm after mixing of 25 μM NADPH with 5 μM nNOS (bottom trace) or 25 μM NADPH with 100 μM NS1 and 5 μM nNOS (upper trace); the dashed lines represent bi-exponential fit of the data. Right panel shows that NS1 inhibited the fast phase in a dose-dependent saturable manner typical for competitive inhibition with NADPH. This fast phase is attributed to hydride transfer from NADPH to FAD. The slow phase remains unaffected by [NS1].

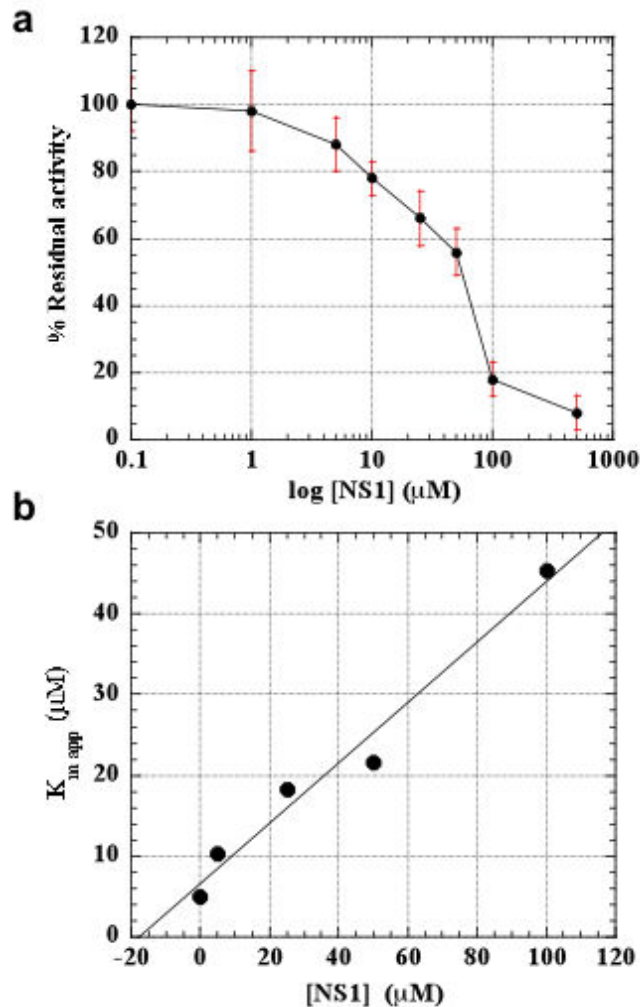


Fig. S6: Inhibition by NS1 of the formation of NO by nNOS: competition experiments between NADPH and NS1. Panel (a) shows the concentration-dependant inhibition of NO formation by NS1 in an assay performed in the presence of 100 μM NADPH. Maximal activity for nNOS was $78 \pm 15 \mu\text{M NO}\cdot\text{min}^{-1}\cdot\text{mM heme}^{-1}$. The IC_{50} value was found to be 65 μM . Using the Cheng-Prusoff ($K_i = \text{IC}_{50}/(1+[\text{NADPH}]/K_d)$), the K_i value was estimated to be 3.4 μM (assuming a K_m value of 5.5 μM). Panel (b) shows secondary plot of $K_{m,app}$ as a function of NS1 concentration ($K_{m,app} = K_m(1+[\text{NS1}]/K_i)$). Intercept with the x-axis indicates a K_i value of 18 μM and the slope indicates a K_i value of 13 μM (assuming $K_m = 5.5 \mu\text{M}$). nNOS was incubated in 50 mM Hepes buffer at pH 7.4 containing 100 μM L-arginine, 100 $\mu\text{g/ml}$ CaM, 1 mM CaCl_2 , 100 U/ml SOD, 100 U/ml catalase and 8-10 μM oxyhemoglobin. Under identical conditions, the IC_{50} values for the endothelial NOS (maximal activity: $12 \pm 5 \mu\text{M NO}\cdot\text{min}^{-1}\cdot\text{mM heme}^{-1}$) and the inducible NOS (maximal activity: $150 \pm 25 \mu\text{M NO}\cdot\text{min}^{-1}\cdot\text{mM heme}^{-1}$) were $80 \pm 15 \mu\text{M}$ and $\geq 200 \mu\text{M}$, respectively. The specific activities measured by hemoglobin and C^{14} arginine to citrulline conversion methods were in good agreement with each other and are as follows:

nNOS: $260 \pm 50 \text{ nmole}\cdot\text{min}^{-1}\cdot\text{mg prot}^{-1}$ ($78 \pm 15 \text{ s}^{-1}$)
iNOS: $600 \pm 100 \text{ nmole}\cdot\text{min}^{-1}\cdot\text{mg prot}^{-1}$ ($150 \pm 25 \text{ s}^{-1}$)
eNOS: $45 \pm 22 \text{ nmole}\cdot\text{min}^{-1}\cdot\text{mg prot}^{-1}$ ($12 \pm 5 \text{ s}^{-1}$)

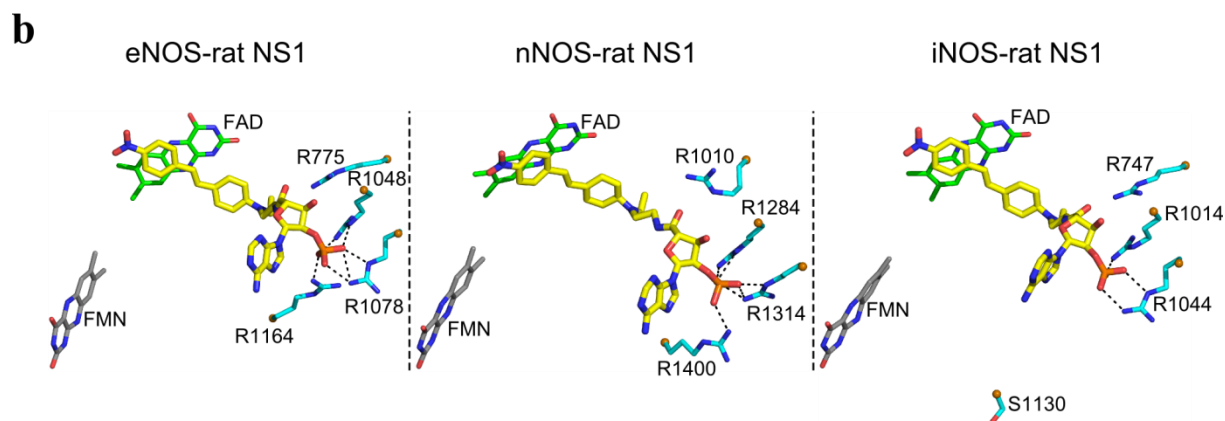
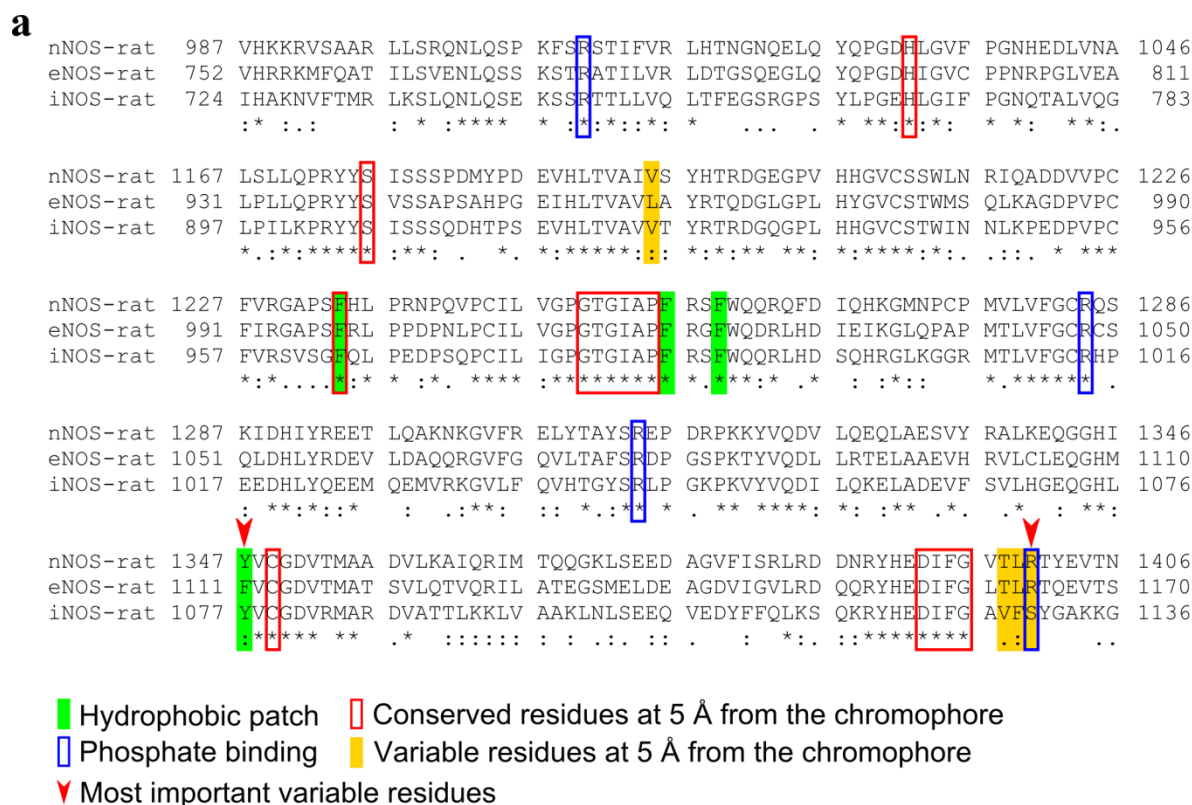


Fig. S7: (a) Alignment of NOS reductase domains and identification of residues within 5 Å to NS1. (b) Comparison of NS1 binding in the NADPH site of eNOS, nNOS and iNOS reductase domains. The 3D-structures of eNOS (left) and iNOS (right) were generated by homology modeling as described (2) (see also supplementary methods). Docking of NS1 in iNOS differed from that in nNOS (or eNOS) by the replacement of R1400 (or R1164) by S1130; thus, the electrostatic interaction between NS1 phosphate and R1400 (or R1164) found in nNOS (or eNOS) lacks in iNOS.

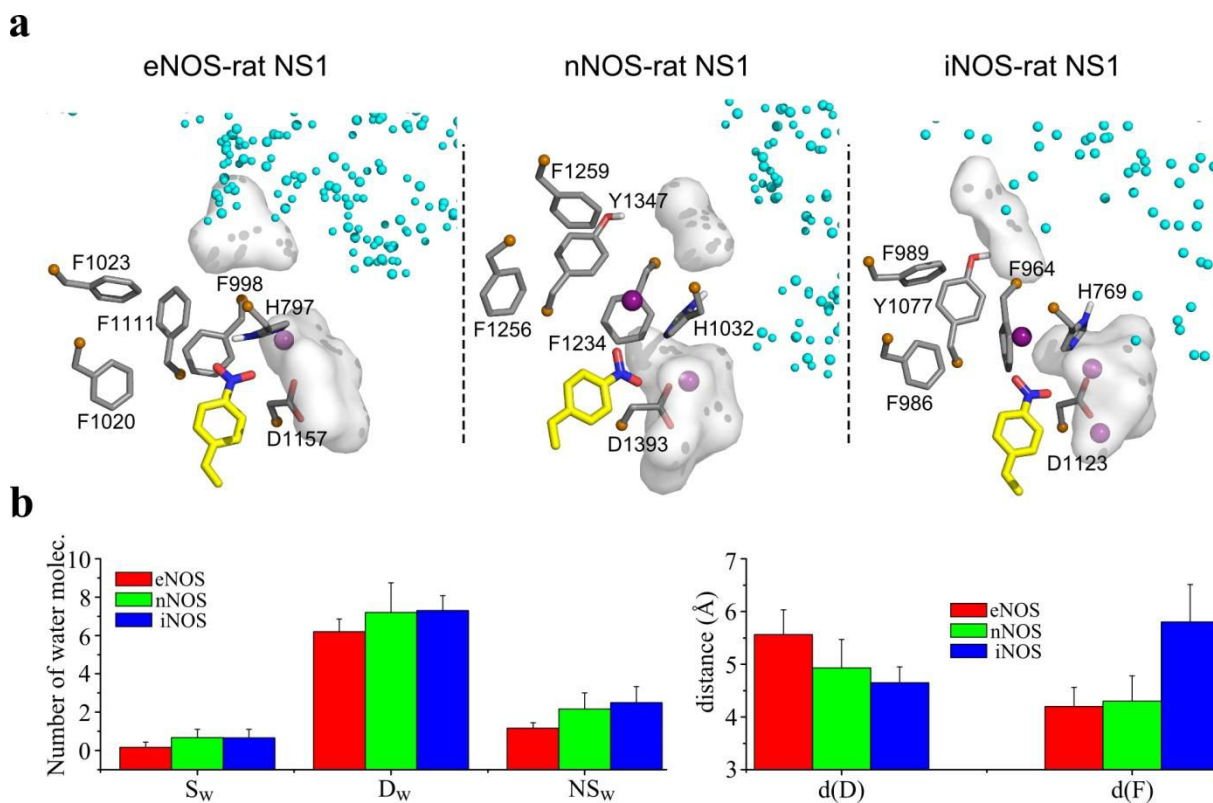


Fig. S8: (a) Structural insight on the solvation and hydrophobic patch in NS1 binding site zoomed at NS1 nitrophenyl terminal in three NOS isoforms. Solvation of D1393 and Y1347 is highlighted by white surfaces; water at 3.5 Å from the nitro group of NS1 is shown by large purple spheres while the water at 3.5 Å from the interface between NOS monomers is depicted by small cyan spheres. **(b) Comparison of selected distances and solvation around the NO₂ terminal of NS1 in the three NOS isoforms as defined in the text below.**

To get quantitative estimates on the differences in solvation around NS1 between the three isoforms, we characterized the following:

- NS_w , the number of water at a distance of 3.5 Å to the nitro group of NS1, related to the residence of water molecules around NS1 chromophore; panels (a) and (b) show that NS_w is lowest in eNOS compared to the water found in nNOS and iNOS.
- D_w , the number of water molecules solvating D1393; D_w is within the error similar in eNOS, nNOS or iNOS, accounting for 6 to 8 water molecules.
- S_w , the solvation of Ser1176 by “catalytic” water and/or by His1032. The lowest number of water molecules around S940 is found in eNOS while S940 is closest to H797 in eNOS compared to both nNOS and iNOS. Previous point mutation studies have shown that the water molecule (“catalytic” water) around Ser1176 (nNOS) has a key role in the proton transfer as part of the hydride transfer step (in a general acid/base in the protonation / deprotonation of the N1 atom of the flavin that is necessary during catalysis (3-5).
- d_D , the minimum distance between side-chain heavy atoms of D1393, D1157 or D1123 (n/e/iNOS) to the N atom of nitro group, d_D is largest in eNOS and decreases in nNOS and iNOS (panel (a)).
- d_F , the minimum distance between side-chain heavy atoms distance of F1234, F998 or F964 (n/e/iNOS) to the the N atom nitro group, d_F is largest in iNOS compared to eNOS and nNOS.

Additional comment to Fig. S8:

Therefore, the NO₂ group in iNOS probes a more solvated environment. In contrast, the NO₂ group of NS1 in eNOS is located in the relatively more hydrophobic environment than in the two other NOS isoforms, characterized by the lowest distance to the conserved F998 and closest to the hydrophobic patch as compared to nNOS and iNOS (see also Fig. 3). Altogether, NS1 probes a more hydrophobic environment in eNOS by a combination of light sequences changes, resulting in stronger hydrophobic interactions and less solvation. This effect is gradual from eNOS, through nNOS to iNOS. These hypotheses perfectly explain the decrease of fluorescent yield of NS1 from eNOS to iNOS, (NS1 in eNOS being the highest, Fig. 3) by local environment effects. This is in agreement with the previously reported decrease in the nitroaminostilbene fluorescence yield in DMSO as compared to CH₂Cl₂ (6). We cannot exclude that global effects at larger distance from NS1 arising from water at the protein – solvent interface could also contribute to explain the experimental findings. We did not observe a distortion of NS1 chromophore from planarity which is expected to affect the overall dipolar moment and the fluorescence yield by some character of “twisted” charge transfer state. It is likely that twisting around the double bond is impeded by steric effects in the NADPH binding site.

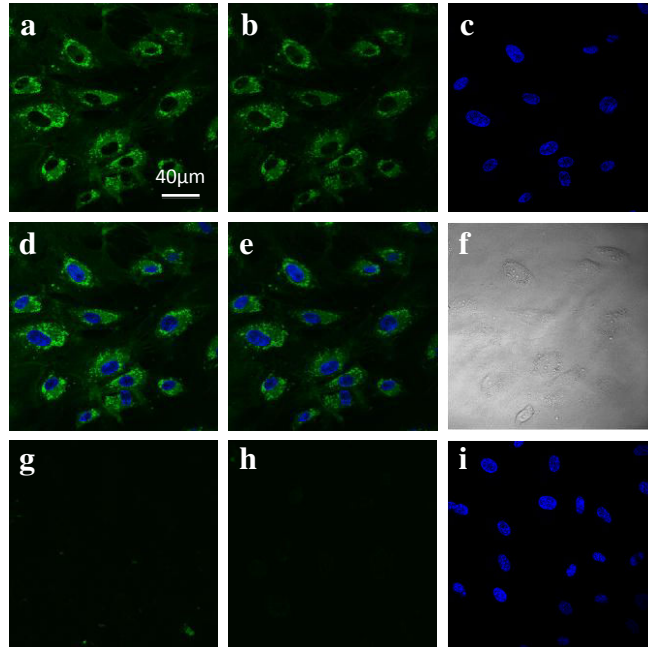


Fig. S9: Imaging of living HUVECs using one- or two-photon excitation of NS1. HUVECs were treated with NS1 (5 μ M) and further observed under either one-photon excitation (confocal microscopy; excitation, 488 nm) **(a)** or two-photon excitation (multiphoton microscopy; excitation, 840 nm) **(b)**. Emission setting was 520-680 nm. Panel **(c)** shows the nucleus staining of NS1-treated HUVECs by Hoechst 33342 (two-photon excitation, 740 nm; emission setting: 410-510 nm). Panels **(d)** and **(e)**: corresponding merges for one- and two-photon images, respectively. Panel **(f)**, DIC transmission image. Control cells (not treated with NS1) were observed under one-photon **(g)** or two-photon **(h)** excitation using the same settings as described for panels **(a)** and **(b)**, respectively. Panel **(i)** shows the nucleus staining of control HUVECs (not treated with NS1) by Hoechst 33342 (two-photon excitation, 740 nm).

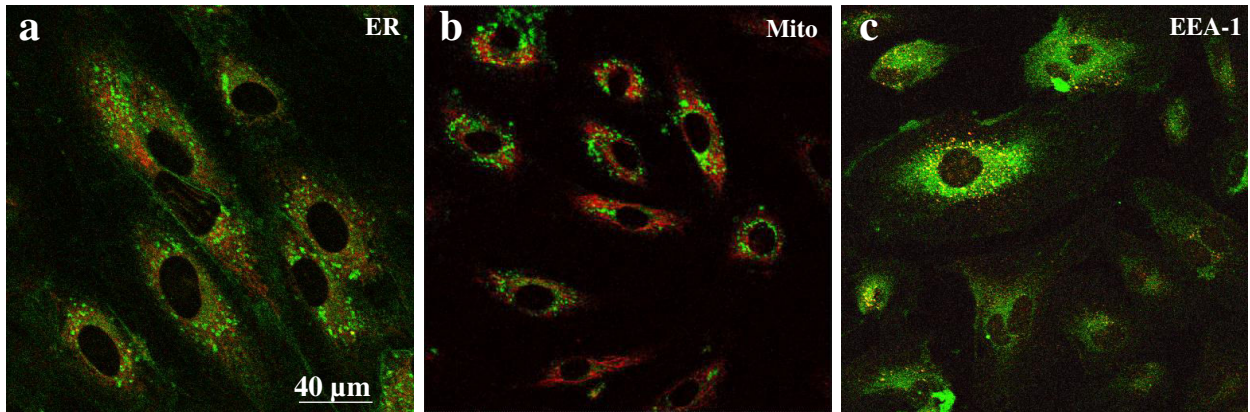


Fig. S10: Co-localization imaging of NS1 and Endoplasmic Reticulum (ER), Mitochondria or Early Endosome (EEA1). (a) Merged image of NS1 and ER. (b) Merged image of NS1 and mitochondria. Living HUVECs were treated with NS1 (5 μ M) and ER tracker (ER-TrackerTM Red dye; 100 nM) or MitoTracker (MitoTracker[®] Deep Red FM; 50 nM) for 30 min and further observed under confocal microscopy. (c) Merged image of NS1 and EEA1. Living HUVECs were treated with NS1 (10 μ M) for 60 min prior to fixation and immuno-staining of EEA1, and further observed under confocal microscopy. Primary and secondary antibodies for immuno-staining were rabbit polyclonal to EEA1-Early Endosome Marker and Alexa Fluor[®] 594 donkey anti-rabbit IgG (H+L), respectively. Excitation and emission settings: NS1 (exc. 488 nm; em. 520-680 nm), ER (exc. 543 nm; em. 590-670 nm), mitochondria (exc. 633 nm; em. 650-700 nm), EEA1 (exc. 543 nm; em. 590-700 nm).

SUPPLEMENTARY METHODS:

Molecular modelling. The MD simulations of the nNOS-NS1 and nNOS-NT1 complexes and eNOS-NS1, iNOS-NS1 complexes (the reductase domains of eNOS and iNOS were generated by homology modelling, see below) were carried out using the program NAMD (7) with the CHARMM27 force field (8). The solvent was treated explicitly using the TIP3P model for water molecules (9). The system formed by nNOS (or eNOS rat or iNOS rat) dimeric enzyme, FAD, FMN and NS1 (or NT1) was centred in a cubic cell of pre-equilibrated water molecules. The electrostatic interactions were calculated with no truncation, using the particle mesh Ewald summation algorithm (10). The system was made electrostatically neutral by adding sodium cations at coordinates of minimum electrostatic energy. The ion concentration of the system was set to 0.15 M by adding randomly sodium and chloride ions. The van der Waals interactions were smoothly shifted to zero between 10.0 Å and 12.0 Å. The list of the non-bonded interactions was truncated at 13.5 Å. The energy of the system was minimized during 5000 steps using the conjugate gradient energy minimization algorithm while the solute atoms were harmonically restrained to their initial positions with a force constant of 50.0 kcal/mol/Å². The system was heated linearly to 300 K over 60 ps. The lengths of the bonds containing hydrogen atoms were fixed with the SHAKE algorithm (11) and the equations of motion were iterated using a time step of 2 fs in the velocity Verlet integrator. Molecular dynamics simulation was further used to equilibrate the system and for production run. During the equilibration phase, the restraints applied on the solute atoms were gradually reduced from 5.0 kcal/mol/Å² to zero. The pressure and temperature were restrained to 1 atm and 300 K, respectively. Each system was simulated for 10 ns.

Homology modelling of eNOS-rat and iNOS-rat reductase domains. Homology modeling was performed using the x-ray structure of the neuronal NOS (nNOS-rat, PDB-ID: 1TLL) as template. The structure of the eNOS-rat was solved by homology modeling as reported previously (1). The iNOS-rat sequence was aligned on the nNOS-rat sequence using the ClustalX 2.1 program (11). Based on the sequence alignment and the coordinates of the monomeric form of the nNOS-rat (PDB id 1TLL), a Swiss-PdbViewer (12) project was made and submitted to the homology modeling website Swiss-Model Workspace (13). The sequence alignment (shown in Fig S7) revealed for the eNOS-rat 374 identical (56.3 %) and 139 similar (20.9 %) positions, accounting for a 77.3 % total homology. For the iNOS-rat there were found 305 identical (45.9%) and 139 similar (20.9%) positions, accounting for a 66.9 % total homology and a QMEAN score (14) of 0.659.

Chemistry, General. All reagents and solvents were from Sigma-Aldrich (Saint-Quentin-Fallavier, France) and were of the highest purity commercially available. High-purity argon (99.9995%) was obtained from Air Products. Phthalimidoacetaldehyde diethyl acetal (**1**) and 2',3'-*O*-isopropylidene adenosine carboxylic acid (**6**) were prepared from aminoacetaldehyde diethyl acetal and 2',3'-*O*-isopropylidene adenosine, respectively, according to known procedures (12, 13).

TLC was performed on pre-coated plates of Silica Gel 60F-254 (Merck, Lyon, France); compounds were detected by UV light. ¹H and ¹³C NMR spectra were recorded with a Bruker (Wissembourg, France) Biospin Avance II 250 MHz spectrometer, and chemical shifts refer to an internal standard of Me₄Si. Mass spectra were recorded by electrospray ionization (ESI) in both positive (ESI⁺) and negative (ESI⁻) ionization detection modes with a LCQ Advantage ion trap mass spectrometer (Thermo, Les Ulis, France). Elemental analyses were performed at ICSN (Gif sur Yvette, France) and high-resolution mass spectra (HRMS) were obtained by ESI in time-of-flight (TOF) detection mode on a LCT (Waters-Micromass, Guyancourt, France) spectrometer at ICSN (Gif sur Yvette, France).

Synthesis of NS1: The NADPH analogue NS1 was prepared as described in Fig. S2.

N-[2-(*N*-Ethylanilino)ethyl]phthalimide (**2**): NaBH(OAc)₃ (3.05 g, 14.4 mmol) was added to a solution of *N*-ethylaniline (1.16 g ; 9.6 mmol) and **1** (2.72 g, 14.4 mmol) in CH₂Cl₂ (28 mL). After 24 h at 20 °C, CH₂Cl₂ was added and the organic phase was washed with H₂O, dried (MgSO₄) and evaporated. The crude product was purified by chromatography over silica gel (80:20 CH₂Cl₂–cyclohexane) to afford **2** as a yellow solid (2.71 g, 96 %). ¹H NMR (250 MHz, CDCl₃): δ 7.85 (m, 2H), 7.71 (m, 2H), 7.24 (t, J = 7.8 Hz, 2H), 6.86 (d, J = 7.8 Hz, 2H), 6.67 (t, J = 7.8 Hz, 1H), 3.91 (dd, J = 6.5, 8.1 Hz, 2H), 3.58 (dd, J = 6.5, 8.1 Hz, 2H), 3.46 (q, J = 6.9 Hz, 2H), 1.22 (t, J = 7.0 Hz, 3H). ¹³C NMR (63 MHz, CDCl₃): δ 168.0 (C), 147.2 (C), 133.7 (CH), 131.8 (C), 129.2 (CH),

123.0 (CH), 116.0 (CH), 111.9 (CH), 47.8 (CH₂), 44.6 (CH₂), 35.0 (CH₂), 12.2 (CH₃). MS: *m/z* = 295 (MH⁺). Anal. calcd for C₁₈H₁₈N₂O₂ (294.14), C 73.45, H 6.16, N 9.52. Found C 73.33, H 6.17, N 9.62.

N-[2-(*N*-Ethyl-4-formyl-anilino)ethyl]phthalimide (**3**): POCl₃ (5.24 mL) was added dropwise to a solution of **2** (2.71 g, 9.2 mmol) in anhydrous pyridine (4.50 mL) and DMF (55 mL), at 0 °C under an argon atmosphere. After 24 h at 20 °C, ice (~ 600 g) was added and stirred for 30 min. The precipitate was filtered, washed and dissolved with CH₂Cl₂. The organic phase was separated from H₂O, dried (MgSO₄) and evaporated. The crude product was filtered over silica gel (Et₂O) to afford **3** as a pale yellow solid after evaporation of the solvent (2.84 g, 96 %). ¹H NMR (250 MHz, CDCl₃): δ 9.67 (s, 1H), 7.82 (m, 2H), 7.69 (m, 4H), 6.81 (d, *J* = 8.9 Hz, 2H), 3.89 (dd, *J* = 6.6, 7.3 Hz, 2H), 3.63 (dd, *J* = 6.6, 7.3 Hz, 2H), 3.50 (q, *J* = 7.3 Hz, 2H), 1.21 (t, *J* = 7.3 Hz, 3H). ¹³C NMR (63 MHz, CDCl₃): δ 189.9 (CH), 168.0 (C), 152.0 (C), 134.0 (CH), 132.1 (CH), 131.6 (C), 125.2 (C), 123.2 (CH), 111.8 (CH), 47.6 (CH₂), 44.9 (CH₂), 34.6 (CH₂), 12.1 (CH₃). MS: *m/z* = 323 (MH⁺). Anal. calcd for C₁₉H₁₈N₂O₃ (322.13), C 70.79, H 5.63, N 8.69. Found C 70.28, H 5.62, N 8.62.

N-[2-[*N*-Ethyl-(4-nitro-phenyl)-vinyl-anilino]ethyl]phthalimide (**4**): A solution of 4-nitrophenyl acetic acid (1.55 g, 8.6 mmol) and piperidine (655 mg, 7.7 mmol) in CH₂Cl₂ (~ 10 mL) was stirred at 20 °C for 10 min. Aldehyde **3** (2.48 g, 7.7 mmol) was then added to the mixture. After 10 min at 20 °C, CH₂Cl₂ was evaporated, and the reaction was heated at 100 °C under vacuum (15 mm Hg) for 3 h, then at 150 °C / 15 mm Hg for 3 h. The crude product was purified by chromatography over silica gel (80:20 CH₂Cl₂-cyclohexane) to afford **4** as a red solid (2.21 g, 65 %). ¹H NMR (500 MHz, CDCl₃): δ 8.16 (d, *J* = 8.9 Hz, 2H), 7.83 (m, 2H), 7.70 (m, 2H), 7.53 (d, *J* = 8.9 Hz, 2H), 7.40 (d, *J* = 8.8 Hz, 2H), 7.14 (d, *J* = 16.2 Hz, 1H), 6.87 (d, *J* = 16.2 Hz, 1H), 6.80 (d, *J* = 8.9 Hz, 2H), 3.88 (dd, *J* = 6.7, 8.1 Hz, 2H), 3.58 (dd, *J* = 6.7, 8.1 Hz, 2H), 3.46 (q, *J* = 7.0 Hz, 2H), 1.20 (t, *J* = 7.0 Hz, 3H). ¹³C NMR (63 MHz, CDCl₃): δ 168.3 (C), 148.0 (C), 145.9 (C), 145.0 (C), 134.1 (CH), 133.5 (CH), 132.0 (C), 128.7 (CH), 126.1 (CH), 124.5 (C), 124.1 (CH), 123.3 (CH), 121.7 (CH), 112.1 (CH), 48.0 (CH₂), 45.1 (CH₂), 35.1 (CH₂), 12.4 (CH₃). MS: *m/z* = 442 (MH⁺). Anal. calcd for C₂₆H₂₃N₃O₄ (441.17), C 70.73, H 5.25, N 9.52. Found C 70.19, H 5.13, N 9.53.

2-[*N*-Ethyl-(4-nitro-phenyl)-vinyl-anilino]ethylamine (**5**): NaBH₄ (806 mg, 21.5 mmol) was added to a suspension of **4** (1.88 g, 4.3 mmol) in a mixture of 2-propanol / water (6 / 1, 120 mL). After 1 h at 60 °C, acetic acid (8 mL) was added at 20 °C and the reaction was kept at 80 °C for 48 h. 2-Propanol was evaporated and the precipitate was filtered. The crude product was purified by chromatography over silica gel (MeOH:CH₂Cl₂:NH₄OH = 3:97:0.25) to afford **5** as a red solid (1.02 g, 77 %). ¹H NMR (250 MHz, DMSO-*d*₆): δ 8.17 (d, *J* = 8.9 Hz, 2H), 7.75 (d, *J* = 8.9 Hz, 2H), 7.49 (d, *J* = 8.9 Hz, 2H), 7.41 (d, *J* = 16.4 Hz, 1H), 7.10 (d, *J* = 16.4 Hz, 1H), 6.76 (d, *J* = 8.9 Hz, 2H), 3.42 (m, 4H), 2.83 (t, *J* = 6.6 Hz, 2H), 1.09 (t, *J* = 7.0 Hz, 3H). ¹³C NMR (63 MHz, DMSO-*d*₆): δ 148.1 (C), 145.2 (C), 145.1 (C), 133.9 (CH), 128.7 (CH), 126.3 (CH), 124.0 (CH), 123.6 (C), 120.9 (CH), 111.6 (CH), 49.8 (CH₂), 44.4 (CH₂), 37.8 (CH₂), 12.0 (CH₃). HRMS (ESI) calcd for C₁₈H₂₂N₃O₂ (MH⁺) *m/z* 312.1712, found 312.1701.

Compound 7: Et₃N (0.8 mL) and HBTU (2.18 g, 5.7 mmol) were added to a solution of **5** (1.19 g, 3.8 mmol) and 2',3'-*O*-isopropylidene adenosine carboxylic acid **6** (1.23 g, 3.8 mmol) in anhydrous DMF (130 mL). After 48 h at 20 °C under an argon atmosphere, DMF was evaporated and the usual work-up with EtOAc / H₂O gave the crude product which was purified by chromatography over silica gel (60:40 EtOAc-CH₂Cl₂) to afford **7** as a red solid (1.64 g, 70 %). ¹H NMR (250 MHz, DMSO-*d*₆): δ 8.29 (s, 1H), 8.17 (d, *J* = 8.8 Hz, 2H), 8.11 (s, 1H), 7.75 (d, *J* = 8.8 Hz, 2H), 7.72 (s, 1H, D₂O exchangeable), 7.45 (d, *J* = 8.8 Hz, 2H), 7.39 (d, *J* = 16.4 Hz, 1H), 7.33 (s, 2H, D₂O exchangeable), 7.08 (d, *J* = 16.4 Hz, 1H), 6.67 (d, *J* = 8.8 Hz, 2H), 6.37 (d, *J* = 1.6 Hz, 1H), 5.43 (dd, 1H, *J* = 1.9, 6.1 Hz, 1H), 5.40 (dd, 1H, *J* = 1.6, 6.1 Hz, 1H), 4.57 (d, *J* = 1.9 Hz, 1H), 3.31-3.24 (m, 6H), 1.54 (s, 3H), 1.34 (s, 3H), 1.03 (t, *J* = 7.0 Hz, 3H). ¹³C NMR (63 MHz, DMSO-*d*₆): δ 168.9 (C), 156.0 (C), 152.4 (CH), 148.8 (C), 148.1 (C), 145.3 (C), 145.1 (C), 140.5 (CH), 133.9 (CH), 128.7 (CH), 126.2 (CH), 124.0 (CH), 123.4 (C), 120.7 (CH), 118.9 (C), 112.9 (C), 111.3 (CH), 89.5 (CH), 86.0 (CH), 83.2 (CH), 83.1 (CH), 47.7 (CH₂), 44.2 (CH₂), 35.7 (CH₂), 26.7 (CH₃), 25.0 (CH₃), 12.0 (CH₃). MS: *m/z* = 615 (MH⁺). Anal. calcd for C₃₁H₃₄N₈O₆ (614.26), C 60.58, H 5.58, N 18.23. Found C 59.98, H 5.53, N 18.11.

Compound 8: HCl (1M, 20 mL) was added to a solution of **7** (0.75 g, 1.2 mmol) in THF (30 mL). After 24 h at 60 °C, saturated K₂CO₃ was added (pH ~ 10) and THF was evaporated. The precipitate was filtered, washed (pH ~ 7) and dried to afford **8** as a red solid (0.67 g, 96 %). ¹H NMR (250 MHz, DMSO-*d*₆): δ 9.16 (bt, 1H, D₂O exchangeable), 8.37 (s, 1H), 8.18 (d, *J* = 8.9 Hz, 2H), 8.08 (s, 1H), 7.76 (d, *J* = 8.9 Hz, 2H), 7.48 (d, *J* = 8.5 Hz, 2H), 7.41 (d, *J* = 16.3 Hz, 2H), 7.09 (d, *J* = 16.3 Hz, 2H), 6.78 (d, *J* = 8.5 Hz, 2H), 5.97 (d, *J* = 7.3 Hz, 1H), 5.78 (d, *J* = 4.3 Hz, 1H, D₂O exchangeable), 5.57 (d, *J* = 6.2 Hz, 1H, D₂O exchangeable), 4.62 (m, 1H), 4.33 (bs, 1H), 4.17 (dd, *J* = 4.3, 3.5 Hz, 1H), 3.42 (m, 6H), 1.08 (t, *J* = 6.9 Hz, 3H). ¹³C NMR (125 MHz, DMSO-*d*₆): 170.0 (C), 161.8 (C), 156.2 (C), 152.6 (CH), 149.0 (C), 148.2 (C), 145.4 (C), 145.3 (C), 140.8 (CH), 134.1 (CH), 128.9 (CH), 126.4 (CH), 124.2 (C), 123.6 (CH), 120.9 (CH), 111.6 (CH), 87.9 (CH), 84.7 (CH), 73.0 (CH), 71.9 (CH),

48.7 (CH₂), 44.6 (CH₂), 36.5 (CH₂), 12.1 (CH₃). HRMS (ESI) calcd for C₂₈H₃₁N₈O₆ (MH⁺) *m/z* 575.2367, found 575.2386.

Compounds 9 and 10: nBu₂SnO (52 mg, 0.21 mmol) was added to a suspension of **8** (93 mg, 0.16 mmol) in anhydrous toluene (10 mL). After 2 h at 130°C under an Ar atmosphere, toluene was evaporated. Anhydrous CH₂Cl₂ (10 mL) and ClP(O)(OEt)₂ (47 μL, 0.32 mmol) were added to the reaction. After 48 h at RT, CH₂Cl₂ was evaporated off. THF (3 mL) and HCl (37%, 1.5 mL) were added and the mixture was stirred at RT for 2.5 h (TLC monitoring: 30:65:4:1 CH₃OH–CH₂Cl₂–H₂O–Et₃N). After addition of an aq. NH₃ solution (2%, until pH ~ 7), the deep-red solid was filtered, washed with H₂O. The crude product was dissolved in DMF and purified by chromatography over C₁₈ silica gel (25:75:1 CH₃CN–H₂O–2% NH₄OH) to provide a mixture of the two regioisomers **9** and **10** in a ratio of 40:60 after lyophilization (76 mg, 70% from diol **8**).

Compound 9 (2'-PO₄H₂, 40 %): ¹H NMR (500 MHz, DMSO-*d*₆): δ 9.16 (bt, 1H), 8.40 (s, 1H), 8.17 (d, 2H, J = 8.9 Hz), 8.02 (s, 1H), 7.76 (d, 2H, J = 8.9 Hz), 7.48 (d, 2H, J = 9.1 Hz), 7.40 (m, 3H), 7.10 (d, 2H, J = 16.4 Hz), 6.78 (d, 2H, J = 9.1 Hz), 6.07 (d, 1H, J = 7.1 Hz), 4.83 (m, 1H), 4.49 (d, 1H, J = 3.8 Hz), 4.45 (bs, 1H), 3.44-3.35 (m, 6H), 1.09 (t, 3H, J = 7.0 Hz).

Compound 10 (3'-PO₄H₂, 60 %): ¹H NMR (500 MHz, DMSO-*d*₆): δ 9.26 (bt, 1H), 8.40 (s, 1H), 8.17 (d, 2H, J = 8.9 Hz), 8.02 (s, 1H), 7.76 (d, 2H, J = 8.9 Hz), 7.48 (d, 2H, J = 9.1 Hz), 7.40 (m, 3H), 7.10 (d, 2H, J = 16.4 Hz), 6.78 (d, 2H, J = 9.1 Hz), 5.97 (d, 1H, J = 8.2 Hz), 4.62 (m, 1H), 4.71 (m, 1H), 4.36 (bs, 1H), 3.44-3.35 (m, 6H), 1.09 (t, 3H, J = 7.0 Hz).

¹³C NMR (125 MHz, DMSO-*d*₆): δ 169.9 (C), 169.5 (C), 156.2 (C), 152.4 (CH), 148.9 (C), 148.0 (C), 145.3 (C), 145.0 (C), 140.5 (CH), 134.0 (CH), 128.8 (CH), 126.2 (CH), 124.0 (CH), 123.4 (C), 120.8 (CH), 111.4 (CH), 88.3 (CH), 83.9 + 83.6 (CH), 75.7 (CH), 72.3 (CH), 48.7 + 48.6 (CH₂), 44.8 + 44.5 (CH₂), 36.4 (CH₂), 12.0 (CH₃).

HRMS (ESI) calcd for C₂₈H₃₀N₈O₉P [M-H]⁻ 653.1873, found 653.1877.

Biochemistry, General. L-Arginine, (6R)-5,6,7,8-tetrahydrobiopterin (H₄B), calmodulin (CaM), Hepes, Tris-HCl, CaCl₂, NADPH, glycerol, cytochrome *c* (cyt *c*), myoglobin, ferredoxin reductase (ferredoxin_{red}) and ferredoxin (from spinach), isocitrate dehydrogenase, glucose 6-phosphate dehydrogenase were purchased from Sigma-Aldrich.

Expression and purification of proteins. Recombinant full-length rat nNOS, murine iNOS and bovine eNOS were expressed in *Escherichia coli* cell line BL21 (DE3) and purified as previously described (14-17). The heme content was determined optically from the [CO-reduced]-[reduced] difference spectrum using Δε_{444-470 nm} = 76,000 M⁻¹ cm⁻¹ (18). Recombinant reductase domain of eNOS (eNOS_{red}) was overexpressed in yeast and purified as described (15, 19). Purified nNOS, eNOS, iNOS and eNOS_{red} were more than 95 % pure as determined by SDS-PAGE stained with Coomassie Blue. Fatty acid binding protein (FABP) was a generous gift of Dr Jiayao Li (LBPA). Cytochrome P450 reductase (P450_{red}) was a gift of Dr Lee-Ho Wang (UTHSC, TX, USA). Lens epithelium-derived growth factor (LEDGF) and *E. Coli* RecQ helicase were prepared as reported in (20, 21). Protein contents were measured using the Bradford reagent from BioRad and bovine serum albumin as a standard.

Spectroscopic methods: Characterization of free or NOS-bound NS1. UV-visible absorption spectrum of NS1 was carried out with an Uvikon XL spectrophotometer. NS1-binding isotherms were build using NOS in 50 mM Tris pH 7.5 containing 150 mM NaCl at 25 °C, either under one-photon (1-PE) or two-photon excitation (2-PE) conditions. For one-photon experiments, fluorescence excitation and emission spectra were recorded on a Eclipse (Varian) spectrofluorimeter, equipped with a thermostated cell holder, using aerated 80 μl solutions placed in micro cells (Hellma, Paris, France). The emission spectra were recorded with excitation and emission slits set at 5 nm. Two-photon excitation and emission spectra were recorded using a home-built set-up. Briefly, a 80-MHz mode-locked Mai-Tai® Ti:Sapphire tunable laser (690-1040 nm, 100 fs laser pulse; Spectra Physics, Mountain View, CA, USA) was focused onto the sample (80 μl) placed in a quartz micro cell. The two-photon fluorescence was collected at 90 degrees and was further filtered by a Semrock FF01-842/SP filter to reject the residual excitation light. The fluorescence signal was focused into an optical fiber connected to a SpectraPro-275 digital spectrograph (300 lines/mm) coupled to a liquid nitrogen cooled CCD detector (1024 × 256 pixels; Princeton Instruments Acton, MA, USA). The wavelength calibration of the spectrograph was done using a high pressure mercury lamp. Excitation power was set between 50 and 100 mW and the acquisition time varied between 1 and 60 s.

Stopped-flow experiments. Kinetics of the reaction between nNOS and NADPH were measured at 24 °C in an anaerobic chamber (Coy Laboratory Products Inc., Michigan, USA), using a Bio-SEQUENTIAL DX-18MV stopped-flow instrument (Applied Photophysics, Leatherhead, UK). Measurements were carried out using an anaerobic solution of 5 μ M nNOS (in 50 mM Hepes buffer, pH 7.7 containing 0.1 M NaCl, 10% glycerol, 1 mM L-arginine, 1 mM calcium and 25 μ M CaM) and monitored at different wavelengths. The solutions of 25 μ M NADPH and NS1 (0-100 μ M) were prepared in oxygen-free buffer (50 mM Hepes, 0.1 M NaCl, 10 glycerol, pH 7.7). Kinetic rates were calculated by fitting data to a single or double-exponential functions using Applied Photophysics software.

Effect of NS1 on the formation of NO catalysed by nNOS. The initial rates of NO formation were determined at 37 °C in 1-cm path-length cuvettes (total volume of 150 μ l) using the oxyhemoglobin assay for NO (22). Usual incubation mixtures were performed in 50 mM Hepes buffer (pH 7.4) containing, 0.1 M KCl, 5 mM DTT, 10-20 μ M oxyhemoglobin, 100 U/ml each of SOD and catalase, 10 μ M H₄B, 100 μ M L-arginine, 1 mM CaCl₂, 10 μ g/ml CaM, 4-6 μ g/ml nNOS, and 0-100 μ M NS1. The mixtures were preincubated for 2 min at 37 °C prior to initiation of the reactions by the addition of NADPH (10-100 μ M) to both cuvettes. The NO-mediated conversion of oxyhemoglobin to methemoglobin was monitored by repetitive scanning between 380 and 480 nm every 0.2 min on a Uvikon 941 spectrophotometer and quantified using an extinction coefficient of 77,000 M⁻¹.cm⁻¹ between peak at 401 nm and valley at 420 nm. Control incubations were performed in the presence of similar amounts of buffer without inhibitor. All values are expressed relative to the control and are means \pm S.D. from 3-4 experiments.

Imaging of living HUVEC cells in the presence of NS1 and co-localization experiments. HUVECs (human umbilical vein endothelial cells, purchased from Sigma) were prepared as previously described (23). NS1 (final concentration, 5 μ M) was incubated with HUVECs (at the fourth passage) for 30 min and the medium was changed before observation. One-photon images of living HUVECs were obtained using a SP2 confocal microscope (Leica MicroSystems, France) equipped with an incubation chamber (37°C, CO₂ 5%). A laser line at 488 nm was used for the excitation of NS1 and the emission range was set between 520 and 680 nm. A similar set up was used for two-photon images except that the excitation source was a 80-MHz mode-locked Mai-Tai® Ti:Sapphire tunable laser (720-920 nm, 100 fs laser pulse; Spectra Physics, Mountain View, CA, USA) tuned to 840 nm. The image of nucleus was monitored using Hoechst 33342 using two-photon excitation (740 nm; emission setting: 410-510 nm).

Co-localization experiments of NS1 with endoplasmic reticulum (ER), mitochondria or Golgi complex were performed on living HUVEC cells (4-7th passage). ER-Tracker™ Red dye (Ref. no. E34250) for ER labeling, MitoTracker® Deep Red FM (Ref. no. M22426) for mitochondria labeling or BODIPY® TR Ceramide complexed to BSA (Ref. no. B34400) for Golgi complex labeling were purchased from Invitrogen (France).

Co-localization of NS1 with early endosome (EEA1) or eNOS was performed by immuno-staining on fixed HUVEC cells according to standard procedure (23, 24) with modifications: PBS-0.5% Saponin was used as permeabilization solution for 10 min at room temperature instead of PBS-0.2% Triton X-100 / 2 mg/ml BSA / 1 mM NaN₃ on ice. Blocking solution was PBS-3% BSA instead of PBS / 0.02% Triton X-100 / 3% BSA / 1 mM NaN₃. Purified mouse anti-eNOS/NOS Type III (BD-Biosciences, France); ref. no. 610297) and rabbit polyclonal to EEA1-Early Endosome Marker (abcam®, Cambridge, UK; ref. no. ab2900) primary antibodies were used at final concentrations of 10 and 4 μ g/mL, respectively, in PBS-0.5% Saponin / 3% BSA. Secondary antibodies, AlexaFluor® 594 goat anti-mouse IgG (H+L) (Ref. no. A-11005) and AlexaFluor® 594 donkey anti-rabbit IgG (H+L) (Ref. no. A-11012) were purchased from Invitrogen (France) and used at final concentrations of 4 and 2 μ g/mL, respectively, in PBS-0.5% Saponin / 3% BSA. The fixation buffer BD Cytifix™ was purchased from BD-Biosciences. Saponin from Quillaja bark and BSA were purchased from Sigma life science. The mounting medium CITIFLUOR™PERMAFIX 1 (HRF) was purchased from Bivalley (France). Excitation and emission settings are indicated in figure legends.

SUPPLEMENTARY REFERENCES:

1. Oivanen ML, H. (1989) Kinetics and mechanisms for reactions of adenosine 2'- and 3'-monophosphates in aqueous acid: competition between phosphate migration, dephosphorylation, and depurination. *J. Org. Chem.* 54:2556–2560.
2. Lambry JC, Beaumont E, Tarus B, Blanchard-Desce M, & Slama-Schwok A (2010) Selective probing of a NADPH site controlled light-induced enzymatic catalysis. *J Mol Recognit* 23:379-388.
3. Garcin ED, *et al.* (2004) Structural basis for isozyme-specific regulation of electron transfer in nitric-oxide synthase. *J Biol Chem* 279:37918-37927.
4. Panda SP, *et al.* (2006) The role of a conserved serine residue within hydrogen bonding distance of FAD in redox properties and the modulation of catalysis by Ca²⁺/calmodulin of constitutive nitric-oxide synthases. *J Biol Chem* 281:34246-34257.
5. Zhang J, Martasek, P, Paschke, R., Shea, T., SilverMasters, B.S., Kim, JJ (2001) Crystal structure of the FAD/NADPH-binding domain of rat neuronal nitric-oxide synthase. Comparisons with NADPH-cytochrome P450 oxidoreductase. *J. Biol. Chem.* 276:37506-37513.
6. Lapouyade R, Kuhn, A., Letard, J.F., Rettig, W. (1993) Multiple relaxation pathways in photoexcited dimethylaminonitro- and dimethylaminocyno-stilbenes. *Chem Phys. Lett.* 208:48-58.
7. Phillips JC, *et al.* (2005) Scalable molecular dynamics with NAMD. *J Comput Chem* 26:1781-1802.
8. Folloppe N, MacKerell, A.D. (2000) All-atom empirical force field for nucleic acids: I. Parameter optimization based on small molecule and condensed phase macromolecular target data. *J. Comp. Chem* 21:86-104.
9. Jorgensen WL, Chandrasekhar J, Madura JD, Impey RW, & Klein ML (1983) Comparison of simple potential functions for simulating liquid water. *J. Chem. Physiol.* 79:926-935.
10. Darden T, York DM, & Pedersen L (1993) Particle mesh Ewald: An N×log(N) method for Ewald sums in large systems. *J. Chem. Phys.* 98:10089-10092.
11. Ryckaert JP, Ciccotti G, & Berendsen HJC (1977) Numerical-integration of Cartesian equations of motion of a system with constraints: Molecular dynamics of n-alkanes. *J. Comp. Phys.* 23:327-341.
12. Safavy A, Smith DC, Jr., Bazooband A, & Buchsbaum DJ (2002) De novo synthesis of a new diethylenetriaminepentaacetic acid (DTPA) bifunctional chelating agent. *Bioconjug Chem* 13(2):317-326.
13. Ha SB, Nair, V. (1996) An Improved Approach to the Synthesis of Adenosine-5'-N-Ethyluronamides of Interest as Adenosine Receptor Agonists *Tetrahedron letters* 37:1567-1570.
14. Berka V, Wang LH, & Tsai AL (2008) Oxygen-induced radical intermediates in the nNOS oxygenase domain regulated by L-arginine, tetrahydrobiopterin, and thiol. *Biochemistry* 47:405-420.
15. Du M, Yeh HC, Berka V, Wang LH, & Tsai AL (2003) Redox properties of human endothelial nitric-oxide synthase oxygenase and reductase domains purified from yeast expression system. *J Biol Chem* 278:6002-6011.
16. Moali C, Boucher JL, Sari MA, Stuehr DJ, & Mansuy D (1998) Substrate specificity of NO synthases: detailed comparison of L-arginine, homo-L-arginine, their N omega-hydroxy derivatives, and N omega-hydroxynor-L-arginine. *Biochemistry* 37:10453-10460.

17. Wu C, Zhang J, Abu-Soud H, Ghosh DK, & Stuehr DJ (1996) High-level expression of mouse inducible nitric oxide synthase in *Escherichia coli* requires coexpression with calmodulin. *Biochem Biophys Res Commun* 222:439-444.
18. Stuehr DJ & Ikeda-Saito M (1992) Spectral characterization of brain and macrophage nitric oxide synthases. Cytochrome P-450-like heme proteins that contain a flavin semiquinone radical. *J Biol Chem* 267:20547-20550.
19. Raman CS, *et al.* (1998) Crystal structure of constitutive endothelial nitric oxide synthase: a paradigm for pterin function involving a novel metal center. *Cell* 95:939-950.
20. Li N, *et al.* (2010) Multiple *Escherichia coli* RecQ helicase monomers cooperate to unwind long DNA substrates: a fluorescence cross-correlation spectroscopy study. *J Biol Chem* 285:6922-6936.
21. Cherepanov P, *et al.* (2003) HIV-1 integrase forms stable tetramers and associates with LEDGF/p75 protein in human cells. *J Biol Chem* 278:372-381.
22. Murphy ME & Noack E (1994) Nitric oxide assay using hemoglobin method. *Methods Enzymol* 233:240-250.
23. Martinive P, *et al.* (2009) Impact of cyclic hypoxia on HIF-1 α regulation in endothelial cells--new insights for anti-tumor treatments. *FEBS J* 276:509-518.
24. Kodiha MR, L.; Stochaj, U. (2009) Optimized immunofluorescence staining protocols to detect the nucleoporin Nup98 in different subcellular compartments. *Nature Protocol- Protocol Exchange*:doi:10.1038/protex.2010.1211

Supplementary data II

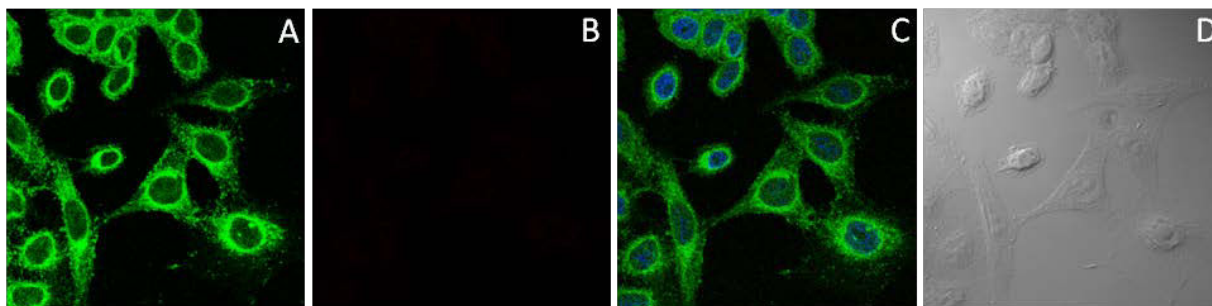


Fig. 17 Colocalization imaging experiments of NS1 and eNOS in HeLa cells.

Living HeLa cells were treated with NS1 (5 μ M) for 60 min prior to fixation and immunostaining of eNOS. Primary and secondary antibodies for immunostaining were purified mouse anti-eNOS/NOS Type III and AlexaFluor 594 goat anti-mouse IgG (H+L), respectively. (A) Imaging channel of NS1 (1-PE, 488 nm); emission slit 520–680 nm]; (B) imaging channel of eNOS (1-PE, 543 nm; emission slit 590–700 nm); no detectable fluorescence signal was observed in this channel; (C) merged image of A and B; nucleus staining by DAPI is also shown in blue; (D) shows the corresponding differential interference contrast microscopy transmission image.

The internalization of NS1 was also observed in HeLa cells using fluorescence imaging, however with a different pattern than in HUVEC cells. First, no plasma membrane signal was detected in HeLa cells compared with HUVECs; second, the distribution of fluorescence emission was located and homogeneously distributed around the nucleus, i.e. in a non-polar manner, whereas in HUVECs, the distribution of fluorescence emission displayed a strong polarity in the perinucleus region, which corresponds to the Golgi-complex. No eNOS was evidenced in HeLa cells, in contrast to that observed in HUVECs, raising the question of the origin of the fluorescence signal observed around nuclei of HeLa cells. This signal may originate from non-specific binding in the perinucleus region leading to a symmetrical distribution of the fluorescence signal around the nuclei. In the case of HUVECs, the presence of eNOS at the Golgi level modified the distribution of the fluorescence signal of NS1 around the nuclei, leading to an asymmetrical NS1 distribution.

Introduction of “Addressing to NADPH-dependent NO and Reactive Oxygen Species signaling with a photoactive NADPH Analogue”

Romero-Perez, Miguel; Lobysheva, Irina; Wang, Huan; Ramassamy, Booma; Rouaud, Florian; Henry, Etienne; Giacchero, Damien; Dhimane, Hamid; Tauc, Patrick; Rocchi, Stéphane; Deprez, Eric; Dessy, Chantal; Boucher, Jean-Luc; Slama-Schwok, Anny

This manuscript is an extended study of NS1 in a more physiologically relevant environment. NS1, as a new prototype of NOS inhibitor, was proved to efficiently bind to the reductase domain of NOS and inhibit NO catalysis *in vitro*. Moreover, NS1 as a novel fluorescent probe under two-photon excitation was found to co-localize with eNOS in HUVEC cells. We next addressed the question of inhibition of NO at the cellular or tissue level. In the vasculature system, NO is well known for its modulation effects: up-regulation of NO production will lead to vasodilation, whereas decreased NO will cause vasoconstriction. At the tissue level, we expected a NO-dependent vasoconstriction as the direct consequence of NS1-induced NO inhibition in isolated mice aortic rings. However, experiments performed on isolated aortic rings reveal an apparent contradictory vasorelaxation, which was later proved to be H₂O₂-driven. Indeed, only in the presence of catalase which converts H₂O₂ into H₂O and O₂, the NO-dependent vasoconstriction by NS1 was observed in pre-relaxed aortic rings treated with Ach (Acetylcholine chloride). This unexpected finding then leads to several questions: in the complex biological environment, what is the participation of NS1 in NOS-related pathways in addition of electron flow blockage? How does NS1 contribute to the basal level of ROS in the endothelium system? Moreover, is there any other target(s) besides NOS? To note, in the previous section, we observed a clear fluorescence signal of NS1 in the absence of eNOS in Hela cells. Which target(s) could possibly interact with NS1 and what is the consequence? To address these questions, we carried out extensive studies to investigate the pharmacological effects of NS1 on (i) NO and ROS levels in endothelium at cellular and tissue levels, as well as on (ii) the uncoupling of nNOS *in vitro*.

The NO formation in endothelial cells (BAECs), pre-stimulated by a calcium ionophore, was significantly inhibited by NS1 (30 μM) as measured using EPR (Electron Paramagnetic Resonance) spin-trapping. Notable, no significant inhibition effect was observed on the basal NO level under non Ca²⁺-stimulated conditions. A similar NS1-induced NO inhibition effect was also observed in isolated aortic rings, the IC₅₀ value (40 ± 20 μM) obtained was close to that measured in endothelial cells.

The effect of NS1 to endothelium dependent relaxation was performed in isolated mice aorta rings. A contraction curve by measuring the length-tension was constructed by using

single dose of Ach on the basis of KCl-induced pre-contraction. As mentioned above, the expected NS1-induced vasoconstriction was observed in the catalase context only. Without catalase, NS1 exerted surprisingly a vasorelaxation effect. This result indicates that NS1 may target more than NOS in the endothelium system, and the consequence of these interactions may hinder the pure effect of NS1 on NOS. In vascular system, H₂O₂ is another important factor capable of modulating the vascular tone and our result highly suggested the participation of H₂O₂; thereby NS1 may also affect ROS-related enzymes. Anyhow, the result obtained in the catalase context confirmed that NS1 actually inhibits the NO production in endothelial cells and aortic vessels.

Next, the fluorescence emission of a ROS indicator was used in NS1-treated endothelial cells (HUVECs) to assess the ROS modulation by NS1, detected by flow cytometer. The data showed that NS1 led to a biphasic response of ROS formation in the cellular context. Indeed, below 1-2 μM, NS1 significantly increased the ROS production while above 2 μM it caused a continuous decrease in the ROS production, a plateau was reached up to 20 μM. The increasing phase in endothelial cells may correspond to the production of H₂O₂, which confirmed the dual effect of NS1 on isolated aorta, where the observed decrease in the NO production was accompanied by H₂O₂ production. However, high concentrations of NS1 led to a reduced formation of H₂O₂. There are two possible but not exclusive explanations for the inhibition phase: (i) NS1 probably inhibits the ROS production derived from uncoupling in NOS. Accordingly, *in vitro* experiments performed by colorimetric assay and EPR spin-trapping detection on uncoupled nNOS showed that, both H₂O₂ and O₂⁻ productions were inhibited by NS1. (ii) NS1 could target NADPH oxydase (NOX) since NS1 inhibits the O₂⁻ production in PMA stimulated mouse macrophages (RAW 264.7), as measured by EPR spin-trapping. Moreover, the experiments of ROS detection in rat aorta smooth muscle cells (A7R5) displayed a distinct feature than in endothelial cells, where only stimulating effect of H₂O₂ by NS1 was observed. To further investigate the mechanism behind the differential behaviors of NS1 in different types of cells lines, a careful comparative and quantitative analysis of NOS expression as well as NOX isoforms in different cell lines is required and will be performed in the near future.

The above-mentioned data highlight that NS1 inhibits NO formation by NOS in endothelial cells and isolated aorta. Additionally, the inhibition of ROS produced by either NOX or uncoupled NOS is strongly suggested. Regarding the vascular response to NS1 performed in aortic rings, we observed vasorelaxation instead of vasoconstriction in the absence of catalase, implying a burst of H₂O₂ which accounts for NO-independent vasorelaxation; in other words, the burst of H₂O₂ may hinder the expected vasoconstriction effect, which is actually observed in the presence of catalase. This result was in accordance with the biphasic behavior of ROS production in response to NS1 observed in flow cytometry experiments with HUVEC cells. A biphasic response was also observed in EPR detection experiments applied to

isolated aorta. Altogether, our data suggests that there might be a third target of NS1, the interaction of NS1 with this target could lead to an increased ROS production simultaneously to NO inhibition. This third potential target of NS1 remains unclear yet. One reasonable hypothesis could be that NS1 inhibits G6PD (glucose-6-phosphate dehydrogenase), which is an enzyme related to vasoconstriction (238) (239). Indeed, G6PD is involved in the conversion of NADP^+ into NADPH, a cofactor of glutathione reductase which in turn decreases the level of H_2O_2 . It is important to note that the augmented ROS level induced by NS1 is still within the non-toxic concentration.

Furthermore, in the angiogenesis assays that probe the endothelial network formation, the extension of endothelial cells (HUVECs) stimulated by VEGF (Vascular Endothelial Growth Factor) was strongly inhibited by NS1 treatment. Altogether, our results show that NS1 appears to affect two important activities of endothelium: NO production and angiogenesis. In addition, NS1 inhibited the proliferation of melanoma cells A375 in a time- and dose-dependent manners, while no inhibition effect was observed in normal melanocytes.

In summary, NS1 displayed interesting potentialities for pharmacological applications: as an inhibitor of NOS, NS1 efficiently inhibits the NO production in endothelium, and as an “extra bonus” it also inhibits ROS derived from electron leakage under uncoupled conditions, while the conventional oxygenase-domain-targeting NOS inhibitors are unable to avoid uncoupling that occurs at the level of the reductase domain; it inhibits NO in aortic rings and exerts NO-dependent vasoconstriction. In addition, it presents anti-angiogenic effects in VEGF-induced endothelial sprouting and selectively inhibits the proliferation of melanoma cells. Even though H_2O_2 or other ROS species may be formed in the presence of NS1, it appears that the NS1-dependent ROS burst is not toxic. Ideally, we expect a selective effect of NS1 on NO production. However, at the cellular level, the small amount of NS1 also leads to an increase in the ROS production, in accordance with the result obtained using aortic ring (i.e. H_2O_2 -dependent vasodilation in the absence of catalase). The experiments performed on endothelial cells indicate that, depending on the NS1 concentration used, the inhibition of ROS may be also observed. Therefore, the influence of catalase should be tested on the whole NS1 concentration range at the tissue level; Altogether, our results predict that a NS1 concentration range probably exists compatible with the observation of vasoconstriction even in the absence of catalase. Alternatively, the selectivity of NS1 for the three NOS isoforms versus the other proteins (for instance G6PD) could be improved by molecular modelling in order to minimize the impact of H_2O_2 modulation. On the other hand, it was shown that H_2O_2 is a signaling molecule at low concentrations (240) (241). In this context, it is important to note that a molecular tool such as NS1 capable of modulating the H_2O_2 level within a non-toxic concentration range, could be useful for future biological studies (at fundamental and application levels) of H_2O_2 -dependent signaling pathways.

Addressing to NADPH-dependent NO and Reactive Oxygen Species signaling with a photoactive NADPH Analogue

Miguel Romero-Perez^{1#}, Irina Lobysheva¹, Huan Wang², Booma Ramassamy³,
Florian Rouaud⁴, Etienne Henry², Damien Giaccherio⁵, Hamid Dhimane³, Patrick Tauc²,
Stéphane Rocchi⁴, Eric Deprez², Chantal Dessy¹, Jean-Luc Boucher^{3*}, Anny
Slama-Schwok^{6*}.

¹ Pole of Pharmacology and Therapeutics, FATH5349, IREC, UCL Medical Sector, B-1200 Brussels, Belgium;

² Laboratoire de Biologie et Pharmacologie Appliquée (LBPA), CNRS UMR 8113, Institut d'Alembert, ENS-Cachan, 61 avenue du président Wilson, 94235 Cachan, France ;

³ CNRS UMR 8601, Université Paris Descartes, 45 rue des Saints Pères, 75270 Paris, France ;

⁴ INSERM U1065 team 1, Université de Nice Sophia Antipolis et Centre Méditerranéen de Médecine Moléculaire, Nice, France

⁵ Service de Dermatologie, Hôpital Archet II, CHU Nice, France

⁶ Virologie et Immunologie Moléculaires, UR 892, INRA, 78352 Jouy en Josas, France.

*Corresponding authors:

Dr Jean-Luc Boucher, Laboratoire de Chimie et Biochimie Pharmacologiques et Toxicologiques CNRS UMR 8601, Université Paris Descartes, 45 rue des Saints Pères, 75270 Paris, France. Email: Jean-Luc.Boucher@parisdescartes.fr; Phone +331 42 86 21 91 Fax: +331 42 86 83 87

Dr Anny Slama-Schwok, Virologie et Immunologie Moléculaires, UR 892, INRA, Domaine de Vilvert, 78352 Jouy en Josas, France. Email : Anny.Schwok@gmail.com. Phone: [+33134652615](tel:+33134652615), Fax: [+33124652621](tel:+33124652621)

Running title (*36 characters*): Modulation of NO and ROS by a NADPH analogue.

Number of text words: 4976

Abstract: 247 words

Discussion: 1437 words

Number of tables: 2

Number of figures: 7

Number of references: 42

Abstract

Background and purpose: Excess of Reactive oxygen species, ROS and Nitric Oxide, NO levels contribute to cardiovascular diseases and cancer. Here, we investigate the pharmacological modulation of NO and ROS by a novel NADPH analogue, called nanoshutter NS1 (Li et al, (2012) PNAS 109: 12526). By NS1 targeting the NADPH site of Nitric Oxide Synthase (NOS) and blocking the electron flow, NS1 was expected at inhibiting both NO and ROS formed by uncoupled NOS with interest for inhibition of redox stress.

Experimental approach: EPR spin trapping and a ROS fluorescent probe were used for NO and superoxide ions measurements in cells and isolated aorta, wire-myograph experiments measured changes of the vascular tone, and several assays determined cell viability, proliferation and endothelial tubes formation.

Key results: NS1 inhibited NO formed in aortic rings and ROS formed by uncoupling as expected from its design. NS1 modulated the vascular tone of aortic rings by blockade of NO-dependent and NO-independent pathways at low micromolar concentrations. NS1 induced a biphasic regulation of ROS. NS1 inhibited NO-dependent formation of endothelial tubes in a 3D model of angiogenesis. Moreover, NS1 specifically decreased the proliferation of metastatic melanoma cells but not of normal cells.

Conclusions and Implications: The specific and dual inhibition of NO and ROS by NS1 is exerted by targeting eNOS and likely NADPH oxidase(s) mainly in the endothelium. NS1 is a promising nano-tool with broad applicability for reducing redox stresses and great potential for targeted vascular therapies, in particular against melanoma invasion.

Keywords: Modulation of cellular signaling, Angiogenesis, NADPH analogue; EPR spectroscopy; Fluorescence, cell proliferation

Abbreviations used:

Ach, acetylcholine;

BAEC, bovine aortic endothelial cells;

CaM, calmodulin;

CAT-1H, 1-hydroxy-2,2,6,6-tetramethylpiperidin-4-yl-trimethylammonium chloride;

DEPMPO, 5-diethoxyphosphoryl-5-methyl-1-pyrroline *N*-oxide;

Na-DETC, diethyldithiocarbamate, sodium salt;

DTPA, diethylenetriaminepentaacetic acid;

EPR, electron spin resonance;

FCS, fetal calf serum;

HUVEC, human umbilical vein endothelial cells;

n-, i-, and eNOS, neuronal, inducible and endothelial nitric oxide synthase, respectively;

H₄B, (6R)-5,6,7,8-tetrahydrobiopterin; LPS, lipopolysaccharide;

MTT, 3-[4,5-dimethylthiazol-2-yl]-2,5-diphenyl tetrazolium bromide;

NOX, NADPH oxidase;

PMA, phorbol 12-myristate 13-acetate;

ROS, reactive oxygen species.

Introduction

Nitric oxide, NO, is an endogenously produced free radical that exerts key biological functions in the cardiovascular, nervous and immune systems (Li and Forstermann, 2009; Moncada, 1991). The signalling pathways regulated by NO are predominantly linked to its ability to activate soluble guanylate cyclase whereas the cytotoxic activities of NO have been associated with formation of NO-derived species such as peroxynitrite ($\text{O}=\text{N}-\text{O}-\text{O}^-$), nitroxyl (NO^-) and nitrosyl (NO^+) ions able to perform nitration of tyrosine residues, nitrosylation of thiols or deamination of DNA (Ischiropoulos, 2003). Numerous pathologies including cancers are linked to the concomitant formation of superoxide and NO, which form the highly reactive peroxynitrite (Szabó C, 2007). In some cancers, NO is an endothelial growth factor that mediates metastasis (Kostourou et al., 2011). NO is synthesized by oxidation of L-arginine (L-arg) catalyzed by three mammalian isoforms of NO synthases (NOS) (Forstermann and Sessa, 2012; Garcin et al., 2004; Jachymova, 2005): the constitutive neuronal (nNOS) and endothelial NOS (eNOS) and the inducible NOS (iNOS) expressed in response to an immune challenge. NOS are active as homodimers, each monomer containing an N-terminal (oxygenase) domain with binding sites for substrate L-arg, heme and cofactor (6R)-5,6,7,8-tetrahydrobiopterin (H_4B), and a C-terminal (reductase) domain binding NADPH, flavins FAD and FMN (Jachymova, 2005). A calmodulin (CaM) binding domain regulates the electron-flow from the reductase to the oxygenase domain. NOS inhibitors would be of high therapeutic value for the treatment of the above-mentioned diseases (Silverman, 2009). Most current NOS inhibitors target the heme site, based on crystallographic structures (Crane BR, 1998; Li et al., 2006; Raman et al., 1998). However, these inhibitors cannot prevent ROS formation at the reductase domain. Compounds specifically targeting the reductase domain were scarcely designed despite that the availability of the X-ray structure of nNOS reductase domain (Garcin et al., 2004): only diphenyl-iodonium (DPI) and some analogues are known to irreversibly react with flavins (Stuehr et al., 1991). Inhibition of ROS formed via eNOS uncoupling by H_4B depletion or NADPH oxidases (NOX) is highly requested for pharmacological treatments of cardiovascular diseases and in cancers (Wind et al., 2010).

Recently, we designed and synthesized a novel prototype of NOS inhibitor, called nanoshutter (NS1) that specifically recognized the NADPH site by a phosphorylated adenosine

moiety, linked to a photoactive stilbene chromophore substituted with an acceptor and a donor group (Li et al., 2012). Using molecular dynamic simulations, we demonstrated that NS1 fitted into the NADPH site of nNOS in a similar manner than our previously reported dienic analogue, called nanotrigger NT1. While NT1 activated NOS catalysis in a synchronous manner upon biphotonic light activation (Beaumont et al., 2009; Beaumont et al., 2007; Beaumont et al., 2008; Lambry et al., 2010), NS1 reversibly inhibited NO formed by recombinant nNOS competitively with NADPH binding (Li et al., 2012). A specific enhancement of NS1 fluorescence by binding to constitutive NOS was observed upon two-photon excitation, allowing NS1 imaging eNOS in living HUVEC cells (Li et al., 2012).

In the present manuscript, we hypothesize that our novel photoactive NADPH analogue NS1 would regulate cellular signaling mediators as Nitric oxide and Reactive Oxygen species through molecular recognition of the NADPH site of selected enzymes. This hypothesis was suggested by NS1 co-localizing with eNOS in living HUVEC cells (Li et al., 2012) and simulations studies suggesting differences between NADPH sites of various proteins (Lambry et al., 2010). To investigate the molecular targets of NS1 in a cellular context and its pharmacological effect, we used endothelial cells, macrophages and isolated aorta. NS1 affected NO levels, NO-mediated vasorelaxation and angiogenesis and modulated ROS levels, which suggested NS1 inhibition of membrane-located enzymes as eNOS and/or NOX's in the endothelium. Furthermore NS1 specifically reduced the number of metastatic melanoma cells while being non-toxic to endothelial cells and normal melanocytes. Modulation of downstream signalling may be useful to inhibit kinase activation as for example the PI3K/Akt pathway overexpressed in many cancers without requiring specific kinase inhibitors and modulate redox sensitive post-translational modifications. Thus, NS1 combined interesting pharmacological and imaging properties, with great interest for targeted vascular therapies.

Experimental

Reagents: NS1 was synthesized as previously described (Li et al., 2012). Acetylcholine (Ach), catalase, calmodulin (CaM) diethyldithiocarbamate sodium salt (DETC-Na), KCl, Fe(SO₄)₂, Na₂S₂O₄, diethylenetriaminepentaacetic acid (DTPA), Hepes, phorbol 12-myristate 13-acetate (PMA), 3-[4,5-dimethylthiazol-2-yl]-2,5-diphenyl tetrazolium bromide (MTT), recombinant mouse IFN- γ , glutathione reductase (from baker's yeast) (GR), glucose 6-phosphate dehydrogenase (from baker's yeast) (G6PDH), oxidized glutathione (GSSG), L-NG-nitroarginine methyl ester (L-NAME) and *E. coli* lipopolysaccharide (LPS) were purchased from Sigma-Aldrich (Saint-Quentin Fallavier, France). 5-diethoxyphosphoryl-5-methyl-pyrroline *N*-oxide (DEPMPO) was from Radical Vision (Marseille, France). 1-Hydroxy-2,2,6,6-tetramethylpiperidin-4-yl-trimethylammonium chloride (CAT-1-H) and 1-hydroxy-3-methoxycarbonyl-2,2,5,5-tetramethylpyrrolidine hydrochloride (CM-H) were from Enzo Life Sciences Inc. (Farmingdale, NY, USA). DMEM culture media and endotoxin-low fetal calf serum (FCS) were from Gibco-InVitrogen. CellROX® Deep Red Reagent was purchased from Invitrogen.

Experiments with recombinant nNOS: Recombinant rat brain nNOS was expressed and purified as described (Moali et al, 1998). Superoxide anion formed by nNOS was detected by spin-trapping with DEPMPO and EPR detection of the spin adducts. The following instrument settings were used, field modulation frequency, 100 kHz; field modulation amplitude, 2 G; time constant, 40.96 ms; conversion time, 40.96 ms; microwave power, 10 mW; field width, 140 G; center field, 3490 G; scan time, 41.94 s; number of scans, 16. DEPMPO-OOH spectrum (hyperfine splitting constants, AN, 13.4G, AP, 52.5 G, and AH 11.9 G) was identified by comparison with incubations performed in the presence of xanthine/xanthine oxidase as previously described (Frejaille et al., 1995). The DEPMPO-OOH spin adduct slowly decomposed to the DEPMPO-OH spin adduct (half-life of about 25 min) and the amounts of DEPMPO-OH spin adduct were neglected under our conditions.

The changes in the amplitude of the first peak of the DEPMPO-OOH adduct (maximum, 3448 G; minimum, 3450 G) as a function of time were used to quantify the amounts of

superoxide generated in the experiments and the rates of these changes were plotted for 10 min after the addition of nNOS. Hydrogen peroxide released by nNOS was determined by measuring the oxidation of ferrous thiocyanate to ferric thiocyanate as previously described (Heinzel et al., 1992). The reaction mixture contained NADPH (200 μ M), CaCl_2 (1.0 mM), and CaM (10 μ g/mL) in 50 mM Hepes buffer pH 7.4. The incubation was initiated by the addition of aliquots of nNOS (40-100 nM) and stopped after 10 min at 37°C by the addition of 6M HCl; 10 μ L of 0.5 M NH_4SCN (in water) and 50 μ L of $\text{Fe}(\text{SO}_4)_2$ (freshly prepared) were added to the mixture, the absorbance at 492 nm of the ferric thiocyanate complex was read on a microplate reader after 10 min. The H_2O_2 release was determined by comparison with a calibration curve using known amounts of H_2O_2 (0–25 μ M); H_2O_2 concentration was determined using $\epsilon_{240 \text{ nm}} = 39.4 \text{ M}^{-1} \cdot \text{cm}^{-1}$ (Nelson and Kiesow, 1972).

Cell culture and treatments: Cultured mouse macrophage cell line RAW 264.7 cells were grown to confluence in 75 cm^2 flasks containing 15 mL DMEM growth medium supplemented with 5% FCS, 10 U/mL penicillin and 100 μ g/mL streptomycin under a 5% CO_2 atmosphere at 37°C. Endothelial (HUVECs and BAECs) and vascular smooth muscle cells (A7r5) were cultured in P100 dishes or 96-well plates (10^4 cells/well) at 37 °C to ~95% confluence in Eagle's Minimal Essential Medium containing 10% fetal calf serum, 5 mM glutamine, penicillin–streptomycin (100 U/mL), 2.5 μ g/mL amphotericin, and 125 μ g/mL gentamycin. Human melanocyte suspensions were obtained from foreskins of Caucasian children as previously described (Botton et al., 2009). Human primary melanocytes were grown in MCDB153 medium supplemented with 2% fetal calf serum, 0.5 mg/ml hydrocortisone, 5 mg/ml insulin, 16 nM phorbol-12 myristate 13- acetate, 1 ng/ml basic fibroblast growth factor, 20 mg/ml bovine pituitary extract, 10 mM forskolin, and penicillin/streptomycin (100U/ml /50 mg/ml) (Botton et al., 2011). Human A375 (CRL-1619) melanoma cells were purchased from American Tissue Culture Collection (Molsheim, France) and grown in DMEM medium supplemented with 10% FCS and penicillin/streptomycin (100 U/ml /50 mg/ml). For each experiment, cells were starved with or without 1% SVF in appropriate medium during 14 h before drug stimulation.

Cell viability tests: Serial dilutions of NS1 (1 μ M - 100 μ M) were added to the cells that were further incubated at 37°C for up to 24 or 48 hours. MTT analysis was performed

following a standard method. At the chosen time, 20 μ L of 5 mg/mL MTT in PBS was added to the cells and further incubated at 37 °C. After washing, 100 μ l of DMSO were added in each well and absorbance at 570 nm was measured on a multi-well Plate Reader (Model VICTORTM X4, PerkinElmer) with subtraction of blank value at 630 nm. In additional experiments, crystal violet reagent was used to detect living cells. At the chosen time, crystal violet reagent (100 μ l of 2mg/ml in distilled water) was added to the cells and further incubated at 37°C for 15 min. After washing of the cells, 100 μ l of DMSO were added in each well and the absorbance at 570 nm was measured on a multi-well Plate Reader with subtraction of the blank value at 630 nm. Results were expressed as percentage versus control condition. In additional experiments, crystal violet reagent was used to detect living cells and cell growth cultured in the presence of NS1 was recorded by videomicroscopy using an Axiocam camera.

Cellular number of melanocytes and melanoma A375 cells: viable cells were counted using trypan blue dye exclusion method as previously described (Tomic et al., 2011).

Mouse isolated vessels experiments: Aorta rings were dissected from 15 weeks-old male C57Bl/6J mice (Elevage Janvier, Le Genest-St-Isle, France) anesthetized with ketamine/xylazine before sacrifice. All experimental procedures and protocols were approved by the local Ethics Committee according to National Care Regulations. ***Vascular reactivity studies protocol:*** Briefly (Rath et al., 2012), vessels were mounted on two 40 mm stainless steel wires in the jaws of a multi wire myograph system (Model 610M, Danish Myo Technology A/S, Aarhus, Denmark) and the myograph baths filled with physiological saline solution at 37 °C saturated with 95% O₂/5% CO₂ at pH=7.4. Aorta were loaded to a tension equivalent to an *in vivo* pressure and then left to equilibrate for 1 h, after which they were stimulated with 50 mM KCl or with 10 μ M phenylephrine (Phe). A concentration-response curve was constructed by a single dose of Ach (10 μ M). Then, vessels were washed and pre-incubated in presence or absence of catalase 500 U/mL during 20 minutes. A contraction curve with 50 mM KCl was performed and once a maximal contraction had been achieved, a single dose of NS1 (10 μ M) was added and changes in tension recorded for 2 hours. At the end of this period, a new concentration-response curve was constructed by the addition of Ach (10 μ M). Ach relaxation responses were expressed as percentage of relaxation to KCl contraction. All experiments were

performed in the presence of indomethacin (10 μ M). Results are expressed as means \pm SEM and n reflects the number of animals. Significant differences between groups were calculated by ANOVA followed by a Bonferroni test. $p < 0.05$ was considered significant.

Measurements of nitric oxide production from endothelial cells and isolated aortic rings in situ by Electron Paramagnetic Resonance (EPR) spin trapping: Production of NO was assayed by EPR spin trapping as by the concentration of paramagnetic NO adduct formed in presence of the spin trap ([Fe(II)-(DETC)₂] in KREBS-Hepes buffer) in BAECs and isolated aortic rings incubated with NS1 or vehicle (1hr at 37°C) and stimulated or not with calcium ionophore (A23187, 2 μ M or ionomycin, 2 μ M) at 37°C during 30 minutes (Lobysheva et al., 2011). [Fe(II)NO-(DETC)₂] EPR signal ($g_1 = 2.035$; $A_{\text{hfs}} = 1.3$ mT) was recorded on a Bruker EMX100 spectrometer (X-band, microwave frequency \sim 9.35 GHz, modulation frequency, 100 kHz).

Measurements of superoxide anion production by Electron Paramagnetic Resonance: Superoxide anion formation was assayed by EPR using spin probes (cell non-permeable CAT1-H or cell-permeable CM-H) (Dikalov et al. 2007) with some modification: aortic rings (about 1-mm length) were dissected from mouse thoracic artery, preincubated on ice (1 hour) in KREBS-DTPA-Hepes buffer (0.1 mM DTPA, 20 mM HEPES, pH 7.5) with or without NS1, catalase (100U/ml) or SOD (100U/mL), and inserted into the capillary after addition of spin probe (CM-H or CAT1-H, 2.5 and 5 mM, respectively). The kinetics of EPR signals formation of the CM. or CAT1. species were recorded on-line during 10 minutes at 37°C in capillary interposed into cavity of EPR spectrometer (MiniScop MS400, Magnetech, equipped with bio-temperature controller). The following instrumental settings were used, modulation frequency, 100 kHz; microwave frequency, \sim 9.4 GHz; MP, 20 mW; MA, 0.1 mT. The rate of aortic basal ROS formation was calculated as a slope of linearized kinetic curve, obtained from automatically recording of radical signal formation (first hf component) using Magnetech kinetic software, and normalized by the length of aortic rings or protein content after subtraction of the basal signal (without aortic rings). Preincubation of aortic rings with SOD (100U/ml, 30 minutes on ice) decreased EPR signal accumulation by 80%.

Experiments with RAW 264.7 cells: Cultured RAW 264.7 cells were stimulated by PMA and superoxide anions generated by the NADPH oxidase activity were trapped with the cyclic

nitron DEPMPO and measured by EPR detection of the DEPMPO-OOH spin-adduct. Measurements of the rates of formation of the DEPMPO-OOH spin adduct were carried out at 21°C using the same settings as for experiments with nNOS.

Fluorescence detection of ROS generation: CellROX[®] Deep Red Reagent (Invitrogen) was used for oxidative stress detection. HUVEC plated in 12-well plates at 85% confluence were pre-incubated with increasing concentrations of NS1 for 30 min at 37°C, and then further incubated with 2 µM CellROX[®] Deep Red Reagent for 30 min. Tert-butyl hydroperoxide (TBHP) (Sigma), an oxidative stress inducer, was used as a positive control. After centrifugation at 1,000 rpm for 5 min, the cell pellets were resuspended in PBS containing 30% of enzyme-free Cell Dissociation Buffer (Gibco[®]) and analysed by FACS Calibur flow cytometer (Becton-Dickinson). To address the modulation effect of NS1 on ROS formation, the MFI (Mean Fluorescence Intensity) related to fluorescence emission of the CellROX[®] Deep Red Reagent, detected in FL-4 channel and measured in the presence of a given concentration of NS1, was normalized by the MFI obtained in the absence of NS1 (*i.e.* CellROX[®] Deep Red Reagent alone; also measured in FL-4 channel), giving the fluorescence enhancement factor.

Angiogenesis assays: To assess in vitro the angiogenic process, an assay of endothelial network formation by plating of endothelial cells (HUVECs (passage 3-5)) on Matrigel was used as previously reported (Brouet et al., 2001). Results are expressed as endothelial network percentage ± SEM versus control condition and *n* reflects the number of experiments.

Results

NS1 inhibits the formation of NO by endothelial cells and isolated mice aortic rings. NO production, sensitive to L-N^G-nitroarginine methyl ester (L-NAME), a nitric oxide synthase inhibitor, was assessed by EPR spin trapping as formation of the paramagnetic [Fe(DETC)₂NO] complex in bovine aortic endothelial cells (BAECs) in the presence of Fe(DETC)₂. The addition of 30 μM NS1 had no significant effect on the formation of NO by BAECs under basal conditions (basal level was normalized at 100, Fig. 1A). After stimulation with Ca²⁺-ionophore, A23187, we observed a 2.6-fold increase in NO formation in comparison with basal conditions (256 ±30 % of control, n=8). One-hour incubation with NS1 (30 μM) significantly inhibited stimulated-NO production in BAECs by 1.7 times (down to 153±19% of control, n=6, Figure 1A), leading to an estimated IC₅₀ value of about 30 μM (see also Table 1).

NO formation by isolated mice aortic rings stimulated with ionomycin was monitored by EPR spin trapping as described above in the presence or absence of NS1. NO decreased in a monotonic manner, the extent of inhibition increasing with NS1 concentration up to a plateau. Further addition of a NOS inhibitor did not change the plateau value within experimental error. These data yielded a half inhibitory concentration IC₅₀ = 40 ± 20 μM, a similar value than that observed with BAECs (Table 1 and Figure 1B).

NS1 inhibits the endothelium- dependent relaxation of mice aortic rings. Mice aorta rings mounted on a wire myograph were pre-contracted with KCl and the tension developed by the rings was measured. KCl stimulation promoted smooth muscle cells depolarization and prevented influences of endothelium-derived hyperpolarization (factors) in the presence of indomethacin (to inhibit cyclooxygenase-dependent modulation of tone). Ach (10 μM) afforded relaxation of pre-contraction by KCl which was inhibited by the addition of L-NAME, a NOS inhibitor (Fig. 2A). Surprisingly, NS1 (1-10 μM) induced a strong vasorelaxation of the aortic rings, which was delayed in the presence of 100μM NADPH and fully abolished by adding of 500U/ml catalase (Fig. 2B). Similar vasorelaxation was observed when the rings were pre-contracted with phenylephrine or with aortic rings without functional endothelium (Supplementary figure 1). In contrast, addition of SOD did not modify the vasorelaxation effect of NS1 (Supplementary figure 2), suggesting a hydrogen peroxide and not a superoxide ion-dependent effect.

In aorta, both NO and H₂O₂ are signaling molecules able to modulate the vascular tone. In order to evaluate the effect of NS1 on the NO-dependent relaxation, vessels were stimulated by high potassium in the presence of catalase (to repress the endothelium-independent effects of NS1) and Ach (10 μM) was added to KCl pre-contracted rings. As expected from NS1 inhibiting eNOS, a NO-dependent vasoconstriction was observed (Figure 2B). In these conditions, the relaxation of mice aortic rings induced by muscarinic receptors stimulation uniquely resides on NO produced by endothelial cells. Our data indicated that in these conditions NS1 inhibited the relaxation induced by acetylcholine, as expected for an inhibitor of eNOS (Figure 2A, L-NAME).

The endothelium-independent vasorelaxation induced by NS1 could be related to the release of H₂O₂ as suggested by the effects of catalase. Hydrogen peroxide is a signaling molecule (Toledano et al., 2010) with vasoconstriction and vasodilation properties depending on the vascular bed and experimental conditions (Santiago et al., 2013). Figure 2A suggested that NS1 could affect other targets than NOS, in particular NADPH- (reductase) or NADP-(dehydrogenase) dependent enzymes and led us to promptly investigate the effects of NS1 on the formation of ROS in isolated aorta and in HUVECs, including purified nNOS and activated macrophages.

Effect of NS1 on the formation of ROS by mice aortic rings. ROS production, sensitive to addition of SOD, was measured by two EPR spin probes: cell permeable CM-H and CAT1-H, the charged analogue that cannot easily cross cellular membrane. Pre-incubation of mice aortic rings for 30 min on ice with 100 U/mL SOD decreased EPR signals by 80% (Figure 3A). One-hour incubation of isolated aortic rings with 10 μM NS1 inhibited the formation of CAT1[•] radicals by 60 ± 19 %, a similar level than that observed with SOD within experimental error. The same NS1 concentration did not change within experimental error the intracellular level of CM[•] radical in isolated aortic rings assayed by *in situ* EPR signal formation at 37°C. Interestingly, incubation with a higher NS1 concentration (30 μM) significantly increased ROS (Figure 3B) detected by changes in the CM[•] EPR signal in aortic rings isolated from the same thoracic aorta. These levels of superoxide ions were low and did not trigger deleterious effects on endothelial cells (HUVECs) and vascular smooth muscle cells (A7r5) as detected by crystal violet staining (Table 2). Furthermore, the growth of HUVECs in the presence of 30 μM NS1

was recorded by video-microscopy for 24 h and did not significantly differ from that of cells treated by vehicle alone (data not shown). These data confirmed the low toxicity of NS1 in these cells.

The unexpected complex effect of NS1 on superoxide ions levels results prompted us at using well-established conditions for O_2^- produced by uncoupled NOS and by activated NOX, thus at testing the hypothesis of inhibition by NS1 of ROS formed by NOS and NOX.

NS1 inhibits H_2O_2 and superoxide formation by nNOS under uncoupling conditions. NOS catalysis involves binding of Ca^{2+}/CaM allowing electron flow to the heme and rapidly leads to a Fe^{II} -heme- O_2 complex formation. In the absence of substrate and/or cofactor H_4B , this complex dissociates to form superoxide and regenerate Fe^{III} -heme (uncoupling) (Stuehr et al., 2004). In addition, NOS can also generate ROS from O_2 reduction by flavins of the reductase domain. We tested the effects of NS1 on the levels of both hydrogen peroxide and superoxide ions formed by uncoupled nNOS: H_2O_2 in a colorimetric assay and O_2^- monitored by EPR spectroscopy using spin-trapping experiments in the presence of the cyclic nitrono DEPMPPO. In the absence of substrate L-arginine and in the presence of low amounts of H_4B , H_2O_2 formation by nNOS was $145 \pm 22 \text{ nmol} \cdot \text{min}^{-1} \cdot \text{mg prot}^{-1}$. The addition of increasing amounts of NS1 inhibited the formation of H_2O_2 by nNOS under uncoupling conditions with an IC_{50} value of $75 \pm 12 \mu\text{M}$ (Table 1). Incubations of recombinant nNOS in the presence of NADPH, Ca^{2+}/CaM and DEPMPPO but in the absence of L-arginine and H_4B led to the gradual appearance of the characteristic 8-lines features on the EPR spectra corresponding to the nitroxide DEPMPPO-OOH spin-adduct (Insert Fig. 4A). The rate of formation of the DEPMPPO-OOH spin-adduct was reduced by the addition of $100 \mu\text{M}$ L-arginine and $10 \mu\text{M}$ H_4B (Figure 4A). The addition of increasing amounts of NS1 inhibited the rate of formation of the EPR signals of the DEPMPPO-OOH spin-adduct with an $IC_{50} = 105 \pm 15 \mu\text{M}$ without formation of other detectable paramagnetic species. The results supported that NS1 inhibited electron leakage in nNOS as expected from NS1 design that targets the reductase domain and blocks the overall electron flow.

NS1 inhibits superoxide formation by PMA- activated macrophages. Treatment of RAW 264.7 cells by PMA led to activation of NADPH oxidase with release of superoxide anion radical. This radical was trapped by the cyclic nitrono DEPMPPO and the nitroxide

DEPMPO-OOH spin-adduct was detected by EPR. The characteristic 8-lines features on the EPR spectra corresponding to the nitroxide DEPMPO-OOH spin-adduct gradually appeared and the rates of its formation were measured as described above. The addition of increasing amounts of NS1 to the PMA-stimulated cells led to half-inhibition of the accumulation of DEPMPO-OOH spin-adduct with an $IC_{50} = 120 \pm 25 \mu M$ (Fig. 4B and Table 1). These results supported the hypothesis that NS1 inhibited NOX activity in this cell line.

Biphasic effect of NS1 on ROS formation in HUVECs detected by a fluorescent probe.

The modulation effect of NS1 on ROS formation in HUVECs was addressed by performing cytometry experiments using the CellROX[®] Deep Red oxidative stress detector (Figure 5). ROS formation is shown by an enhancement of the probe fluorescence (absorption/emission maxima at ~644/665 nm) as observed using tert-butyl hydroperoxide (TBHP) as a positive control for ROS formation. Fluorescence signals of NS1 and CellROX[®] Deep Red were measured by using FL-1 and FL-4 channels, respectively. To minimize differences in basal cellular ROS among different experiments, the fluorescence signal in the presence of NS1 was normalized by the signal monitored in the same cells without NS1. This normalization gave a fluorescence enhancement factor, which accounts for ROS formation as a function of NS1 concentration (Fig. 5A). ROS detection in HUVECs presented a bell-shaped response, with an increasing phase up to 1-2 μM of NS1, followed by a decrease in fluorescence intensity below 1 at higher (above 2 μM) NS1 concentrations, indicating that NS1 inhibited the basal production of ROS in HUVECs. This biphasic behavior probably results from the combination from a main inhibition phase of ROS by NS1 with a minor enhancement of ROS formation, resembling the dual detection of ROS in isolated aorta by the two spin traps CAT1-H and CM-H. The CAT1-H spin probe showed that NS1 inhibited ROS formed by membrane-bound enzymes in aorta. Therefore, NS1 may target and inhibit not only ROS formed by eNOS as expected from the *in vitro* experiments with uncoupled nNOS but also ROS formed by NOX, a hypothesis further confirmed by RAW macrophages experiments. Fluorescence data qualitatively supported the endothelium-dependent inhibition of ROS by NS1; an additional target for NS1 in HUVECS or aortic rings should be responsible for the NS1 formation of ROS detected by CM-H and observed in the vasorelaxation experiments in the absence of catalase and in the absence of endothelium.

NS1 inhibits VEGF-dependent angiogenesis of HUVECs. To extend the pharmacological response of NS1 to another eNOS-dependent process besides the modulation of the vascular tone, we investigated the effect of NS1 on VEGF-induced angiogenesis. To assess the effects of NS1 on the angiogenic process, an assay of endothelial network formation (plating of HUVECs on Matrigel) was used and the formation of cord capillary structures in the absence or presence of 1% serum as previously reported (Brouet et al., 2001; Dessy et al., 2005) was monitored as a function of time (Figure 6A). Addition of 100 μ M significantly slowed down the rate and the amount of tube formation compared to control experiments that showed significant increase in capillary structures formation 24 h after plating. Addition of increasing concentrations of NS1 to the cells led to a strong reduction of their ability to form capillary structures in serum free buffer or in the presence of 1% serum (Figure 6B). All the experiments showed significant differences between groups and demonstrated the anti-angiogenic effect of NS1 on these endothelial cells.

NS1 effect on normal melanocytes and melanoma cells. Melanoma is characterized by its high propensity to metastasize and its proliferation has been linked to altered redox signalling in which NOX4, uncoupled eNOS and sustained iNOS expression is involved (Godoy et al., 2012; Melo et al., 2011; Yamaura et al., 2009). Because NS1 should affect these cellular targets associated with redox stress, we tested whether NS1 may affect the number of metastatic melanoma A375 cells. Normal human melanocytes were used as a control. Figure 7A shows that increasing concentrations of NS1 had minimal effect on these healthy cells after 24 and 48 hours, in agreement with the lack of toxicity of NS1 on endothelial and smooth vascular cells (Table 2). In contrast, NS1 reduced the proliferation of melanoma cells in a time- and dose-dependent manner (Fig. 7B and C). 48 hours incubation with 50 μ M NS1 reduced cell proliferation to 55% and 66% of the controls in serum-free and serum-enriched conditions, respectively while additional incubation with NS1 led to further decrease to 25 and 5% after 96 hours. The dose dependence of NS1 seems to be a monotonic decrease of number of A375 cells in the presence of serum (Figure 7B). In serum-free conditions, NS1 seems to have a more complex effect. This initial study showed a differential and specific effect of NS1 on melanoma and not on their healthy cells counterpart and more work will be required for dissecting the mechanisms involved in NS1 effect.

Discussion

Our recent *in vitro* data (Li et al., 2012) showed that NS1 was a new prototype of a reversible inhibitor of NOS targeting their reductase domain. NS1 was designed by molecular modelling, by replacing the imbedded NADP cofactor in nNOS reductase domain (Garcin et al., 2004; Li et al., 2012). The nucleotide moiety of NS1 allows proper targeting to the NADPH site; thus, NS1 competes with NADPH binding (Beaumont et al., 2007; Lambry et al., 2010; Li et al., 2012). This nucleotide moiety is linked to a photoactive chromophore. Therefore, NS1 was also a novel fluorescent probe upon two-photon excitation that co-localized with eNOS in HUVEC cells in the Golgi complex and at the cell membrane. In this work, we tested the broad potential pharmacological applications of NS1 in terms of NO and ROS modulation in vascular biology using various cells and *ex vivo* systems.

Inhibition of NO by NS1 targeting eNOS in the endothelium: NS1 inhibited NO formed by eNOS expressed in BAEC and isolated aortic rings. The IC₅₀ values for NO inhibition were similar in these systems (Table 1) and corresponded to IC₅₀ previously determined *in vitro*, IC₅₀ = 30 ± 10 μM (Li et al., 2012). We further investigated the effects of NS1 in vasomodulation of the vascular tone. NS1 inhibited 80% of the acetylcholine-mediated relaxation of pre-contracted mice aortic rings in the presence of catalase in the low μM range (Figure 2B, Table 1), which is an NO-dependent process. NS1 modulation of another NO-dependent effect: endothelial sprouting of HUVEC cells in a 3-D model of angiogenesis was also investigated (Sonveaux et al., 2004). As expected from VEGF-mediated signalling combined with NS1 inhibition of eNOS, NS1 exhibited anti-angiogenic effects in a dose-dependent manner (Figure 6). Taken together, the data show that NS1 inhibited two important NO-dependent processes in endothelial cells and in aortic rings: vasodilation (in the presence of catalase) and angiogenesis. This result is in agreement with NS1 targeting the NADPH site of constitutive NOS (Li et al., 2012). The anti-angiogenic property of NS1 offers great perspectives for therapeutic strategies aimed at targeting deleterious effects of NO produced by iNOS or eNOS in metastasis (Kostourou et al., 2011; Lim et al., 2008).

Modulation of ROS levels by NS1 in endothelium-dependent and independent processes: Further experiments aimed at testing whether NS1 inhibited ROS formation in isolated aorta and endothelial cells. ROS inhibition was a consequence of NS1 blocking the

electron flow in NOS, which resulted in superoxide and hydrogen peroxide inhibition formed by purified nNOS *in vitro* under uncoupling conditions. This is an expected intrinsic advantage of NS1 over other NOS inhibitors directed against the oxygenase domain, thus unable to avoid uncoupling at the level of the reductase domain. Besides uncoupled e/nNOS (Maron and Michel, 2012), the main sources of ROS in the vasculature are NADPH oxidases and the mitochondrial respiratory chain. ROS levels also depend on the redox homeostasis, on oxygen and NO levels. Since NS1 inhibited superoxide ions formed by NADPH-oxidase(s) in PMA-stimulated RAW 264.7 macrophages, NS1 also likely inhibited these enzymatic targets in the endothelium of mice aorta. These results are consistent with on the one hand NS1 inhibition of ROS formed in aorta monitored by a cell impermeable spin trap and on the other hand several NOX isoforms and eNOS being found in endothelial cells membranes (BelAiba et al., 2007).

In fully functional aortic rings with a COX inhibitor in the absence of catalase (Fig 2A), NS1 induced vasorelaxation by a burst of hydrogen peroxide that could be inhibited by adding catalase (by reduction of H₂O₂ into H₂O). This showed that NO-dependent vasoconstriction was masked by H₂O₂-mediated processes that affected the vascular tone. Such relaxation was partly dependent on NADPH (Figure 2A), and was also observed using endothelium-depleted aortic rings (data not shown), both effects suggesting that NS1 targets additional enzymes besides eNOS and NOX in vascular smooth muscle cells. H₂O₂ is a signalling molecule at low concentration (Santiago et al., 2013; Toledano et al., 2010) and may promote vasorelaxation or vasoconstriction depending upon the vascular bed and the redox conditions: under oxidative stress, H₂O₂ induces vasoconstriction, a process dependent on COX-1, on the presence of endothelium and reversed by catalase (Santiago et al., 2013); under anti-oxidant treatment as tempol, H₂O₂ induces vasorelaxation that can be partly abolished by a NOS inhibitor (Puri et al., 2013). A number of enzyme(s) could be involved in the NS1-induced H₂O₂ burst in an indirect manner:

(i) KCl-induced depolarization of aorta was reported at activating glucose 6-phosphate dehydrogenase (G6PD) and derived NADPH, required for NADPH oxidase and glutathione reductase activities. This led at coronary aorta contraction, possibly via an NADPH oxidase-dependent effect (Gupte et al., 2011). NS1 inhibition of G6PD by blocking its NADP

site may therefore lead to vasodilation in an endothelium-independent manner. Preliminary *in vitro* experiments suggested that NS1 inhibited purified G6PD with an EC50 of about 60 to 100 μ M, which may be consistent with the small inhibition of cell metabolism observed in A7R5 cells (MTT tests, Table 2), in agreement with the role of G6PD in the pentose-phosphate pathway (Gupte et al., 2011).

(ii) Beside catalase, H₂O₂ can be scavenged by glutathione via glutathione peroxidase GP, itself coupled with glutathione reductase GR, an enzyme requiring NADPH (Weldy et al., 2012). This cycle can take place without endothelium and is only partly inhibited by a NOS-inhibitor. In that scenario, NS1 may inhibit glutathione reductase, leading to an unbalanced glutathione/ redox homeostasis. However, preliminary *in vitro* experiments did not support a significant inhibition of GR by NS1 (EC50 > 250 μ M).

Taken together, the data support that NS1 binds eNOS and NADPH oxidase(s) in the HUVECs / endothelium of aortic rings and affords NO and ROS inhibition. NS1 probably reaches a third target, possibly in present both in endothelium and in smooth vascular cells, the candidates being mitochondrial or Golgi-located enzymes as G6PD. This hypothesis is supported by (1) ROS formation detected by a cell permeable EPR probe at high NS1 concentrations in aorta; (2) H₂O₂-dependent vasorelaxation of endothelium-depleted aortic rings; (3) ROS formation detected with a fluorescent probe followed by a ROS inhibition phase in HUVECs. Biphasic probing of ROS was observed (Wind et al., 2010) and may reflect concentration and/or redox –dependent effects of NO and H₂O₂.

We emphasize that the modulation of ROS levels induced by NS1 by an increase or decrease by a factor of ~1.5- 2.0 times with respect to basal level in endothelial cells (Figure 5) likely took place within the physiological range. This suggests that NS1 may modulate NO and/or ROS (H₂O₂) signalling without generating toxic concentrations of these mediators in endothelial and smooth muscle vascular cells (Table 2).

Chemical inhibition of NOX that contributes to support aerobic glycolysis in cancer led to inhibition of cancer growth *in vivo* (Lu et al., 2012); altered redox status of cancer cells and their environment promote angiogenesis (Garrido-Urbani et al., 2011). To test potential applications of NS1, we investigated whether NS1 had a specific effect on metastatic melanoma cells compared with normal melanocytes. NS1 induced a specific decrease of metastatic

melanoma cells number (Fig. 7A, B). Both NO and ROS levels affect melanoma growth and invasion: NOX4 is highly expressed in A375 cells and not in melanocytes (Yamaura et al., 2009) and regulates the G2/M transition to promote melanoma growth. Melanoma cells also express iNOS and uncoupled eNOS (Godoy et al., 2012; Melo et al., 2011). Thus, by decreasing NO and ROS levels, NS1 may be useful to reduce melanoma invasion and modulate their abnormal signalling. The mechanisms involved in NS1 reduction of melanoma proliferation are presently under investigation (Tomic et al., 2011).

The ability of NS1 to avoid e/nNOS uncoupling and to inhibit excessive ROS levels formed in endothelial cells and macrophages suggest that NS1 could have great potential to revert from endothelial dysfunction. The pharmacological effects of NS1 were reverted by addition of NADPH, showing that NS1 likely targets NADPH sites of NOS or NOX subunits or NADP sites of G6PD, as expected from its design (Beaumont et al., 2009; Beaumont et al., 2007; Beaumont et al., 2008; Li et al., 2012). This molecular-targeted mode of inhibition is unique. Unspecific ROS inhibition by antioxidants as red wine polyphenol was reported (Idris Khodja et al., 2012). NADPH-oxidase inhibitors prevented NOX subunit assemblies (Wind et al., 2010). In conclusion, NS1 has dual functions of imaging eNOS in endothelial cells and pharmacological effects consistent with NS1 targeting eNOS and likely NADPH oxidase(s), with broad interest for endothelial dysfunction and cancer. Importantly, pharmacological application of NS1 allows vasodilation, redox stress decrease and a specific reduction of metastatic melanoma cells number.

Acknowledgments

This work was supported by Agence Nationale de la Recherche (ANR-PCVI08-006-01, TRIGNOSTUMOR) to AS (PI), JLB and ED.

The authors thank Dr Y. Frapart (UMR 8601 CNRS, Paris) for assistance in EPR experiments, Dr K. Abbas (UMR 8601 CNRS, Paris) for her help with RAW cells experiments and Dr Stuehr for providing NOS samples.

References

Beaumont, E., Lambry, J.C., Blanchard-Desce, M., Martasek, P., Panda, S.P., van Faassen, E.E., Brochon, J.C., Deprez, E., and Slama-Schwok, A. (2009). NO formation by neuronal NO-synthase can be controlled by ultrafast electron injection from a nanotrigger. *ChemBiochem* 10, 690-701.

Beaumont, E., Lambry, J.C., Gautier, C., Robin, A.C., Gmouh, S., Berka, V., Tsai, A.L., Blanchard-Desce, M., and Slama-Schwok, A. (2007). Synchronous photoinitiation of endothelial NO synthase activity by a nanotrigger targeted at its NADPH site. *J Am Chem Soc* 129, 2178-2186.

Beaumont, E., Lambry, J.C., Robin, A.C., Martasek, P., Blanchard-Desce, M., and Slama-Schwok, A. (2008). Two photon-induced electron injection from a nanotrigger in native endothelial NO-synthase. *Chemphyschem* 9, 2325-2331.

BelAiba, R.S., Djordjevic, T., Petry, A., Diemer, K., Bonello, S., Banfi, B., Hess, J., Pogrebniak, A., Bickel, C., and Gorlach, A. (2007). NOX5 variants are functionally active in endothelial cells. *Free Radic Biol Med* 42, 446-459.

Botton T, Puissant A, Bahadoran P, Annicotte JS, Fajas L, Ortonne JP, Gozzerino G, Zamoum T, Tartare-Deckert S, Bertolotto C, Ballotti R, Rocchi S. (2009). In vitro and in vivo anti-melanoma effects of ciglitazone. *J Invest Dermatol.* 129, 1208-18.

Brouet, A., Sonveaux, P., Dessy, C., Moniotte, S., Balligand, J.L., and Feron, O. (2001). Hsp90 and caveolin are key targets for the proangiogenic nitric oxide-mediated effects of statins. *Circ Res* 89, 866-873.

Crane BR, A.A., Ghosh DK, Wu C, Getzoff ED, Stuehr DJ, Tainer JA. (1998). Structure of nitric oxide synthase oxygenase dimer with pterin and substrate. *Science* 279, 2121-2126.

Dessy, C., Saliez, J., Ghisdal, P., Daneau, G., Lobysheva, II, Frerart, F., Belge, C., Jnaoui, K., Noirhomme, P., Feron, O., et al. (2005). Endothelial beta3-adrenoreceptors mediate nitric oxide-dependent vasorelaxation of coronary microvessels in response to the third-generation beta-blocker nebivolol. *Circulation* 112, 1198-1205.

Dikalov, S., Griendling, K.K., and Harrison, D.G. (2007). Measurement of reactive oxygen species in cardiovascular studies. *Hypertension* 49, 717-727.

Forstermann, U., and Sessa, W.C. (2012). Nitric oxide synthases: regulation and function. *Eur Heart J* 33, 829-837, 837a-837d.

Frejaville C, Karoui H, Tuccio B, Le Moigne F, Culcasi M, Pietri S, Lauricella R, Tordo P. (1995). 5-(Diethoxyphosphoryl)-5-methyl-1-pyrroline N-oxide: a new efficient phosphorylated nitron for the in vitro and in vivo spin trapping of oxygen-centered radicals. *J Med Chem.* 38, 258-65.

Garcin, E.D., Bruns, C.M., Lloyd, S.J., Hosfield, D.J., Tiso, M., Gachhui, R., Stuehr, D.J., Tainer, J.A., and Getzoff, E.D. (2004). Structural basis for isozyme-specific regulation of electron transfer in nitric-oxide synthase. *J Biol Chem* 279, 37918-37927.

- Garrido-Urbani, S., Jemelin, S., Deffert, C., Carnesecchi, S., Basset, O., Szyndralewicz, C., Heitz, F., Page, P., Montet, X., Michalik, L., *et al.* (2011). Targeting vascular NADPH oxidase 1 blocks tumor angiogenesis through a PPARalpha mediated mechanism. *PLoS One* 6, e14665.
- Godoy, L.C., Anderson, C.T., Chowdhury, R., Trudel, L.J., and Wogan, G.N. (2012). Endogenously produced nitric oxide mitigates sensitivity of melanoma cells to cisplatin. *Proc Natl Acad Sci U S A* 109, 20373-20378.
- Gupte, R.S., Ata, H., Rawat, D., Abe, M., Taylor, M.S., Ochi, R., and Gupte, S.A. (2011). Glucose-6-phosphate dehydrogenase is a regulator of vascular smooth muscle contraction. *Antioxid Redox Signal* 14, 543-558.
- Idris Khodja, N., Chataigneau, T., Auger, C., and Schini-Kerth, V.B. (2012). Grape-derived polyphenols improve aging-related endothelial dysfunction in rat mesenteric artery: role of oxidative stress and the angiotensin system. *PLoS One* 7, e32039.
- Ischiropoulos, H.B., JS (2003). Oxidative stress and nitration in neurodegeneration: cause, effect, or association? *J Clin Invest* 111, 163-169.
- Jachymova, M., Martasek, P, Panda, S., Roman, L.J., Shea, T.M., Ishimura, Y., Kim, J.J., Masters B.S. (2005). Recruitment of governing elements for electron transfer in the nitric oxide family. *Proc Natl Acad Sci USA* 102, 15833-15838.
- Kostourou, V., Cartwright, J.E., Johnstone, A.P., Boulton, J.K., Cullis, E.R., Whitley, G., and Robinson, S.P. (2011). The role of tumour-derived iNOS in tumour progression and angiogenesis. *Br J Cancer* 104, 83-90.
- Lambry, J.C., Beaumont, E., Tarus, B., Blanchard-Desce, M., and Slama-Schwok, A. (2010). Selective probing of a NADPH site controlled light-induced enzymatic catalysis. *J Mol Recognit* 23, 379-388.
- Li, H., and Forstermann, U. (2009). Prevention of atherosclerosis by interference with the vascular nitric oxide system. *Curr Pharm Des* 15, 3133-3145.
- Li, H., Igarashi, J., Jamal, J., Yang, W., and Poulos, T.L. (2006). Structural studies of constitutive nitric oxide synthases with diatomic ligands bound. *J Biol Inorg Chem* 11, 753-768.
- Li, Y., Wang, H., Tarus, B., Perez, M.R., Morellato, L., Henry, E., Berka, V., Tsai, A.L., Ramassamy, B., Dhimane, H., *et al.* (2012). Rational design of a fluorescent NADPH derivative imaging constitutive nitric-oxide synthases upon two-photon excitation. *Proc Natl Acad Sci U S A* 109, 12526-12531.
- Lim, K.H., Ancrile, B.B., Kashatus, D.F., and Counter, C.M. (2008). Tumour maintenance is mediated by eNOS. *Nature* 452, 646-649.
- Lobysheva, I., Rath, G., Sekkali, B., Bouzin, C., Feron, O., Gallez, B., Dessy, C., and Balligand, J.L. (2011). Moderate caveolin-1 downregulation prevents NADPH oxidase-dependent endothelial nitric oxide synthase uncoupling by angiotensin II in endothelial cells. *Arterioscler Thromb Vasc Biol* 31, 2098-2105.

Lu, W., Hu, Y., Chen, G., Chen, Z., Zhang, H., Wang, F., Feng, L., Pelicano, H., Wang, H., Keating, M.J., *et al.* (2012). Novel role of NOX in supporting aerobic glycolysis in cancer cells with mitochondrial dysfunction and as a potential target for cancer therapy. *PLoS Biol* *10*, e1001326.

Maron, B.A., and Michel, T. (2012). Subcellular localization of oxidants and redox modulation of endothelial nitric oxide synthase. *Circ J* *76*, 2497-2512.

Melo, F.H., Molognoni, F., Morais, A.S., Toricelli, M., Mouro, M.G., Higa, E.M., Lopes, J.D., and Jasiulionis, M.G. (2011). Endothelial nitric oxide synthase uncoupling as a key mediator of melanocyte malignant transformation associated with sustained stress conditions. *Free Radic Biol Med* *50*, 1263-1273.

Moali, C., Boucher, J.L., Sari, M.A., Stuehr, D.J., and Mansuy, D. (1998). Substrate specificity of NO synthases: detailed comparison of L-arginine, homo-L-arginine, their N omega-hydroxy derivatives, and N omega-hydroxynor-L-arginine. *Biochemistry* *37*, 10453-10460.

Moncada, S., Palmer, R.M., Higgs, E.A. (1991). Nitric oxide: physiology, pathophysiology and pharmacology. *Pharmacol Rev* *43*, 109-142.

Nelson DP, Kiesow LA. (1972). Enthalpy of decomposition of hydrogen peroxide by catalase at 25 degrees C (with molar extinction coefficients of H₂O₂ solutions in the UV). *Anal Biochem.* *49*, 474-8.

Puri, N., Zhang, F., Monu, S.R., Sodhi, K., Bellner, L., Lamon, B.D., Zhang, Y., Abraham, N.G., and Nasjletti, A. (2013). Antioxidants condition pleiotropic vascular responses to exogenous H₂O₂: role of modulation of vascular TP receptors and the heme oxygenase system. *Antioxid Redox Signal* *18*, 471-480.

Raman, C.S., Li, H., Martasek, P., Kral, V., Masters, B.S., and Poulos, T.L. (1998). Crystal structure of constitutive endothelial nitric oxide synthase: a paradigm for pterin function involving a novel metal center. *Cell* *95*, 939-950.

Rath, G., Saliez, J., Behets, G., Romero-Perez, M., Leon-Gomez, E., Bouzin, C., Vriens, J., Nilius, B., Feron, O., and Dessy, C. (2012). Vascular hypoxic preconditioning relies on TRPV4-dependent calcium influx and proper intercellular gap junctions communication. *Arterioscler Thromb Vasc Biol* *32*, 2241-2249.

Santiago, E., Contreras, C., Garcia-Sacristan, A., Sanchez, A., Rivera, L., Climent, B., and Prieto, D. (2013). Signaling pathways involved in the HO-induced vasoconstriction of rat coronary arteries. *Free Radic Biol Med* *60C*, 136-146.

Silverman, R.B. (2009). Design of selective neuronal nitric oxide synthase inhibitors for the prevention and treatment of neurodegenerative diseases. *Acc Chem Res* *42*, 439-451.

Sonveaux, P., Martinive, P., DeWever, J., Batova, Z., Daneau, G., Pelat, M., Ghisdal, P., Gregoire, V., Dessy, C., Balligand, J.L., *et al.* (2004). Caveolin-1 expression is critical for vascular endothelial growth factor-induced ischemic hindlimb collateralization and nitric oxide-mediated angiogenesis. *Circ Res* *95*, 154-161.

Stuehr, D.J., Fasehun, O.A., Kwon, N.S., Gross, S.S., Gonzalez, J.A., Levi, R., and Nathan, C.F. (1991). Inhibition of macrophage and endothelial cell nitric oxide synthase by diphenylethylidenehydrazide and its analogs. *FASEB J* 5, 98-103.

Stuehr, D.J., Wei, C.C., Santolini, J., Wang, Z., Aoyagi, M., and Getzoff, E.D. (2004). Radical reactions of nitric oxide synthases. *Biochem Soc Symp*, 39-49.

Szabó C, I.H., Radi R (2007). Peroxynitrite: biochemistry, pathophysiology and development of therapeutics. *Nat Rev Drug Discov* 6, 662-680.

Toledano, M.B., Planson, A.G., and Delaunay-Moisan, A. (2010). Reining in H₂O₂ for safe signaling. *Cell* 140, 454-456.

Tomic, T., Botton, T., Cerezo, M., Robert, G., Luciano, F., Puissant, A., Gounon, P., Allegra, M., Bertolotto, C., Bereder, J.M., *et al.* (2011). Metformin inhibits melanoma development through autophagy and apoptosis mechanisms. *Cell Death Dis* 2, e199.

Weldy, C.S., Luttrell, I.P., White, C.C., Morgan-Stevenson, V., Bammler, T.K., Beyer, R.P., Afsharinejad, Z., Kim, F., Chitale, K., and Kavanagh, T.J. (2012). Glutathione (GSH) and the GSH synthesis gene *Gclm* modulate vascular reactivity in mice. *Free Radic Biol Med* 53, 1264-1278.

Wind, S., Beuerlein, K., Eucker, T., Muller, H., Scheurer, P., Armitage, M.E., Ho, H., Schmidt, H.H., and Winkler, K. (2010). Comparative pharmacology of chemically distinct NADPH oxidase inhibitors. *Br J Pharmacol* 161, 885-898.

Yamaura, M., Mitsushita, J., Furuta, S., Kuniwa, Y., Ashida, A., Goto, Y., Shang, W.H., Kubodera, M., Kato, M., Takata, M., *et al.* (2009). NADPH oxidase 4 contributes to transformation phenotype of melanoma cells by regulating G2-M cell cycle progression. *Cancer Res* 69, 2647-2654.

Figures Legends

Figure 1:

A: Effects of NS1 on NO production by BAECs under basal or Ca²⁺-stimulated conditions. Cells (grown to confluence in gelatinized Petri dishes, $\sim 0.1 \times 10^6/\text{cm}^2$) were pre-incubated for 1 h in the absence or presence of 30 μM NS1 before incubation for 30 min in the presence of $\text{Fe}(\text{DETC})_2$ as described under Experimental procedures. The amount of the $\text{Fe}(\text{DETC})_2\text{NO}$ complex was detected by EPR spectroscopy. Experiments were performed under basal conditions (Control) or under Ca²⁺-stimulation of NOS activity in the presence of ionophore. Results are means \pm SD from 3-9 experiments.

B: NO formation by isolated aorta rings in the absence or presence of increasing concentrations of NS1 ([NS1] = 0, 10, 30, 100 μM). Aorta rings from C57BL/6J male mice, 15 weeks old were incubated for 2 h with NS1 and then stimulated with 2 μM ionomycin. Formation of the $\text{Fe}(\text{DETC})_2\text{NO}$ complex was detected by EPR spectroscopy following a 30 min incubation in the presence of $\text{Fe}(\text{DETC})_2$ complex as described under Experimental procedures. Results are expressed as NO formed (arbitrary units) / 30 minutes / mg of dry tissue and are means \pm SD from 3-6 experiments.

Figure 2:

A: Kinetics of NO-independent relaxation of pre-contracted aortic rings by NS1 in the absence of catalase at times 10, 30, 60 and 90 minutes after addition of NS1; Relaxation of pre-contracted aortic rings with KCl or phenylephrine as a function of NS1 concentration.

B: Effects of NS1 on NO-dependent relaxation of mouse aortic rings. Intact aortic rings were pre-contracted in the presence of KCl and their tension was measured following the addition of 10 μM NS1, 500U/ml catalase, or 10 μM Ach in a second run. This second run followed a first run experiment that determined the full relaxation (100%) of the aorta by acetylcholine as described under Experimental procedures. Data are means \pm SD from 6 experiments. Significant differences between groups were calculated by ANOVA followed by a Bonferroni test. $p < 0.05$ was considered significant.

Figure 3:

A: Effects of NS1 on the formation of basal ROS by isolated aortic rings in the presence of vehicle alone (control) or after addition of 10 μM NS1. The hydroxylamine probe CAT-1H was oxidized to nitroxide CAT-1 radical that was detected by EPR as indicated in Experimental procedures. The basal level corresponded to the oxidation of the probe in the absence of aortic rings (with or without NS1). As expected, the signal is inhibited by SOD but not by catalase (data not shown).

B: CM-H trapping of basal ROS levels formed by aortic rings without and with 10 and 30 μM NS1; the formation of the CM \cdot radical was detected by EPR spectroscopy as indicated in Experimental procedures. Data are expressed as arbitrary units/min/mm of tissues. * Paired t-test, one tailed, $P < 0.05$.

Figure 4

Effects of NS1 on the rates of formation of superoxide anion by nNOS or RAW cells. Superoxide anion was trapped by DEPMPO and the DEPMPO-OOH spin-adduct was detected by EPR spectroscopy. Insert: Spectra of DEPMPO-OOH spin-adduct formed upon production of $\text{O}_2^{\cdot-}$ by nNOS *in vitro*. Horizontal axis represents magnetic field intensity and vertical axis the intensities of the EPR signal (arbitrary units).

A: Formation of the DEPMPO-OOH spin adduct by uncoupled nNOS and effect of NS1.

B: Formation of superoxide by RAW cells and effect of NS1. Data compare the relative changes in the rates of formation of the DEPMPO-OOH spin adduct measured as the differences in the intensity of the first line of the DEPMPO-OOH spin-adduct (arrows on Insert of Fig. 4). Conditions are described in Experimental procedures and data are taken from 3-4 representative experiments.

Figure 5

NS1 modulation of ROS formation in HUVECs. HUVECs were pre-treated with increasing concentration of NS1 for 30 min and further treated with 2 μM CellROX[®] Deep Red Reagent for 30 min before flow cytometry analysis for measurements of the intracellular level of ROS.

A: Fluorescence enhancement factor of the CellROX[®] Deep Red reagent as a function of NS1 concentration. The fluorescence enhancement factor corresponds to the ratio between the MFI (Mean Fluorescence Intensity) values obtained in the presence and in the absence of NS1, respectively, as measured in FL-4 channel. The reported ratios correspond to averages of at least four independent measurements. One representative experiment is shown in panel B.

B: One example of cell population distribution of CellROX[®] Deep Red fluorescence intensity (as measured in FL-4 channel). Left: modulation by NS1. Curve 1: control cells (in the absence of CellROX[®] Deep Red and NS1); curve 2: cells + CellROX[®] Deep Red alone; curves 3-7: cells + CellROX[®] Deep Red in the presence of increasing NS1 concentrations (0.5, 1, 8, 10 or 20 μ M, respectively). Right: modulation by the oxidative stress- inducer TBHP used at a concentration of 400 μ M as a positive control.

Figure 6

Effects of NS1 on a 3D-model of angiogenesis using VEGF-stimulated HUVECs grown on matrigel.

Upper panel: comparison of the kinetics on endothelial tube sprouting without and with 100 μ M NS1; **Bottom panel:** Quantification of the experiments (n=3): length of the tubes formed in 24H in serum free (left) and with 1% serum (right) in the presence of 0, 1, 3, 10, 30 and 100 μ M NS1. * Paired t-test, one tailed, $P < 0.05$, *** $P < 0.01$; Results are expressed as endothelial network percentage \pm SEM versus control condition and n reflects the number of experiments. Significant differences between groups were calculated by ANOVA followed by a Bonferroni test. $P < 0.05$ was considered significant.

Figure 7

Comparison of the number of melanocytes (A) and melanoma A375 cells (B) in the presence of increasing concentrations of NS1 after 24 and 48h incubation Primary human melanocytes and melanoma cell lines A375 were treated with indicated concentrations of NS1. After 24h or 48h, viable cells were counted using trypan blue dye exclusion method NT: untreated, DMSO: cells treated with DMSO 1%, NS1: cells treated with the indicated concentration of NS1 diluted from stock solution in DMSO. **(C) Number of A375 melanoma**

cells as a function of NS1 concentrations after 72 and 96 h incubation. Melanoma A375 cell lines were treated with indicated concentrations of NS1. After 72h or 96h, viable cells were counted using trypan blue dye exclusion method. For each experiment, cell number is expressed in percent of control (100%). Data are mean \pm S.D. of three independent experiments performed in triplicate. Significantly different from the corresponding control *P<0.05; **P<0.01; ***P<0.001

Financial Disclosure, Disclosure: There is no conflict of interest.

Table 1: Summary of the pharmacological activities of NS1 on NO and ROS inhibition in vascular bed and macrophages.

Cell type	NO	ROS	Detection	EC50 μM
BAEC^a	Inhibition of NO inhibited by L-NAME		EPR	20-30
HUVEC^b	Inhibition of tube sprouting		Angiogenesis on matrigel	≈ 30
Aortic rings^c	Inhibition of NO inhibited by L-NAME		EPR	40 ± 20
Aortic rings	relaxation inhibited ^d inhibited by L-NAME	H ₂ O ₂ -dependent relaxation ^e	Wire myograph	< 10 ≈ 4
nNOS uncoupling in vitro^f		Inhibition of H ₂ O ₂ Inhibition of O ₂ ⁻	EPR	75 ± 12 105 ± 15
HUVEC^g		BIPHASIC: Formation of ROS Inhibition of ROS	FACS	Detected at 0.5-2μM NS1 ≈ 5
Aortic rings		BIPHASIC: Inhibition of O ₂ ⁻ Formation of O ₂ ⁻	EPR	≈10 ^h ≈50 ⁱ
Macrophages Raw^j		Inhibition of O ₂ ⁻ DPI Inhibited	EPR	120 ± 25

^a: [NS1] = 10-30 μM, BAECs treated with 2μM A23187, NO detected by EPR spin-trapping

^b: [NS1] = 10-100 μM, HUVECs treated with VEGF.

^c: [NS1] = 10-100 μM, aortic rings treated with Ionomycin

^d: aortic rings treated with catalase and 10 μM NS1

^e: aortic rings without catalase and treated with [NS1] = 1-10 μM

^f: [NS1] = 10-250 μM

^g: [NS1] = 0.5-25 μM

^h: superoxide ions formed by aortic rings detected by the CAT1 probe at 10 μM NS1

ⁱ: superoxide ions formed by aortic rings detected by the CMH probe at 10- 100 μM NS1

^j: Raw macrophage activated by PMA treated with [NS1] = 1-500 μM

Table 2: NS1 displays low toxicity toward endothelial and smooth muscle A7r5 cells and mild interference with the metabolism.

[NS1] (μ M)	Cells	Incubation time	Crystal violet	MTT
0	HUVEC	2h	100	100
	A7r5	2h	100	100
10	HUVEC	2h	108 \pm 7%	72 \pm 5 % (P<0.05)
	A7r5	2h	107 \pm 5%	74 \pm 6% (P<0.05)
30	HUVEC	2h	133 \pm 8%	75 \pm 5 % (P<0.05)
	A7r5	2h	109 \pm 4%	65 \pm 11 (P<0.01)

Effects of NS-1 on cellular viability and metabolic activity have been tested in endothelial (HUVEC) and vascular smooth muscle (A7r5) cells by crystal violet staining and MTT assays respectively. We did not observe any significant reduction of the viability of endothelial cells when they were incubated in the presence of NS1 10 or 30 μ M for short (2h) or long (up to 48h, data not shown) periods of time. Similarly in A7r5, the cell viability was not significantly reduced (P< 0.05, 3-7 experiments done in triplicates). However, we observed a small but significant dose-dependent reduction in the MTT assay when A7r5 were incubated with NS1 10 or 30 μ M for 2 h which suggested that NS1 did not affect the viability of vascular smooth muscle cells but may interfere with components associated with the metabolic activity of these cells. This effect may be also present in HUVECs.

Figures

Figure 1:

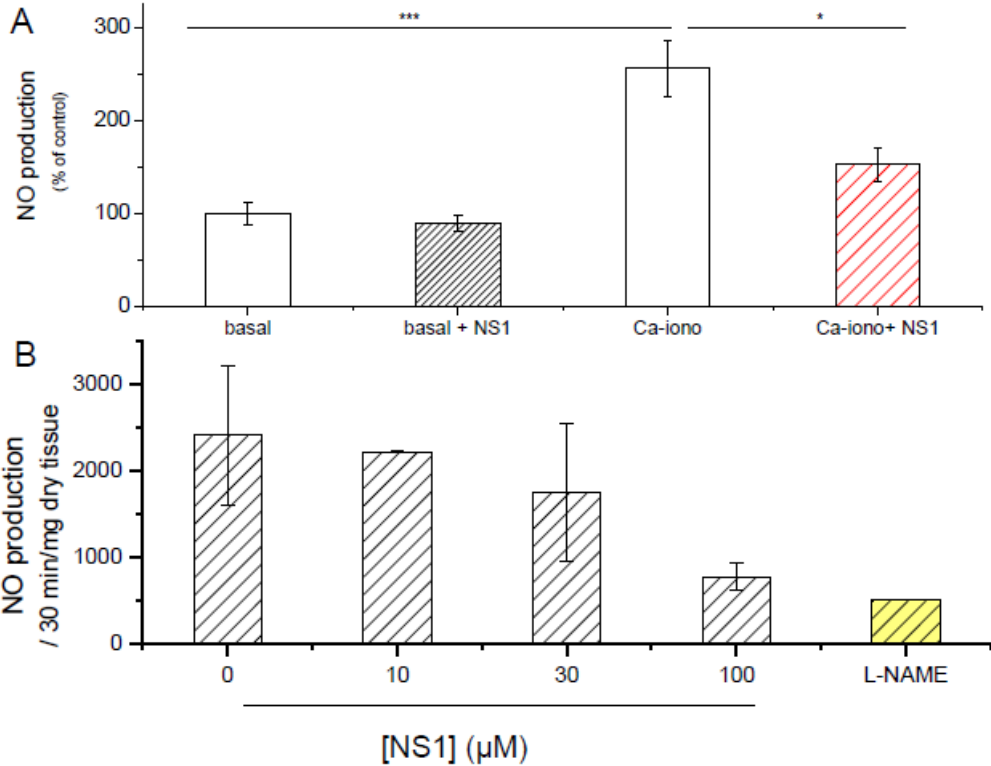
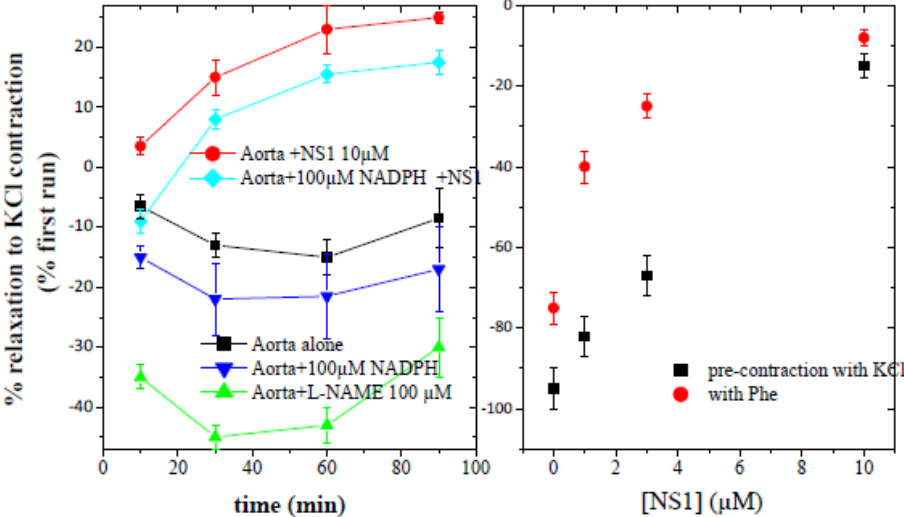


Figure 2:

A- Without catalase



B- With Catalase

NO-dependent relaxation

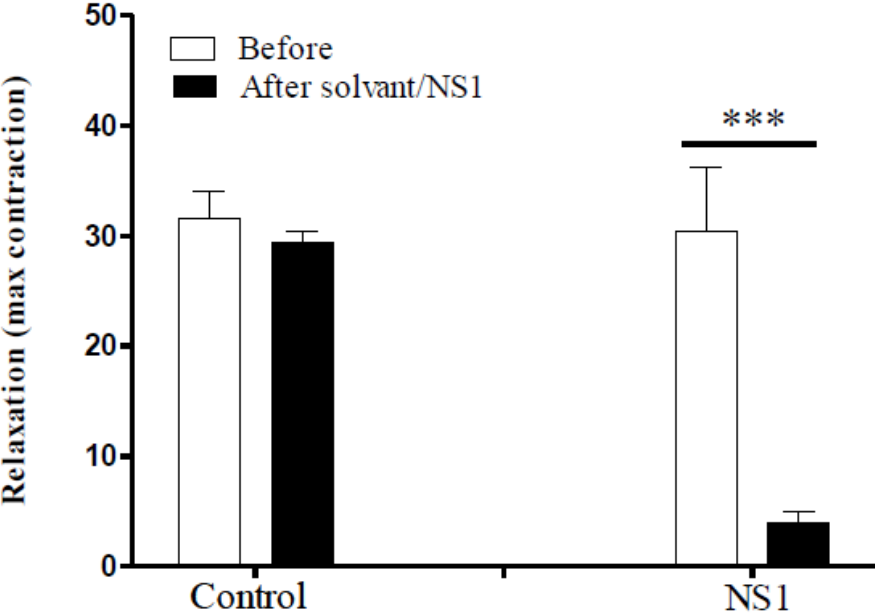


Figure 3:

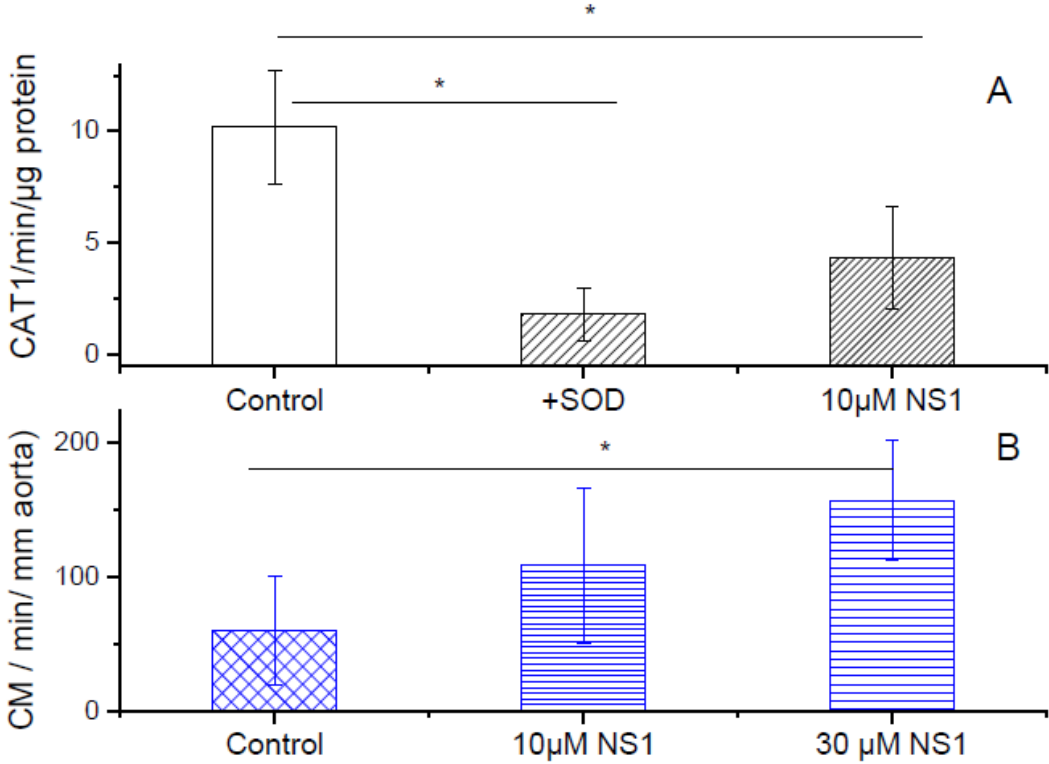


Figure 4:

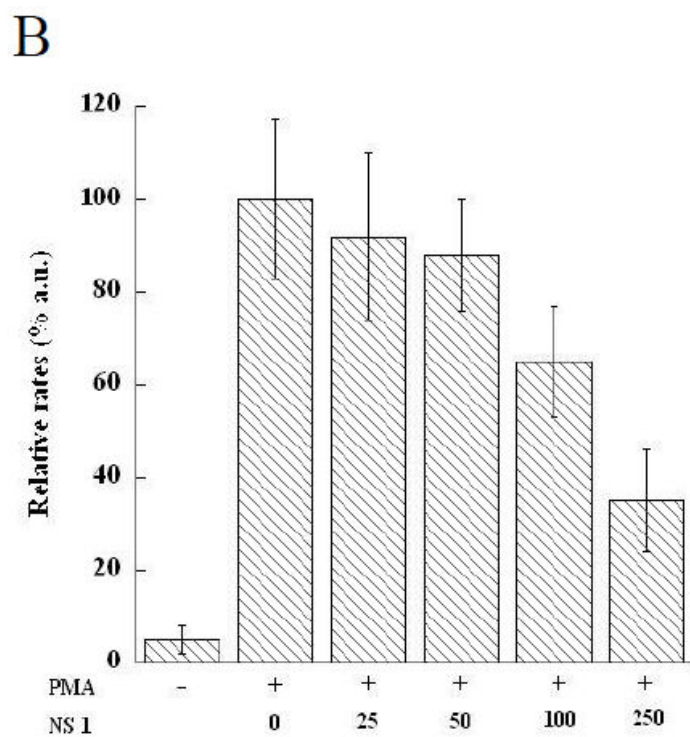
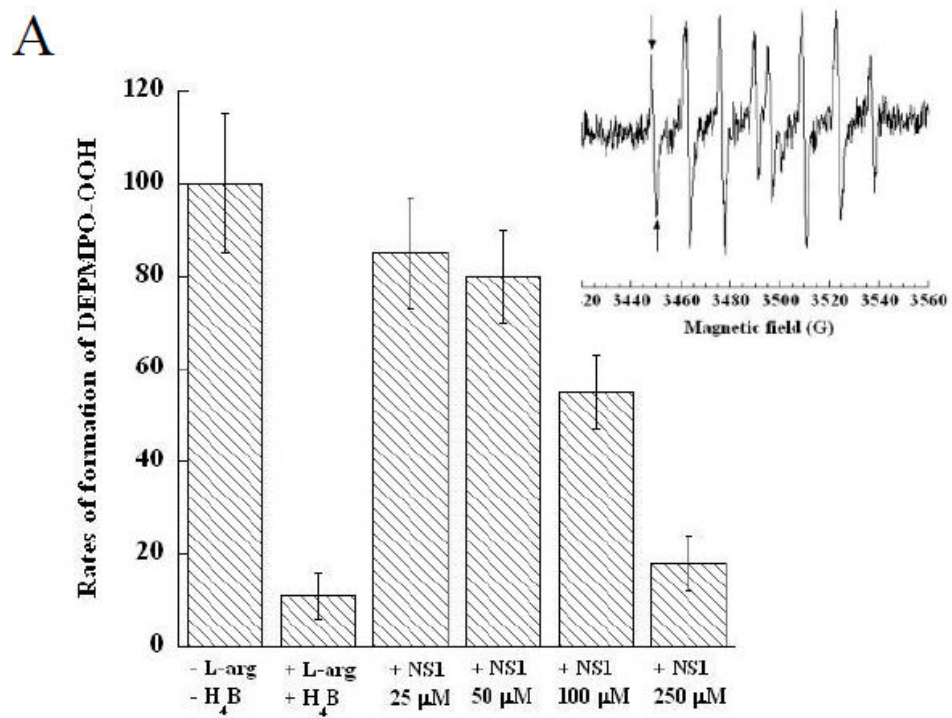
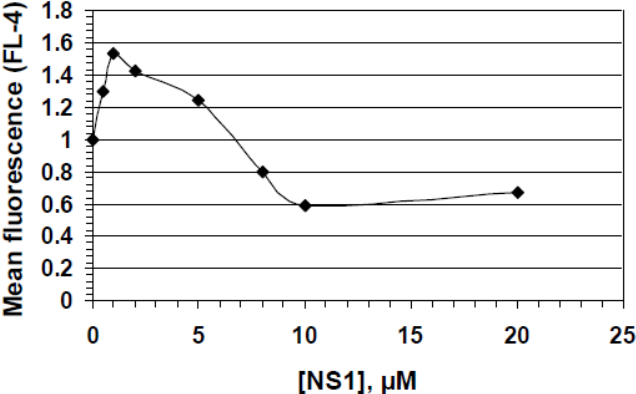


Figure 5:

A



B

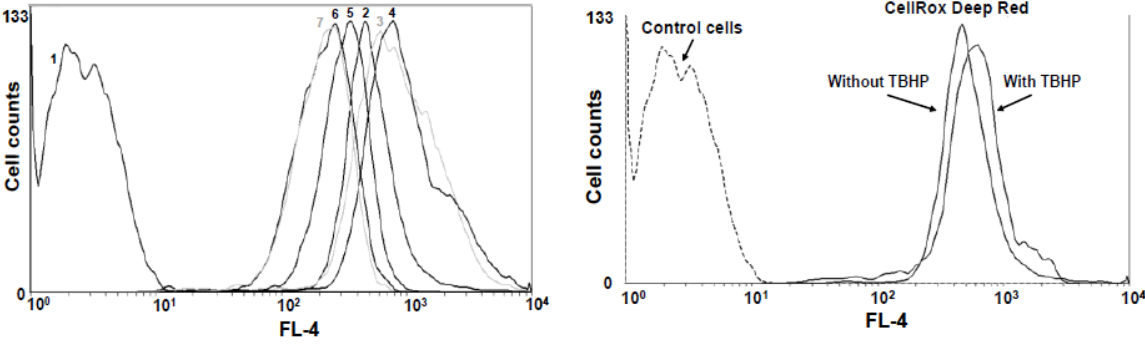
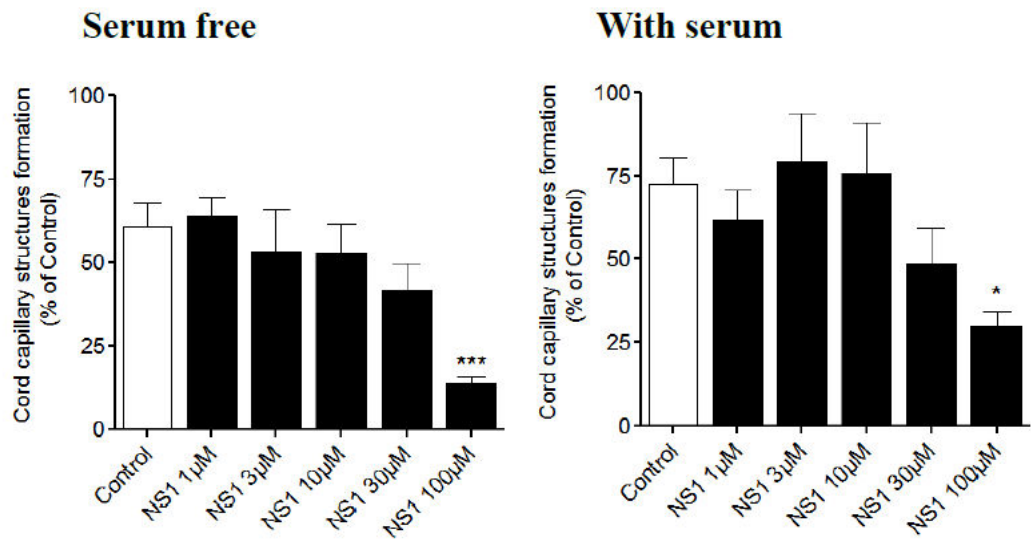
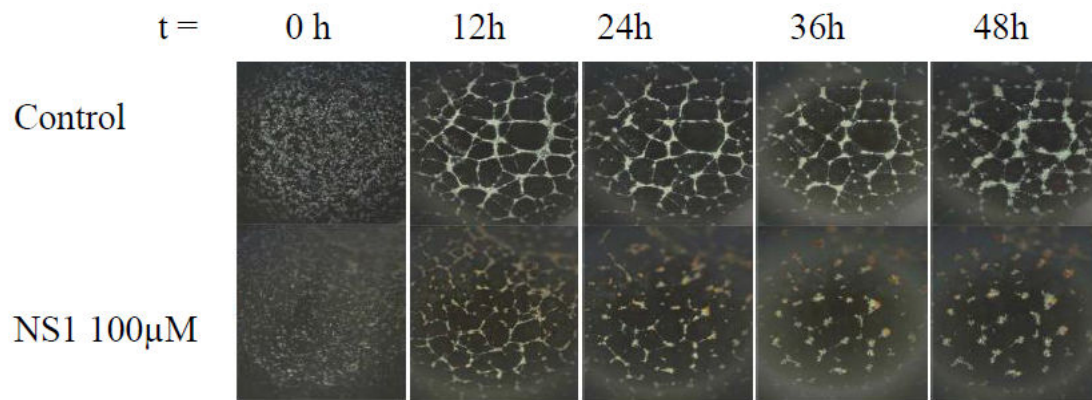
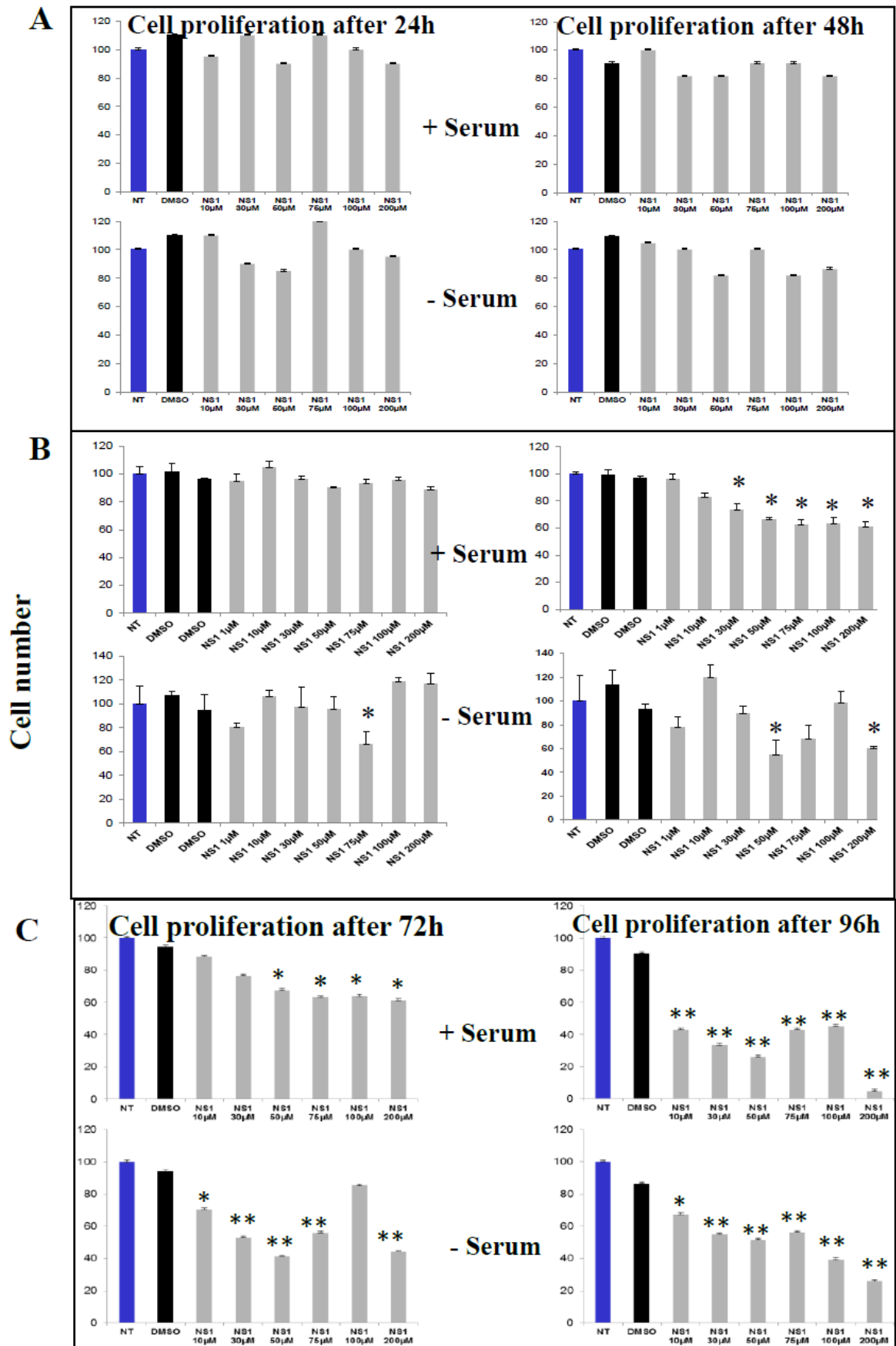


Figure 6:



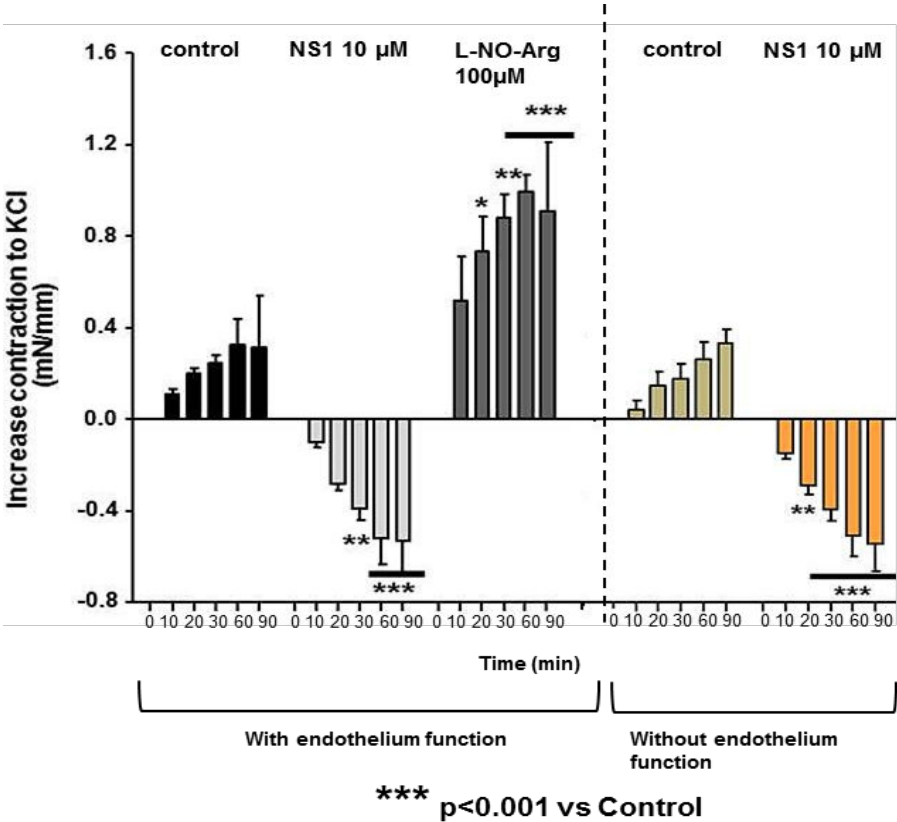
***** P<0.001 vs control; * P<0.05 vs control,**

Figure 7:



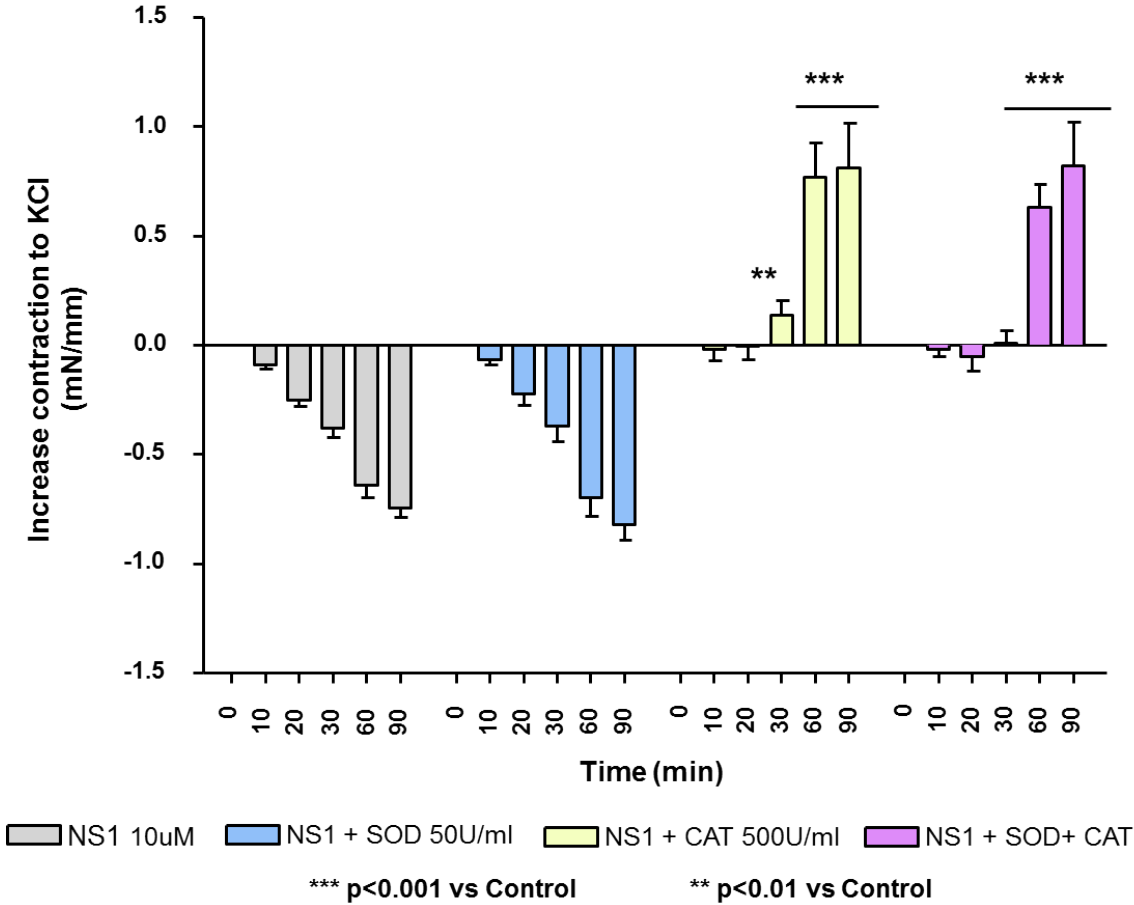
Supplementary data I

Figure S1



The isolated mice aortic rings with (left) or without (right) endothelium function were pre-contracted by 50 mM of KCl under different conditions. The tensions of the aortic rings were recorded by wire-miograph. No significant difference between the effects of NS1 on the aortic rings with or without endothelium function was observed. This result suggests that the observed NS1-mediated vasorelaxation is endothelium-independent.

Figure S2



The vasoconstriction effects of NS1 were performed with aortic rings isolated from mice (n=6). The aortic rings were incubated with either SOD or CAT or both for 20 min, then the contraction of vessels were induced by 50mM of KCl for another 20 min, and 10 μ M of NS1 was added. The tensions of the vessels were recorded up to 90 min after the addition of NS1. Only catalase abolished the vasorelaxation effect. Indeed, under catalase condition, NS1 induced a vasoconstriction effect. In contrast, SOD had no effect on the NS1-mediated vasorelaxation. This result indicates that the NO-independent vasorelaxation led by NS1 was related to the burst of H₂O₂ instead of O₂⁻.

Supplementary data II

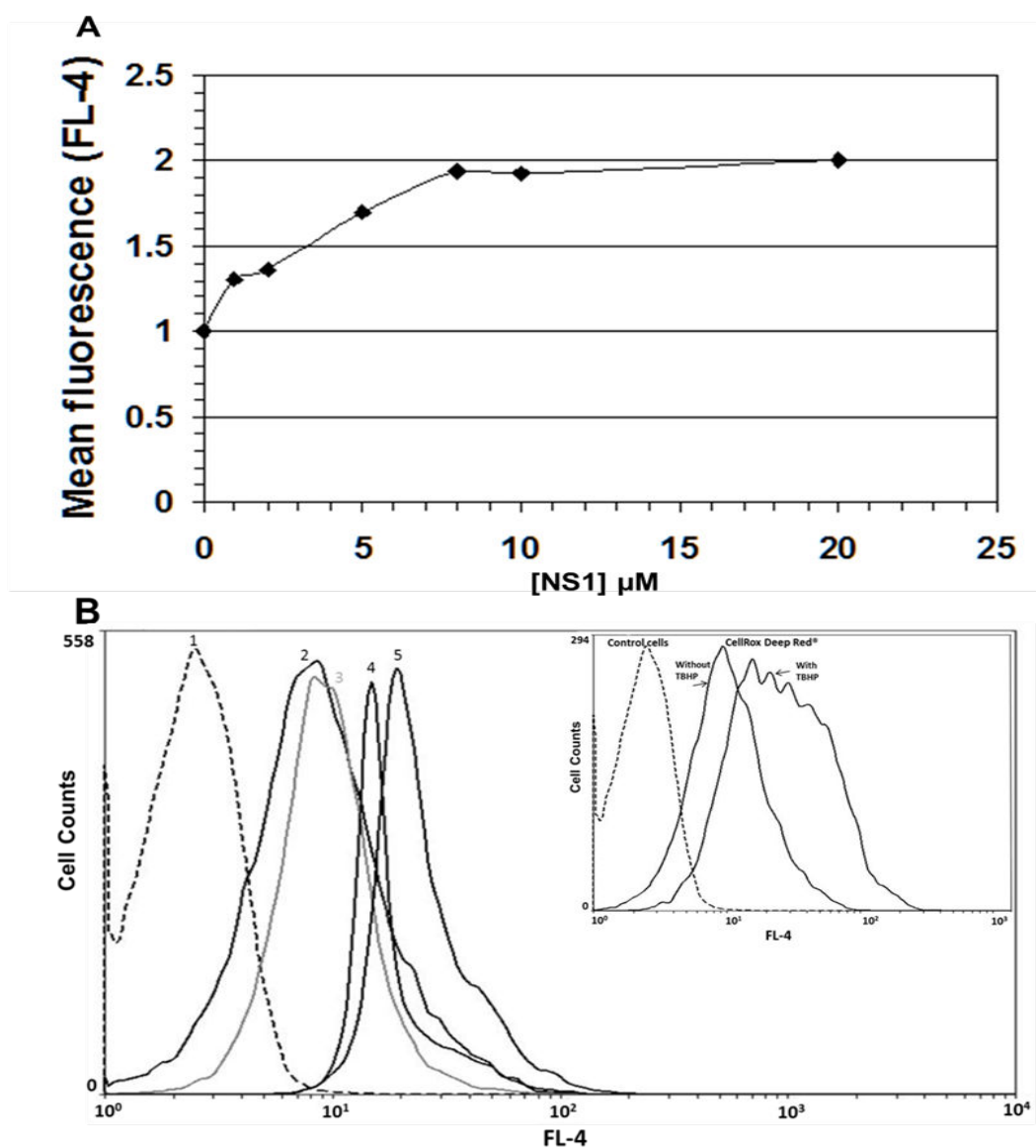


Fig. 18 Detection of ROS formation with NS1 treatment in A7R5 cell line.

A7R5 (smooth muscle cells from rat aorta) between 4-8th passage were pre-incubated with increasing concentrations of NS1 for 30 min, and then further incubated with 2 μM CellROX[®] Deep Red Reagent for 30 min. Tert-butyl hydroperoxide (TBHP), an oxidative stress inducer, was used as a positive control. In this case, cells were pre-treated with 400 μM TBHP for 2 hours before addition of CellROX[®] Deep Red Reagent. The detection of ROS fluorescence emission was analyzed by FACSCalibur flow. Fluorescence signals of NS1 and CellROX[®] Deep Red were measured by using FL-1 and FL-4 channels, respectively. The data were interpreted by the MFI (Mean Fluorescence Intensity) as a function of NS1 concentration. The MFI detected in FL-4 channel is related to the fluorescence emission of the CellROX[®] Deep Red Reagent. The fluorescence enhancement factor was obtained by

normalization of the MFI value obtained in the presence of NS1 by the corresponding value obtained in the absence of NS1.

(A) Fluorescence enhancement factor of the CellROX[®] Deep Red Reagent as a function of NS1 concentration. The fluorescence enhancement factor corresponds to the ratio between the MFI (Mean Fluorescence Intensity) values obtained in the presence and in the absence of NS1, respectively, as measured in FL-4 channel. The reported ratios correspond to averages of at least 4 independent measurements. One representative experiment is shown in panel B. (B) One example of cell population distribution of CellROX[®] Deep Red fluorescence intensity (as measured in FL-4 channel). Curve 1: control cells (in the absence of CellROX[®] Deep Red and NS1); curve 2: cells + CellROX[®] Deep Red alone; curves 3-5: cells + CellROX[®] Deep Red in the presence of increasing NS1 concentrations (1, 5 and 20 μ M, respectively). Inset: modulation by the oxidative stress inducer TBHP as a positive control.

Unlike the bell-shaped curve observed in the case of HUVEC cells, the response of ROS formation in A7R5 cells displayed a monophasic behavior that continuously increases until it reached a plateau. With the increasing concentration of NS1, the fluorescence emission of ROS increased up to 2-fold higher than the basal level. This discrepancy probably results from the differential dominant effects of NS1 interacting with different target(s) among cell lines. Firstly, the increasing phases observed in both HUVECs and A7R5 are in common, suggesting that the effect of NS1 on ROS production is reproducible in different cells lines (a similar behavior was observed with Hela cells (data not shown)). The increase in ROS production in both cases could probably due to the dominant effect of NS1 to other NADPH site containing protein(s), for instance G6PD as previously suggested, the inhibition of which by NS1 would account for a burst of ROS. Secondly, regarding the decreasing phase observed at higher NS1 concentrations in HUVECs, the mechanism probably lies in the inhibition of ROS produced by either NADPH Oxidase (NOX) or uncoupling of NOS or a combination of both. Regarding the possibility that NOS could be responsible for the decreasing phase, it is important to note that no inhibition of ROS was observed in the case of A7R5 cells, despite the fact that NS1 co-localized with eNOS in A7R5 cells (data not shown). This qualitative observation alone cannot exclude the participation of NOS in the differential response between HUVEC and A7R5 cells since, until now, we do not know whether the level of eNOS produced in A7R5 is comparable to that in HUVECs. On the other hand, NOX has been shown to mediate the NS1-dependent inhibition of ROS production in macrophages. Again, an extensive study of NOX expression profiles in HUVEC/A7R5 cells is required to conclude about the participation of NOX in the differential response observed between the different cell types. At this stage, no clear conclusion can be drawn from the present data. A careful quantitative study (e.g. Western blot analysis) is then required to assess and conclude about the participation of NOS/NOX in the decreasing phase.

DISCUSSION, CONCLUSIONS AND PERSPECTIVES

NS1 was designed as a NADPH analogue targeting the NADPH site of NOS and displaying differential fluorescence properties between its free or bound state. It is non-fluorescent in aqueous solvent, but a significant fluorescence recovery occurs upon NS1 binding to NOS under both one- and two-photon excitation conditions. The estimated K_d value indicated a good affinity of NS1 for the three NOS isoforms, which is comparable to that of the natural NADPH substrate. To note, the two-photon excitation condition displayed an obvious advantage in extracting the pure binding information by eliminating the contribution of the auto-fluorescence signal of NOS originating from the flavins. NS1 was proved to compete with NADPH and reversibly inhibited NO formation both *in vitro* and in the cellular context. As NS1 was designed to be a NOS inhibitor, functionally it fulfilled the goal. In the binding test of NS1 to the three NOS isoforms and to other proteins containing or not a NADPH binding site, NS1 displayed surprisingly selectivity for the NOS isoforms. Among the NOS isoforms, NS1 lead to differential effects, depending on the nature of the NOS protein, in terms of fluorescence quantum yield, most likely because NS1 probes a different environment in terms of water molecule content in the vicinity of the nitro group. The eNOS-bound NS1 has a higher quantum yield over nNOS and much higher over iNOS. We took advantage of this feature in the imaging study at cellular level, in endothelial cells (HUVECs) which produce eNOS. A significant fluorescence emission appeared rapidly after the addition of NS1 into the culture dish, suggesting a fast and efficient internalization of NS1. Most importantly, the fluorescence emissions of NS1 and immuno-labeling of eNOS showed a consistent asymmetrical localization at the perinucleus region and a sporadic localization at the plasma membrane, as well as a co-localization between the NS1 and eNOS signals, showing that NS1 targets eNOS in endothelial cells. A signal also appears in Hela cells (which do not produce eNOS) but in this case the perinucleus signal has a symmetrical pattern around the nucleus. This result indicates that the NS1 emission signal in cells is not fully explained by its binding to eNOS.

In the studies of NS1-induced physiological response *in vivo*, NS1 was found to inhibit NO and modulate ROS production at the cellular and tissue levels; The NS1 effect on ROS complicates the analysis of its proper effect on NO-dependent vasodilation/vasoconstriction. Besides, NS1 exhibited an anti-angiogenesis effect on endothelial cells and prevents the proliferation of melanoma. The NS1 induced NO-dependent vasoconstriction in isolated mouse aorta was observed in the presence of catalase only, where the measured production of NO showed an inhibition effect of NS1, as well as in endothelial cells. However, the response of vascular to NS1 appeared to be opposite in the absence of catalase, where a NO-independent vasorelaxation was observed, suggesting an additional target of NS1 than eNOS in the aorta. The interaction of NS1 with this target would probably account for the

NS1-dependent formation of ROS. G6PD could be a candidate, since inhibition of its activity is expected to increase the ROS level (238) (239). Accordingly, in the fluorescence detection of ROS in endothelial cells treated with NS1, the modulation of ROS production displayed a clear but complex biphasic pattern in response to increasing NS1 concentrations: the enhancement of fluorescence intensity occurred at low concentration of NS1 (below 2 μM), whereas using higher NS1 concentrations (up to 20 μM), the ROS level decreased continuously. The decreasing phase could be related to the reduced ROS derived from electron leakage in NOS and/or inhibition of ROS produced by NADPH oxidase. The supportive evidences were provided by (i) *in vitro* experiments of ROS production that originates from uncoupling of nNOS and (ii) O_2^- detection in activated mouse macrophages: in both cases, NS1 behaves as an inhibitor of ROS production.

In summary, NS1 competitively binds to the reductase domain of NOS and efficiently inhibits NO catalysis by blocking the electron flow, including in endothelial cells and isolated mouse aorta; it may induce the NO-dependent vasoconstriction, and inhibits both angiogenesis in endothelial cells and proliferation of melanoma. Different from conventional NOS inhibitors, it is the first inhibitor targeting the reductase domain of the enzyme. Meanwhile, this molecule tool exhibits a unique two-photon property with an excellent signal-to-noise ratio in fluorescence emission. Finally, in addition to its role as a NOS inhibitor, NS1 was also proved to modulate ROS formation in endothelial cells and macrophages.

Designed as a NOS inhibitor that displays fluorescence property, NS1 reached the initial purpose. However, the results of *in vitro* protein-binding assays and fluorescence cell imaging highly suggest the existence of other potential target(s) than NOS. NS1-NOS isoforms exhibited much higher fluorescence emission than NS1 in other protein context, regardless they contain or not a NADPH binding site. Regarding the fluorescence quantum yield, NS1 appeared to be selective for NOS isoforms, yet we cannot conclude that NS1 displays specificity in terms of binding properties. Indeed, NS1 could have others targets than NOS, but their interactions may lead to non-fluorescence or a poor fluorescence signal. Accordingly, NS1 displays differential quantum yields as a function of the NOS isoform, even though the estimated K_d values characterizing the different complexes were similar (5-10 μM). Furthermore, we performed NS1 internalization in several cell lines, such as HUVECs, Hela (cervical cancer cells) and MCF cells (breast cancer cell line), and found that the fluorescence signal of NS1 was not exclusively detectable in endothelial cells, but also in tumor cells, despite of the observed differences in the fluorescence distribution in the different cell lines. Indeed, the fluorescence emission in endothelial cells was more polarized in the peri-nucleus region, corresponding to the Golgi-complex region, and with sporadic signals at the plasma membrane. By contrast, the fluorescence emission in Hela cells was more evenly located around the nucleus forming a ring shape (non-polarized pattern) and no detectable signal at the plasma membrane was observed. The fluorescence emission in

MCF7 cells was observed consistently along the plasma membrane, and with a similar pattern in peri-nucleus region as observed in HeLa cells. It is known that endothelial cells contain much higher amounts of eNOS than tumor cells, and we proved that NS1 targets eNOS in HUVECs. In contrast, eNOS was not detected in HeLa cells. Nevertheless, the fluorescence emission was consistently detected in the three cell lines, despite of the different patterns. The possible explanations are: (i) Besides targeting eNOS in endothelial cells, the detectable fluorescence signal may also originate from non-specific binding of NS1 (i.e. trapping of NS1 within organelles). Such a non-specific signal could explain the symmetrical distribution of the signal around the nucleus in HeLa cells, with a re-distribution/re-localization of the signal into the Golgi region in the case of HUVECs. (ii) The fluorescence emission of NS1 in tumor cells could be due to NS1 binding to other protein targets than eNOS. Although NS1 can be considered as a promising fluorescence probe for NOS labeling, especially eNOS based on quantum yield consideration, the current data also highlight the requirement to improve the NS1 selectivity to NOS isoforms over other proteins to ensure selectivity in terms of biological response (see below).

Based on the spectroscopic characterization, fluorescence properties and in vivo imaging studies, an extensive study concerning the physiological effect of NS1 was carried out in endothelial cells, macrophages and isolated mouse aorta. The results once again confirmed the desired goal of NS1 as a NOS inhibitor. Besides the expected NO inhibition and vasoconstriction effect induced by NS1, we also observed a substantial variation of ROS formation in various types of cell lines and in isolated mouse aortic ring. This observation highly suggested that in a biological environment, NOS is not the exclusive target of NS1. The supportive evidences are:

(i) Depending on the absence or presence of catalase, the response of aortic ring to NS1 is opposite; the expected vasoconstriction is obtained only in the presence of catalase, an enzyme which converts H_2O_2 into H_2O and O_2 . In the vascular system, besides NO, H_2O_2 is another main factor which modulates the vascular tone, suggesting that NS1-induced vasorelaxation in the absence of catalase could be due to a burst of H_2O_2 , which in turn accounts for dilation of the aortic ring in a NO-independent manner. Thus only in the presence of catalase which counters the H_2O_2 effect, a NO-dependent vasoconstriction effect induced by NS1 was revealed. At this step, the observed physiological effects of NS1 include the modulation of NO, as well as the modulation of reactive oxygen species. Therefore, NS1 could also target ROS-related enzymes. As previously mentioned, G6PD could be targeted by NS1.

(ii) The O_2^- production was found to be suppressed by NS1 in mouse macrophages activated by PMA, suggesting that the NADPH oxidase, a major source of superoxide in vascular cells (242), could be an additional target. Further experiments are needed to understand the differential effect of NS1 on ROS inhibition in different cell lines (HUVEC, HeLa,

and A7R5). This implies: a quantitative study of eNOS and NADPH oxidase expression profiles in endothelial, Hela and A7R5 cells. It could be also interesting to perform *in vitro* studies regarding (i) the effect of NS1 on the NADPH oxidase-derived ROS formation and (ii) two-photon fluorescence measurements of NS1-NADPH oxidase complex formation.

ROS modulation by NS1 in the cell context is complex and leads to a biphasic response in endothelial cells. The increasing phase in the ROS detection as a function of NS1 that occurs at low NS1 concentration is in accordance with the NS1-induced vasorelaxation/vasoconstriction in the absence and presence of catalase, respectively. These observations show that NS1, in a certain concentration range, could activate the ROS production, suggesting the existence of a third target in addition to NOS and NOX. It is then reasonable to interpret the biphasic effect of NS1 in endothelial cells and mouse aorta as follows: NS1 may target certain enzyme(s), leading to the up-regulation of ROS, whereas other enzymes such as NOS and NOX could be involved in the net decrease in the ROS production observed in the presence of NS1. These two inverse processes are probably in competition in living systems, however depending on the cell line. The overall effect could be dependent on the NS1 concentration used and the expression levels of the targeted proteins in a given cell line. Preliminary *in vitro* experiments performed by J-L Boucher (Paris V) indicated that NS1 inhibits G6PD (Glucose-6-phosphate dehydrogenase), an enzyme containing a NADP binding site and that reduces NADP^+ to NADPH (personal communication). The inhibition of the G6PD activity is known to promote the endothelial cell oxidant stress (239). Since NS1 was designed as a NADPH analogue, it is likely to target and inhibit G6PD, explaining the increasing phase of ROS formation in endothelial cells and the observed vasorelaxation effect due to the burst of H_2O_2 in mouse aortic rings. Further experiments should be addressed to correlate the ROS production and the co-localization of NS1/G6PD in the cell context.

Besides the detection of ROS in endothelial cells treated with NS1, we performed parallel experiments in A7R5 cells (rat aortic smooth muscle cells) using the same protocol. By contrast to the results obtained with HUVECs, the response of ROS to NS1 in A7R5 appeared to be monophasic, i.e. only the increasing phase was observed without any inhibition of ROS production up to 20 μM of NS1. The increasing phases observed in both HUVECs and A7R5 suggested that the effect of NS1 on ROS production is reproducible in different cells lines; probably the inhibition of NS1 to other NADPH site containing protein(s), as for instance G6PD as suggested above, accounts for the burst of ROS. Regarding the decreasing phase observed at higher NS1 concentrations in HUVECs, the preliminary *in vitro* study provided one possible explanation: under condition of nNOS uncoupling, NS1 inhibited both H_2O_2 and O_2^- productions. Another possible explanation for the decreasing phase observed in HUVEC cells probably lies in the inhibition of ROS produced by NADPH Oxidase (NOX) as observed in macrophages. Altogether, the inhibition of ROS production in HUVECs

may be due to either the inhibition of NOX or inhibition of NOS uncoupling or a combination of both. Regarding the possibility that NOS could be responsible for the decreasing phase, no inhibition of ROS was observed in the case of A7R5 cells, despite the fact that eNOS was evidenced in A7R5 cells by immuno staining experiments (data not shown). However, this – only – qualitative observation is insufficient to provide definitive conclusion about the participation of NOS in the decreasing phase. A quantitative approach by western blot analysis is required (and will be performed in the near future) in order to compare the expression levels of NOS in HUVEC and A7R5 cell lines. On the other hand, NOX is another possible candidate for the decreasing phase. Currently the expression profiles of NOX in HUVEC/A7R5 cells remain unknown. Again, the expression profile of NOX in both cell lines must be evaluated. Generally speaking, to further investigate the targets responsible for both increasing/decreasing phases, it is needed to quantify the different enzyme expression levels, such as eNOS, NADPH oxidase and G6PD, among the different cell lines.

The biosafety issue is an important factor to evaluate the feasibility of a new drug. Firstly, in our study, the MTT assay was performed in HUVECs and A7R5 cell lines, with the treatment of NS1 dissolved in aqueous buffer, up to concentration at 30 μ M, no significant cell viability change was observed. Secondly, during the cell exposure to light excitation, the factor of photodamage should also be taken into account. Since the two-photon excitation rate depends on the square of the illumination intensity, the out-of-focus background excitation falls as the reciprocal 10^4 of distance above and below the focal volume, thus the excitation and the subsequent photodamage are avoided along the out-of-focus beam path way. By comparison, UV-induced damage occurs for power values of about three orders of magnitude lower than the mean values of NIR femtosecond laser pulses. Reduced damage outside of the focal volume may have tremendous advantages in multiphoton studies of thick specimens. Since the first commercial multiphoton microscopes were introduced in 1996, multi-photon microscopy has been widely applied to a variety of imaging tasks and has now become the technique of choice for fluorescence microscopy of thick tissues as well as small animals. In the optical window of two-photon excitation in the NIR region (700-1200 nm), the absorption and light scattering in biological tissues are also much lower than in the UV/VIS region of the spectrum.

As mentioned above, further progress should be dedicated to improve the selectivity of NS1 for NOS isoforms over the other proteins. Based on the molecular modelling (A. Slama-Schwok & Bogdan Tarus, INRA, personal communication), by adding a molecular hook to NS1, the recognition of the inhibitor to NOS isoforms is supposed to be improved since the steric fit between NS1 and NOS is expected to be tighter. To note, there is a specific position in NS1 (or NT) between the chromophoric moiety and the docking moiety that could be compatible with the attachment of such a function (red color in **Fig.19**). The group of Joanne Xie (PPSM, ENS-Cachan) is currently working on the synthesis of new compounds that belong

to the NT family with a hook inserted between the nucleotidic and the chromophoric parts. Such a strategy can be also applied to the NS family since the NS and NT share similarity in these overall structures (except the electron donor/acceptor group in the chromophoric moiety which are different). By analogy, in the near future, the structural improvement of NS could be then addressed, by synthesizing new NS compounds containing a similar molecular hook.

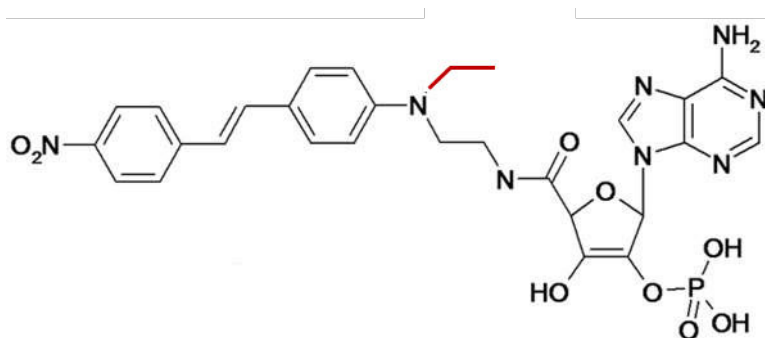


Fig. 19 Scheme of NS1 highlighting the available position (in red) for the attachment of a new function.

Another improvement of the NS strategy concerns the photo-control of the binding step of NS1 to NOS. The possibility to “switch on/off” the NOS inhibition can be realized by modulating the *trans-cis* steric configuration of NS1. Based on molecular modelling (A. Slama-Schwok & Bogdan Tarus, personal communication), only the *trans* configuration of NS is expected to efficiently bind to NOS, corresponding to the “switch on”. By contrast, the binding of NS to NOS would be impeded when it is in the *cis* configuration, corresponding to the “switch off” function. By means of light illumination, it is possible to change the steric configuration of NS between the *trans/cis* isoforms, to further control the “switch on/off” effect of NS. For example, starting from a *cis* isoform (inactive: no binding to NOS -> no inhibition), it would be possible to trigger NOS inhibition by light illumination which converts the *cis* into the *trans* configuration (active: binding to NOS -> inhibition). During the time course of my thesis, I performed preliminary *trans-cis* isomerization experiments by UV/VIS light illumination on NS series, which contain various electron acceptor groups (data not shown). In the case of NS1, the attempt for modulating *trans-cis* isomerization showed a failure, due to the non-rotatable nitro group which is known to inhibit the steric transition from *trans-to-cis* isoform, as well as the fluorescence (243). However, my results suggested a more promising perspective for a NS derivative which contains a CN group instead of NO₂. The preliminary experiment for this compound showed the possibility of a *trans-to-cis* conversion, there was a significant variation in the absorption spectra before and after light illumination. Unfortunately, in the *trans-to-cis* photoisomerization experiments performed on the NS derivatives containing a CN group, the absorption maximum of the *trans* isoforms only

decreased 50% after the light illumination, and only 10% recovery of absorption was observed in the *cis-to-trans* photoisomerization experiments, suggesting that the reversibility of the phenomena was limited by photo-damage. In the future, other NS derivatives containing other electron acceptor groups will be tested.

In summary, NS1 as a novel molecular tool displayed the efficient inhibition effect on NOS and induced expected physiological response in cells and isolated aorta, as well as a unique two-photon property with high signal-to-noise ratio imaging; these features provide broad perspectives in pharmacological applications concerning enzymatic modulation, with interesting anti-angiogenesis properties. However, several aspects should be improved such as the binding selectivity and the photo-control of isomerization which in turn could control the binding of NS to NOS in a spatial and temporal manner.

REFERENCES

1. **Moncada S, Palmer RM, Higgs EA.** Nitric oxide: physiology, pathophysiology and pharmacology. *Pharmacol.Rev.* 1991, Vol. 43, pp. 109-42.
2. **Moncada S, Palmer RM, Higgs EA.** The discovery of nitric oxide as the endogenous nitrovasodilator. *Hypertension.* Oct 1988, Vol. 12, pp. 365-72.
3. **Andrade SP, Bakhle YS, Piper PJ.** Decreased response to platelet activating factor (PAF), endothelin-1 (ET-1) and angiotensin II (All) in tumour blood vessels in mice. *Br J Pharmacol.* 1991, Vol. 104, p. 422.
4. **Sinzinger H, Fitscha P, O'Grady J, et al.** Synergistic effect of prostaglandin E1 and isosorbide dinitrate in peripheral vascular disease. *Lancet.* Mar 1990, Vol. 335, pp. 627-8.
5. **Mellion BT, Ignarro LJ, Ohlstein EH, et al.** Evidence for the inhibitory role of guanosine 3', 5'-monophosphate in ADP-induced human platelet aggregation in the presence of nitric oxide and related vasodilators. *Blood.* May 1981, Vol. 57, pp. 946-55.
6. **Radomski MW, Palmer RM, Moncada S.** The role of nitric oxide and cGMP in platelet adhesion to vascular endothelium. *Biochem Biophys Res Commun.* Nov 1987, Vol. 148, pp. 1482-9.
7. **Radomski MW, Palmer RM, Moncada S.** Endogenous nitric oxide inhibits human platelet adhesion to vascular endothelium. *Lancet.* Nov 1987, Vol. 2, pp. 1057-8.
8. **Vidal MJ, Romero JC, Vanhoutte PM.** Endothelium-derived relaxing factor inhibits renin release. *Eur J Pharmacol.* May 1988, Vol. 149, pp. 401-2.
9. **Griffith TM, Edwards DH, Lewis MJ, et al.** The nature of endothelium-derived vascular relaxant factor. *Nature.* Apr 1984, Vol. 308, pp. 645-7.
10. **RF, Furchgott.** The role of endothelium in the responses of vascular smooth muscle to drugs. *Annu Rev Pharmacol Toxicol.* 1984, Vol. 24, pp. 195-97.
11. **Busse R, Trogisch G, Bassenge E.** The role of endothelium in the control of vascular tone. *Basic Res Cardiol.* 1985, Vol. 80, pp. 475-90.
12. **RF, Furchgott.** Studies on relaxation of rabbit aorta by sodium nitrite: The basis for the proposal that the acid activatable inhibitory factor from bovine retractor penis is inorganic nitrite and the endothelium-derived relaxing factor is nitric oxide. [book auth.] Vanhoutte PM. *Vasodilatation: vascular smooth muscle, peptides, autonomic nerves, and endothelium.* s.l. : Raven Press, New York, 1988, pp. 401-414.

13. **Palmer RM, Ferrige AG, Moncada S.** Nitric oxide release accounts for the biological activity of endothelium-derived relaxing factor. *Nature*. Jun 1987, Vol. 327, pp. 524-6.
14. **Palmer RM, Ashton DS, Moncada S.** Vascular endothelial cells synthesize nitric oxide from L-arginine. *Nature*. Jun 1988, Vol. 333, pp. 664-6.
15. **Moncada S, Higgs EA.** *Nitric oxide from L-arginine: a bioregulatory system*. s.l. : Elsevier, Amsterdam, 1990. pp. 19-33.
16. **JS, Beckman.** *Nitric Oxide: Principles and Actions*. [ed.] Lancaster JR. s.l. : Academic Press, San Diego, 1996. pp. 1-82. Vol. The physiological and pathological chemistry of nitric oxide.
17. **Wise DL, Houghton G.** Diffusion coefficients of neon, krypton, xenon, carbon monoxide and nitric oxide in water at 10-60 °C. *Chem Eng Sci*. 1968, Vol. 23, pp. 1211-6.
18. **Wise DL, Houghton G.** Solubilities and diffusivities of oxygen in hemolyzed human blood solutions. *Biophys J*. 1969, Vol. 9, pp. 36-53.
19. **Porterfield DM, Laskin JD, Jung SK, et al.** Proteins and lipids define the diffusional field of nitric oxide. *Am J Physiol Lung Cell Mol Physiol*. 2001, Vol. 281, pp. L904-912 .
20. **Miersch S, Espey MG, Chaube R, et al.** Plasma membrane cholesterol content affects nitric oxide diffusion dynamics and signaling. *J Biol Chem*. 2008, Vol. 283, pp. 18513-21 .
21. **Bellamy TC, Griffiths C, Garthwaite J.** Differential sensitivity of guanylyl cyclase and mitochondrial respiration to nitric oxide measured using clamped concentrations. *J Biol Chem*. 2002, Vol. 277, pp. 31801-7 .
22. **Liu X, Srinivasan P, Collard E, et al.** Nitric oxide diffusion rate is reduced in the aortic wall. *Biophys J*. Mar 2008, Vol. 94, pp. 1880-9.
23. **Hall CN, Garthwaite J.** What is the real physiological NO concentration in vivo? *Nitric Oxide*. 2009, Vol. 21, pp. 92-103 .
24. **Jr, Lancaster JR.** Diffusion of free nitric oxide. *Methods Enzymol*. 1996, Vol. 268, pp. 31-50.
25. **Möller M, Botti H, Batthyany C.** Direct measurement of nitric oxide and oxygen partitioning into liposomes and low density lipoprotein. *J Biol Chem*. Mar 2005, Vol. 280, pp. 8850-4.
26. **Möller MN, Li Q, Lancaster JR Jr, Denicola A.** Acceleration of nitric oxide autoxidation and nitrosation by membranes. *IUBMB Life*. Apr-May 2007, Vol. 59, pp. 243-8.

27. **Freeman BA, Baker PR, Schopfer FJ.** Nitro-fatty acid formation and signaling. *J Biol Chem.* 2008, Vol. 283, pp. 15515-9.
28. **Thomas LP, Eric FJ.** *Structures of cytochrome P450 enzymes-Structure, Mechanism, and Biochemistry.* [ed.] P.R.Ortiz de Montellano. s.l. : Kluwer Academic/Plenum Publishers, New York, 2005. pp. 87-111.
29. **B.Mayer, M. John, E. Bohme.** Purification of a Ca²⁺/calmodulin-dependent nitric-oxide synthase from porcine cerebellum-cofactor-role of tetrahydrobiopterin. *FEBS Lett.* 1990, Vol. 277, pp. 215-219.
30. **Fischmann TO, Hruza A, Niu XD, et al.** Structural characterization of nitric oxide synthase isoforms reveals striking active-site conservation. *Nat Struct Biol.* Mar 1999, Vol. 6, pp. 233-42.
31. **Raman CS, Li H, Martásek P, Král V, et al.** Crystal structure of constitutive endothelial nitric oxide synthase: a paradigm for pterin function involving a novel metal center. *Cell.* Dec 1998, Vol. 95, pp. 939-50.
32. **Crane BR, Arvai AS, Ghosh DK, et al.** Structure of nitric oxide synthase oxygenase dimer with pterin and substrate. *Science.* Mar 1998, Vol. 279, pp. 2121-6.
33. **Bredt DS, Hwang PM, Glatt CE, et al.** Cloned and expressed nitric oxide synthase structurally resembles cytochrome P-450 reductase. *Nature.* 1991, Vol. 351, pp. 714-718.
34. **Garcin ED, Bruns CM, Lloyd SJ.** Structural basis for isozyme-specific regulation of electron transfer in nitric-oxide synthase. *J Biol Chem.* 2004, Vol. 279, pp. 37918-27.
35. **Wang M, Roberts DL, Paschke R, et al.** Three-dimensional structure of NADPH-cytochrome P450 reductase: prototype for FMN- and FAD-containing enzymes. *Proc Natl Acad Sci U S A.* 1997, Vol. 94, pp. 8411-6.
36. **Alderton WK, Cooper CE, Knowles RG.** Nitric oxide synthases: structure, function and inhibition. *Biochem J.* 2001, Vol. 357, pp. 593-615.
37. **Bredt DS, Snyder SH.** Isolation of nitric oxide synthetase, a calmodulin-requiring enzyme. *Proc Natl Acad Sci U S A.* 1990, Vol. 87, pp. 682-5.
38. **Michel T, Feron O.** Nitric oxide synthases: which, where, how, and why? *J Clin Invest.* 1997, Vol. 100, pp. 2146-52.
39. **Nathan C, Xie Q.** Nitric oxide synthase: roles, tolls, and controls. [*J*]. *Cell.* 1994, Vols. 78(6):915-18.

40. **Moncada S, Higgs A, Furchgott R.** International Union of Pharmacology Nomenclature in Nitric Oxide Research. *Pharmacol Rev.* Jun 1997, Vol. 49, pp. 137-42.
41. **Vallance P, Collier J, Moncada S.** Effects of endothelium-derived nitric oxide on peripheral arteriolar tone in man. *Lancet.* Oct 1989, Vol. 2, pp. 997-1000.
42. **Förstermann U, Li H, Schwarz P, Kleinert H.** *Signal Transduction by Reactive Oxygen and Nitrogen Species: Pathways and Chemical Principles.* [ed.] Fukuto J, Torres M Forman H. s.l. : Springer, Netherlands, 2004. pp. 119-54. Vol. NO Synthesis and NOS regulation.
43. **Balligand JL, Mayer B.** *Nitric Oxide.* s.l. : Springer, 2000. pp. 1-667. 3540661220 9783540661221.
44. **Ignarro, L.J., [ed.].** *Nitric Oxide-Biology and Pathobiology.* s.l. : Academic Press, San Diego, 2000. pp. 1-1003.
45. **Cho HJ, Xie QW, Calaycay J, et al.** Calmodulin is a subunit of nitric oxide synthase from macrophages. *J Exp Med.* Aug 1992 Aug, Vol. 176, pp. 599-604.
46. **Brenman JE, Chao DS, Gee SH, et al.** Interaction of nitric oxide synthase with the postsynaptic density protein PSD-95 and alpha1-syntrophin mediated by PDZ domains. *Cell.* Mar 1996, Vol. 84, pp. 757-67.
47. **Roman LJ, Martásek P, Masters BS.** Intrinsic and extrinsic modulation of nitric oxide synthase activity. *Chem Rev.* Apr 2002, Vol. 102, pp. 1179-90.
48. **S, Daff.** Calmodulin-dependent regulation of mammalian nitric oxide synthase. *Biochem Soc Trans.* Juna 2003, Vol. 31, pp. 502-5.
49. **Li H, Shimizu H, Flinspach M, et al.** The novel binding mode of N-alkyl-N'-hydroxyguanidine to neuronal nitric oxide synthase provides mechanistic insights into NO biosynthesis. *Biochemistry.* Nov 2002, Vol. 41, pp. 13868-75.
50. **S, Daff.** NO synthase: structures and mechanisms. *Nitric Oxide.* 2010, Vol. 23, pp. 1-11.
51. **Matter H, Kumar HS, Fedorov R, et al.** Structural analysis of isoform-specific inhibitors targeting the tetrahydrobiopterin binding site of human nitric oxide synthases. *J Med Chem.* Jul 2005, Vol. 48, pp. 4783-92.
52. **Aoyagi M, Arvai AS, Tainer JA, Getzoff ED.** Structural basis for endothelial nitric oxide synthase binding to calmodulin. *EMBO J.* Feb 2003, Vol. 22, pp. 766-75.
53. **Tochio H, Zhang Q, Mandal P, et al.** Solution structure of the extended neuronal nitric oxide synthase PDZ domain complexed with an associated peptide. *Nat Struct Biol.* May 1999, Vol. 5, pp. 417-21.

54. **Panda K, Ghosh S, Stuehr DJ.** Calmodulin activates intersubunit electron transfer in the neuronal nitric-oxide synthase dimer. *J Biol Chem.* Jun 2001, Vol. 276, pp. 23349-56.
55. **Sagami I, Daff S, Shimizu T.** Intra-subunit and inter-subunit electron transfer in neuronal nitric-oxide synthase: effect of calmodulin on heterodimer catalysis. *J Biol Chem.* Aug 2001, Vol. 276, pp. 30036-42.
56. **Siddhanta U, Presta A, Fan B, et al.** Domain swapping in inducible nitric-oxide synthase. Electron transfer occurs between flavin and heme groups located on adjacent subunits in the dimer. *J Biol Chem.* Jul 1998, Vol. 273, pp. 18950-8.
57. **Pant K, Bilwes AM, Adak S, et al.** Structure of a nitric oxide synthase heme protein from *Bacillus subtilis*. *Biochemistry.* Sept 2002, Vol. 41, pp. 11071-9.
58. **Crane BR, Rosenfeld RJ, Arvai AS, et al.** N-terminal domain swapping and metal ion binding in nitric oxide synthase dimerization. *EMBO J.* Nov 1999, Vol. 18, pp. 6271-81.
59. **Venema RC, Ju H, Zou R, et al.** Subunit interactions of endothelial nitric-oxide synthase. Comparisons to the neuronal and inducible nitric-oxide synthase isoforms. *J Biol Chem.* Jan 1997, Vol. 272, pp. 1276-82.
60. **Masters BS, Martasek P, Roman LJ.** *Pathophysiology and Clinical Applications of Nitric Oxide.* [ed.] Rubyani GM. s.l. : Harwood Academic Publishers, Amsterdam, 1999. pp. 17-37. Vol. Structural variations on a theme of nitric oxide production by three isoforms of nitric oxide synthase. 9057024152.
61. **DJ, Stuehr.** Mammalian nitric oxide synthases. *Biochim Biophys Acta.* May 1999, Vol. 1411, pp. 217-30.
62. **Klatt P, Schmidt K, Lehner D, et al.** Structural analysis of porcine brain nitric oxide synthase reveals a role for tetrahydrobiopterin and L-arginine in the formation of an SDS-resistant dimer. *EMBO J.* Aug 1995, Vol. 14, pp. 3687-95.
63. **McMillan K, Adler M, Auld DS, et al.** Allosteric inhibitors of inducible nitric oxide synthase dimerization discovered via combinatorial chemistry. *Proc Natl Acad Sci USA.* Feb 2000, Vol. 97, pp. 1506-11.
64. **Abu-Soud HM, Stuehr DJ.** Nitric oxide synthases reveal a role for calmodulin in controlling electron transfer. *Proc Natl Acad Sci USA.* Nov 1993, Vol. 90, pp. 10769-72.
65. **Daff S, Sagami I, Shimizu T.** The 42-amino acid insert in the FMN domain of neuronal nitric-oxide synthase exerts control over Ca(2+)/calmodulin-dependent electron transfer. *J Biol Chem.* Oct 1999, Vol. 274, pp. 30589-95.

66. **Adak S, Ghosh S, Abu-Soud HM, Stuehr DJ.** Role of reductase domain cluster 1 acidic residues in neuronal nitric-oxide synthase. Characterization of the FMN-FREE enzyme. *J Biol Chem.* Aug 1999, Vol. 274, pp. 22313-20.
67. **Garnaud PE, Koetsier M, Ost TW, Daff S.** Redox properties of the isolated flavin mononucleotide- and flavin adenine dinucleotide-binding domains of neuronal nitric oxide synthase. *Biochemistry.* Aug 2004, Vol. 43, pp. 11035-44.
68. **Li H, Das A, Sibhatu H, et al.** Exploring the electron transfer properties of neuronal nitric-oxide synthase by reversal of the FMN redox potential. *J Biol Chem.* Dec 2008, Vol. 283, pp. 34762-72.
69. **Noble MA, Munro AW, Rivers SL, et al.** Potentiometric analysis of the flavin cofactors of neuronal nitric oxide synthase. *Biochemistry.* Dec 1999, Vol. 38, pp. 16413-8.
70. **Gachhui R, Presta A, Bentley DF, et al.** Characterization of the reductase domain of rat neuronal nitric oxide synthase generated in the methylotrophic yeast *Pichia pastoris*. Calmodulin response is complete within the reductase domain itself. *J Biol Chem.* Aug 1996, Vol. 271, pp. 20594-602.
71. **Stuehr DJ, Ikeda-Saito M.** Spectral characterization of brain and macrophage nitric oxide synthases. Cytochrome P-450-like heme proteins that contain a flavin semiquinone radical. *J Biol Chem.* Oct 1992, Vol. 267, pp. 20547-50.
72. **Siddhanta U, Wu C, Abu-Soud HM, et al.** Heme iron reduction and catalysis by a nitric oxide synthase heterodimer containing one reductase and two oxygenase domains. *J Biol Chem.* Mar 1996, Vol. 271, pp. 7309-12.
73. **Shirran S, Garnaud P, Daff S, et al.** The formation of a complex between calmodulin and neuronal nitric oxide synthase is determined by ESI-MS. *J R Soc Interface.* Dec 2005, Vol. 2, pp. 465-76.
74. **Spratt DE, Taiakina V, Palmer M, Guillemette JG.** Differential binding of calmodulin domains to constitutive and inducible nitric oxide synthase enzymes. *Biochemistry.* Jul 2007, Vol. 46, pp. 8288-300.
75. **Abu-Soud HM, Yoho LL, Stuehr DJ.** Calmodulin controls neuronal nitric-oxide synthase by a dual mechanism. Activation of intra- and interdomain electron transfer. *J Biol Chem.* Dec 1994, Vol. 269, pp. 32047-50.
76. **Nishida CR, de Montellano PR.** Control of electron transfer in nitric-oxide synthases. Swapping of autoinhibitory elements among nitric-oxide synthase isoforms. *J Biol Chem.* Jun 2001, Vol. 276, pp. 20116-24.

77. **Chen PF, Wu KK.** Characterization of the roles of the 594-645 region in human endothelial nitric-oxide synthase in regulating calmodulin binding and electron transfer. *J Biol Chem.* Apr 2000, Vol. 275, pp. 13155-63.
78. **Montgomery HJ, Romanov V, Guillemette JG.** Removal of a putative inhibitory element reduces the calcium-dependent calmodulin activation of neuronal nitric-oxide synthase. *J Biol Chem.* Feb 2000, Vol. 275, pp. 5052-8.
79. **Nishida CR, Ortiz de Montellano PR.** Autoinhibition of endothelial nitric-oxide synthase. Identification of an electron transfer control element. *J Biol Chem.* May 1999, Vol. 274, pp. 14692-8.
80. **Nishida CR, Ortiz de Montellano PR.** Electron transfer and catalytic activity of nitric oxide synthases. Chimeric constructs of the neuronal, inducible, and endothelial isoforms. *J Biol Chem.* May 1998, Vol. 273, pp. 5566-71.
81. **Roman LJ, Martásek P, Miller RT, et al.** The C termini of constitutive nitric-oxide synthases control electron flow through the flavin and heme domains and affect modulation by calmodulin. *J Biol Chem.* Sept 2000, Vol. 275, pp. 29225-32.
82. **Roman LJ, Masters BS.** Electron transfer by neuronal nitric-oxide synthase is regulated by concerted interaction of calmodulin and two intrinsic regulatory elements. *J Biol Chem.* Aug 2006, Vol. 281, pp. 23111-8.
83. **Tiso M, Tejero J, Panda K, et al.** Versatile regulation of neuronal nitric oxide synthase by specific regions of its C-terminal tail. *Biochemistry.* Dec 2007, Vol. 46, pp. 14418-28.
84. **Jones RJ, Smith SM, Gao YT, et al.** The function of the small insertion in the hinge subdomain in the control of constitutive mammalian nitric-oxide synthases. *J Biol Chem.* 279, Aug 2004, pp. 36876-83.
85. **Haque MM, Panda K, Tejero J, et al.** A connecting hinge represses the activity of endothelial nitric oxide synthase. *Proc Natl Acad Sci USA.* May 2007, Vol. 104, pp. 9254-9.
86. **Feng C, Tollin G, Hazzard JT, et al.** Direct measurement by laser flash photolysis of intraprotein electron transfer in a rat neuronal nitric oxide synthase. *J Am Chem Soc.* May 2007, Vol. 129, pp. 5621-9.
87. **Feng C, Tollin G, Holliday MA, et al.** Intraprotein electron transfer in a two-domain construct of neuronal nitric oxide synthase: the output state in nitric oxide formation. *Biochemistry.* May 2006, Vol. 45, pp. 6354-62.

88. **Welland A, Garnaud PE, Kitamura M, et al.** Importance of the domain-domain interface to the catalytic action of the NO synthase reductase domain. *Biochemistry*. Sept 2008, Vol. 47, pp. 9771-80.
89. **Adak S, Sharma M, Meade AL, Stuehr DJ.** A conserved flavin-shielding residue regulates NO synthase electron transfer and nicotinamide coenzyme specificity. *Proc Natl Acad Sci USA*. Oct 2002, Vol. 99, pp. 13516-21.
90. **Craig DH, Chapman SK, Daff S.** Calmodulin activates electron transfer through neuronal nitric-oxide synthase reductase domain by releasing an NADPH-dependent conformational lock. *J Biol Chem*. Sept 2002, Vol. 277, pp. 33987-94.
91. **Knight K, Scrutton NS.** Stopped-flow kinetic studies of electron transfer in the reductase domain of neuronal nitric oxide synthase: re-evaluation of the kinetic mechanism reveals new enzyme intermediates and variation with cytochrome P450 reductase. *Biochem J*. Oct 2002, Vol. 367, pp. 19-30.
92. **Guan ZW, Kamatani D, Kimura S, Iyanagi T.** Mechanistic studies on the intramolecular one-electron transfer between the two flavins in the human neuronal nitric-oxide synthase and inducible nitric-oxide synthase flavin domains. *J Biol Chem*. Aug 2003, Vol. 278, pp. 30859-68.
93. **Matsuda H, Iyanagi T.** Calmodulin activates intramolecular electron transfer between the two flavins of neuronal nitric oxide synthase flavin domain. *Biochim Biophys Acta*. Dec 1999, Vol. 1473, pp. 345-55.
94. **Konas DW, Zhu K, Sharma M, et al.** The FAD-shielding residue Phe1395 regulates neuronal nitric-oxide synthase catalysis by controlling NADP⁺ affinity and a conformational equilibrium within the flavoprotein domain. *J Biol Chem*. Aug 2004, Vol. 279, pp. 35412-25.
95. **Page CC, Moser CC, Dutton PL.** Mechanism for electron transfer within and between proteins. *Curr Opin Chem Biol*. Oct 2003, Vol. 7, pp. 551-6.
96. **Shimanuki T, Sato H, Daff S, et al.** Crucial role of Lys(423) in the electron transfer of neuronal nitric-oxide synthase. *J Biol Chem*. Sept 1999, Vol. 274, pp. 26956-61.
97. **Crane BR, Arvai AS, Gachhui R, et al.** The structure of nitric oxide synthase oxygenase domain and inhibitor complexes. *Science*. 1997, Vol. 278, pp. 425-431.
98. **Panda K, Haque MM, Garcin-Hosfield ED, et al.** Surface charge interactions of the FMN module govern catalysis by nitric-oxide synthase. *J Biol Chem*. Dec 2006, Vol. 281, pp. 36819-27.

99. **Montellano, P.R. Ortiz de, [ed.].** *Cytochrome P450: Structure, Mechanism, and Biochemistry, third ed.* s.l. : Kluwer Academic/Plenum Publishers, New York, 2005. pp. 1-659. 978-0306483240.
100. **Gorren AC, Mayer B.** Nitric-oxide synthase: a cytochrome P450 family foster child. *Biochim Biophys Acta.* Mar 2007, Vol. 1779, pp. 432-45.
101. **Stuehr DJ, Kwon NS, Nathan CF, et al.** N omega-hydroxy-L-arginine is an intermediate in the biosynthesis of nitric oxide from L-arginine. *J Biol Chem.* Apr 1991, Vol. 266, pp. 6259-63.
102. **Griffith OW, Stuehr DJ.** Nitric oxide synthases: properties and catalytic mechanism. *Annu Rev Physiol.* 1995, Vol. 57, pp. 707-36.
103. **Stuehr DJ, Santolini J, Wang ZQ, et al.** Update on mechanism and catalytic regulation in the NO synthases. *J Biol Chem.* Aug 2004, Vol. 279, pp. 36167-70.
104. **Wei CC, Wang ZQ, Hemann C, et al.** A tetrahydrobiopterin radical forms and then becomes reduced during Nomega-hydroxyarginine oxidation by nitric-oxide synthase. *J Biol Chem.* Nov 2003, Vol. 278, pp. 46668-73.
105. **Wei CC, Crane BR, Stuehr DJ.** Tetrahydrobiopterin radical enzymology. *Chem Rev.* Jun 2003, Vol. 103, pp. 2365-83.
106. **Bec N, Gorren AC, Voelker C, et al.** Reaction of neuronal nitric-oxide synthase with oxygen at low temperature. Evidence for reductive activation of the oxy-ferrous complex by tetrahydrobiopterin. *J Biol Chem.* May 1998, Vol. 273, pp. 13502-8.
107. **Abu-Soud HM, Gachhui R, Raushel FM, Stuehr DJ.** The ferrous-dioxy complex of neuronal nitric oxide synthase. Divergent effects of L-arginine and tetrahydrobiopterin on its stability. *J Biol Chem.* Jul 1997, Vol. 272, pp. 17349-53.
108. **Berka V, Yeh HC, Gao D, et al.** Redox function of tetrahydrobiopterin and effect of L-arginine on oxygen binding in endothelial nitric oxide synthase. *Biochemistry.* Oct 2004, Vol. 43, pp. 13137-48.
109. **Ost TW, Daff S.** Thermodynamic and kinetic analysis of the nitrosyl, carbonyl, and dioxy heme complexes of neuronal nitric-oxide synthase. The roles of substrate and tetrahydrobiopterin in oxygen activation. *J Biol Chem.* Jan 2005, Vol. 280, pp. 965-73.
110. **Laursen JB, Somers M, Kurz S, et al.** Endothelial regulation of vasomotion in apoE-deficient mice: implications for interactions between peroxynitrite and tetrahydrobiopterin. *Circulation.* Mar 2001, Vol. 103, pp. 1282-8.

111. **Landmesser U, Dikalov S, Price SR, et al.** Oxidation of tetrahydrobiopterin leads to uncoupling of endothelial cell nitric oxide synthase in hypertension. *J Clin Invest.* Apr 2003, Vol. 111, pp. 1201-9.
112. **Cai S, Khoo J, Mussa S, et al.** Endothelial nitric oxide synthase dysfunction in diabetic mice: importance of tetrahydrobiopterin in eNOS dimerisation. *Diabetologia.* Sept 2005, Vol. 48, pp. 1933-40.
113. **Tsutsui M, Shimokawa H, Morishita T, et al.** Development of genetically engineered mice lacking all three nitric oxide synthases. *J Pharmacol Sci.* Oct 2005, Vol. 102, pp. 147-54.
114. **Tsutsui M, Shimokawa H, Otsuji Y, et al.** Nitric oxide synthases and cardiovascular diseases: insights from genetically modified mice. *Circ J.* Jun 2009, Vol. 73, pp. 986-93.
115. **Park CS, Pardhasaradhi K, Gianotti C, et al.** Human retina expresses both constitutive and inducible isoforms of nitric oxide synthase mRNA. *Biochem Biophys Res Commun.* Nov 1994, Vol. 205, pp. 85-91.
116. **Park CS, Park R, Krishna G.** Constitutive expression and structural diversity of inducible isoform of nitric oxide synthase in human tissues. *Life Sci.* 1996, Vol. 59, pp. 219-25.
117. **Morrissey JJ, McCracken R, Kaneto H, et al.** Location of an inducible nitric oxide synthase mRNA in the normal kidney. *Kidney Int.* Apr 1994, Vol. 45, pp. 998-1005.
118. **McNaughton L, Puttagunta L, Martinez-Cuesta MA, et al.** Distribution of nitric oxide synthase in normal and cirrhotic human liver. *Proc Natl Acad Sci USA.* Dec 2002, Vol. 99, pp. 17161-6.
119. **Asano K, Chee CB, Gaston B, et al.** Constitutive and inducible nitric oxide synthase gene expression, regulation, and activity in human lung epithelial cells. *Proc Natl Acad Sci USA.* Oct 1994, Vol. 91, pp. 10089-93.
120. **Roberts PJ, Riley GP, Morgan K, et al.** The physiological expression of inducible nitric oxide synthase (iNOS) in the human colon. *J Clin Pathol.* Apr 2004, Vol. 54, pp. 293-7.
121. **Shimizu Y, Sakai M, Umemura Y, Ueda H.** Immunohistochemical localization of nitric oxide synthase in normal human skin: expression of endothelial-type and inducible-type nitric oxide synthase in keratinocytes. *J Dermatol.* Feb 1997, Vol. 24, pp. 80-7.
122. **Laughlin MH, Pollock JS, Amann JF, et al.** Training induces nonuniform increases in eNOS content along the coronary. *J Appl Physiol.* Feb 2001, Vol. 90, pp. 501-10.
123. **Chambliss KL, Shaul PW.** Estrogen modulation of endothelial nitric oxide. *Endocr Rev.* Oct 2002, Vol. 23, pp. 665-86.

124. **Harris MB, Blackstone MA, Ju H, et al.** Heat-induced. *Am J Physiol Heart Circ Physiol*. Jul 2003, Vol. 285, pp. H333-40.
125. **Lam CF, Peterson TE, Richardson DM, et al.** Increased blood flow causes coordinated upregulation of arterial. *Am J Physiol Heart Circ Physiol*. Feb 2006, Vol. 290, pp. H786-93.
126. **Balligand JL, Feron O, Dessy C.** eNOS activation by physical forces: from short-term regulation of contraction to chronic remodeling of cardiovascular tissues. *Physiol Rev*. Apr 2009, Vol. 89, pp. 481-534.
127. **S, Moncada.** Nitric oxide: discovery and impact on clinical medicine. *J R Soc Med*. Apr 1999, Vol. 92, pp. 164-9.
128. **López A, Lorente JA, Steingrub J, et al.** Multiple-center, randomized, placebo-controlled, double-blind study of the nitric oxide synthase inhibitor 546C88: effect on survival in patients with septic shock. *Crit Care Med*. Jan 2004, Vol. 32, pp. 21-30.
129. **Petros A, Lamb G, Leone A, et al.** Effects of a nitric oxide synthase inhibitor in humans with septic shock. *Cardiovasc Res*. Jan 1994, Vol. 28, pp. 34-9.
130. **Kuhn, Cl.** *The Biochemical Basis of Pulmonary Function (Lung Biology in Health and Disease)*. [ed.] Lenfant C. s.l. : Dekker, New York, 1976. pp. 3-48. Vol. The cells of the lung and their organelles.
131. **Fagan KA, Tyler RC, Sato K, et al.** Relative contributions of endothelial, inducible, and neuronal NOS to tone in the murine pulmonary circulation. *Am J Physiol*. Sept 1999, Vol. 277, pp. L472-8.
132. **Förstermann U, Dun N.** Immunohistochemical localization of nitric oxide synthases. *Methods Enzymol*. 1996, Vol. 268, pp. 510-5.
133. **Zhan X, Li D, Johns RA.** Immunohistochemical evidence for the NO cGMP signaling pathway in respiratory ciliated epithelia of rat. *J Histochem Cytochem*. Nov 1999, Vol. 47, pp. 1369-74.
134. **Ermert M, Ruppert C, Günther A, et al.** Cell-specific nitric oxide synthase-isoenzyme expression and regulation in response to endotoxin in intact rat lungs. *Lab Invest*. Apr 2002, Vol. 82, pp. 425-41.
135. **Ricciardolo FL, Sterk PJ, Gaston B, et al.** Nitric oxide in health and disease of the respiratory system. *Physiol Rev*. Jul 2004, Vol. 84, pp. 731-65.
136. **Andreadis AA, Hazen SL, Comhair SA, et al.** Oxidative and nitrosative events in asthma. *Free Radic Biol Med*. Aug 2003, Vol. 35, pp. 213-25.

137. **Langen RC, Korn SH, Wouters EF.** ROS in the local and systemic pathogenesis of COPD. *Free Radic Biol Med.* Aug 2003, Vol. 35, pp. 226-35.
138. **Tsujino I, Nishimura M, Kamachi A, et al.** Exhaled nitric oxide--is it really a good marker of airway inflammation in bronchial asthma? *Respiration.* 2000, Vol. 67, pp. 645-51.
139. **Kanazawa H, Shiraishi S, Hirata K.** Decreased peroxynitrite inhibitory activity in induced sputum in patients with bronchial asthma. *Thorax.* Jun 2002, Vol. 57, pp. 509-12.
140. **Wei CL, Khoo HE, Lee KH, Hon WM.** Differential expression and localization of nitric oxide synthases in cirrhotic livers of bile duct-ligated rats. *Nitric Oxide.* Sept 2002, Vol. 7, pp. 91-102.
141. **Knolle PA, Gerken G.** Local control of the immune response in the liver. *Immunol Rev.* Apr 2000, Vol. 174, pp. 21-34.
142. **McConell GK, Wadley GD.** Potential role of nitric oxide in contraction-stimulated glucose uptake and mitochondrial biogenesis in skeletal muscle. *Clin Exp Pharmacol Physiol.* Dec 2008, Vol. 35, pp. 1488-92.
143. **Steensberg A, Keller C, Hillig T, et al.** Nitric oxide production is a proximal signaling event controlling exercise-induced mRNA expression in human skeletal muscle. *FASEB J.* Sept 2007, Vol. 21, pp. 2683-94.
144. **Buchwalow IB, Minin EA, SamoiloVA VE, et al.** Compartmentalization of NO signaling cascade in skeletal muscles. *Biochem Biophys Res Commun.* May 2005, Vol. 330, pp. 615-21.
145. **Heydemann A, McNally E.** NO more muscle fatigue. *J Clin Invest.* Mar 2009, Vol. 119, pp. 448-50.
146. **Kobayashi YM, Rader EP, Crawford RW, et al.** Sarcolemma-localized nNOS is required to maintain activity after mild exercise. *Nature.* Nov 2008, Vol. 456, pp. 511-5.
147. **Guo ZL, Longhurst JC.** Responses of neurons containing VGLUT3/nNOS-cGMP in the rVLM to cardiac stimulation. *Neuroreport.* Feb 2006, Vol. 17, pp. 255-9.
148. **Chang AY, Chan JY, Chan SH.** Differential distribution of nitric oxide synthase isoforms in the rostral ventrolateral medulla of the rat. *J Biomed Sci.* May-Jun 2003, Vol. 10, pp. 285-91.
149. **Barouch LA, Harrison RW, Skaf MW, et al.** Nitric oxide regulates the heart by spatial confinement of nitric oxide synthase isoforms. *Nature.* Mar 2002, Vol. 416, pp. 337-9.

150. **Fulton D, Fontana J, Sowa G, et al.** Localization of endothelial nitric-oxide synthase phosphorylated on serine 1179 and nitric oxide in Golgi and plasma membrane defines the existence of two pools of active enzyme. *J Biol Chem.* Feb 2002, Vol. 277, pp. 4277-84.
151. **Schilling K, Opitz N, Wiesenthal A, et al.** Translocation of endothelial nitric-oxide synthase involves a ternary complex with caveolin-1 and NOSTRIN. *Mol Biol Cell.* Sept 2006, Vol. 17, pp. 3870-80.
152. **Zimmermann K, Opitz N, Dedio J, et al.** NOSTRIN: a protein modulating nitric oxide release and subcellular distribution of endothelial nitric oxide synthase. *Proc Natl Acad Sci USA.* Dec 2002, Vol. 24, pp. 17167-72.
153. **Schleicher M, Brundin F, Gross S, et al.** Cell cycle-regulated inactivation of endothelial NO synthase through NOSIP-dependent targeting to the cytoskeleton. *Mol Cell Biol.* Sept 2005, Vol. 25, pp. 8251-8.
154. **Dreyer J, Hirlinger D, Müller-Esterl W, et al.** Spinal upregulation of the nitric oxide synthase-interacting protein NOSIP in a rat model of inflammatory pain. *Neurosci Lett.* Oct 2003, Vol. 350, pp. 13-6.
155. **Dedio J, König P, Wohlfart P, et al.** NOSIP, a novel modulator of endothelial nitric oxide synthase activity. *FASEB J.* Jan 2001, Vol. 15, pp. 79-89.
156. **Gilchrist M, McCauley SD, Befus AD.** Expression, localization, and regulation of NOS in human mast cell lines: effects on leukotriene production. *Blood.* Jul 2004, Vol. 104, pp. 462-9.
157. **Yuan Z, Liu B, Yuan L, et al.** Evidence of nuclear localization of neuronal nitric oxide synthase in cultured astrocytes of rats. *Life Sci.* May 2004, Vol. 74, pp. 3199-209.
158. **Giordano A, Tonello C, Bulbarelli A, et al.** Evidence for a functional nitric oxide synthase system in brown adipocyte nucleus. *FEBS Lett.* Mar 2002, Vol. 514, pp. 135-40.
159. **Coggins MP, Bloch KD.** Nitric oxide in the pulmonary vasculature. *Arterioscler Thromb Vasc Biol.* Sept 2007, Vol. 27, pp. 1877-85.
160. **Bove PF, van der Vliet A.** Nitric oxide and reactive nitrogen species in airway epithelial signaling and inflammation. *Free Radic Biol Med.* Aug 2006, Vol. 41, pp. 515-27.
161. **Shaw DE, Berry MA, Thomas M, et al.** The use of exhaled nitric oxide to guide asthma management: a randomized controlled trial. *Am J Respir Crit Care Med.* Aug 2007, Vol. 176, pp. 231-7.

162. **Donnelly LE, Barnes PJ.** Expression and regulation of inducible nitric oxide synthase from human primary airway epithelial cells. *Am J Respir Cell Mol Biol.* Jan 2002, Vol. 26, pp. 144-51.
163. **Ayuse T, Brienza N, Revelly JP, et al.** Alternations in liver hemodynamics in an intact porcine model of endotoxin shock. *Am J Physiol.* Mar 1995, Vol. 268, pp. H1106-14.
164. **H, Spapen.** Liver perfusion in sepsis, septic shock, and multiorgan failure. *Anat Rec (Hoboken).* Jun 2008, Vol. 291, pp. 714-20.
165. **Kishi T, Hirooka Y, Sakai K, et al.** Overexpression of eNOS in the RVLM causes hypotension and bradycardia via GABA release. *Hypertension.* Oct 2001, Vol. 38, pp. 896-901.
166. **Giulivi C, Kato K, Cooper CE.** Nitric oxide regulation of mitochondrial oxygen consumption I: cellular physiology. *Am J Physiol Cell Physiol.* Dec 2006, Vol. 291, pp. C1225-31.
167. **Cooper CE, Giulivi C.** Nitric oxide regulation of mitochondrial oxygen consumption II: Molecular mechanism and tissue physiology. *Am J Physiol Cell Physiol.* Jun 2007, Vol. 292, pp. C1993-2003.
168. **Gachhui R, Abu-Soud HM, Ghosha DK, et al.** Neuronal nitric-oxide synthase interaction with calmodulin-troponin C chimeras. *J Biol Chem.* Mar 1998, Vol. 273, pp. 5451-4.
169. **Villanueva C, Giulivi C.** Subcellular and cellular locations of nitric oxide synthase isoforms as determinants of health and disease. *Free Radic Biol Med.* Aug 2010, Vol. 49, pp. 307-16.
170. **Earp HS, Smith P, Huang Ong SH, Steiner AL.** Regulation of hepatic nuclear guanylate cyclase. *Proc Natl Acad Sci USA.* Mar 1977, Vol. 74, pp. 946-50.
171. **Gobeil F Jr, Zhu T, Brault S, Geha A, et al.** Nitric oxide signaling via nuclearized endothelial nitric-oxide synthase modulates expression of the immediate early genes iNOS and mPGES-1. *J Biol Chem.* Jun 2006, Vol. 281, pp. 16058-67.
172. **Sessa WC, García-Cardeña G, Liu J, et al.** The Golgi association of endothelial nitric oxide synthase is necessary for the efficient synthesis of nitric oxide. *J Biol Chem.* July 1995, Vol. 270, pp. 17641-4.
173. **García-Cardeña G, Oh P, Liu J, et al.** Targeting of nitric oxide synthase to endothelial cell caveolae via palmitoylation: implications for nitric oxide signaling. *Proc Natl Acad Sci USA.* Jun 1996, Vol. 93, pp. 6448-53.

174. **Jagnandan D, Sessa WC, Fulton D.** Intracellular location regulates calcium-calmodulin-dependent activation of organelle-restricted eNOS. *Am J Physiol Cell Physiol.* Oct 2005, Vol. 289, pp. C1024-33.
175. **Wang H, Wang AX, Liu Z, et al.** The trafficking/interaction of eNOS and caveolin-1 induced by insulin modulates endothelial nitric oxide production. *Mol Endocrinol.* Oct 2009, Vol. 23, pp. 1613-23.
176. **Michel JB, Feron O, Sacks D, Michel T.** Reciprocal regulation of endothelial nitric-oxide synthase by Ca²⁺-calmodulin and caveolin. *J Biol Chem.* Jun 1997, Vol. 272, pp. 15583-6.
177. **Symons JD, McMillin SL, Riehle C, et al.** Contribution of insulin and Akt1 signaling to endothelial nitric oxide synthase in the regulation of endothelial function and blood pressure. *Circ Res.* May 2009, Vol. 104, pp. 1085-94.
178. **Corson MA, James NL, Latta SE, et al.** Phosphorylation of endothelial nitric oxide synthase in response to fluid shear stress. *Circ Res.* 1996, Vol. 79, pp. 984-91.
179. **Fisslthaler B, Dimmeler S, Hermann C, et al.** Phosphorylation and activation of the endothelial nitric oxide synthase by fluid shear stress. *Acta Physiol Scand.* Jan 2000, Vol. 168, pp. 81-8.
180. **Dimmeler S, Fleming I, Fisslthaler B, et al.** Activation of nitric oxide synthase in endothelial cells by Akt-dependent phosphorylation. *Nature.* Jun 1999, Vol. 399, pp. 601-5.
181. **Fulton D, Gratton JP, McCabe TJ, et al.** Regulation of endothelium-derived nitric oxide production by the protein kinase Akt. *Nature.* Jun 1999, Vol. 399, pp. 597-601.
182. **McCabe TJ, Fulton D, Roman LJ, Sessa WC.** Enhanced electron flux and reduced calmodulin dissociation may explain "calcium-independent" eNOS activation by phosphorylation. *J Biol Chem.* Mar 2000, Vol. 275, pp. 6123-8.
183. **Hayashi Y, Nishio M, Naito Y, et al.** Regulation of neuronal nitric-oxide synthase by calmodulin kinases. *J Biol Chem.* Jul 1999, Vol. 274, pp. 20597-602.
184. **Nakane M, Mitchell J, Förstermann U, Murad F.** Phosphorylation by calcium calmodulin-dependent protein kinase II and protein kinase C modulates the activity of nitric oxide synthase. *Biochem Biophys Res Commun.* Nov 1991, Vol. 180, pp. 1396-402.
185. **Mount PF, Kemp BE, Power DA.** Regulation of endothelial and myocardial NO synthesis by multi-site eNOS phosphorylation. *J Mol Cell Cardiol.* Feb 2007, Vol. 42, pp. 271-9.
186. **Chen ZP, Mitchelhill KI, Mitchell BJ, et al.** AMP-activated protein kinase phosphorylation of endothelial NO synthase. *FEBS Lett.* Jan 1999, Vol. 443, pp. 285-9.

187. **Bauer PM, Fulton D, Boo YC, et al.** Compensatory phosphorylation and protein-protein interactions revealed by loss of function and gain of function mutants of multiple serine phosphorylation sites in endothelial nitric-oxide synthase. *J Biol Chem.* Apr 2003, Vol. 278, pp. 14841-9.
188. **Michell BJ, Harris MB, Chen ZP, et al.** Identification of regulatory sites of phosphorylation of the bovine endothelial nitric-oxide synthase at serine 617 and serine 635. *J Biol Chem.* Nov 2002, Vol. 277, pp. 42344-51.
189. **Matsubara M, Hayashi N, Jing T, Titani K.** Regulation of endothelial nitric oxide synthase by protein kinase C. *J Biochem.* Jun 2003, Vol. 133, pp. 773-81.
190. **MA, Marletta.** Mammalian synthesis of nitrite, nitrate, nitric oxide, and N-nitrosating agents. *Chem Res Toxicol.* Sep-Oct 1988, Vol. 1, pp. 249-57.
191. **Dinerman JL, Lowenstein CJ, Snyder SH.** Molecular mechanisms of nitric oxide regulation. Potential relevance to cardiovascular disease. *Circ Res.* Aug 1993, Vol. 73, pp. 217-22.
192. **RM, Palmer.** The discovery of nitric oxide in the vessel wall. A unifying concept in the pathogenesis of sepsis. *Arch Surg.* Apr 1993, Vol. 128, pp. 396-401.
193. **Evans CH, Stefanovic-Racic M.** Nitric Oxide in Arthritis. *Methods.* Aug 1996, Vol. 10, pp. 38-42.
194. **Vallance P, Leone A, Calver A, et al.** Accumulation of an endogenous inhibitor of nitric oxide synthesis in chronic renal failure. *Lancet.* Mar 1992, Vol. 339, pp. 572-5.
195. **MacAllister RJ, Whitley GS, Vallance P.** Effects of guanidino and uremic compounds on nitric oxide pathways. *Kidney Int.* Mar 1994, Vol. 45, pp. 737-42.
196. **Schini VB, Vanhoutte PM.** Inhibitors of calmodulin impair the constitutive but not the inducible nitric oxide synthase activity in the rat aorta. *J Pharmacol Exp Ther.* May 1992, Vol. 261, pp. 553-9.
197. **Werner ER, Pitters E, Schmidt K, et al.** Identification of the 4-amino analogue of tetrahydrobiopterin as a dihydropteridine reductase inhibitor and a potent pteridine antagonist of rat neuronal nitric oxide synthase. *Biochem J.* Nov 1996, Vol. 320, pp. 193-6.
198. **Bömmel HM, Reif A, Fröhlich LG, et al.** Anti-pterins as tools to characterize the function of tetrahydrobiopterin in NO synthase. *J Biol Chem.* Dec 1998, Vol. 273, pp. 33142-9.
199. **Levine RA, Miller LP, Lovenberg W.** Tetrahydrobiopterin in striatum: localization in dopamine nerve terminals and role in catecholamine synthesis. *Science.* Nov 1981, Vol. 214, pp. 919-21.

200. **Kapatos G, Hirayama K, Hasegawa H.** Tetrahydrobiopterin turnover in cultured rat sympathetic neurons: developmental profile, pharmacologic sensitivity, and relationship to norepinephrine synthesis. *J Neurochem.* Dec 1992, Vol. 59, pp. 2048-55.
201. **Wolff DJ, Datto GA, Samatovicz RA, et al.** Calmodulin-independent nitric-oxide synthase. Mechanism of inhibition by imidazole and phenylimidazoles. *J. Biol. Chem.* (1993), Vol. 268, pp. 9425-9429.
202. **Stuehr DJ, Fasehun OA, Kwon NS, et al.** Inhibition of macrophage and endothelial cell nitric oxide synthase by diphenyleneiodonium and its analogs. *FASEB J.* Jan 1991, Vol. 5, pp. 98-103.
203. **Beaumont E, Lambry JC, Gautier C, et al.** Synchronous photoinitiation of endothelial NO Synthase activity by a Nanotrigger targeted at its NADPH site. *J Am Chem Soc.* 2007, Vol. 129, pp. 2178-86.
204. **Beaumont E, Lambry JC, et al.** NO formation by neuronal NO-Synthase can be controlled by ultrafast electron injection from a Nanotrigger. *ChemBioChem.* 2009, Vol. 10, pp. 690-701.
205. **Robin AC, Gmouh S, Mongin O, et al.** A NADPH substitute for selective photo-initiation of reductive bioprocesses via two-photon induced electron transfer. *Chem Commun (Camb).* Apr 2007, Vol. 7, pp. 1334-6.
206. **Porrés L, Alain V, Hapiot P, et al.** Optical and electrochemical properties of soluble donor-p-donor compounds as potential molecular wires and electrochemically triggered optical switches. *Phys Chem Chem Phys.* 2003, Vol. 5, pp. 4576-82.
207. **Rogers JE, Slagle JE, McLean DG, et al.** Insight into the nonlinear absorbance of two related series of two-photon absorbing chromophores. *J Phys Chem A.* Mar 2007, Vol. 111, pp. 1899-906.
208. **Herschel, Sir JFW.** On a case of superficial colour presented by a homogeneous liquid internally colourless. *Phil Trans Roy Soc (London).* 1845, Vol. 135, 02610523, pp. 143-5.
209. **Lakowicz, Joseph R.** *Principles of Fluorescence Spectroscopy, 3rd ed.* s.l. : Springer, 2006. pp. 1-25. 978-0-387-31278-1.
210. **Markus S, Johan H, Jörg E.** *Handbook of Fluorescence Spectroscopy and Imaging.* s.l. : WILEY-VCH Verlag GmbH & Co. KGaA, Weinheim, 2011. pp. 7-10. 978-3-527-31669-4.
211. **Cox, Guy.** *Optical Imaging Techniques in Cell Biology.* s.l. : CRC Press, Taylor & Francis Group, 2007. pp. 101-7. Vol. Nonlinear Microscopy.

212. **Barry R. Masters, Peter So.** *Handbook of Biomedical Nonlinear Optical Microscopy*. s.l. : Oxford University Press, 2008. 0195162609.
213. **Lakowicz, Joseph R.** *Principles of fluorescence spectroscopy, 3rd ed.* s.l. : Springer, 2006. pp. 607-21. Vol. Multiphoton excitation and microscopy. 978-0-387-31278-1.
214. **Masters BR, So PT.** Antecedents of two-photon excitation laser scanning microscopy. *Microsc Res Tech.* Jan 2004, Vol. 63, pp. 3-11.
215. **Lakowicz, Joseph R.** *Topics in Fluorescence Spectroscopy, Vol. 5: Nonlinear and Two-Photon-Induced Fluorescence*. s.l. : Springer, 1997. pp. 471-99. Vols. Nonlinear and Two-Photon-Induced Fluorescence. 0306455536.
216. **So PT, Dong CY, Masters BR, Berland KM.** Two-photon excitation fluorescence microscopy. *Annu Rev Biomed Eng.* 2000, Vol. 2, pp. 399-429.
217. **Ishikawa-Ankerhold HC, Ankerhold R, Drummen GP.** Advanced fluorescence microscopy techniques--FRAP, FLIP, FLAP, FRET and FLIM. *Molecules.* Apr 2012, Vol. 17, pp. 4047-132.
218. **Cox, Guy.** *Optical imaging techniques in cell biology*. s.l. : CRC Press, Taylor & Francis Group, 2007. pp. 57-68. Vol. The confocal microscopy.
219. **Kaiser W, Garrett CGB.** Two-Photon Excitation in CaF₂: Eu²⁺. *Phys Rev Lett* 7. 1961, Vol. 7, pp. 229-31.
220. **Denk W, Strickler JH, Webb WW.** Two-photon laser scanning fluorescence microscopy. *Science.* Apr 1990, Vol. 248, pp. 73-6.
221. **Xu C, Zipfel W, Shear JB, et al.** Multiphoton fluorescence excitation: New spectral windows for biological nonlinear microscopy. *Proc Natl Acad Sci USA.* Oct 1996, Vol. 93, pp. 10763-8.
222. **Greulich KO, Weber G.** The light microscope on its way from an analytical to a preparative tool. *J Microsc.* Aug 1992, Vol. 167, pp. 127-51.
223. **Pawley, J.B.,ed.** *Handbook of Biological Confocal Microscopy.2nd edn.* s.l. : Plenum Press, New York., 1995.
224. **Tyrrell RM, Keyse SM.** New trends in photobiology. The interaction of UVA radiation with cultured cells. *J Photochem Photobiol B.* Mar 1990, Vol. 4, pp. 349-61.
225. **Duck, Francis A.** *Physical Properties of Tissue: A Comprehensive Reference book*. s.l. : Academic Press,London, 1990. 0122228006.

226. **Hale GM, Query MR.** Optical constants of water in the 200nm to 200mm wavelength region. *Appl Opt.* Mar 1973, Vol. 12, pp. 555-63.
227. **Conn, P. Michael.** *Techniques in Confocal Microscopy.* s.l. : Elsevier Science, 2010. p. 273. 9780123846587.
228. **König K, Becker TW, Fischer P, et al.** Pulse-length dependence of cellular response to intense near-infrared laser pulses in multiphoton microscopes. *Opt Lett.* Jan 1999, Vol. 24, pp. 113-5.
229. **K, König.** Two-photon near-infrared excitation in living cells. *J Near Infrared Spectrosc.* 1997, Vol. 5, pp. 27-34.
230. **Schönle A, Hell SW.** Heating by absorption in the focus of an objective lens. *Opt Lett.* Mar 1998, Vol. 23, pp. 325-7.
231. **Squirrell JM, Wokosin DL, White JG, Bavister BD.** Long-term two-photon fluorescence imaging of mammalian embryos without compromising viability. *Nat Biotechnol.* Aug 1999, Vol. 17, pp. 763-7.
232. **Moali C, Boucher JL, Sari MA, et al.** Substrate specificity of NO synthases: detailed comparison of L-arginine, homo-L-arginine, their N omega-hydroxy derivatives, and N omega-hydroxynor-L-arginine. *Biochemistry.* Jul 1998, Vol. 37, pp. 10453-60.
233. **Du M, Yeh HC, Berka V, et al.** Redox properties of human endothelial nitric-oxide synthase oxygenase and reductase domains purified from yeast expression system. *J Biol Chem.* Feb 2003, Vol. 278, pp. 6002-11.
234. **Na L, Etienne H, Elvire G, et al.** Multiple Escherichia coli RecQ Helicase Monomers Cooperate to Unwind Long DNA Substrates. *J Biol Chem.* March 2010, Vol. 285, pp. 6922-6936.
235. **Li, Na.** *Application pour la caractérisation des interactions entre macromolécules d'intérêt biologiques et l'étude enzymologique de l'activité hélicase.* s.l. : PhD thesis, LBPA, ENS-Cachan, 2009.
236. **Li J, Henry E, Wang L, et al.** Comparative Study of the Fatty Acid Binding Process of a New FABP from *Cherax quadricarinatus* by Fluorescence Intensity, Lifetime and Anisotropy. *PLoS One.* 2012. 2012, Vol. 7, p. e51079.
237. **Zou MH, Shi C, Cohen RA.** Oxidation of the zinc-thiolate complex and uncoupling of endothelial nitric oxide synthase by peroxynitrite. *J Clin Invest.* 2002, Vol. 109, pp. 817-26.
238. **Gupte RS, Ata H, Rawat D, et al.** Glucose-6-phosphate dehydrogenase is a regulator of vascular smooth muscle contraction. *Antioxid Redox Signal.* Feb 2011, Vol. 14, pp. 543-58.

239. **Leopold JA, Cap A, Scribner AW, et al.** Glucose-6-phosphate dehydrogenase deficiency promotes endothelial oxidant stress and decreases endothelial nitric oxide bioavailability. *FASEB J.* Aug 2001, Vol. 15, pp. 1771-3.
240. **Toledano MB, Planson AG, Delaunay-Moisan A.** Reining in H₂O₂ for safe signaling. *Cell.* Feb 2010, Vol. 140, pp. 454-6.
241. **Santiago E, Contreras C, García-Sacristán A, et al.** Signaling pathways involved in the H₂O₂-induced vasoconstriction of rat coronary arteries. *Free Radic Biol Med.* Jul 2013, Vol. 60, pp. 136-46.
242. **Griendling KK, Sorescu D, Ushio-Fukai M.** NAD(P)H oxidase: role in cardiovascular biology and disease. *Circ Res.* Mar 2000, Vol. Mar, pp. 494-501.
243. **Gruen Henry, Goerner Helmut.** Trans-cis photoisomerization, fluorescence, and relaxation phenomena of trans-4-nitro-4'-(dialkylamino)stilbenes and analogues with a nonrotatable amino group. *J. Phys. Chem.* 1989, Vols. 93 (20), pp 7144–7152.

Abstract

In this study, we introduced a NADPH derivative named as Nanoshutter (NS). NS was designed to inhibit the catalytic activity of NOS, *i.e.* synthesis of NO, by occupying the NADPH site in the reductase domain of NOS. In mammals, NO participates in extensive physiological/pathological processes in the cardiovascular, nervous and immune systems. The pathway of mammal NO synthesis is the oxidation of L-arginine catalyzed by NOS, which occurs in its oxygenase domain. The catalysis requires three co-substrates (L-arginine, NADPH, and O₂) and five cofactors groups (FAD, FMN, calmodulin, BH₄ and heme). Guided by molecular modelling, the structure of NS contains two conjugated subunits: (i) the nucleotide recognition motif of NADPH was retained in NS, allowing a proper targeting to the NADPH binding site of NOS; (ii) the nicotinamide moiety of NADPH is replaced by a stilbene moiety linked with a terminal electron acceptor group, preventing electron flow from the reductase to the oxygenase domain of NOS. Furthermore, this moiety is characterized by a large two-photon absorption cross-section ($\sigma_2 = 130$ GM at 840 nm).

NS1, the first compound of the NS family, contains a NO₂ terminal group as an electron acceptor group. NS1 displayed distinct fluorescence properties in its free and NOS-bound states. The K_d value (≈ 4.2 μ M) was estimated in titration experiments performed under one- or two-photon excitation conditions, suggesting an effective binding of NS1 to NOS with a good affinity. Surprisingly, in terms of fluorescence quantum yield, NS1 displayed a good selectivity to the NOS isoforms over other proteins which contain or not a NADPH binding site. Furthermore, NS1 was shown to competitively inhibit nNOS in a dose-dependent manner. In fluorescence imaging experiments with endothelial cells (HUVEC), NS1 displayed a rapid and efficient internalization, with highlighted fluorescence signal at the perinucleus region and sporadic signal at the plasma membrane. This observation was in accordance with the colocalization imaging between NS1 and eNOS as shown by immunostaining, showing that NS1 actually targets eNOS in endothelial cells. The expected NO-dependent vasoconstriction in isolated mouse aortic rings was only evidenced in the presence of catalase, which converts H₂O₂ into H₂O and O₂. By contrast, in the absence of catalase, a contradictory vasorelaxation was observed. This result indicates that NS1 may target more than NOS in endothelium system, which is (are) likely related to Reactive Oxygen Species (ROS) production. Accordingly, NS1 led to a biphasic response of ROS production in HUVEC cells: An increasing phase occurred at low NS1 concentration (below 2 μ M) and followed by a decreasing phase (ROS inhibition) at higher NS1 concentrations. Furthermore, NS1 was shown to inhibit O₂⁻ production in mouse macrophages and H₂O₂ and O₂⁻ production in uncoupled nNOS *in vitro*. Altogether, the possible but not exclusive explanations for current data are: in addition to its inhibition effect on NO production, NS1 probably also inhibits the ROS production either produced by NADPH Oxidase or by electron leakage from uncoupled NOS, or a combination of both. The origin of the increasing phase remains more elusive but could correspond to the targeting of glucose-6-phosphate-dehydrogenase (G6PD). Additionally, NS1 displayed anti-angiogenesis effect on endothelial cells and prevented proliferation of melanoma.

In conclusion, NS1 fulfilled the goal as a new NOS inhibitor targeting the reductase domain and displayed a unique two-photon property *in vitro* and *in vivo*, these features may provide a promising future for non-invasive real-time imaging, and to potential clinical applications in the NO-dependent diseases.

Key words: NanoShutter (NS); Nitric Oxide (NO); Nitric Oxide Synthase (NOS); NADPH derivative; Reactive Oxygen Species (ROS); two-photon fluorescence; confocal microscopy; fluorescence imaging